



HAL
open science

Development of uniform surface sources by functionalization for decommissioning

Dilan Tüzün

► **To cite this version:**

Dilan Tüzün. Development of uniform surface sources by functionalization for decommissioning. Radiochemistry. Université Paris-Saclay, 2024. English. NNT : 2024UPASP013 . tel-04521519

HAL Id: tel-04521519

<https://theses.hal.science/tel-04521519v1>

Submitted on 26 Mar 2024

HAL is a multi-disciplinary open access archive for the deposit and dissemination of scientific research documents, whether they are published or not. The documents may come from teaching and research institutions in France or abroad, or from public or private research centers.

L'archive ouverte pluridisciplinaire **HAL**, est destinée au dépôt et à la diffusion de documents scientifiques de niveau recherche, publiés ou non, émanant des établissements d'enseignement et de recherche français ou étrangers, des laboratoires publics ou privés.

Development of uniform surface sources by functionalization for decommissioning

*Développement de sources surfaciques uniformes par
fonctionnalisation pour le démantèlement*

Thèse de doctorat de l'université Paris-Saclay

École doctorale n° 576, Particules, Hadrons, Énergie et Noyau : Instrumentation,
Image, Cosmos et Simulation (PHENIICS)
Spécialité de doctorat : Sciences de l'Aval du Cycle Nucléaire, de la Radioprotection
et de la Radiochimie
Graduate School : Physique. Référent : Faculté des sciences d'Orsay

Thèse préparée au **Laboratoire national Henri Becquerel (Université Paris-Saclay, CEA)**, sous la direction de **Martin LOIDL**, Directeur de recherche, et le co-encadrement de **Valérie LOURENÇO**, Ingénieure Chercheuse

Thèse soutenue à Paris-Saclay le 22 Février 2024, par

Dilan TÜZÜN

Composition du Jury

Membres du jury avec voix délibérative

Gilles MONTAVON

Directeur de recherche CNRS, Subatech, Université de Nantes Président

Marielle CROZET

Directrice de recherche CEA, Université Claude Bernard (Lyon 1) Rapportrice & Examinatrice

Pascal FICHET

Chercheur HDR CEA, Sorbonne Université ED 388 Rapporteur & Examineur

Pierino DE FELICE

Chercheur, ENEA, INMRI, Italie Examineur

Céline GAUTIER

Chercheuse CEA, Université Paris-Saclay Examinatrice

Titre : Développement de sources surfaciques uniformes par fonctionnalisation pour le démantèlement

Mots clés : source radioactive, traçabilité, modification de surface, démantèlement, ^{152}Eu , ^{241}Am

Résumé : La thèse vise à développer des sources radioactives surfaciques pour améliorer la traçabilité des mesures de la contamination surfacique. En particulier, le sujet vise à fournir in fine des sources radioactives traçables et utilisables sur le terrain pour caractériser les performances des moniteurs de contamination surfacique. Les sources qui répondent aux exigences des normes internationales ont des caractéristiques très différentes des surfaces à contrôler dans le cadre des activités de l'assainissement et démantèlement (A&D). Elles sont constituées d'un substrat en aluminium rigide sur lequel l'activité est déposée en surface puis recouverte d'une couche de protection. L'approche de la thèse vise à lier chimiquement les éléments radioactifs aux substrats sélectionnés. L'étude a consisté à mettre au point des méthodes de modification de deux types de substrats, polymériques et aluminium, pour y attacher des éléments radioactifs (lanthanide et actinide trivalents). La modification des surfaces d'aluminium à l'aide d'oxydes de manganèse ou de chrome a été réalisée ainsi que leur silanisation et leur greffage avec des acides phosphoniques. Les surfaces polymériques ont quant à elles été d'abord oxydées puis fonctionnalisées avec des acides sulfoniques.

Le processus se divise en plusieurs étapes : préparer la surface, la fonctionnaliser/modifier, y attacher la radioactivité et quantifier l'uniformité de la distribution radioactive. Chaque étape a fait l'objet d'optimisations et de caractérisations (MEB, IRTF, scintillation liquide et autoradiographie). Le substrat Aluminium, tout en étant flexible, permet de conserver un point de comparaison avec les normes en vigueur et le substrat polymérique peut être modifié pour s'approcher des contraintes du terrain (charge en sable, rugosité, moulage de formes complexes). Enfin, une évaluation de la conformité des sources aux normes existantes a été réalisée, même si ces normes ne permettent pas de répondre aux besoins complexes des mesures sur les chantiers d'A&D. Avec les substrats polymériques modifiés avec de l'oxyde de manganèse, il a été possible de fixer près de 100 % de l'Eu-152 ou de l'Am-241 après quelques heures d'immersion dans des solutions radioactives, soit respectivement 74 ou 57 pmol sur $\sim 50 \text{ cm}^2$. L'uniformité de la radioactivité de ces sources a atteint 90 %.

Title : Development of uniform surface sources by functionalization for decommissioning

Keywords : radioactive source, traceability, surface modification, decommissioning, ^{152}Eu , ^{241}Am

Abstract : The thesis aims to develop radioactive surface sources to improve the traceability of surface contamination measurements carried out during dismantling operations. In particular, the ultimate aim is to provide radioactive sources that can be traceable and used in the field to characterize the performance of surface contamination monitors. The sources that meet the requirements of international standards have very different characteristics from the surfaces to be monitored during decontamination and dismantling (D&D) activities. They consist of a rigid aluminum substrate on which surface the activity is deposited and then covered with a protective layer. The study involved developing methods for modifying two types of substrates, polymeric and aluminum, to attach radioactive elements (trivalent lanthanide and actinide). For aluminum substrates, coating with manganese or chromium oxides was tested, along with silanol functionalization and phosphonic acid grafting. The surface modification of polymeric substrates was based on oxidation followed by sulfonic acid grafting.

Whatever the substrate, the study was divided into several stages: preparing the surface, functionalizing/modifying it, attaching the radioactivity and quantifying the uniformity of the radioactive distribution. Each stage was optimised and characterised using SEM, ATR-FTIR, liquid scintillation and autoradiography. The aluminum substrate, while flexible, allows to compare with current standard sources. Additionally the polymeric substrates can be adapted to mimic the real constraints of the D&D sites (sand load, roughness, moulding of complex shapes). Finally, an assessment of the compliance of the sources with existing standards was carried out, even though these standards do not meet the complex needs of measurements on D&D sites. The polymeric substrates coated with manganese oxide could uptake close to 100% of ^{152}Eu or ^{241}Am when immersed in acidic radioactive solutions for a few hours, respectively 74 or 57 pmol on $\sim 50\text{ cm}^2$. For these sources, the uniformity of the radionuclide distribution reached 90%.

Acknowledgements

Ever since I was a little, I had a dream of living abroad in my heart. Life began to shape some plans for me in October 2018 and I was accepted into a prestigious scholarship program from Turkey to pursue my Ph.D. studies in the field of radiation metrology in France. I owe this opportunity to the vision of our esteemed leader, Mustafa Kemal Atatürk, whom I deeply admire, and I would like to extend my first thanks to him for creating this scholarship program and giving me the opportunity to improve myself. Being a part of this scholarship program was a great pleasure for me. On one hand, as a chemical engineer who had worked in different field before, and as someone who would be living abroad alone for the first time, I had my concerns from the very beginning. When I came to France in February 2020 to start a language course, little did I know that I would be stranded in a small town in the midst of a pandemic. This unexpected beginning was enough to turn any ordinary Ph.D. program into a transformative journey. Finally, I had the chance carry out my three years and three months of thesis within the Laboratory National Henri Becquerel of CEA-Saclay. Therefore, I would like to express my gratitude to head of LNHB, Mark Kellett, for welcoming me into this laboratory. Also, I am deeply grateful to Olivier Gal for his unwavering support and efforts. Without his efforts, this Ph.D. study may not have been possible.

First and foremost, I wish to express my heartfelt gratitude to our esteemed jury members. Thank you to my reviewers: Marielle Crozet and Pascal Fichet for their thorough reading of the manuscript, their insightful remarks and the exchanges we had before and during the defense. Thank you to Pierino De Felice, for your kind words and supportive demeanor in my work. Céline Gautier, for the insightful comments and engaging discussions during my defense. Finally, I want to thank Gilles Montavon for chairing the jury and the important remarks on the enriching the explanation of the best results. Then, I want to extend my heartfelt gratitude to my supervisor, Valérie Lourenço. I am immensely grateful to have had her guidance. Thank you for your patience, kindness, and support. It was a pleasure for me to work and learn alongside you. Your unwavering support and mentorship have been invaluable to me throughout this journey. Despite the challenges, you always believed in my potential and stood by me from the very beginning, even offering this position to me, taking the risk that I could have some troubles with the subject. Your trust in me bolstered my determination, and your mentorship surely has left your marks on both my academic and personal development. I also extend my sincere thanks to my thesis director, Martin Loidl. Your willingness to lend an ear and provide insights made a significant difference during these years. Your wisdom offered clarity during times of uncertainty, for which I am truly grateful. I also express my deepest appreciation to Lucille Chambon, my lab partner, an "excel" woman and the target of my fire questions, your support and guidance throughout this journey have been my greatest source of strength and encouragement.

During the analysis process, I had several opportunities to collaborate and get some help from experts. Therefore, I would like to extend my deepest gratitude to Denis Doizi from SPC/LC2R for his unwavering support and kind assistance in ATR-FTIR analysis. Your support was always there whenever I needed it, and I am so grateful for it. Stéphanie Heinkele from SPRE/SRL, whose invaluable help facilitated the completion of LSC analysis. For the SEM, the support provided by Pierre-François Orfila from SPEC/GQ, along with his insightful comments and guidance on

obtaining better images. I am also thankful to Clotaire Chevalier for his meaningful comments during the writing process. Thank you Yann Kergadallan, for your assistance during spontaneously occurring scientific discussions, I will miss these fruitful talks. Finally, I extend my deepest gratitude to Christophe Bobin, for your kind efforts from the very beginning of the Ph.D. process.

Having been a member of LNHB, I found myself fortunate because, by the end of the three-year doctoral journey, I had become surrounded by a bunch of friends, not just colleagues. A big thank you to Sylvie, for our tea talks and sharing the precious moments during this period. Thank you to Sylvain, for showing how to walk like a cat 57 "elli yedi" times a day in the corridor, answering my bunch of questions, and reminding me of cats to relieve the ups and downs of regular Ph.D. life. Thank you to Johanna for her supportive friendship. And thank you to Sophie, Margot, Malvina, Camille, Marie-Noelle, and Cory for their support and always smiling faces. As well as, I would like to thank the internship students I have worked with; Charles, your strong work and effort on polymeric substrates opened new doors to my study, thank you for your efforts and for bringing laughter to our office. Ambra, thank you for the little physics facts that you explained to me and the studies you performed on autoradiography calibration. Thank you to all my Ph.D. fellows: my dear friend Loki for the laughter you brought to me, and the guys from room 114, I will miss our chit-chats that I bothered you to come and try to talk about everything and nothing to relieve some stress: Gael, Triem, Quentin, and Inigo, and fresh doctors, Arsh, Stephanie. Finally, I would like to thank each member of our lab; everyone was an integral part of the journey, and I will keep all the memories in my heart.

This Ph.D. study was funded by the FOCUSDEM project, for which I am sincerely grateful. Additionally, I would like to extend my heartfelt thanks to the YLSY scholarship program sponsored by the Turkish National Ministry of Education, which enabled me to come here and receive education on behalf of Turkish Energy, Nuclear, and Mineral Research Agency (TENMAK). I am deeply appreciative of the opportunity provided by this scholarship program to fulfill my dreams of living abroad. All of these sources of funding provided support during my studies and enabled me to pursue my academic goals.

Besides all of this, I want to thank my dear family for supporting me at every moment. I am heartfully grateful to them, even in the moments when they miss me a lot; they were supporting me for my decisions. First of all, dear grandfather "Hacıbaba," my constant source of motivation; thank you for everything. I will always remember how you supported me, giving me motivation in every situation. Wherever you are now (I'm sure you're in the best place), you can see that I finished my studies, as you had never doubted that. I am so lucky to have you. My lovely mother Ayşe Ardiç, thank you for listening to my daily journeys of every evening and reminding me that in every occasion everything will be fine at the end. My father Mesut Tüzün, thank you for making fun of every occasion and bringing some joy to this process. Dear Dilge Tüzün, the best sister ever, thank you for encouraging me and being there all the time. And my dear aunt Gülüzar Kuşgözoğlu and my lovely grandmother Ayhan Ardiç, I am grateful for your presence in my life, I felt your heart with me all the time. I would like to extend my sincere gratitude to my supervisor from my master's studies, Prof. Suna Balcı, for all the support provided since the beginning of my journey and for offering the best advice at all times. Additionally I want to express my heartfelt thanks to my literature professor from high school, who has now become my dearest friend, Nursel Temir.

You have been my strongest support throughout these years, and I am incredibly fortunate to have you in my life. I cannot forget about the support of my Turkish community in France that makes my life easier, as I could share my feelings in my native language with my dear group of friends Ezel, Evren, Safa, Fatih, and Gülçin. I also want to thank the mother of the stray cats, and my academic struggle-sharing fellow, Gizem. I am grateful for the emotional support you provided during our one-hour-long video calls that ended with meditation and a wishes session. Hopefully, we will see the days when you thank me in your master's thesis soon. Lastly, another heartfelt thanks for my dear friend Aslı, whom I met in the last six months of my Ph.D., and we became very close. Thank you for your support and that of your little lovely baby boy, Mehdi. If we made it through that time, we can be stronger friends than ever later. Our weekly meetings play an important role for me in releasing the stress of the entire writing process. I am so lucky to know you.

And lastly, dear Dorian, thank you for always being by my side with patience and calmness. I am so happy for your kind presence in my life and your invaluable support. Thank you for the guitar and piano solos that inspired my manuscript. Now, you can repeat them a hundred times a day without concern for me. Finally, I should not forget those who worked hard with me: precious Yoda (British Whiskas/5 years old), who tirelessly contributed to my master's thesis (mostly by sleeping on the keyboard). And to my little co-author Luna (Birman/3 years old) for the efforts in my doctoral thesis (sudden jumps on the keyboard and trying to take the place of the screen by putting her head just in front of it), I can't even imagine how to write a thesis without your supervision and lovely hugs.

Finally, to conclude these few pages of acknowledgments, I'd like to share an honest fact about myself. When I took my first step into France, I didn't know anywhere else, so I saved the address of LNHB as "home" on my map for a sense of security. From that moment, it felt like home to me. As I begin this new chapter of my life, I am grateful for the great beginning I had with the LNHB team. Now, I am more excited than ever about what will come next. What could be better than this?

Résumé étendu

Introduction

Dans l'Union Européenne, 95 réacteurs sont en cours de démantèlement et la plupart des 131 réacteurs restants devraient l'être également d'ici une vingtaine d'années. Le coût estimé de ces opérations atteint les 100 milliards d'euros. Cela implique une gestion juste des millions de tonnes de déchets générés, en partie radioactifs, afin de les orienter vers les filières adéquates pour éviter les surcoûts et tenir compte des espaces restreints d'entreposage et stockage. Une caractérisation précise et juste de l'activité des déchets et des matières suspectes permet d'assurer des étapes d'assainissement et de démantèlement (A&D) plus sûres, réalisées avec un risque minimal pour le personnel, la population et l'environnement. Lors des opérations de démantèlement, une des premières étapes de caractérisation du chantier consiste à inspecter des milliers de m² de surface avec des systèmes de détection de type contaminamètres. Cette étape de caractérisation radiologique est cruciale car elle contribue à classer le déchet qui sera produit dans la filière la plus adaptée (déchets TFA pour Très Faible Activité, FA/MA pour faible et moyenne activité, HA pour haute activité ; on tient aussi compte de la période radioactive via la distinction VC/VL pour vie courte et vie longue au-delà de 30 ans en général), mais aussi à maîtriser le coût global du démantèlement, intimement lié au coût de traitement des déchets selon leur niveau d'activité. Le LNHB-MA est le laboratoire national français de métrologie des rayonnements ionisants, en charge de la mesure primaire de l'activité. Il propose grâce à cette thèse de contribuer à améliorer la traçabilité des mesures d'activité surfacique grâce au développement de sources surfaciques uniformes par fonctionnalisation. L'approche choisie devrait également permettre de reproduire des surfaces complexes et non uniformes, fournissant ainsi un étalonnage plus adapté des moniteurs de contamination surfacique ou de toute technique d'analyse de surface non destructive.

Dans d'A&D, une majorité des caractérisations sont réalisées à l'aide de méthodes destructives, qui nécessitent un échantillonnage et une analyse chronophage en laboratoire. Des mesures radiométriques directes sont également effectuées sur site, à l'aide d'appareils de mesure de la contamination de surface, qui doivent être étalonnés correctement avec des sources radioactives surfaciques (ISO 8769). Il est donc intéressant de réaliser du premier coup ces mesures de manière juste et, pour cela, de connaître les performances des appareils utilisés dans des conditions représentatives des conditions de terrain. Les chantiers d'A&D présentent une complexité particulière où la nature des surfaces est variée (béton, peinture, métal), avec des textures lisses ou rugueuses, des surfaces planes mais également des structures plus complexes telles que des tuyaux, tout cela avec une large palette de radionucléides (RN) potentiels. Les conditions de mesures in-situ donc bien différentes des conditions d'étalonnage avec les sources de référence (ISO 8769) et des biais de mesures sont introduits et doivent être corrigés lors de la mesure de surfaces réelles. C'est pour répondre à ces besoins que l'objectif de ce travail est de réaliser des sources surfaciques traçables et de natures plus variées que l'existant afin de reproduire la complexité du terrain. En particulier, cette thèse vise à développer des sources modulables tant dans leur forme qu'en termes de radionucléides disponibles.

Il n'existe aujourd'hui qu'un choix très restreint de sources permettant de caractériser une contamination surfacique. Ces sources sont essentiellement métalliques, rigides et de surfaces

assez modestes puisqu'inférieures à $0,015 \text{ m}^2$. Il est intéressant de noter par ailleurs que dans le domaine de l'A&D, le terme de « point chaud », c'est-à-dire une tache de radioactivité, est utilisé pour désigner une surface présentant une activité alpha de 500 Bq sur $0,1 \text{ m}^2$ (soit un carré d'environ 32 cm de côté). Parmi les radionucléides présents sur les sites en cours d'A&D, les émetteurs alpha et bêta de faible énergie sont les plus délicats à mesurer, en raison de leur faible parcours dans la matière. L'énergie typique d'une particule alpha sur ces chantiers varie entre 4 et 7 MeV , tandis que celle des particules bêta vaut de quelques keV à 2 MeV . L'épaisseur (de plastique) nécessaire pour arrêter de tels rayonnements est seulement de quelques dizaines de micromètres pour les particules alpha et va jusqu'au centimètre pour les particules bêta.

Traçabilité et démantèlement : les limites des sources surfaciques réglementaires

Lors des opérations d'assainissement et de démantèlement, les surfaces sont inspectées avec des systèmes de détection de type moniteurs de contamination de surface (Fig. i). Les performances de ces appareils doivent être caractérisées sur la base de la norme NF EN 60325 et leur étalonnage se fait à partir des sources surfaciques dont les caractéristiques sont décrites dans la norme ISO 8769. Actuellement, les meilleures sources surfaciques disponibles sur le marché sont des sources dont l'uniformité de la répartition de l'activité est comprise entre 90 et 95% . Il s'agit de sources métalliques planes et rigides (support en aluminium de 3 mm d'épaisseur), d'une surface maximale de seulement 150 cm^2 (Fig. i), avec une uniformité à peine supérieure à 90% .



Figure i: Exemples de sources surfaciques commerciales et de contaminamètres de surface

Ces sources sont le plus souvent fabriquées par séchage de solutions radioactives sur de l'aluminium et sont ainsi peu représentatives de la réalité du terrain. Plusieurs autres techniques de production de sources sont décrites dans la littérature, telles que les sources réalisées par dépôt de gouttes, celles électrodéposées, les sources anodisées ou celles sur membranes d'échange d'ions. Ces sources sont étalonnées en termes de taux d'émission de particules par unité de surface et en activité. Une dizaine de techniques de préparation de sources surfaciques, disponibles commercialement ou non, ont été décrites. Leur conformité avec l'ISO 8769 et leur capacité à mimer des surfaces contaminées réalistes des sites en A&D ont été évaluées.

Nouvelle approche pour la réalisation de sources surfaciques traçables

Pour réaliser des sources de grande taille, un changement d'approche est nécessaire. Les sources présentées sur la Figure i sont fabriquées par adsorption de l'activité sur une surface, parfois poreuse, ensuite, puisque le dépôt n'est que séché sur la surface, il est nécessaire de le protéger afin de rendre la source non contaminante. Cette étape réduit le rendement d'émission des rayonnements de faible parcours dans la matière comme les émissions alpha ou bêta pures, du fait de l'auto-absorption. L'approche de ce travail vise à augmenter drastiquement l'affinité du radionucléide pour la surface en l'y fixant chimiquement (i.e. par fonctionnalisation). Le choix de la méthode de fonctionnalisation dépend du substrat sur lequel l'accroche a lieu (métallique, polymère, conducteur ou non, souple ou rigide). Contrairement à la physisorption (adsorption réversible comme dans le cas d'un dépôt simplement séché) pour laquelle les énergies de liaison avec la surface sont faibles (\sim kJ/mol), la chimisorption permet d'atteindre des valeurs beaucoup plus importantes (centaine de kJ/mol) par création d'une liaison chimique forte, qui garantit une plus grande stabilité de la couche formée (Fig. ii).

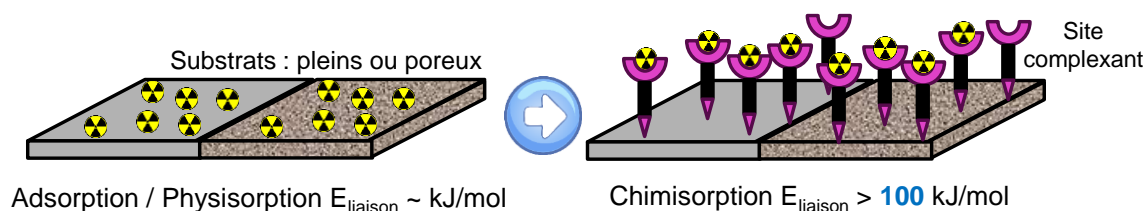


Figure ii: Illustration du changement d'approche choisi pour l'amélioration des performances des sources surfaciques

Pour répondre aux besoins de l'A&D en termes de développement de sources traçables, deux pistes principales ont été suivies : d'une part les sources sur substrat métallique proches de celles décrites par la norme qui permettront un point de comparaison avec les performances des sources existantes, d'autre part des sources déformables voire cylindriques, non disponibles actuellement. Pour ces dernières, des supports polymériques de type plastique (PET, type Mylar®) ou résine (époxy) ont été retenus, ce qui modifie les approches en termes de fonctionnalisation ou d'encapsulation de l'activité par rapport aux surfaces métalliques. Les trois types de sources qui ont fait l'objet de ce travail de thèse sont décrites Figure iii.

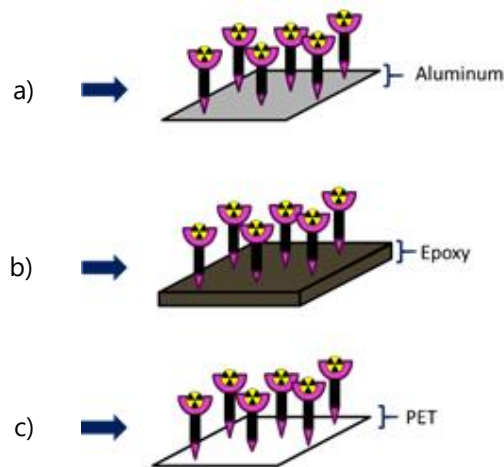


Figure iii: Sources surfaciques produites avec la nouvelle approche a) à partir de feuilles d'aluminium plus ou moins fines, b) à partir de résine époxy, c) à partir de films de PET

Dans tous les cas, la principale approche retenue est la fonctionnalisation du substrat pour immobiliser et répartir de manière uniforme les radionucléides sans trop atténuer les rayonnements, tout en garantissant que la surface reste non contaminante. La formation de liaisons chimiques fortes avec la surface doit garantir la stabilité de la couche formée et l'affinité chimique avec les molécules complexantes immobilisées sur la surface, vise à fixer durablement l'activité. Cette approche est nécessairement itérative puisque les contraintes d'accroche du radionucléide dépendent de la nature du substrat retenu pour la source (Fig. iv).

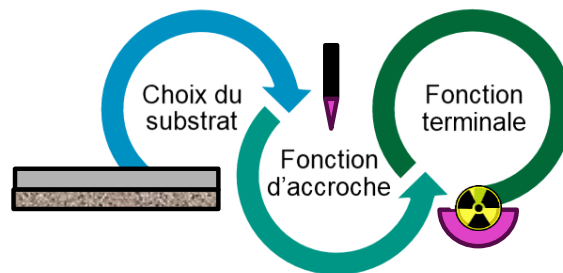


Figure iv : Approche choisie pour l'amélioration des performances des sources surfaciques.

Les émetteurs alpha étant parmi les plus difficiles à mesurer, cette étude s'est concentrée sur la production de sources d'actinides car les éléments transuraniens tels que le neptunium, le plutonium, l'américium et le curium, produits dans les réacteurs et les explosions nucléaires, sont particulièrement intéressants. Les actinides constituent un groupe de 14 éléments, caractérisés par le remplissage d'orbitales 5f, à l'instar des lanthanides, dans lesquels les orbitales 4f sont remplies. Les actinides présentent une chimie plus complexe que les lanthanides, comprenant à la fois des éléments des chaînes de désintégration naturelle et des actinides artificiels. Parmi les actinides, les actinides trivalents sont connus pour leur stabilité, c'est pourquoi de nombreuses

recherches se sont concentrés sur cet état d'oxydation. Parmi les actinides trivalents, l'américium (Am) et le curium (Cm) sont les plus courants. L'américium 241 se distingue par son émission gamma de 59,54 keV, qui facilite sa mesure directe à partir de certains échantillons. C'est pourquoi ce RN a été choisi comme actinide modèle pour cette étude. L'euporium est fréquemment utilisé comme modèle pour la série des lanthanides, en outre, l'euporium 152 présente l'avantage d'émettre des photons gamma facilement mesurables. Enfin, l'euporium étant situé juste au-dessus de l'américium dans la classification périodique, c'est aussi le lanthanide qui est le meilleur analogue chimique de l'américium.

Il a été nécessaire d'optimiser à façon l'accroche du radionucléide sur la surface choisie, via l'adaptation de la fonctionnalisation avec, à une extrémité, une fonction d'accroche adaptée à la surface support et, à l'autre, une fonction spécifique du radionucléide à fixer. Enfin, des molécules commercialement disponibles associant le couple de fonctions recherchées ont été identifiées.

Après avoir examiné la littérature, différentes fonctions ont été identifiées pour leur propension à se fixer sur les deux substrats retenus d'une part (l'aluminium et les surfaces polymériques) mais aussi à retenir l'euporium ou l'américium. Pour les surfaces polymériques, l'accent a été mis sur le groupement acide sulfonique pour se lier au RN, et la 1,4-butane sultone a été choisie pour l'accroche sur les surfaces PET et époxy. Pour l'aluminium, l'utilisation de silanes et d'acides phosphoniques a été envisagée pour le greffage, et pour attacher les RN, les fonctions ammonium quaternaire, acide sulfonique et acide phosphonique ont été choisies. De plus, des méthodes de revêtements de conversion à base d'oxydes de manganèse ou de chrome ont également été sélectionnés pour le substrat en aluminium, en raison de leur capacité à former un revêtement de surface, susceptible de retenir des cations tels que Eu^{3+} et Am^{3+} . La disponibilité commerciale des molécules a été vérifiée et a conduit à définir la liste des produits présentés dans le Tableau i et le Tableau ii.

Tableau i : Fonction chimique retenue pour les substrats polymériques (et mention de l'approche par revêtement, étape intermédiaire pour la fonctionnalisation)

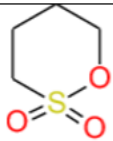
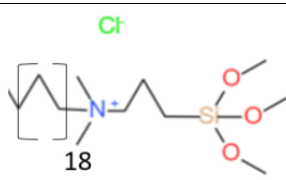
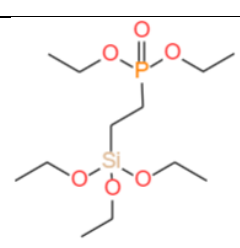
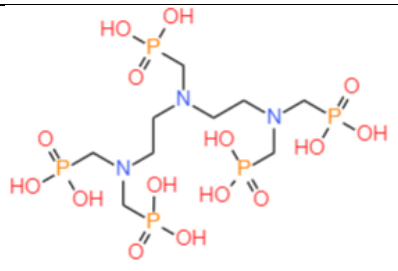
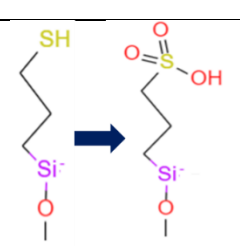
Substrats polymériques	
Fonctionnalisation	 1,4 butane sultone Fonction pour lier le RN: Acide sulfonique
Revêtement	Revêtement à base de manganèse KMnO_4

Tableau ii : Fonctions chimiques retenues pour le substrat aluminium et types de revêtement testés

		Substrat Aluminium	
Fonctionnalisation	 <p>18</p> <p>DMOAC</p>	<p>3-(Trimethoxysilyl)propyl-<i>N,N,N</i>-trimethylammonium-¹⁵N chloride (DMOAC)</p> <p>Fonction d'accroche : Silanes</p> <p>Fonction pour lier le RN: ammonium quaternaire</p>	
	 <p>DPTES</p>	<p>(2-Diethylphosphatoethyl) Triethoxysilane (DPTES)</p> <p>Fonction d'accroche: Silanes ou acide phosphonique</p> <p>Fonction pour lier le RN : acide phosphonique</p>	
	 <p>DTPMP</p>	<p>Diethylene triaminepentakis(methylphosphonic acid) (DTPMP)</p> <p>Fonction d'accroche : acide phosphonique</p> <p>Fonction pour lier le RN: acide phosphonique</p>	
	 <p>MPTMS</p>	<p>(3-Mercaptopropyl)trimethoxysilane (MPTMS)</p> <p>Fonction d'accroche : Silanes</p> <p>Fonction pour lier le RN: Acide sulfonique</p>	
Revêtement	<p>Revêtement à base de manganèse</p>		<p>KMnO₄</p>
	<p>Revêtement à base de chrome</p>		<p>K₂Cr₂O₇</p>

Caractérisations chimiques et radiologiques réalisées sur les sources produites

Plusieurs méthodes de caractérisation chimique ont été utilisées afin d'estimer le niveau de succès de chaque étape de modification des surfaces. La principale technique de caractérisation utilisée est la spectroscopie infrarouge à transformée de Fourier à réflexion totale atténuée (ATR-FTIR) pour identifier les fonctions chimiques présentes à la surface des échantillons par l'identification de leurs vibrations caractéristiques. La surface des échantillons d'aluminium a été observée par microscopie optique et leur topographie par microscopie électronique à balayage (MEB).

La capacité des surfaces modifiées à fixer les RN a été évaluée à l'aide de techniques radiométriques comme la scintillation liquide et l'autoradiographie numérique. En effet, suite à la modification chimique des substrats, leur marquage avec l'activité est réalisé par trempage dans une solution radioactive (contenant soit ^{152}Eu , soit ^{241}Am). Il est donc possible de déduire l'activité fixée sur la surface par une mesure de l'activité massique de cette solution avant et après trempage. Ces mesures ont été réalisées par scintillation liquide et ont permis d'estimer la capacité des surfaces à fixer la radioactivité.

La cinétique de fixation des RN sur les surfaces a pu être suivie en effectuant des échantillonnages réguliers de la solution en contact avec la surface et en mesurant ces aliquotes par scintillation liquide, ce qui a permis d'évaluer le rendement de fixation maximal atteint par les sources (Fig. v).

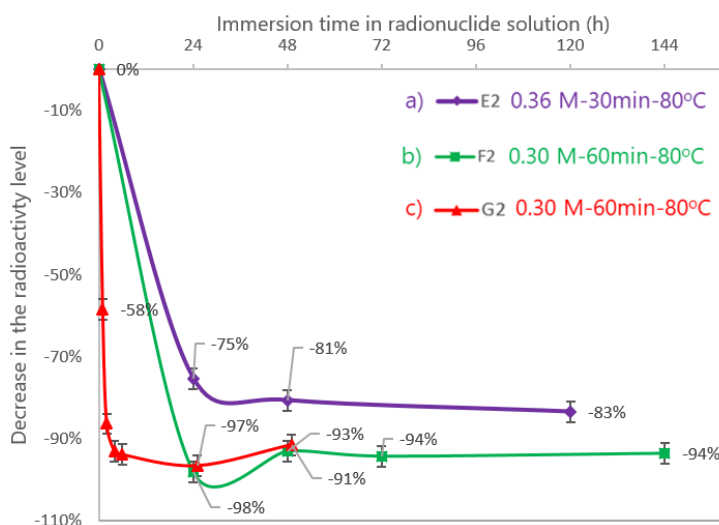


Figure v : Exemple de suivi cinétique de la fixation de l'europlu 152 sur 3 échantillons de résine époxy modifiée.

L'autoradiographie numérique a ensuite permis de visualiser la distribution de la radioactivité sur les sources les plus prometteuses et d'évaluer leur uniformité. La répétabilité des meilleures méthodes de production identifiées a été testée avec l'américium 241. Enfin, des tests par frottis secs et humides ont été effectués sur les meilleures sources, pour estimer leur non-contamination.

Résultats obtenus avec les sources surfaciques développées sur substrats polymériques

Le chapitre trois rassemble un aperçu complet des méthodes de production de sources surfaciques sur substrats polymériques, à savoir des films de PET et de la résine époxy. Les deux substrats ont subi deux types de traitements chimiques : un traitement au permanganate de potassium (KMnO_4) et une sulfonation, en testant différents protocoles. L'efficacité de chaque traitement a été évaluée par des méthodes de caractérisation chimique et radiologique (cf. paragraphe précédent). La capacité des échantillons modifiés de PET à fixer l'activité a été testée avec l'euporium 152, tandis que les échantillons de résine époxy ont été testés avec l'euporium 152 d'une part et l'américium 241 d'autre part. Avec le PET, des surfaces sulfonées ont été obtenues après un protocole en trois étapes, et les surfaces traitées au KMnO_4 ont été obtenues en une seule étape. Pour la résine époxy, le traitement au KMnO_4 a été utilisé avant la sulfonation, pour oxyder les surfaces.

Sur les échantillons de PET, la sulfonation a nécessité des étapes préliminaires d'hydrolyse et de réduction, afin d'augmenter le nombre de fonctions hydroxyle à sa surface et le rendre plus réactif pour la suite. L'analyse par infra-rouge (ATR-FTIR) a confirmé que le PET avait été modifié avec succès après la réaction d'hydrolyse. Les mesures de scintillation liquide ont démontré que chaque étape de traitement améliorait la fixation de l'euporium 152 sur les surfaces, avec des échantillons sulfonés atteignant un rendement de fixation maximal d'environ 15 % (~ 10 pmol sur 50 cm^2). Les échantillons modifiés au KMnO_4 , produits en conditions basiques, ont atteint un rendement de fixation plus élevé, atteignant 47 % (soit ~ 32 pmol d'Eu sur $\sim 50 \text{ cm}^2$). Ce rendement élevé était probablement dû à la formation d'une couche d'oxyde de manganèse (MnOx) à la surface du PET d'une part, ainsi qu'à l'oxydation de la surface d'autre part. Cependant, le mécanisme exact de la formation du revêtement n'est pas précisément connu. La comparaison entre les photographies et les images d'autoradiographie des échantillons de PET traités au KMnO_4 , a montré que la présence du revêtement sur la surface était corrélée avec la fixation des RN, soutenant l'hypothèse d'un revêtement d'oxyde de manganèse (MnOx). Cependant, les valeurs d'uniformité pour ces échantillons n'ont atteint qu'environ 20 % au mieux, contrairement à l'échantillon sulfoné, qui présentait une uniformité maximale d'environ 40 %. Le meilleur échantillon parmi toutes les sources de PET est celui produit par traitement au KMnO_4 (échantillon H5, ~ 32 pmol d'Eu sur $\sim 50 \text{ cm}^2$). Cependant, les résultats n'étaient pas suffisamment prometteurs, et l'amélioration de la fonctionnalisation du PET n'a pas été poursuivie davantage.

Les échantillons de résine époxy ont subi un traitement similaire avec le KMnO_4 puis une réaction de sulfonation avec la 1,4-butane sultone. L'analyse infra-rouge (ATR-FTIR) de ces échantillons a indiqué que la modification de la surface était réalisée dans les deux cas. De plus, la présence d'oxyde de manganèse (MnOx) a été confirmée par infra-rouge, ce qui indique qu'un revêtement s'est formé lors de l'oxydation du KMnO_4 sur ces surfaces. Lors de l'immersion des échantillons dans les solutions radioactives, les échantillons oxydés ont atteint des taux de fixation plus élevés par rapport aux échantillons sulfonés à la fois avec l'euporium 152 et l'américium 241. Le rendement de fixation maximal voisin de 100 % a été atteint avec les surfaces d'époxy oxydées en et mises en contact avec l'euporium 152 (échantillon F2, ~ 51 pmol sur $\sim 50 \text{ cm}^2$, $\sim 860 \text{ Bq}$). Les échantillons sulfonés ont également atteint des rendements de fixation importants quoique légèrement inférieurs aux échantillons oxydés testés avec l'euporium 152, avec environ 87 % de rendement de fixation pour le meilleur échantillon de cette série (échantillon F3, ~ 46 pmol sur

~ 50 cm², ~ 785 Bq). Le Tableau iii présente les résultats obtenus avec les meilleurs échantillons polymériques en contact avec l'euporium 152.

Tableau iii : Comparaison des meilleurs échantillons de PET et de résine époxy mis en contact avec de l'euporium 152

Echantillon	Conditions de préparation	Total amount of Eu in solution (picomol)	Maximum fixation yield, standard uncertainty ($k = 1$)	A_{\max} (Bq) ($k = 1$)
PET traité au KMnO ₄ H5	~0.30 M-60min-80°C	68	-(47.1 ± 2.5)%	(520 ± 30)
PET sulfoné E7	ACN-3h@70°C+16h@22°C	70	-(14.0 ± 2.7)%	(165 ± 30)
Résine époxy traitée au KMnO ₄ F2	~0.30 M-60min-80°C	52	-(98.0 ± 2.9)%	(860 ± 25)
Résine époxy sulfonée F3	ACN-3h@70°C+16h@22°C	53	-(87.4 ± 2.7)%	(786 ± 25)

La Figure vi, page suivante, présente les photographies, les images d'autoradiographie et les principales caractéristiques des deux meilleurs échantillons de résine époxy modifiée produits avec d'une part l'euporium 152 et l'américium 241 d'autre part. L'uniformité des sources d'euporium 152 a atteint environ 80 % pour les échantillons oxydés et sulfonés. Là encore, la comparaison entre les photographies des échantillons et les images d'autoradiographie a montré une corrélation entre les zones présentant un revêtement noir et les endroits où l'activité est présente. Cela suggère que pour améliorer l'uniformité des sources, la distribution du revêtement doit d'abord être améliorée.

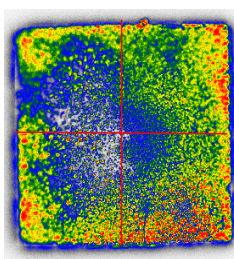
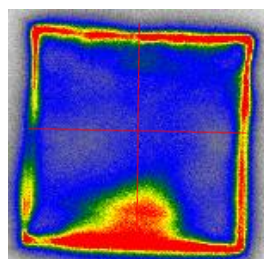
Dans le cas des échantillons d'époxy testés avec l'américium 241, des résultats répétables ont été obtenus, avec des rendements de fixation d'environ 100 % pour les échantillons oxydés (~ 46 pmol sur ~ 50 cm²), et supérieurs à 90 % (~ 35 pmol sur ~ 50 cm²) pour les échantillons sulfonés. Les échantillons oxydés présentaient des valeurs d'uniformité d'environ 90 %, tandis que les échantillons sulfonés atteignaient 85 %.

En conclusion, les paramètres optimaux pour la modification de la résine époxy avec le permanganate de potassium d'une part (0,36 M-60 min-80 °C) et la sulfonation d'autre part (utilisation de deux fois le rapport molaire de 1,4-butane sultone dans l'acétonitrile pendant 3 heures à 70 °C, suivi de 16 heures à 22 °C) ont été identifiés avec succès. Cette étude a démontré non seulement le potentiel de ces traitements pour produire des sources radioactives sur des surfaces polymériques, mais elle offre également des perspectives précieuses pour les futures

recherches dans ce domaine.

F2 (~0.30M-60 min-80°C) ^{152}Eu

K3 (Oxidized) ^{241}Am



U: $(82 \pm 10)\%$

A_{end} : (820 ± 25) Bq

A_s : (16.4 ± 0.5) Bq/cm²

U: $(90 \pm 10)\%$

A_{end} : (1100 ± 33) Bq

A_s : (22.2 ± 0.6) Bq/cm²

Figure vi : Photographies, images d'autoradiographie et caractéristiques des deux meilleurs échantillons de résine époxy modifiés produits avec l'euporium 152 et l'américium 241. U représente l'uniformité de l'échantillon, A_{end} son activité en fin d'immersion dans la solution radioactive et enfin A_s est l'activité surfacique (en supposant que l'activité est uniformément répartie).

Résultats obtenus avec les sources surfaciques développées sur substrat d'aluminium

La production de sources surfacique sur support d'aluminium a été étudiée selon la même approche expérimentale que la section précédente. Des feuilles d'aluminium de plusieurs épaisseurs ont été modifiées en utilisant deux méthodes principales : le greffage de molécules sur leur surface ou la production de revêtements à base de manganèse ou de chrome. Avant les modifications, l'aluminium a dû subir quelques étapes de préparation. Des étapes de nettoyage, de polissage et de décapage chimique ont été réalisées de diverses manières. Ensuite, le greffage de quatre molécules permettant de fixer la radioactivité a été réalisé à la surface de l'aluminium : le DMOAC (Si-N), le DPTES (Si-PO₃), le DTPMP (PO₃-PO₃) et le MPTMS (Si-SH puis Si-SO₃).

Pour la caractérisation chimique de l'aluminium, en plus de l'infra-rouge (ATR-FTIR), il a été possible d'utiliser l'analyse par microscopie électronique à balayage (MEB) pour observer la topographie de l'aluminium modifié. En plus du greffage, la formation de revêtements a été explorée en utilisant de l'oxyde de manganèse, connu pour sa capacité à fixer les RN divalents, et de l'oxyde de chrome en tant qu'alternative. La formation de ces revêtements a été testée dans différentes conditions de pH et de concentrations. Les revêtements de chrome ont permis de

tester une méthodologie en milieu acide, tandis que ceux à base d'oxyde de manganèse ont été réalisés en condition soit acide, soit basique. Encore une fois, la capacité de ces sources à fixer soit l'euporium 152, soit l'américium 241 a été testée et suivie par scintillation liquide et par autoradiographie numérique.

Parmi toutes les méthodes de fonctionnalisation explorées, le greffage Si-SO₃ (MPTMS modifié) s'est distingué par sa stabilité en immersion dans la solution de marquage acide jusqu'à 72 heures. Cependant, la plupart des RN se sont détachés de la surface après 48 heures. Le greffage Si-SO₃ a été choisi parmi les méthodes de greffage et des améliorations ultérieures ont conduit à des rendements de fixation de 15 % pour l'euporium 152 et de 68 % pour l'américium 241. La comparaison des feuilles d'aluminium sulfonées avec ces deux RN a montré que l'américium 241 pouvait se fixer à la surface de l'aluminium modifié de manière plus importante (~ 20 pmol) que l'euporium 152 (~ 10 pmol). Malgré cela, les RN fixés ont fini par se détacher de la surface, indiquant que le groupement acide sulfonique greffé sur l'aluminium ne tenait pas des immersions prolongées dans des solutions acides (pH 2, HCl).

En ce qui concerne les essais de revêtement, deux méthodes ont été appliquées : le revêtement à base d'oxyde de manganèse et d'oxyde de chrome, dans diverses conditions de pH et de concentration. Le revêtement de chrome a été testé dans des conditions acides, avec deux durées de revêtement différentes. La durée la plus longue a donné un meilleur rendement de fixation des RN par rapport à l'autre. Le revêtement de manganèse dans des conditions basiques s'est avéré plus efficace, avec des rendements de fixation plus élevés et une meilleure stabilité dans le temps. Des ajustements de température pendant la production du revêtement se sont révélés affecter la rugosité de la surface résultante, suggérant que des températures plus élevées pourraient améliorer les propriétés du revêtement. L'analyse par autoradiographie a révélé des motifs différents sur les surfaces, probablement liés aux surfaces revêtues. Ces motifs variaient en uniformité selon la face de l'échantillon, la plupart du temps une face était mieux revêtue que l'autre, ce qui a impacté la fixation des RN. Les photographies des échantillons ont également indiqué qu'avant immersion dans la solution radioactive acide et après, le revêtement avait en partie disparu. Il semble que le revêtement situé près des bords se soit dégradé en premier, ce qui peut être dû à l'agitation continue pendant la fixation du radionucléide, qui met la feuille d'aluminium en contact régulier avec les parois du bécher.

En conclusion, parmi tous les échantillons, les échantillons revêtus d'oxyde de manganèse produit dans des conditions basiques ont donné les meilleurs résultats, avec des niveaux de radioactivité variant de 15 à 20 Bq/cm². Les futures études devraient se concentrer sur le perfectionnement des méthodes de greffage et des conditions de production de revêtement à base de manganèse pour améliorer la stabilité et l'efficacité de la fixation des radionucléides.

Conclusion

Dans cette étude, une nouvelle approche a été proposée pour produire des sources surfaciques traçables par le biais de la formation de liaisons chimiques entre le substrat et les radionucléides choisis. Trois substrats différents ont été utilisés dans les méthodes de production : le PET, la résine époxy et l'aluminium, qui ont été choisis pour leur capacité à imiter les surfaces courbes et/ou rugueuses, et qui permettraient in fine de se rapprocher des surfaces réelles des chantiers en A&D.

Le PET et la résine époxy ont subi des modifications chimiques similaires, à savoir le traitement au permanganate de potassium (KMnO_4) et la sulfonation. L'échantillon traité au KMnO_4 (H5) a été identifié comme le plus réussi parmi toutes les sources à base de PET. Il a fixé environ 47 % de l'euporium disponible en solution (~ 32 pmol d'Eu, y compris stable), ce qui a conduit à une source d'environ 520 Bq de part et d'autre de l'échantillon de 25 cm². Néanmoins, à la fin de l'immersion, l'activité était plus faible (environ 370 Bq) avec une faible uniformité proche de 20 %.

Les échantillons de résine époxy ont subi un traitement au KMnO_4 puis une sulfonation avec la 1,4-butane sultone. Les échantillons oxydés ont donné des rendements de fixation de l'activité plus élevés pour l'euporium 152 et l'américium 241 que les échantillons sulfonés. Le meilleur échantillon de résine époxy oxydé (F2) a permis de fixer quasiment 100 % de l'euporium en solution avec une activité finale de 860 Bq sur les 2 faces de l'échantillon de 25 cm² (~ 51 pmol d'Eu y compris stable). En revanche, le meilleur échantillon sulfoné (F3) a montré un rendement de fixation d'environ 85 % avec une activité maximale de 786 Bq (~ 46 pmol d'Eu y compris stable). L'uniformité des sources d'euporium 152 a dépassé les 80 %. Pour les échantillons mis en contact avec l'américium 241, des résultats très répétables ont été obtenus avec des rendements de fixation plus élevés, voisins de 100 % pour les échantillons oxydés (entre 36 et 57 pmol de ²⁴¹Am), et d'environ 92 % pour le meilleur échantillon sulfoné (L3, soit ~ 35 pmol de ²⁴¹Am). Les échantillons oxydés présentaient des valeurs d'uniformité d'environ 90 %, tandis que les échantillons sulfonés atteignaient 85 %. Ce rendement de fixation plus élevé des échantillons oxydés pourrait être lié au fait que le revêtement d'oxyde de manganèse a une affinité plus élevée pour les RN que les fonctions acide sulfonique des échantillons sulfonés.

En résumé, les paramètres optimaux pour le traitement au KMnO_4 (0,36 M, 60 minutes, 80 °C) et la sulfonation ont été déterminés avec succès (en utilisant deux fois le rapport molaire de la 1,4-butane sultone dans l'acétonitrile pendant 3 heures à 70 °C, suivi de 16 heures à 22 °C).

De manière générale, les résines époxy modifiées ont pu fixer plus de radioactivité que leurs homologues à base de PET. La résine époxy ayant une structure de réseau réticulé en trois dimensions, des pores peuvent s'y former plus facilement que sur les feuilles de PET de 18 µm d'épaisseur. De plus, la rugosité plus importante de la surface des résines époxy augmente considérablement le nombre de groupements pouvant lier les RN, ce qui permet de fixer plus d'activité. Toutefois, cette rugosité peut également affecter l'émission des particules alpha par la source produite. L'étude de cet aspect pourrait constituer une perspective intéressante pour les études à venir.

Deux méthodes principales de modification de la surface ont été employées sur les échantillons d'aluminium : le greffage et la production d'un revêtement. Les études de greffage ont fait appel

à quatre produits chimiques qui pouvaient se lier à la surface d'un côté et fixer les RN de l'autre. Des fonctions alcoxy-silanes et acide phosphonique ont été utilisées pour le greffage sur l'aluminium, tandis que des ammoniums quaternaires, des acides phosphoniques et des acides sulfoniques ont été utilisés pour la fixation des RN. Les méthodes de production de revêtement ont été réalisées en variant les conditions de pH (de 1 à 13), afin d'obtenir une couche d'oxyde de manganèse qui permette de fixer la radioactivité. Des essais de revêtements à base de chrome ont également été réalisés.

Parmi toutes les méthodes de fonctionnalisation testées sur l'aluminium, c'est le greffage Si-SO₃ qui s'est distingué. C'est pourquoi une optimisation de cette méthode a été réalisée. Les meilleures conditions se sont avérées être 20 heures de réaction de fonctionnalisation. Le rendement de fixation pour l'euprotium 152 a atteint environ 15 % (~ 10 pmol, y compris stable), tandis que pour l'américium 241, il atteignait 68 % au maximum (~ 20 pmol). En outre, avec l'américium 241, les essais de répétabilité ont été plutôt réussis, à condition de ne laisser les échantillons que 4 heures immergés dans la solution radioactive, puisque sinon l'activité tend à repasser en solution. Ceci indique que le groupement acide sulfonique greffé pourrait manquer de stabilité pour maintenir les molécules greffées sur la surface pendant plus de 48 heures, en solution acide (pH 2, HCl). Les recherches futures devraient se concentrer sur l'optimisation du processus de greffage afin d'améliorer son uniformité pour optimiser celle de la radioactivité lors de l'étape suivante.

Le revêtement d'oxyde de chrome sur la surface a été obtenu dans des conditions acides et a été étudié comme une alternative aux revêtements d'oxyde de manganèse. L'étude a montré que la durée du processus de revêtement affectait de manière significative ses performances. Des durées de revêtement plus longues, jusqu'à 8 heures, ont permis d'obtenir une meilleure stabilité. Dans le cas du revêtement d'oxyde de manganèse en conditions basiques, il a été observé que le revêtement avait tendance à s'enlever en conditions acides. C'est pourquoi les conditions expérimentales ont été améliorées en modifiant des paramètres tels que la durée et la température de la réaction. Des tests de répétabilité ont été réalisés dans trois conditions différentes en produisant trois échantillons pour chaque méthode : 15 minutes à 50 °C (série Y), 15 minutes à 80 °C (série T), et enfin 40 minutes à 80 °C (série R). Parmi ces conditions, les meilleures se sont avérées être 40 minutes à 80 °C avec l'échantillon R2 avec 77 % de rendement de fixation du RN (soit ~ 23 pmol de ²⁴¹Am). Il a été observé que le maintien d'une température plus basse lors de la production du revêtement pouvait conduire à la détérioration de ce dernier après 4 heures (série Y). En revanche, des températures plus élevées semblent améliorer les propriétés du revêtement et augmenter la fixation de l'américium 241, en la triplant presque (~ 23 pmol de ²⁴¹Am pour R2 par rapport à ~ 8 pmol pour T1).

Pour la plupart des échantillons, l'analyse par autoradiographie a montré une corrélation claire entre la surface revêtue (visible sous la forme d'un revêtement brunâtre) et les zones de détection de l'activité. Le revêtement tend à se détériorer notamment sur les bords en fonction de la durée d'immersion dans la solution radioactive. Les valeurs d'uniformité pour la série Y étaient d'environ 80 %. De la série Y à la série T, l'uniformité a chuté à environ 60 %, avec l'apparition d'un motif central notable, reflétant peut-être la forme du fond du cristalliseur utilisé pendant la synthèse du revêtement. L'échantillon T1, comparé à R2, a montré qu'une durée d'immersion plus longue dans la solution d'enrobage améliorait l'uniformité de la source jusqu'à 85 %. Cependant, alors qu'un

côté de la source présentait un meilleur revêtement, l'autre ne fixait pas d'activité.

Parmi ces échantillons, les meilleurs résultats ont été obtenus avec les échantillons J3 (0.27 M-15 min-50 °C, ~ 41 pmol de ^{241}Am) et R2 (0.28 M-40 min-80 °C) recouverts d'oxyde de manganèse en conditions basiques. Les sources surfaciques obtenues avaient des activités surfaciques de 15 à 20 Bq.cm⁻². Ces niveaux d'activité peuvent être facilement ajustés pour obtenir des activités plus faibles pour les besoins de l'A&D. Avec des activités plus faibles, le rendement de fixation de certaines surfaces peut être amélioré, mais il sera toujours nécessaire de parvenir à une distribution uniforme des modifications de surface réalisées afin d'obtenir une source radioactive uniforme in fine.

Perspectives

Dans cette étude, les efforts ont porté sur la production de sources surfaciques traçables sur deux types de substrats : des polymères et de l'aluminium. Certaines améliorations peuvent être envisagées pour les études futures.

Un aspect critique, tel qu'énoncé dans la norme ISO 8769, est que les sources de référence ne doivent présenter qu'une seule face radioactive. Pour cela, la conception et l'utilisation de cellules de réaction spécifiques peuvent être envisagées, de manière similaire à celle décrite dans une étude réalisée au LNHB par Tsouanko-Sitnikov. Une telle stratégie est non seulement conforme aux normes établies par la norme ISO 8769, mais elle simplifie aussi potentiellement la manipulation et l'utilisation de ces sources. Pour améliorer l'étape de fixation des RN et prévenir la dégradation du revêtement ou de la couche fonctionnalisée, l'utilisation d'un distributeur de microgouttes pourrait être envisagée. Cet appareil est constitué d'un bras robotisé, capable de déposer des gouttes de solution (radioactive dans notre cas) de quelques microlitres, régulièrement réparties sur la surface (tous les millimètres par exemple). De telles gouttelettes ont tendance à sécher en quelques secondes, limitant l'effet de la solution acide sur la surface. En outre, en contrôlant la zone où les modifications peuvent être appliquées sur une surface, il serait possible de produire des sources volontairement non uniformes si la présence d'un point chaud s'avérait nécessaire par exemple.

Concernant la fixation des RN, la production de sources d'émetteurs alpha purs, par exemple le curium 244, pourrait être réalisée. Cela permettrait de mieux comprendre les mécanismes de liaison et tester l'efficacité des différents traitements avec cet émetteur alpha pur. Il faut également rappeler que les méthodologies développées dans cette étude peuvent être appliquées à tout élément présentant un état trivalent stable, ce qui couvre *a minima* tous les lanthanides et la plupart des actinides.

Dans le cas des échantillons d'époxy, les images autoradiographie ont révélé une corrélation entre les zones brunâtres et les emplacements de fixation de l'activité, ce qui suggère que des améliorations du processus d'oxydation pourraient accroître les rendements de fixation des RN. Par conséquent, pour les sources à base de résine époxy, l'allongement de la durée de la réaction pourrait améliorer la couverture de la surface, ce qui pourrait conduire à une porosité accrue et à un plus grand nombre de groupements fonctionnels disponibles pour la fixation de l'activité. Cette porosité devra être maîtrisée si des émetteurs alpha pur doivent être fixés sur ces sources.

Une question encore ouverte est de savoir si le succès de la sulfonation est uniquement dû au processus d'oxydation ou s'il y a une contribution significative des fonctions acide sulfonique greffées. Une analyse préliminaire par spectroscopie photoélectronique à rayons X (XPS) pourrait permettre d'identifier les éléments liés aux surfaces et leurs interactions. Cette analyse pourrait clarifier les différences entre l'oxydation et la sulfonation en termes de liaison chimique, ce qui permettrait de comprendre les mécanismes sous-jacents du traitement au KMnO_4 et de l'étape suivante, la sulfonation.

Un autre avantage de l'utilisation de la résine époxy comme substrat est sa capacité à incorporer des charges solides. Dans une autre étude au LNHB, des tests ont été réalisés pour incorporer une forte proportion de sable dans cette résine, tout en maintenant la cohésion des grains grâce à la résine. Des proportions de l'ordre de 70 % de sable relativement fin ont pu être incorporées avec succès, rendant la surface naturellement rugueuse et plus représentative du béton, par exemple. Réussir à fonctionnaliser la surface de tels substrats pour fixer la radioactivité serait une étape intéressante vers la production de sources à façon pour le démantèlement (Fig. vii).



Figure vii : Exemples de surfaces obtenues à base de résine époxy permettant de reconstituer a) une surface courbe et lisse, b) un pseudo-béton rugueux, c) une surface rugueuse obtenue par moulage

Table of contents

INTRODUCTION	10
CHAPTER 1: METROLOGY AND DECOMMISSIONING.....	13
1 DECOMMISSIONING AND DISMANTLING.....	13
1.1 Costs of D&D and the French approach.....	13
1.2 The importance of the radiological characterization.....	15
2 TRACEABILITY IN WASTE MEASUREMENT	17
2.1 Detectors used for surface monitoring	18
2.2 Calibration of surface contamination monitors	21
2.3 Reference sources from applicable standards.....	22
3 STATE OF THE ART ON THE PRODUCTION OF SURFACE SOURCES.....	25
3.1 Limitations of calibration in terms of D&D applications.....	25
3.2 Anodized aluminum surfaces sources	26
3.3 Drop deposition and inkjet	27
3.4 Electroplated sources	28
3.5 Ion exchange sources.....	30
3.5.1 Sources from commercial ion exchange membranes	30
3.5.2 Conducting polymer with ion exchange functional groups.....	32
3.5.3 MnO ₂ coated disc.....	33
3.6 Polymeric sources	33
3.6.1 Carbon-14 polymer sources	33
3.6.2 Painted sources.....	34
3.6.3 Epoxy resin.....	34
3.7 Summary of source production methods.....	35

CHAPTER 2: NEW APPROACH TO PROVIDE TRACEABLE SURFACE SOURCES	38
1 SELECTION OF RADIONUCLIDES OF INTEREST.....	41
1.1 Radionuclides encountered in D&D sites.....	41
1.2 Radiochemistry of actinides.....	41
2 APPROACH OF THE STUDY: SURFACE MODIFICATION.....	44
3 THE CHEMICAL FUNCTIONS FOR RADIONUCLIDE BINDING.....	45
3.1 The mechanisms of extraction resins	45
3.2 Common extraction resins for actinides	47
4 ATTACHMENT OF CHEMICALS ON THE SURFACE	50
4.1 Polymeric surfaces	50
4.1.1 The structure of PET	50
4.1.2 The structure of epoxy resin	51
4.1.3 Chemical methods for forming hydroxyl bonds (-OH)	52
4.1.3.1 Formation of hydroxyl bonds on PET substrates	52
4.1.3.2 Formation of hydroxyl bonds on epoxy resin substrates.....	53
4.1.4 Sulfonation of polymeric substrates.....	55
4.2 Aluminum surfaces.....	57
4.2.1 Forming Al-OH bonds by etching	58
4.2.2 The investigation of potential grafting molecules.....	59
4.2.2.1 Grafting molecules containing silanol groups.....	59
4.2.2.2 Grafting molecule containing phosphonic acid groups.....	62
4.2.3 Conversion coating techniques	64
4.2.3.1 Manganese oxide (MnOx) coating.....	65
4.2.3.2 Acidic conversion coating with potassium permanganate	68
4.2.3.3 Basic conversion coating with potassium permanganate	68
4.2.3.4 Chromium oxide (CrOx) coating	69
5 CONCLUSION OF CHAPTER 2	70

CHAPTER 3: PRODUCTION AND CHARACTERIZATION OF POLYMERIC SURFACE SOURCES	72
1 MATERIALS AND METHODS	73
1.1 Materials	73
1.2 Methods	74
1.2.1 Modification of the PET surfaces	74
1.2.1.1 The steps of the PET sulfonation	74
1.2.1.1.1 Hydrolysis of PET	74
1.2.1.1.2 Reduction of hydrolyzed PET	75
1.2.1.1.3 Sulfonation of reduced PET	75
1.2.1.2 KMnO ₄ treatment of PET	75
1.2.2 Functionalization of Epoxy Resin	76
1.2.2.1 Casting and cleaning of the epoxy resin	76
1.2.2.2 KMnO ₄ treatment of epoxy resin	77
1.2.2.3 Sulfonation of the epoxy resin	79
1.2.3 Surface characterization	80
1.2.4 Radionuclide binding experiments for polymeric surface sources	80
1.2.5 Radiometric characterizations	81
2 RESULTS AND DISCUSSION	83
2.1 Chemical Characterization	84
2.1.1 Chemical changes in the PET structure	84
2.1.2 Infrared spectroscopy of PET	85
2.1.3 Chemical changes in the epoxy resin structure	88
2.1.4 Infrared spectroscopy of the epoxy resin	89
2.2 Radiometric characterization	93
2.2.1 Liquid Scintillation Counting analysis	93
2.2.1.1 LSC analysis of the PET samples	94
2.2.1.2 LSC analysis of the epoxy resin samples	96
2.2.1.2.1 Epoxy resin samples spiked with ¹⁵² Eu	96
2.2.1.2.2 Epoxy resin samples immersed in a ²⁴¹ Am solution	102
2.2.1.2.3 Comparison between ¹⁵² Eu and ²⁴¹ Am binding	106
2.2.1.2.4 Comparison between polymeric substrates	107
2.2.2 Phosphor imaging Autoradiography analysis	108
2.2.2.1 Autoradiography analysis of PET samples	110
2.2.2.2 Autoradiography analysis of epoxy resin samples	111
2.2.2.2.1 Epoxy resin samples in contact with ¹⁵² Eu	111
2.2.2.2.2 Epoxy resin samples in contact with ²⁴¹ Am	113
2.2.2.2.3 Uniformity as a function of the emission type on oxidized and sulfonated epoxy samples with ²⁴¹ Am	116

2.2.3	Non-contamination test for oxidized and sulfonated epoxy samples with ²⁴¹ Am	117
3	CONCLUSION OF CHAPTER 3	120
CHAPTER 4: PRODUCTION AND CHARACTERIZATION OF ALUMINUM SURFACE SOURCES		
122		
1	MATERIALS AND METHODS	123
1.1	Materials	123
1.2	Methods	124
1.2.1	Al surface modification methods	125
1.2.1.1	Pre-treatments	126
1.2.1.1.1	Polishing	126
1.2.1.1.2	Cleaning	126
1.2.1.1.3	Chemical etching	126
1.2.1.2	Grafting methods	127
1.2.1.3	Coating Methods	129
1.2.2	Surface Characterization	132
1.2.3	Radionuclide binding experiments for aluminum foil surface sources	132
1.2.4	Radiometric characterization	133
2	RESULTS AND DISCUSSION	133
2.1	Surface characterization	134
2.1.1	Observable differences between the two faces of aluminum foils	134
2.1.2	The effect of polishing and etching	136
2.1.3	Effect of the selected etching methods	138
2.1.4	Impact of different grafting methods	139
2.1.4.1	Improvement of the DMOAC (Si-N) grafting method	147
2.1.4.2	Improvement of the DPTES (Si-PO ₃) grafting method	150
2.1.4.3	Improvement of the DTPMP (PO ₃ -PO ₃) grafting method	152
2.1.5	Coating methods	155
2.1.5.1	KMnO ₄ treatment	155
2.1.5.2	K ₂ Cr ₂ O ₇ treatment	157
2.2	Radiometric analysis	159
2.2.1	Liquid scintillation analysis	159
2.2.1.1	Analysis of the grafted samples (Si-N, Si-PO ₃ , PO ₃ -PO ₃)	159
2.2.1.2	Sulfonated samples production (Si-SO ₃) and optimization studies	160
2.2.1.3	KMnO ₄ and K ₂ Cr ₂ O ₇ coated samples and their optimization studies	164
2.2.1.3.1	K ₂ Cr ₂ O ₇ treated (CrOx coated) samples	164
2.2.1.3.2	KMnO ₄ treated samples	167

Table of contents

2.2.2	Phosphor imaging Autoradiography analysis.....	175
2.2.2.1	Samples produced with grafting methods	176
2.2.2.1.1	Sulfonated (Si-SO ₃) samples	176
2.2.2.2	Coated samples	179
2.2.2.2.1	Autoradiography images of KMnO ₄ treated samples.....	179
3	CONCLUSION OF CHAPTER 4	184
	GENERAL CONCLUSION	186
	APPENDICES	190
1	CHEMICAL CHARACTERIZATION METHODS	190
1.1	Fourier Transform Infrared Spectroscopy.....	190
1.2	Scanning Electron Microscopy analyses	192
2	RADIOLOGICAL CHARACTERIZATION METHODS.....	193
2.1	Liquid Scintillation Counting (LSC).....	193
2.1.1	Principles of LSC	193
2.1.2	Normalization of LSC measurements.....	195
2.2	Phosphor autoradiography imaging.....	197
3	EXTRA ATR-FTIR SPECTRA, SEM OR OPTICAL MICROSCOPE IMAGES AND KINETICS OF RN FIXATION	201
	LISTS OF FIGURES AND TABLES.....	207
	REFERENCES	214

List of Abbreviations

Abbreviation	Definition
ACN	Acetonitrile
APTES	(3-Aminopropyl) triethoxysilane
ASN	French Nuclear Safety Authority
CC	Conversion coating
CMPO	Carbamoyl-methyl phosphine oxide
CTAB	Cetyltrimethylammonium bromide
D&D	Decommissioning and dismantling
DGA	Diglycolamide
DI water	De-ionized water
DMOAC	Dimethyloctadecyl[3-(trimethoxysilyl)propyl]ammonium chloride
DMSO	Dimethyl sulfoxide
DPTES	(2-Diethylphosphatoethyl) triethoxysilane
DSND	French Nuclear Defence Safety Delegate
DTM	Difficult to measure
DTPMP	Diethylenetriaminepentakis (methylphosphonic acid)
ETM	Easy to measure
EtOH	Ethanol
INB	Basic Nuclear Installations
MPTMS	3-mercaptopropyl trimethoxysilane
NDA	Non-destructive analysis
OTMS	Octadecyl trimethoxysilane
PBT	Poly(butylene terephthalate)
PDMS	Poly(dimethyl siloxane)
PEEK	Polyether ether ketone
PEM	Proton exchange membranes
PET	Polyethylene terephthalate
PFO	Perfluoroalkyl triethoxysilane
PMMA	Poly(methyl methacrylate)
PTFE	Polytetrafluoroethylene
RN	Radionuclide
THF	Tetrahydrofuran

INTRODUCTION

Characterization of the radioactivity of the nuclear facilities is one of the first mandatory steps of any decommissioning and dismantling (D&D) process. This step consists in detecting, locating, and estimating the nature and activity of any contamination to adapt the dismantling process accordingly. A large majority of this characterization is performed using destructive methods, which require sampling and dedicated analysis in the laboratory. Direct radiometric measurements are also performed on-site, using surface contamination meters, which need to be calibrated properly with radioactive surface sources. Discriminating low-level radioactive contamination from non-radioactive surfaces is particularly challenging, as the signal is close to the background, necessitating the improvement of measurement systems. In particular, the calibration of these measurement systems with traceable sources is crucial to ensure the accuracy of the measurements. Current calibration sources for contamination detectors are tailored for calibrating radioactivity measurement devices in laboratory conditions but fall short in addressing the unique requirements of D&D sites (ISO 8769, 2020). However, the sites under D&D present varied challenges in terms of proper radioactivity measurements, such as measuring diverse surface types and textures, from flat areas to complex structures like pipes and rough surfaces as well as a wide variety of radionuclides (RNs). Due to the differences between the real sites and the reference sources, biases are introduced during the calibration of the surface contamination meters and need to be taken into account, which impacts both trueness and precision.

Among the radionuclides responsible for contamination in D&D sites, alpha and low energy beta emitters are “difficult to measure” (DTM), due to the high stopping power of their emitted radiations in solid matter. The typical energy of an alpha particle encountered in dismantling application ranges from 4 MeV to 7 MeV, while the typical range of beta particles is from a few keV to 2 MeV. The corresponding thickness of plastic required to stop the radiation is several tens of micrometers for alpha particles, to centimeters for beta particles. Commercial surface sources used for the calibration of contamination detectors are often covered with a micrometer-thick protective layer, which is enough to attenuate the alpha radiation coming from the source. This might also impact the calibration of the devices.

This study aims to produce traceable surface sources that are not only closer to the real conditions of decommissioning sites but also that should be capable of replicating complex, non-uniform surfaces, typical of nuclear sites, providing a more accurate calibration for contamination detectors or any non-destructive surface analysis technique.

In the first chapter, the importance of the traceability of radiological characterization in D&D is underlined and the specifications from international standards are presented. Then, the source production methods found in the literature are described, and their advantages and drawbacks are listed, with the aim to assess their ability to cover the needs of D&D, highlighting the gaps in existing approaches. Among these sources, even the ones that are not commercially available have been considered, and thus about ten techniques of source preparation have been reviewed.

The second chapter is devoted to the description of the approach devised for this thesis, using surface chemistry to modify the surface of a substrate to introduce functions capable to bind to radionuclides (RNs). First, Americium-241 (^{241}Am) and Europium-152 (^{152}Eu) are chosen as target radionuclides, the former because it is the most studied actinide, and an alpha emitter representative of DTM radionuclides, the latter as a chemical analog of Am. Then, aluminum foil and polymeric surfaces are chosen as substrates. Aluminum foils are chosen for comparison with ISO 8769:2020, with the added advantage of being flexible and able to mimic pipes. Polymeric surfaces, polyethylene terephthalate (PET) and epoxy resin, are chosen for their flexibility or their ability to be molded into curved and/or rough surfaces. Next, chemical functions able to bind to trivalent actinides or lanthanides are identified by reviewing the chemistry of ion exchange membranes. Eventually, a literature review is conducted to select commercial molecules that could both attach to the selected substrates, and bind to the selected RNs. For polymeric substrates, a method to produce sulfonic acid functions is selected after identifying ways to increase the reactivity of these surfaces by forming hydroxyl bonds. For grafting onto aluminum, four molecules are selected, bearing alkoxy silane or phosphonic acid moieties to attach to the aluminum surface, and quaternary ammonium, phosphonic acid and sulfonic acid groups to bind to the RNs. For aluminum, conversion coatings composed of manganese oxide and chromium oxide are also identified as potential suitable surface modification methods, the coated layer having a strong affinity for RNs.

Chapter three is the first experimental chapter and it starts with the detailed description of the attempts to produce polymeric surfaces sources, first from PET films and then from a bicomponent epoxy resin. In order to obtain PET surface sources, the two methods tested, sulfonation and a potassium permanganate (KMnO_4) treatment, are described. The sulfonation method involved three steps, while the second method was a one-step KMnO_4 treatment. The production of epoxy resin surface sources, using a sulfonation functionalization method, with a preliminary oxidation step, is then presented. The chapter also covers the chemical characterizations performed after each modification or improvement step in order to assess its level of success. The main characterization technique used was attenuated total reflection Fourier transform infrared spectroscopy (ATR-FTIR) to identify the chemical functions present on the surfaces of the samples. Following the modification of both substrates, their capability to fix radioactivity was tested by immersing them in acidic solutions containing the desired RN (either ^{152}Eu or ^{241}Am). The ability of the modified surfaces to attach the RNs was assessed with radiometric techniques such as liquid scintillation counting (LSC) and phosphor imaging digital autoradiography. The kinetics of RN attachment to the surfaces was followed by performing regular samplings and LSC measurements. This allowed to assess the maximum binding yield reached by the sources while digital autoradiography enabled to visualize the distribution of the radioactivity onto the sources as well as evaluating their uniformity. In the end, the best production methods identified were tested for intermediate precision and some dry and wet smear tests were performed on the best sources, according to ISO 7503 to check their non-contamination.

The production of aluminum surfaces sources is the subject of the fourth chapter, whose structure is similar to that of the previous chapter. Aluminum foils of several thicknesses were modified using two main methods: grafting chemicals onto their surface or applying conversion coating techniques. Before modifications, aluminum needs to go through several preparation steps. The cleaning, polishing and chemical etching stage developments are presented. Then, the grafting of

Introduction

four chemicals were investigated for their ability to attach RNs to the aluminum surface and to fix RNs: DMOAC (Si-N), DPTES (Si-PO₃), DTPMP (PO₃-PO₃) and MPTMS (Si-SH). For aluminum chemical characterization, in addition to ATR-FTIR, it was possible to use scanning electron microscopy (SEM) analysis in order to observe the topography of the modified aluminum. The ability of phosphonic and sulfonic acids to bind RNs (again either ¹⁵²Eu or ²⁴¹Am) was studied with the radiometric techniques (LSC and phosphor imaging digital autoradiography). The kinetics of RN attachment to the surfaces was followed to evaluate the maximum binding yield reached by the surfaces while assessing the uniformity of the distribution of the radioactivity onto the sources. In the end, the best production methods identified were tested for intermediate precision with ²⁴¹Am. In addition to grafting, conversion coating was explored using manganese oxide, known for its ability to bind divalent RNs, and chromium oxide as an alternative. These coatings were applied under different pH and concentration of the used coating reagent. The chromium coatings allowed to test an acidic conversion coating methodology, while two manganese oxide coating were performed in basic conditions. Again, the ability of these sources to fix either ¹⁵²Eu or ²⁴¹Am was tested and followed using LSC and phosphor imaging digital autoradiography.

The conclusion of the manuscript sums up all the outcomes from the numerous and various experiments performed during these three years. Finally, prospects for further studies and improvements are identified in order to achieve the objective of providing more representative sources suitable for decommissioning and dismantling.

Details about characterization techniques such as FTIR spectroscopy, SEM, phosphor imaging autoradiography and LSC are given in appendices, while the tables of illustrations (Figures and Tables) and the Reference sections close the manuscript.

CHAPTER 1: METROLOGY AND DECOMMISSIONING

1 DECOMMISSIONING AND DISMANTLING

The primary objective of decommissioning and dismantling (D&D) nuclear facilities is to safely remove regulatory controls from a site while ensuring the protection of the public, the environment, and decommissioning workers (OECD/NEA, 2003). This process not only safeguards health and environmental standards but also aims to repurpose valuable assets, such as sites and buildings, for unrestricted use while promoting the recycling of materials and the restoration of natural settings.

The D&D process in nuclear facilities, while not universally standardized due to varying legislative frameworks in different countries, encompasses several key components (OECD/NEA, 2003). This process includes techniques for decontaminating various surfaces such as metal and concrete, cutting methods for dismantling installations, and remote control techniques. Additionally, there are environmental protection measures, and methods for treating, preconditioning, and conditioning wastes. Foremost, radioactivity measurement techniques play a crucial role in this process, aiding in the establishment of the radioactive inventory of the nuclear site. This inventory is crucial in making decisions about the appropriate decontamination and dismantling processes, in categorizing materials and wastes for conditioning, storage, and disposal. It is also important in ensuring that materials, buildings, and sites meet the criteria for release from radiological controls when possible, as well as in implementing protective measures for workers (OECD/NEA, 2003).

The management of radioactive waste from D&D activities is a critical aspect of the planning, timing and economics of the process in nuclear facilities. The range of waste types generated during D&D reflects those from the operational phase of these facilities, encompassing high-level waste, intermediate-level long-lived waste, low-level short-lived waste, and low-level waste. The kinds of waste include contaminated materials, plant equipment, structural components, and soil from remediation efforts.

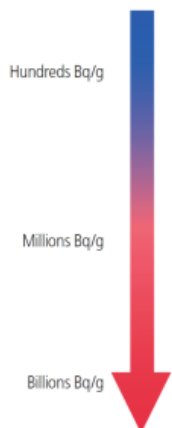
Effective management and disposal of these wastes are integral to D&D operations. The protocols for handling the contaminated materials during D&D are generally analogous to those implemented during regular operational management, highlighting the continuity in waste management practices.

1.1 COSTS OF D&D AND THE FRENCH APPROACH

Economic considerations in D&D are multifaceted, influenced by factors such as assumptions in cost estimation and the specific requirements of D&D elements. These factors include the definitions of facility shutdown, post-operational cleanup, D&D end-state determination, and protocols for managing residual spent fuel and radioactive waste. A noteworthy point is that while only a small percentage (approximately 2%) of radioactive materials is officially categorized under

waste management, these activities account for a substantial portion (around 60%) of the overall D&D costs. This significant cost allocation underscores the importance of accurate radiological characterization to optimize expenses related to the treatment, storage, and disposal of waste.

To discuss radioactive waste management and its economic implications in D&D operations, it is essential to understand the basis of waste classification. Waste classification is based on two fundamental parameters: the activity level of the radioactive elements and their radioactive half-life. This system distinguishes between short-lived waste, characterized by a half-life of less than 31 years, and long-lived waste otherwise. Such a classification is instrumental in aligning each waste category with one or more tailored management solutions, as shown in Figure 1 (ASN, 2016).



		Very short lived waste containing radionuclides with a half-life of < 100 days	Short lived waste in which the radioactivity comes mainly from radionuclides with a half-life ≤ 31 years	Long-lived waste containing a significant quantity of radionuclides with a half-life > 31 years ¹⁰
Hundreds Bq/g	Very low level (VLL)	Waste management by radioactive decay	Recycling or dedicated surface disposal	
Millions Bq/g	Low level (LL)		Surface disposal except for certain tritiated waste and certain sealed sources	Near-surface disposal Solution being examined under Article 4 of the 28 th June 2006 Act
	Intermediate level (IL)			Deep geological disposal Solution being examined under Article 3 of the 28 th June 2006 Act
Billions Bq/g	High level (HL)	Not applicable ¹¹		

Figure 1: Principles of radioactive waste classification in the French legislation (ASN, 2016)

This table is based on the reference act, passed on 28th June 2006. The statement outlines a national policy that focuses on the responsible and sustainable handling of radioactive materials and their waste.”

According to French regulations, all waste from areas within a nuclear facility that are likely to be contaminated or become radioactive must undergo specialized management to ensure traceability, regardless of the radioactivity level of the waste. The regulations require that a detailed "waste study" be conducted. This study includes creating a "zoning" plan for the facility, which must be approved by the French Nuclear Safety Authority (ASN) for Basic Nuclear Installations (INBs) and by the French Nuclear Defense Safety Delegate (DSND) for secret basic nuclear facilities (INBSs) (ASN, 2016). This zoning distinguishes between areas that may generate radioactive waste, termed "nuclear waste zones," and "non-radioactive zones." Waste from non-radioactive zones is directed to conventional management pathways after confirming its non-radioactive status.

In France, the categorization of waste from nuclear facilities as "conventional" waste is determined through successive lines of defense, in contrast to other European countries, which rely on the concept of clearance levels of the waste or release thresholds per unit mass. In France, any waste that is contaminated, activated, or could become so is considered radioactive waste and must be subjected to a dedicated management process designed for radioactive waste. Very recently, in 2022, the Public Health Code has been amended by two decrees (14 February 2022), one on the implementation of recovery operations for low-level radioactive substances, the other on radioactive substances eligible for recycling operations, which allow for derogations.

The significant generation of very low-level waste, particularly from decommissioning operations, is a contributing factor to the cost assumptions. ANDRA (the French National radioactive waste management public agency) foresees the generation of the current facilities to be approximately 2,200,000 cubic meters of very low-level (VLL) waste until their licenses are terminated (ASN, 2016).

Within this context, radiological mapping along with other characterization techniques are necessary for reliable radioactivity assessment. It enables the accurate identification, sentencing, and consignment of the appropriate waste following regulations, which is important from a radiological protection standpoint. Additionally, it has economic benefits; at low activity levels, where volumes of waste are very large, inaccurate metrology close to the sentencing limits between categories can lead to "overclassification" of important volumes of waste, significantly increasing disposal costs and resulting in misuse of space at national repositories. Under classification would result in a breach of the legal requirements.

1.2 THE IMPORTANCE OF THE RADIOLOGICAL CHARACTERIZATION

Radiological mapping is notably complex when dealing with low-level radioactive waste, mainly when radioactivity levels are akin to the non-contaminated surfaces. One of its many technical challenges is the need to measure radioactivity levels across diverse materials (e.g., concrete, metal, coating, etc.) that are present in real sites. Additionally to this complexity, the geometry of the existing surfaces (flat, curved, rough) in the nuclear sites such as those found on ceilings (Figure 2.a) and pipes (Figure 2.b), brings challenges to the measurement of the radioactivity of those surfaces.

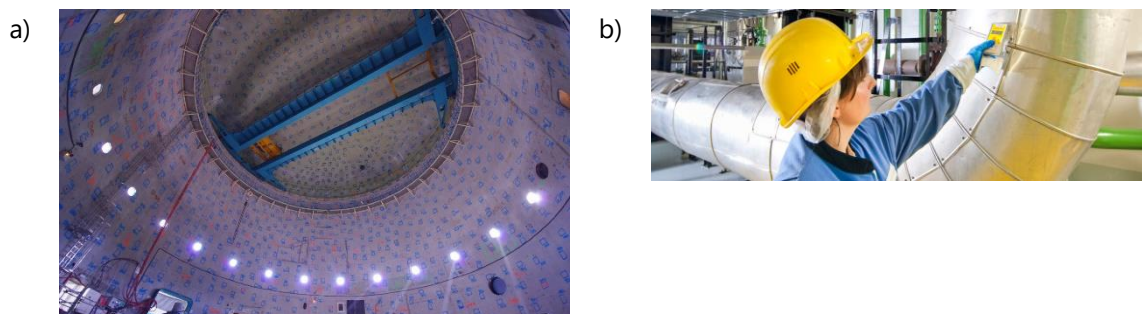


Figure 2: Curved surfaces encountered on nuclear sites: a) ceiling that was checked by hand (blue areas); b) a pipe

Measurement techniques are generally categorized into three distinct groups: bulk monitoring, surface monitoring, and radiochemical analysis. Bulk monitoring is primarily used for assessing gamma (γ) and neutron emitters within bulk materials, ensuring the accurate measurement of radioactivity levels. Surface monitoring is focused mainly on detecting alpha (α) and beta (β) emitters, essential for identifying contamination on various surfaces. Finally, radiochemical analysis is pivotal in establishing a "radionuclide fingerprint" for specific operational areas, but it relies on destructive analyses. Combined with in situ monitoring data, it offers a comprehensive understanding of the present radioactive constituents. These techniques allow the distinction between radionuclides (RNs) that are "easy to measure" (ETM), which can be directly characterized in waste form, and "difficult to measure" RNs (DTM), which require more complex methods for characterization (International Atomic Energy Agency, 2007). This study will primarily focus on DTM RNs, knowing that if DTM RNs can be measured accurately, the effective measurement of ETM RNs should be possible too.

In this context of radioactive waste characterization, both destructive and non-destructive methods are crucial for understanding and accurately assessing the inventory of RN (International Atomic Energy Agency, 2007). Often, employing a combination of these approaches provides the most efficient and effective result (Figure 3). For instance, in the case of activated reactor waste, initial assessments of the expected RNs present and their activity concentrations can be conducted through inference (calculation of the activation). This process is further achieved by scaling the direct measurements of ETM contaminants, which then allows for the inference of the radioactivity levels of DTM RNs (NEA, 2017). Once established, these scaling factors can be applied in conjunction with in situ measurements of ETM RNs. This method allows for a rapid determination of the inventory and activity concentrations of all RNs present in materials or waste water (NEA, 2017).

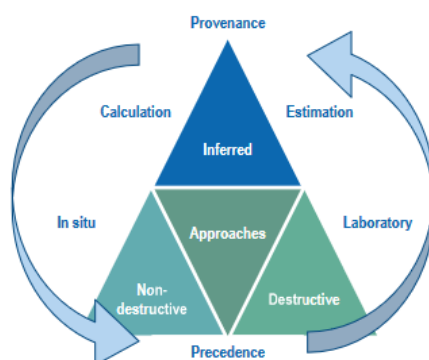


Figure 3: Approach of characterization of the contaminated surfaces (NEA, 2017)

Destructive methods are particularly crucial for the complete determination of DTM nuclides such as alpha, pure beta, X-ray, and low energy gamma emitters. Such measurements are carried out under laboratory conditions, necessitating costly and laborious radioactive measurement procedures. Moreover, the expenses associated with transporting radioactive materials and the complexities in sampling or representativeness must be considered. These methods typically involve a process of sample dissolution, followed by specific chemical separation procedures, and radiometry, tailored according to the chemical and radioactive properties of the nuclides (Baudat et al., 2021; Gautier et al., 2020).

On the other hand, non-destructive assay systems are instrumental in characterizing key nuclides. These systems employ various tools to ascertain the activity levels of RNs and can be applied to the entire production of waste packages (International Atomic Energy Agency, 2007). Non-destructive methods include radiation detection and measurement that can be performed by measuring the emitted radiation. These measurements employ two modes: pulse counting and spectrometry. Pulse counting records the number of pulses, irrespective of their amplitude, whereas spectrometry quantifies the count and amplitude of pulses, sorting them using multichannel analyzers according to their magnitude. This makes spectrometry particularly effective for obtaining detailed information necessary to identify specific radionuclides in a mixture. The best results are generally obtained through the combination of several devices, for example a gamma spectrometry system equipped with a beta probe. However, these probes have often a limited sensitivity to very low energy beta radiations (^3H , ^{14}C , ...) although some improvements have been made (Leblond et al., 2022). Another passive approach was proposed in using digital autoradiography (Fichet et al., 2012; Haudebourg and Fichet, 2016; Leskinen et al., 2013). This studies also highlight that this technique is particularly effective in identifying DTM RNs in a study on the use of autoradiography to target DTM RNs such as ^3H . Digital autoradiography is also sensitive to both labile and fixed contamination. Although this method cannot reach liquid scintillation detection limits, its advantages include simplicity, non-destructiveness, and the ability to map spatial distribution of low energy emitters without needing physical samples.

All of the measurements conducted in D&D areas need to comply with national standards, such as ISO 7503 for radioactivity measurements on solid surfaces for example (ISO 7503-1, 2016). This compliance is crucial for ensuring that the classification of radioactive waste is accurate then reliable. Adhering to these standards provides heightened confidence to regulators and to the public. Furthermore, improved traceability to these standards can reduce the need for additional investigation into measurement discrepancies, thereby fostering public trust and confidence in the secure disposal of radioactive waste.

2 TRACEABILITY IN WASTE MEASUREMENT

There has been a significant focus in the literature on discussing available standards, and calibration processes to achieve traceability in D&D. Efforts include the development of a generic analysis regime for operational areas, and pinpointing stages where traceability can be theoretically established. Several research teams have developed new methodologies for creating "realistic" large-volume standard sources, traceable to standards like ISO 8769, to address this need (Dean et al., 2007; Pérot et al., 2018).

For destructive analyses, laboratories can rely on the use of certified reference materials (CRM) or that comprise ideally similar liquid, solid or gaseous matrices and isotopic tracers, to characterize their methods in real cases. Reference materials are also used to check both precision and trueness of the measurement systems. The accuracy of a measurement method can also be assessed by inter laboratory comparisons following NF ISO 5725:2023 (ISO 5725-1, 2023). For non-destructive surface measurements, reference sources, such as those specified in ISO 8769, can be employed. ISO 7503-2 defines the evaluation of surface contamination throughout with wipe-test samples.

For the purpose of this study, a significant focus is placed on surface contamination monitors, when measuring DTM radionuclides, notably alpha and low energy beta emitters.

The challenge in ensuring traceability to standards arises from the fact that sources complying with ISO 8769, while these are specialized for calibration purposes, are not explicitly designed for the unique contexts of D&D operations. The primary reason for this misalignment is that the calibration sources and reference materials under ISO 8769 are standardized for specific, controlled environments, which may not accurately represent the diverse and complex conditions encountered in D&D operations.

A significant challenge in accurate calibration for D&D relates to the variety of surfaces at these sites. The surfaces to be measured can vary significantly in terms of material composition, geometry, and contamination levels, whereas the calibration standards are often based on uniform and idealized conditions. This discrepancy leads to the limited applicability of these standards to the wide range of samples encountered in D&D activities.

When measuring curved or rough surfaces, the disparity in shape between the flat reference source and the actual surface leads to measurement biases and precision. The surface geometry affects the distribution and intensity of the radiation detected. To address this challenge, geometric correction factors must be applied to the measurements on non-flat surfaces, to account for the differences in surface geometries between the calibration standards and the actual contaminated surfaces in D&D sites. These factors are essential for adjusting the readings to account for geometric differences, ensuring that the radiological assessment remains reliable despite the complexities of the structural geometry of the surfaces in the nuclear site.

Consequently, the complexity and variability of D&D environments call for a more targeted approach to calibration and traceability. This approach is essential to ensure that surface contamination measurements are accurate and then reliable, adapting to the requirements and challenges posed by D&D activities.

Understanding how different detectors used for surface monitoring at nuclear sites align with the requirements of standards such as ISO 7503 is crucial in the context of traceability in D&D. The following section explores the variety of detectors employed for surface monitoring, illustrating the pros and cons in using them to achieve traceable and reliable measurements within the D&D process.

2.1 DETECTORS USED FOR SURFACE MONITORING

A variety of measurement techniques are utilized in surface contamination monitoring, with two main methods being direct and indirect measurements. The direct method involves placing a radiation detector directly on the surface being investigated, the indirect typically employs smear tests to assess contamination. Each methods have its own set of advantages and disadvantages.

Table 1: Types of measurement methods (Amgarou and Herranz, 2021)

Type of method	Advantages	Disadvantages
Direct	Total contamination measurement Areas of sizes up to the size of the detector can be checked	Not suitable for every surface Sensitive to high radiation background
Indirect	Simple concept Access to loose contamination	Variable wiping efficiency Fixed contamination not measured Representativeness

Surface contamination meters play a crucial role in detecting the presence of radioactive substances on accessible surfaces, including low-level ones. The calibration is becoming more challenging when considering the low-level radioactivity close to the level of non-contaminated surfaces. One needs to consider also that the detection efficiencies of these instruments can range from nearly zero up to approximately 30%, for different radionuclides.

Key components of radiation detection systems include the detector itself and the associated processing units. The detector absorbs radiation and converts it into an electrical signal. Various mediums are used for this purpose, including various gases and gas mixtures in gas-filled detectors, as well as solids in solid-state detectors. These detectors are able to measure the main types of radiation produced by radioactive decay, such as alpha, beta, X, or gamma rays. The electrical signals generated are then amplified and processed, to quantify the radiation and to convert it into radiological units.

Gas-filled detectors (Figure 4. a) such as ionization chambers, proportional counters, and Geiger-Müller devices respond to radiation by ionizing the gas within, with the resulting charge being transferred to electrodes and measured by a probe. The applied voltage can influence their ionization response. The scale from the lower to higher voltages is shown from top to bottom in Figure 4.b, c, and d. Ionization chambers cannot discriminate between radiation types, meaning they cannot be used for spectroscopy. Proportional counters experience a gas amplification effect that multiplies the intensity of the output pulse, making them beneficial in spectroscopy applications due to their sensitivity and efficiencies in alpha and beta detection. Geiger-Müller tubes operate at a higher voltage than other gas-filled detectors. Each ionization, regardless of its intensity, causes a gas amplification effect across the entire detector anode, making them suitable primarily as simple counting devices for measuring count rates or dose rates.

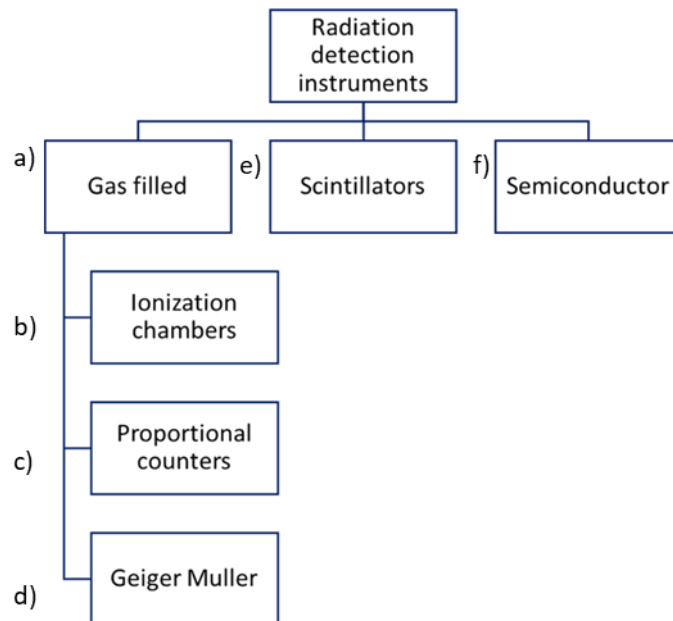


Figure 4: Radiation detection instruments

Scintillators (Figure 4. e) generate a distinct flash of light when it interacts with radiation, allowing them to capture specific spectroscopic profiles. They operate by coupling a scintillator material to a photomultiplier tube. There are two primary types of scintillators: inorganic and organic/plastic.

Inorganic scintillators, such as sodium iodide (NaI(Tl)) and cesium iodide (CsI), have the unique property of being transparent to their own emitted radiation. In these materials, electrons are excited from the valence to the conduction band, and as they de-excite, they emit optical or near-UV photons. The emitted photons generally possess lower energy than the excitation energy, which ensures the scintillator's transparency to its emitted radiation. Often, these crystals are doped with activators, such as thallium in NaI(Tl) scintillators, to enhance their light output.

On the other hand, organic scintillators (liquid or solid), comprise molecules or polymers that have the capability to scintillate. In these scintillators, when submitted to a ionizing radiation, electrons are excited between electronic levels within a molecule and quickly de-excite, emitting photons with less energy than the excitation energy, allowing them to escape the plastic or liquid. Plastic scintillators may exhibit a characteristic blueish glow in light, indicative of a high-frequency emission around 400 nm (Knoll, 2010).

Other solid-state detectors contain lithium drifted silicon detectors, avalanche detectors, photoconductive detectors and position sensitive semiconductor detectors (Figure 4. f).

2.2 CALIBRATION OF SURFACE CONTAMINATION MONITORS

The concepts of calibration and “type test” are important in the context of calibrating radiation detection instruments. The terms “test” and “calibration” are distinct but related. While calibration is the process of quantifying the response of an instrument to a known radioactivity, a “type test” involves a broader examination, which may include an inspection of the mechanical and electrical state of the instrument. This test defines the procedure for assessing the performance of the instrument, thereby determining its suitability, or confirming its continued appropriateness for certain types of radiation measurements.

Before its first utilization, the portable radiation protection instruments should undergo an initial Test Before First Use (TBFU) and, subsequently, Periodic Tests. These tests, which require the immediate supervision of a qualified person and compliance with current national regulations, are compared with past performance test information and the appropriate type tests, to confirm that the instrument is meeting its specification and is suitable for its intended use.

Each contamination meter is designed and type-tested to measure a specific range of contaminants. The response of the instruments depends on several factors, including the type and energy of the radiation, the detection efficiency of the detector, the detection geometry including the dimensions and nature of the contaminated surface as well as the distance between detector and surface. Additionally, the condition of the instruments—factors like inherent electrical noise, wear and tear, and potential malfunctions—also plays a critical role.

The surface contamination instruments need to be calibrated regularly using reference sources that comply with the international standard (ISO 8769, 2020). This process is conducted by traceable methods recognized by the ISO 7503 and requires a set of predefined reference sources, which have certified α , β , or photon surface emission rates. These sources serve as emitters of alpha particles, electrons or photons within specific energy ranges rather than as sources of particular RNs. Consequently, it is crucial for users of the instrument to keep a certificate relating to the last formal test and carry out routine checks on the instrument with these reference sources. Another fact regarding the calibration sources is the requirement to have non-contaminating surfaces to allow their use in real sites and to protect the workers.

ISO 7503 gives guidance on the measurement of surface contamination, which is applicable to many situations where radioactive contamination occurs. Ideally, radiological mapping requires the information regarding the RNs constituting the surface contamination, but it is not always possible to distinguish or identify the different RNs so in most cases the type of radiation is mentioned (α , β , γ). The measurements are typically taken in counts per second (cps or s^{-1}) and must be converted to Bq/cm^2 . Additionally, some of the instruments can be set to measure surface contamination in Bq/cm^2 directly. After qualitative evaluation of the RNs, surface contamination activity should be measured per unit area, and compared with surface contamination guideline values or surface contamination limits.

The traceability of the reference sources is an important factor that needs to be considered. However, for most sources, self-absorption is non-negligible and significantly affects the emission spectrum. ISO 8769 recognizes this issue, indicating that alpha source preparation in particular

necessitates further enhancements.

It is also important to consider the factors contributing to measurement uncertainty, particularly the matrix being analyzed. The large variety in matrices compositions and the inhomogeneous distribution of activity within these matrices, will contribute significantly to the overall uncertainty of the measurement values.

2.3 REFERENCE SOURCES FROM APPLICABLE STANDARDS

In this part, the information regarding current reference sources is given with their details. Reference sources should comply with the ISO 8769 standard. First, the sources should be constructed with an electrically conductive backing material, ideally 3 mm thick, which has a radionuclide or radionuclides permanently attached to or embedded in one side. The backing of the sources should prevent radiation emission through the back of the source. Alternatively, sources can consist of a material layer containing uniformly distributed RN. For this type of sources, the thickness of the layer should not exceed the saturation layer of the particulate radiation.

In order to measure the surface emission rate directly, a threshold must be set which corresponds to a minimum energy. For alpha counting, the threshold must be just above the electronic noise of the system. The threshold should align with a photon energy of 590 eV for beta counting and it should encompass the photon peak and the whole Compton continuum in photon counting.

The active area of the sources must be at least 100 cm², and recommended sizes typically include 10 x 10 cm², 10 x 15 cm², and 15 x 20 cm². These sources are designed to be as close to a 3 mm thick aluminum backing material as possible. Additionally, extending the backing material at least 10 mm beyond the active area of the source is recommended to allow its manipulation. Self-absorption (particularly for alpha and low energy beta emitters) cannot be neglected for reference sources. This leads to a degradation of the emission spectrum and might affect measurements with windowed transfer measurement devices.

A National Metrology Institutes should conduct the measurement of surface emission rate for standards. During this process, relative standard uncertainties must not exceed 3% for alpha standards, 3% for beta standards with an end-point energy greater than 150 keV, 5% for beta standards with an end-point energy below 150 keV, and 10% for photon standards.

The uniformity of a sample is expressed as 1 minus the standard deviation of the surface emission rates (σ_n) of each individual portion of the entire sample divided by the mean value of these emission rates (n) as shown in Equation 1.

$$\left(1 - \frac{\sigma_n}{n}\right) \times 100 (\%) \quad \text{Equation 1}$$

The uniformity of sources should be greater than 90% to be acceptable for the ISO 8769 standard. The subareas of each portion should be 10 cm² or less. If the active area of the reference source is 10 cm x 10 cm and 10 cm x 15 cm they should be divided into 16 rectangular portions in a four-by-four pattern.

Uniformity may be measured by using the image plate technique, position-sensitive measurement systems, or by inserting a masking plate between the reference and the detector. The masking device should provide sufficient thickness for complete shielding.

Radionuclides that are preferred, and some alternatives, in the alpha-emitting standards (Table 2) and beta-emitting standard sources (Table 3) are given below, along with the maximum energy range of the RNs.

Table 2: Radionuclides for alpha-emitting standard sources (ISO 8769, 2020)

Radionuclide	Half-life in years	Maximum energy in keV
Preferred		
^{241}Am	432.6	5 486
^{230}Th	75 380	4 687
Alternative		
^{238}Pu	87.7	5 499

Table 3: Radionuclides for beta emitting standard sources (ISO 8769, 2020)

Radionuclide	Half-life in years	Maximum energy in keV
Preferred		
^{14}C	5 700	156
^{99}Tc	211 500	294
^{36}Cl	302 000	710
$^{90}\text{Sr}/^{90}\text{Y}$	28.80 (^{90}Sr) ^{90}Y in equilibrium	546 (^{90}Sr) 2 279 (^{90}Y)
$^{106}\text{Ru}/^{106}\text{Rh}$	1.02 (^{106}Ru) ^{106}Rh in equilibrium	39 (^{106}Ru) 3 546 (^{106}Rh)
Alternatives		
^{147}Pm	2.62	224
^{204}Tl	3.79	764
^{60}Co	5.27	317
^3H	12.31	19
^{63}Ni	98.7	67

The “preferred” RNs include the RNs that are widely available, possess long half-lives, high specific activities, and can cover energy levels typically required in monitoring scenarios. On the other hand, the “alternative” radionuclides might not be as suitable due to several factors. These include their shorter half-lives, which necessitates frequent replacement, lower specific activities making

it challenging to achieve the desired activity level in a very thin active layer, the emission of additional, non-desirable types of radiation, and the complications in achieving high levels of radioactive purity.

When conducting alpha radiation surveys with hand-held detectors, due to the short range of emitted alpha particles there is no significant impact of the alternative or preferred RNs on the detection. Therefore, in large area alpha surveys, the approach is mainly qualitative. Only representative locations are typically checked for alpha radiation, as this provides a sufficient overview of the safety of the areas and contamination levels.

The characterization of reference measurement standards in the context of radiation detection and measurement involves two distinct types of standards, known as Class 1 and Class 2. Class 1-reference measurement standards are calibrated directly in terms of both activity and surface emission rate. This calibration is carried out at a national metrology institute (possibly abroad), ensuring the highest level of accuracy and traceability to international standards. These standards are crucial as they serve as the primary reference, directly linked to the fundamental units of activity measurement. On the other hand, Class 2 reference measurement standards are calibrated slightly differently. They are calibrated in terms of surface emission rate using a reference transfer instrument. However, the accuracy of this instrument is first established by calibrating it with a Class 1 standard of the same radionuclide and similar construction, under the same geometrical conditions. This process is conducted in laboratories that follow the ISO/IEC 17025 standards for such measurements. While Class 2 standards are considered secondary due to their indirect calibration method, they are still highly reliable and provide a practical means of calibration when direct measurement at a metrology institute is not accessible. Both Class 1 and Class 2 standards are used in the field of radiation measurement, ensuring precision and trueness in various applications.

To sum up, the aforementioned ideal sources, while not explicitly tailored for calibration in D&D activities, are quite effective in the general calibration of surface contamination monitors. Their design and function are well suited to the broader objective of ensuring accurate calibration of these devices. However, it is important to acknowledge the limitations in their specificity when it comes to D&D applications. The production of specific sources for D&D purposes aims at enhancing the reliability of measurement system while covering the unique requirements of D&D processes. However, these sources might not always align with national standards. This refinement addresses the specific challenges and demands encountered in D&D, ensuring that calibration is not only general but also acutely relevant to the particular conditions and needs of D&D operations.

3 STATE OF THE ART ON THE PRODUCTION OF SURFACE SOURCES

3.1 LIMITATIONS OF CALIBRATION IN TERMS OF D&D APPLICATIONS

Regularly calibrating the surface contamination monitors is an essential procedure that ensures the accuracy and reliability of measurements. This process must comply with the national measurement standards, as stated in ISO 7503 (ISO 7503-1, 2016), through a traceability pathway employing certified reference sources and well calibrated measurement devices.

The surface sources presently used in surface monitoring calibration are designed to calibrate devices under controlled, specific conditions. However, these sources do not represent the complex shapes and varied surfaces encountered at D&D sites. The sources can be efficiently used for the calibration of the detectors, to check that they function properly, however they are not specialized for D&D purposes. For this reason, these sources should be adapted in a way that can reflect the contamination characteristic of the nuclear sites. Thereby, the potential error in calibration techniques can be minimized for D&D purposes.

Another assertion of the reference sources can be that they yield results with considerable uncertainty, particularly for alpha and beta emitters, which must not exceed 10%. These uncertainties arise due to self-absorption, where emitted particles from the RNS are absorbed into the material rather than being detected, or lose a significant portion of their energy before leaving the material and potentially being detected. Hence, this fact presents a challenge in ensuring accurate and reliable measurements. According to ISO 8769, it has been established that self-absorption is not negligible and influences the emission spectrum of the sources (ISO 8769, 2020). Further efforts should be made to minimize this feature.

Furthermore, ISO 8769 (ISO 8769, 2020) stated that LARS should be flat and maintain uniformity above 90% for operational tests and calibration of surface contamination monitors. Achieving this uniformity is an ongoing challenge, as highlighted in various studies (Burgess and Iles, 1983; Nähle and Kossert, 2012; Ohshiro et al., 2016). Deviations from this uniformity standard can introduce bias in instrument efficiency estimates and an increase of the uncertainties (Silva et al., 2020).

Challenges associated with current large area reference sources (LARS) and their features, are linked with their preparation techniques. Notably, parameters such as backscattering, self-absorption and uniformity mostly depend on the production methods and the layer thickness on which the activity is deposited upon.

To address the gap in reliable calibration of surface contamination meters in D&D, this study aims to develop traceable LARS specialized for this application. Various types of LARS, such as drop-deposited, electro-deposited, anodized, and ion-exchange membrane sources, are commercially available. These sources are calibrated regarding particle surface emission rates and activity, with different traceability methods reported in the literature (Janssen and Klein, 1994; Janßen and Thieme, 2000; Švec et al., 2006). Several other source production techniques are described in the literature, even if those sources are not commercially available. The aim of this section is to describe the commercial and non-commercial source preparation techniques, highlighting their compliance (or lack thereof) with ISO 8789, and their suitability to mimic real contaminated

surfaces encountered in D&D. This way, a suitable source preparation method can be devised, to obtain sources tailored for the calibration of monitors used in D&D.

3.2 ANODIZED ALUMINUM SURFACES SOURCES

A conventional method for preparing reference surface sources involves embedding the RN within the porous surface of an anodized aluminum foil (Tsouanko-Sitnikov et al., 2002). This approach involves etching micropores into the aluminum foil, which has a standard thickness of 0.3 mm, and ensuring micropores are less than 0.01 mm in diameter (as shown in Figure 5).

The radioactive substance is then secured within the micropores in a stable chemical form. Subsequently, a chemical sealing process produces a thin layer of Al, exhibiting mechanical robustness and chemical resistance. The anodized aluminum is mounted on a supportive backing plate with a thickness of around 3 mm to construct rigid sources (EZAG, 2022). Typically, the radioactive material is concentrated in a surface layer, ranging from 3 to 10 μm in thickness, composed of aluminum and aluminum oxide.

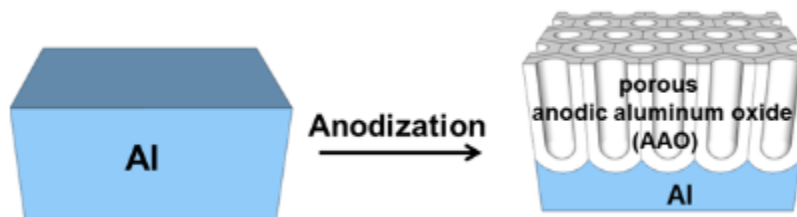


Figure 5: Porous anodic aluminum oxide surface (Lee and Park, 2014)

It exists similar, commercially available reference surface sources referred to as etch pitched surface sources. In the described method, sources embedding radioactive material into pits are constructed through a multi-step process. Initially, fine etch pits are generated on the surface of an aluminum plate. Subsequently, a radioactive material is deposited within these etch pits. The final step involves sealing the surface with a thin film. However, these sources have the disadvantage of self-absorption, due to the protective film. This technique yields a uniform source that is not only durable but also exhibits a high degree of chemical resistance (Isotrak Calibration Sources, 2022). These sources, being made of aluminum, comply with the requirements of ISO 8769. Despite the common usage of these sources, they present some disadvantages. One notable issue is the potential for abrasion on the aluminum surface, which can lead to the removal of radioactivity. This phenomenon, often results in an apparent loss of radioactivity over the years. Consequently, this necessitates periodic recalibration of the sources at regular intervals, in accordance with national standards and recommendations. The activity depth distribution within the source is highly dependent on the preparation procedure which brings a challenge in controlling this variable. (Tsouanko-Sitnikov et al., 2002). The thickness of the active layer, is generally not negligible compared to the range of emitted alpha and low energy beta particles, leading to low effectiveness due to the self-absorption of the radiation.

Additionally, as these sources are only produced flat, therefore they are unable to accurately represent the complex geometries encountered in nuclear sites. Finally, the materials used are also not representative of heavier materials that require contamination checks in D&D processes, such as stainless steel, copper, zinc or concrete, and polymer.

3.3 DROP DEPOSITION AND INKJET

The drop deposition method, applied with an aqueous radioactive solution, is a straightforward method for producing traceable surface sources of limited sizes (up to a few cm of diameter). However, it is limited by its poor resolution due to the self-absorption in the dried deposit layer. Generally, this method is applied with a spreading agent to improve the uniformity of the source and, for alpha sources, the quality of the spectrum. Due to the combination of the solution and spreading agent, the drying period can take up to a few hours. Another significant drawback of this method is the tendency to produce a non-uniform distribution of radioactivity, which often creates clumping or an accumulation of the solid at the periphery (Aggarwal, 2016).

Further expanding on this method, drop deposition can also be employed with an array of drops, on filter paper, allowing for the creation larger area sources (Figure 6). In this method, RNs are deposited onto the filter paper by dripping a solution of RNs, followed by a drying process. Typically, these are encased in a thin plastic film, such as metallized Mylar®, to obtain non-contaminating sources. The advantage of this technique is that the activity can be quantified based on the volume or weight of the solution applied, and the production process is straightforward. However, this method tends to result in lower uniformity compared to other methods, due to the difficulty in reliably producing drops of similar size (Sato et al., 2004). Another significant disadvantage should be self-absorption in the filter paper, in particular for alpha particles.



Figure 6: Drop deposition of radioactive solution on a filter paper (Monsanglant-Louvet et al., 2015)

Another type of drop-deposited sources is ink-jet sources. To produce these sources, the radioactive material is mixed into inks or other liquids compatible with an inkjet printer, and the source is obtained by printing on a sheet of paper by the printer. Printed sources are dried at room temperature, then they are covered with metallized Mylar®. This method provides highly uniform sources with high positional resolution, flat but with arbitrary shapes (Sato et al., 2004; Yamada et al., 2012).

These drop-deposited sources are not reported to comply with ISO 8769, however they could be if used in combination with an Al backing plate, provided that they meet the criteria for uniformity. They can also be adapted for D&D applications, if the drops are deposited onto flexible surfaces, than can be bent to mimic curved surfaces, such as Mylar® or paper.

3.4 ELECTROPLATED SOURCES

The electrodeposition method has been utilized for depositing a wide range of elements onto a cathode through a suitable reduction or precipitation reaction, especially those with a reduction potential lower than water. This method is a widely used surface source production method, especially for actinides, by applying from an aqueous (e.g., diluted HNO₃) or organic medium (e.g. isopropyl alcohol) (Aggarwal, 2016).

While the electrodeposition method is typically used to produce sources for small areas, a few centimeters in size, it can also be adapted for larger areas. In an aqueous medium, the method involves the cathodic deposition of hydrated oxides in mildly acidic (pH: 3-5) or basic media containing various amounts of ammonium or alkali salts (Talvitie, 1972), whereas in an organic medium, molecular plating occurs. The process requires careful optimization of various parameters such as current density, volume of the solution in the cell, voltage, distance between cathode and anode, and the shape of the anode (Aggarwal, 2016). Moreover, it can be improved by the use of different aqueous and/or organic electrolyte solutions or changes in the deposition system itself, e. g. the use of rotating disc cathodes, semi-permeable membranes to prevent platinum precipitation, or improvements in the stirring process of the electrolyte solution (Krmpotić et al., 2018).

This method was also conducted in a cell configuration where the cathode was embedded in the cell wall, and the anode was a cylinder submerged in the solution, which was stirred by a magnetic bar (Becerril et al., 1993).

One example of the improvements of this technique, with rotating disc cathode cells, is shown in Figure 7. The process requires precise control over the rotation speed and careful management of the flow lines from the bulk to the cathode surface. Deviations in the rotation velocity and the presence of a vortex or additional stirring from gas evaluation at the cathode can lead to inaccuracies in the deposition yield (Becerril et al., 1993).

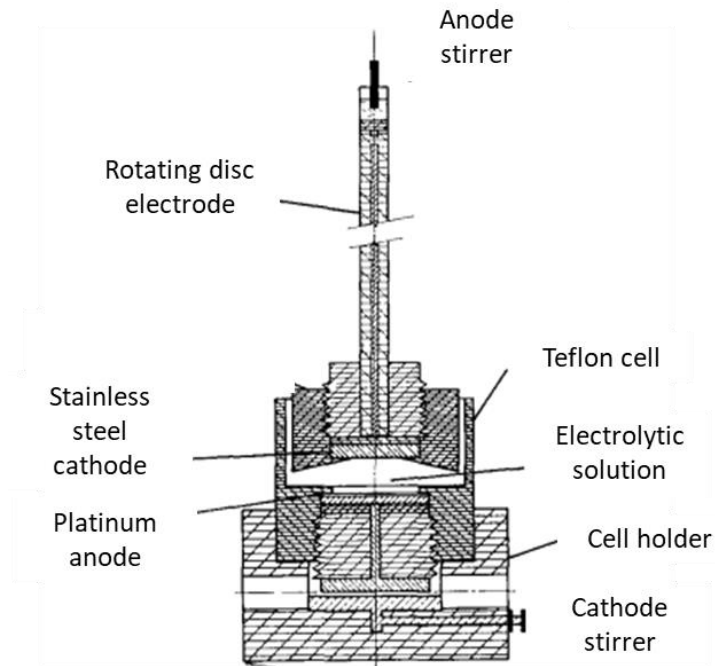


Figure 7: Illustration of the electrodeposition method (Becerril et al., 1993).

This technique is remarkable due to the possibility of achieving a uniform and almost weightless sample, which is crucial for the high-resolution alpha spectrometric determination of actinides (Talvitie, 1972). Additionally, it significantly enhances the stability of the deposited films, providing resistance to higher operational temperatures and offering increased resistance to both corrosion and radiation-induced damage (Balasubramanian, 1997). Nevertheless, electroplated sources can be contaminating if touched.

While electrodeposition is a widely used technique, specific challenges are associated with its application. This method requires an electrochemical system to reach a real steady state and optimized parameters. Over time, the deposited radioactive materials may exfoliate, thus complicating quantitative metrology techniques (Chen et al., 2018).

It is noteworthy that regardless of whether deposition or electrodeposition techniques are employed, there is no chemical interaction between the radioactive materials and the substrate used in the source production. This technique allows to obtain sources that can comply with ISO 8769, if an Al backing is used, and providing that the uniformity of the deposited activity is within the range described in the standard. However, this technique was only reported in the production of flat surfaces, and is not expected to easily yield rough or curved surfaces similar to those encountered in D&D sites.

3.5 ION EXCHANGE SOURCES

3.5.1 Sources from commercial ion exchange membranes

Producing radioactive surface sources through an ion-exchange membrane involves introducing an ionic radioactive solution onto an ion-exchange membrane (Ballard, 1981). This fabrication method is based on the principle of RN uptake from a solution by ion-exchange resins coated on a nylon web. Sources are prepared by cutting the web to a desired size and immersing it in a radioactive solution of the target RN for a duration ranging from a few hours to three days. For example, ^{241}Am sources produced this way reached 90% of uptake within 4 hours (Ballard, 1981). Finally, the sources are rinsed, dried, and sprayed with a vinyl aerosol, to minimize the contamination, improving safety and handling. The following types of resins are utilized in the production methods: cation-type resin containing sulfonic acid groups, anion-type resin containing quaternary ammonium chloride.

The container size used during the production of these sources can significantly affect their uniformity. To enhance uniformity, plastic containers slightly larger than the membrane were employed. In this study, the authors realized that excessively large containers could result in uneven RN distribution, with edges absorbing more ions than the central region (Ballard, 1981). Another research group (Yoshida and Martin, 1990) modified the suspension set up of the membrane in the solution on a glass framework with nylon fishing lines to avoid surface contact Figure 8.

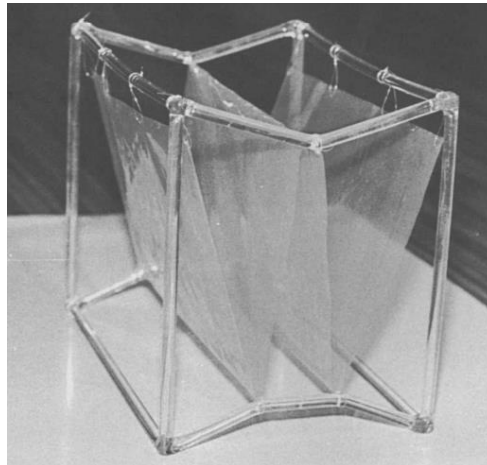


Figure 8: Glass framework for soaking large ion-exchange membrane (Yoshida and Martin, 1990)

The ion exchange resin can be employed with various isotopes, and the production process is repeatable. However, isotopes with weak ionic charges or significant self-absorption might not be suitable for this technique. The underlying low efficiency of these sources presents limitations on the accurate control of RN concentrations. This constraint often results in the production of sources that do not consistently exhibit the specified levels of radioactivity.

Despite having a good uniformity, a notable loss of activity was observed over the years. Thin sources pose practical challenges due to their fragility and finite self-absorption for alpha and low energy beta radiations.

Another disadvantage of using an ion exchange membrane is that during the preparation process, the dipping step may result in wrinkles on the membrane, complicating the task of adhering the membrane closely and smoothly to a backing material. A research group (Chen et al., 2018) focused on developing a convenient method for preparing homogeneous and chemically stable reference sources, utilizing Nafion HP membrane with sulfonic acid functional groups, with a 4 mm thick anodized aluminum plate as backing (as seen in Figure 9).

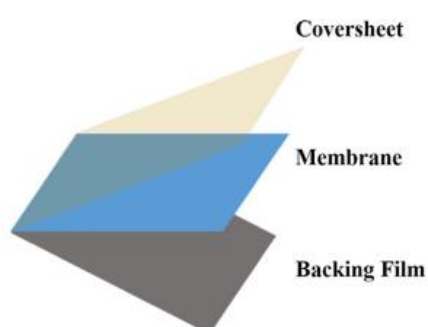


Figure 9: The structure of Nafion HP membrane (Chen et al., 2018)

The necessary equipment for preparing the source is illustrated in Figure 10. The membrane and backing were placed in a quartz glass reaction tank, and polydimethylsiloxane (PDMS) was added and polymerized on the surface, to form a well. Then, the RN solution was placed in the well.

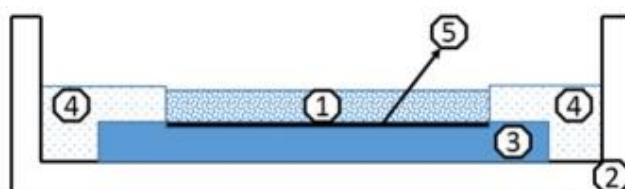


Figure 10: Diagram of the schematic device to prepare the source 1: RN solution, 2: quartz glass tank, 3: aluminum backing material, 4: PDMS, 5: ion exchange membrane (Chen et al., 2018)

This approach can reach a uniformity of approximately 96% for ^{241}Am , in compliance with ISO 8769 standard. However, the efficiency of the source was notably lower (31%) than the Class 1 reference source requirement specified in ISO 8769 standards (45%) (Chen et al., 2018). The reduced efficiency was attributed to the membrane structure, which limited emission rates, especially for α emitters.

These sources could however be used to mimic curved surfaces encountered in D&D sites, provided that the membrane is bent after binding the RN.

3.5.2 Conducting polymer with ion exchange functional groups

Another method utilizing ion exchange groups to immobilize RN onto a surface is the electrodeposition of modified polypyrrole films, to bind actinides (Stéphan and Carrier, 1997). This method involves forming a thin, insoluble film of a conducting polymer ion exchanger through the electrochemical polymerization of an organic monomer on a large-area conducting support. A radioactive nuclide is then incorporated into the film from an aqueous solution with a specific composition by an ion exchange mechanism.

Another study used the same technique with bivalent cations such as ^{90}Sr and ^{60}Co , and a polypyrrole functionalized with carboxylic cation exchange groups was utilized (Tsoukko-Sitnikov et al., 2002). This forms regular, well-adhering films when electrochemically prepared on small-area electrodes made of glass coated with semiconducting tin oxide (Figure 11).

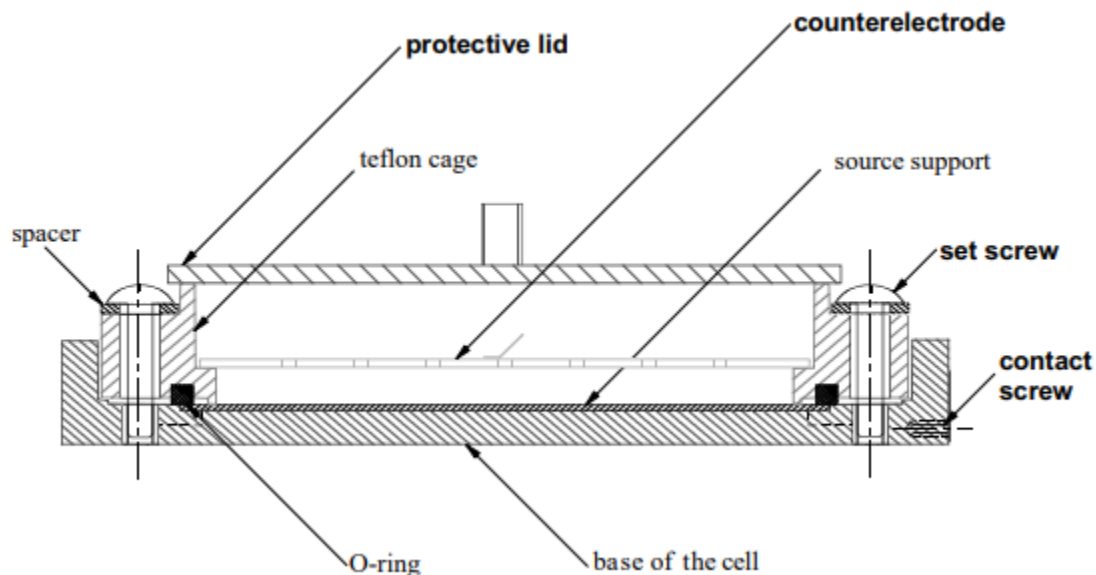


Figure 11: Illustration of the cell for electrochemical polymerization (Tsoukko-Sitnikov et al., 2002)

This method has certain drawbacks. One significant limitation is the need for a cover layer over the conducting polymer that decreases the efficiency of the source due to the attenuation of the emitted radiation. Moreover, the production process is inherently complicated and demands precise control and careful execution. This technique necessitates a stainless steel flat surface, in order to proceed with the electropolymerization. This material can be representative of some real contaminated surfaces in D&D sites.

In theory, these sources could comply with ISO 8769 requirements, provided that a suitable Al backing is used, and that they meet the requirements for uniformity.

3.5.3 MnO₂ coated disc

In the literature, 24 mm diameter discs coated with MnO₂ are utilized for the extraction of radium and uranium from water samples by adsorption of the RN onto the disc. However, the aim of this treatment is not to produce reference sources, but samples to be analyzed. On the other hand, this approach could be extended to manufacture reference sources in the context of our study. The resolution offered by this method is sufficiently good for identification purposes and could potentially be adapted for larger sizes of sources.

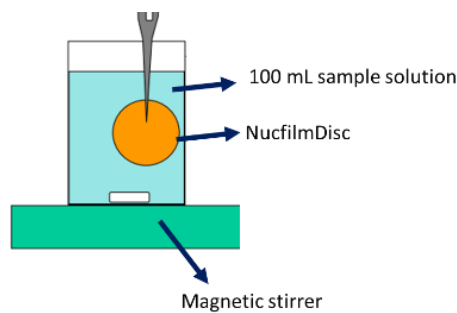


Figure 12: Immersion of the MnO₂ coated thin film in RN solution (Surbeck, 2000)

This product is also commercially available from Triskem (Nuc Film Discs, 2015). These particular discs were prepared using polyvinyl polymer-based substrates, which were washed with ethanol, hydrochloric acid, and isopropyl alcohol. Subsequently, the substrate was immersed in a potassium permanganate solution with stirring at 70 °C for two hours. The manganese dioxide (MnO₂) coated discs were then rinsed with deionized water, air-dried, and immersed in a RN-containing solution for radium adsorption. A pH of 7.5 was maintained for the solution, and quantitative adsorption of radium was achieved within 24 hours from the water samples. The discs were then washed with water, dried at room temperature, and used for alpha spectrometric analysis (Surbeck, 2000).

Since this technique was not designed to produce reference sources, the MnO₂ discs do not comply with ISO 8769. However, a MnO₂ coating could be deposited on flexible, curved or even rough surfaces, to yield sources that are more representative of contaminated surfaces in D&D sites.

3.6 POLYMERIC SOURCES

3.6.1 Carbon-14 polymer sources

Carbon-14 sources, are 1 mm thick, 10 cm² plate composed of pure poly[mety/L⁴C] methacrylate (PMMA). Unlike some other sources, this particular design does not incorporate any backing material. Instead, it is supported by a Perspex ring. Notably, the manufacturer does not conduct direct measurements of the output from these sources. Instead, an approximate output is provided, which is based on the specific activity of the source (Burgess and Iles, 1983). This approach has significant drawbacks. The only available radionuclide with this approach is ¹⁴C, and

it requires the synthesis of radioactive PMMA through organic chemistry.

It should be possible for these sources to comply with ISO 8769, if deposited on an Al backing. The PMMA polymer could also be molded to mimic curved or rough surfaces.

3.6.2 Painted sources

Painted sources are produced by applying a lacquer containing radioactive material onto a substrate, which is then, in some instances, sintered to enhance durability. The uniformity of the sources can be improved by repeating the painting process, as multiple layers help to achieve a more consistent distribution of radioactivity (Sato et al., 2004). In those sources, the activity is distributed in the painted layer, which is typically thicker than the mean free path of alpha particles. Therefore, the self-absorption should be a significant phenomenon for alpha sources prepared with this technique.

The article describing these sources does not specify their compliance with ISO 8769. However, various surfaces, including curved and rough, could be painted upon, to mimic contaminated surfaces of D&D sites. Furthermore, it is likely that some painted areas of nuclear sites have been contaminated, and therefore, painted sources would be close to real contaminated surfaces.

3.6.3 Epoxy resin

In the previous study applied by LNHB research team has initiated a study involving polymeric epoxy resin to produce large area surface sources ranging from 25 to 400 cm², designed to mimic various contaminated surfaces typically found in D&D sites (curved or rough surfaces). This exploration forms a part of ongoing investigations into the use of polymeric resin as surface sources (Chambon et al., 2022).

The production method involves encapsulating alpha, beta, and gamma-emitting RNs within an epoxy matrix, utilizing the strength of a cross-linked polymeric network to trap RNs and prevent their leaching. The process entails mixing two components of epoxy resin in a beaker, followed by the introduction of the radioactive solution. After achieving a homogenized mixture, it is poured into molds. After sources are cured, they can be coated with a thin gold layer, to ensure conductivity for the proper measurement process, or used without coating.

The study highlights several advantages of this approach. The sources demonstrate high uniformity, around 95% for 25 cm² surface sources, and are traceable to national standards in terms of activity and surface emission rate. However, the approach has some drawbacks. One of the disadvantages is the low efficiency for alpha-emitting RNs, approximately 1%. This is mainly due to the thickness of the resin, which varies from 0.5 to 1 mm and significantly exceeds the mean free path of alpha particles in the resin, estimated to be around 30 μm. This case is illustrated in Figure 13. It was challenging to control the thickness of the sources below 0.5 mm, so obtaining sources thinner than the mean free path of alpha particles was impossible.

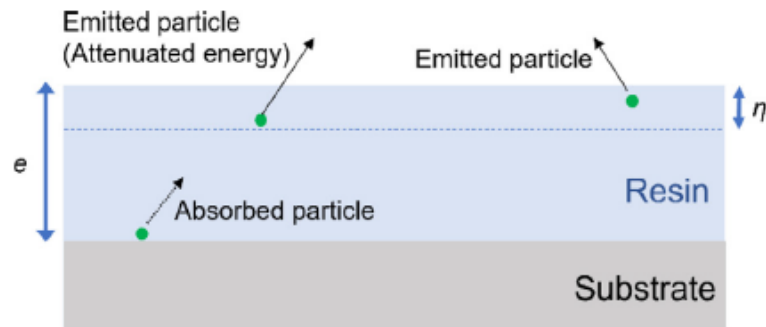


Figure 13: Scheme of the low efficiency alpha emitting resin sources (Chambon et al., 2022).

This low efficiency was a drawback of the epoxy resin spiking approach, because it meant that most of the alpha RNs used were wasted, since they could not be detected. Additionally, the production process required RN solutions with even higher activity for high alpha surface emission rate sources. These sources, being specialized to meet the specific needs of D&D areas and to mimic real contaminated surfaces, do not fully comply with ISO 8769 standards.

In summary, while the polymeric resin method offers valuable insights and utility, particularly in D&D scenarios, its limitations, particularly in terms of alpha-emitting RN efficiency and control over resin thickness, highlight areas that require further research and development.

3.7 SUMMARY OF SOURCE PRODUCTION METHODS

A summary of various source production methods, derived from reference articles and catalog information, is presented in Table 4. This summary not only details the production methods but also evaluates their compliance with ISO standards. Additionally, the table assesses the applicability of these methods to the D&D process, particularly in terms of their ability to represent real surfaces encountered in nuclear sites.

Table 4: Production methods for LARS

Technique and references	RN studied	Sizes and surface activity	Advantages and drawbacks	Compliance with ISO 8769	Applicable to D&D ?
Anodized aluminum source (Burgess and Iles, 1983) Eckert and Ziegler Nuclitec anodized aluminum source	$^{90}\text{Sr}/^{90}\text{Y}$, ^{204}Tl , ^{147}Pm , ^{14}C , ^{36}Cl Beta emitters	10 x 15 cm ² 5-30 Bq 10 x 10 cm ² Depth of active layer: 6 μm 3 mm Al backing	Loss of activity Non-uniformity less than 10% By the improvements in the uniformity can comply with ISO	Can comply	No
Ion exchange resin (Burgess and Iles, 1983) (Ballard, 1981)	$^{90}\text{Sr}/^{90}\text{Y}$, ^{204}Tl , ^{147}Pm Alpha and beta sources	10 x 10 cm ² 18.5 Bq 47 mm discs or 10 x 14 ft roll For alpha sources 370 Bq to 37 MBq For beta sources lower limit is 3700 Bq	Low uniformity values Uniform Low wipe off factors Applicable to a wide range of RNs	No	Yes
Nafion ion exchange resin (Chen et al., 2018)		Thickness 20 μm 10 x 10 cm ² Source efficiency 31.3% 3210 Bq	Feasible and effective Source efficiency does not comply to the standard	No	Yes
Conducting polymer ion exchange resins (Tsoumpko-Sitnikov et al., 2002)	Beta sources	Active deposit d= 44 mm on a 50 mm x 3 mm thick stainless steel support Source efficiency around 75%	Uniform Reproducible	Yes	Yes

Technique and references	RN studied	Sizes and surface activity	Advantages and drawbacks	Compliance with ISO 8769	Applicable to D&D ?
Anion exchange polymer resins (Stéphan and Carrier, 1997)	Alpha sources, actinides U(III), Pu(III), Am(III)	Deposit area: 4 cm ² For alpha sources 370 Bq to 37 MBq For beta sources lower limit is 3700 Bq	Thin and uniform	No	Yes
¹⁴ C Polymer source (Burgess and Iles, 1983)	¹⁴ C	10 x 10 x 1.2 cm ³ 96.2 Bq	Not have backing material	No	Yes
JRIA Inkjet source (Ohshiro et al., 2016) (Yamada et al., 2012)	³⁶ Cl Beta emitters	10 x 10 cm ² Depth of active layer: 5 µm 3 mm Al backing 0.9 mg·cm ² aluminized mylar used as a window 1.5 Bq/cm ² sources are prepared Polyester film with an Al backing (4 mm) covered with aluminized mylar 61.6 Bq	Uniform Reproducible Long term stability	Yes	Yes
Electro deposition (Becerril et al., 1993)	Actinides	15 mm diameter disc It is covered with a plastic sheet after the production	Uniform and weightless Requires stable conditions With time exfoliation occurs No chemical interaction between the substrate and deposited RN	Yes	No
(Surbeck, 2000) Adsorption by MnO ₂ coated polymeric resin	²²⁶ Ra, ²³⁸ U and ²³⁴ U, ²¹⁰ Po	2 x 2 cm ² film on a polyamide substrate 1.5 Bq/cm ² sources are prepared	Adsorption technique for removal of the RNs	No, source for measurement systems	No
(Chambon et al., 2022) Polymeric surface sources	²⁴¹ Am but applicable to alpha beta and gamma	3.8 to 400 cm ² Thickness varied 0.75 to 1.14 mm 344-18800 Bq/g	Low emission efficiency for alpha sources Uniformity	No	No

CHAPTER 2: NEW APPROACH TO PROVIDE TRACEABLE SURFACE SOURCES

In the previous chapter, a literature investigation was conducted to assess the limitations associated with commercial surface sources and their production methods. This chapter introduces novel approaches to address and overcome the identified disadvantages and to provide surface sources more suited to the needs of D&D.

The production of commercial surface sources is carried out by established methods, as discussed in the first chapter. These sources are flat, rigid aluminum surfaces with areas of 150 cm² (as illustrated in Figure 14). Subsequently, this substrate is fixed to a 3 mm thick stainless steel support to ensure structural integrity (Orano, 2023).

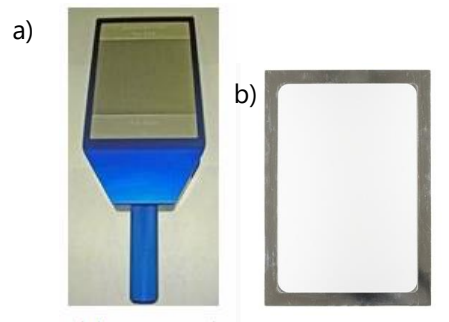


Figure 14: Commercial surface sources produced on a 150 cm² sized aluminum plaque a) alpha-beta hand source, Eckert & Ziegler b) © LEA - Cyril Crespeau, Orano

These commercial sources must conform to the ISO 8769 standards, which cover specific requirements, including material, geometry, and uniformity. Even though these commercially available sources are used to calibrate surface contamination meters in nuclear sites for decommissioning purposes, they are not specifically tailored for the needs of D&D. In particular, they are used to check that the device is operating correctly, and are not aimed to mimic the real surfaces encountered in D&D sites.

There have been efforts to mimic the volume, activity levels, and density of the samples under D&D process (Dean et al., 2007; Pérot et al., 2018). Nevertheless, due to the difference between reference commercial sources and real surfaces, a bias is introduced during measurements whose uncertainties are increased. Within the context of the production of sources, some previous attempts have been made by LNHB research team by using the epoxy resins to provide curved and rough resin sources to mimic the complex shapes in the D&D sites (Chambon et al., 2022).

Furthermore, sources should be non-contaminating to be used on-site safely. Current sources are often covered with a protective layer to fulfill this need. However, this protective layer can cause attenuation, leading to decreased efficiency, especially for sources emitting alpha and low energy beta particles. The reasons mentioned above highlight the importance of developing new surface

sources capable of addressing these concerns and improve the assessment of the performance of contamination monitors used in D&D.

This research aims to create non-contaminating surfaces by establishing robust chemical bonds between the substrate and RNs, thereby eliminating the need for a protective layer. This approach is expected to enhance the efficiency of the sources, particularly concerning alpha and beta particles. Furthermore, immobilizing radioactive elements only on the surface of the sources can help to minimize the self-absorption of the emitted particles. Figure 15 illustrates the difference between commercial sources and the approach of this study.

This study seeks to attach RNs onto selected substrates through surface modification, moving beyond the reliance on weak adsorption bonds, which typically have energies in the range of a few kJ/mol. Instead of physisorption, which involves physical adsorption, the aim is to enable the formation of stronger interactions, including hydrogen bonding, covalent and ionic bonds through chemisorption (chemical adsorption). The enthalpy of adsorption for chemisorption ranges from 80 to 240 kJ/mol. These bonds are formed between the substrate and the RNs through a process known as surface modification, involving grafting or coating techniques. The modifying molecule serves as a bridge between the substrates and the RNs, as illustrated in Figure 15.b. The methods of these chemical modifications, tailored to their respective substrates, are detailed in the following sections.

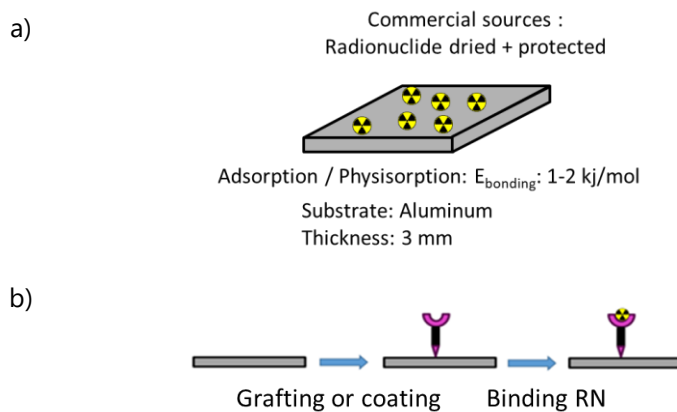


Figure 15: The comparison of the production methods of commercial surface sources (a) and approach (b)

While tailoring modification methods for radioactive surface source production, addressing the specific requirements of D&D areas is crucial. Polymeric surfaces, with their adaptability to mimic various shapes and properties will be described first. Polyethylene Terephthalate (PET) is commonly available as foils and can easily be bent to mimic the shape of a pipe. PET is chosen as primary option for polymeric surface sources. Moreover, the unmodified areas of the PET will maintain their chemical inertness, which is also an interesting feature for the use of these sources on-site. The inherent flexibility and ability to return to its original shape even after deformation, make PET an ideal substrate for source production. Another option is epoxy resins, which can be molded into various shapes, and can maintain structural integrity once cured.

This feature allows for examining the impacts of surface shape on radioactivity distribution (especially roughness). These modified epoxy resins can attach RNs on their surface, replicating the exact shapes of some surfaces found in nuclear sites.

Following the focus on polymers, the study also considers aluminum foil an alternative substrate. Its flexibility and the possibility of being compatible with the ISO 8769 standard makes aluminum foil an alternative substrate for the source production methods. For initial experiments, an aluminum foil with a thickness of 0.3 mm was selected, offering a thinner yet flexible option compared to standard reference sources and the ability to mimic complex shapes. Figure 16 illustrates the three substrates that were chosen in this study.

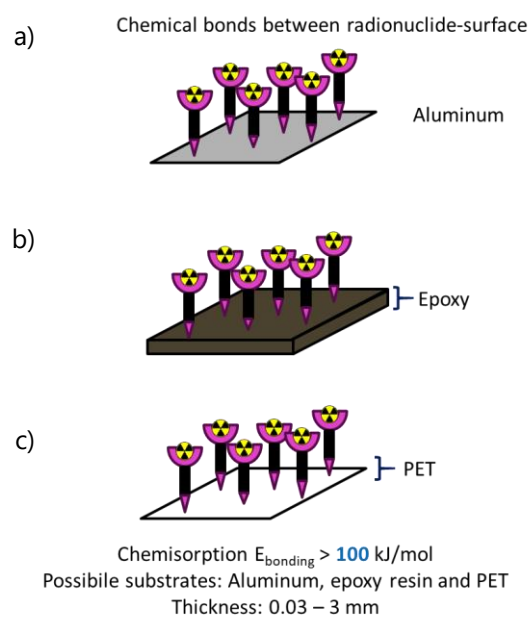


Figure 16: Surface sources produced with approach of the study a) aluminum foil, b) epoxy resin, c) PET

It is important to note that the primary goal of this study is to establish and refine effective methods for surface source production across three different substrates. The initial emphasis is on developing reproducible production techniques, with subsequent adaptations to adjust the diverse shapes and structures encountered in D&D environments.

The custom synthesis of specific complexing molecules to bind RNs (Fryxell et al., 2004) is not compatible with the duration of the thesis. We have therefore chosen to look for commercially available molecules or to carry out relatively standard surface modifications. A specific investigation regarding commercial chemicals capable of efficiently binding RNs to the surface of the substrates was conducted. In particular, molecules capable of attaching radioactivity in an acidic environment (pH 2 or less) would be ideal, which has led us to take an interest in RN separation techniques, including ion exchange resins and ion chromatography.

1 SELECTION OF RADIONUCLIDES OF INTEREST

1.1 RADIONUCLIDES ENCOUNTERED IN D&D SITES

Nuclear D&D activities, depending on the past operations conducted in the facility, are likely to encompass various forms of contamination. Radionuclides have unstable nuclei; this instability arises from a nucleus having excessive mass or an inappropriate neutron-to-proton ratio for stability. The radioactive decay process allows the nucleus to dispose of its excess mass and adjust to neutron to proton ratio towards stability. There are four main radioactive decay modes: fission, alpha, beta, and electron capture (Lehto and Hou, 2011). In the context of D&D, the focus is on characterizing alpha, low energy beta, and low energy gamma emitters, which constitute a significant portion of common waste.

Alpha decay is a typical decay mode for heavier radionuclides, it involves emitting a helium nucleus (positively charged alpha particle (α)) and is prevalent in actinide isotopes like uranium or thorium decay chains. The energies of the emitted alpha particles are always high, typically between 4 and 7 MeV. Often, the decay process leads not only to the ground state of the daughter but also to excited energy levels, leading to gamma emissions (^{241}Am).

Beta decay, common for lighter RNs, involves adjusting the neutron-to-proton ratio by converting a neutron into a proton or vice versa. This process emits either a beta minus particle, physically identical to an electron, having the same mass and electrical charge of -1, and an anti-neutrino, or a beta plus particle, identical with a positron, and a neutrino. Internal transition refers to the de-excitation of the daughter nuclide, occurring through gamma-ray emission or internal conversion, i. e. emission of a bound electron, referred to as conversion electron.

Alpha and low energy betas are challenging to measure accurately in-situ, due to their short range even in air and due to the complexity of the matrices. Therefore, rough or curved surfaces contaminated with radionuclides emitting such radiations are especially difficult to characterize, due to the different source-to-detector distances in the same sample. To handle this issue, the development of specialized reference sources designed to replicate rough surfaces would be instrumental in enhancing the accuracy and reliability of this measurement system.

As alpha emitters are among the most difficult to measure, the focus of this study was placed on producing sources of actinides. The transuranic elements such as neptunium, plutonium, americium, and curium, produced in nuclear reactors and explosions, are particularly interesting.

1.2 RADIOCHEMISTRY OF ACTINIDES

In the context of D&D, the primary focus has been placed on alpha emitters, given their significant presence on D&D sites. Within this scope, actinides, being predominantly characterized by alpha emitters with some low-level gamma emissions, are focused on. Consequently, this section is dedicated to investigating the radiochemistry of actinides.

Actinides constitute a group of 14 elements, characterized by the filling of 5f orbitals, similarly to lanthanides, in which the 4f orbitals are filled. The actinides display a more complex chemistry compared to lanthanides, including both natural decay series elements and artificial actinides. This group is divided into light actinides and transuranium elements.

Among actinides, trivalent actinides are known for their stability, therefore many research efforts were focused on this redox state. Among the trivalent actinides, Americium (Am) and Curium (Cm) are identified as the most common one. The electronic configurations of these elements are [Rn] 7s² 5f⁷ for Am and [Rn] 7s² 5f⁷ 6d¹ for Cm (Lehto and Hou, 2011). Their characteristic oxidation state is +III, like most lanthanides.

Americium and curium are part of the transuranium group and are formed by successive neutron captures and beta decays originating from uranium and plutonium in nuclear fuel and nuclear explosions. All the americium and curium isotopes undergo the alpha decay mode. Their distinct energy levels associated with alpha energies permit simultaneous measurement through alpha spectrometry. While curium isotopes exhibit multiple gamma emissions, the intensities of these emissions are generally too low to be used for the detection of this RN. In contrast, ²⁴¹Am stands out due to its 59.54 keV gamma emission, facilitating direct measurement from some samples. Therefore, ²⁴¹Am has been selected as the model actinide for this research, aligning with the specific requirements and challenges encountered in D&D.

Frequently, europium represents all trivalent actinides; additionally, it has the advantage of emitting an easily measured gamma emission compared to the actinides (Lehto and Hou, 2011). Europium is the nearest lanthanide analog for americium, while gadolinium corresponds to curium. Although americium can occur in several oxidation states from +II to +VII, +III is most relevant under ordinary redox conditions prevalent in natural systems (as seen in Figure 17).

The +IV oxidation state becomes relevant primarily within basic conditions. Therefore, this discussion exclusively concerns the +III oxidation state, which is the most stable. The hydrolysis behavior of Eu and Am is similar to that of other actinides and lanthanides, starting around pH 5-6.

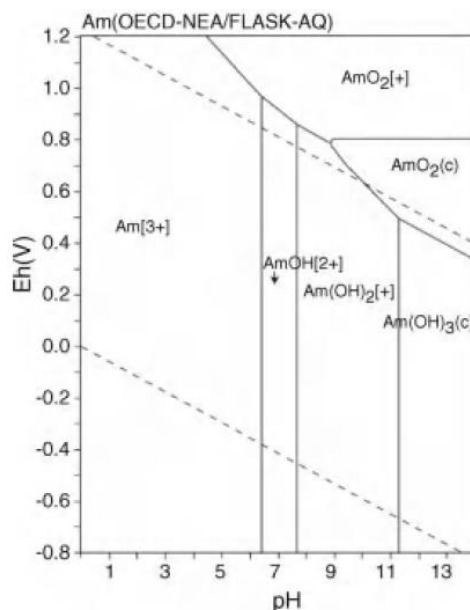


Figure 17: E-pH diagram of americium in 10^{-10} M solutions (Lehto and Hou, 2011).

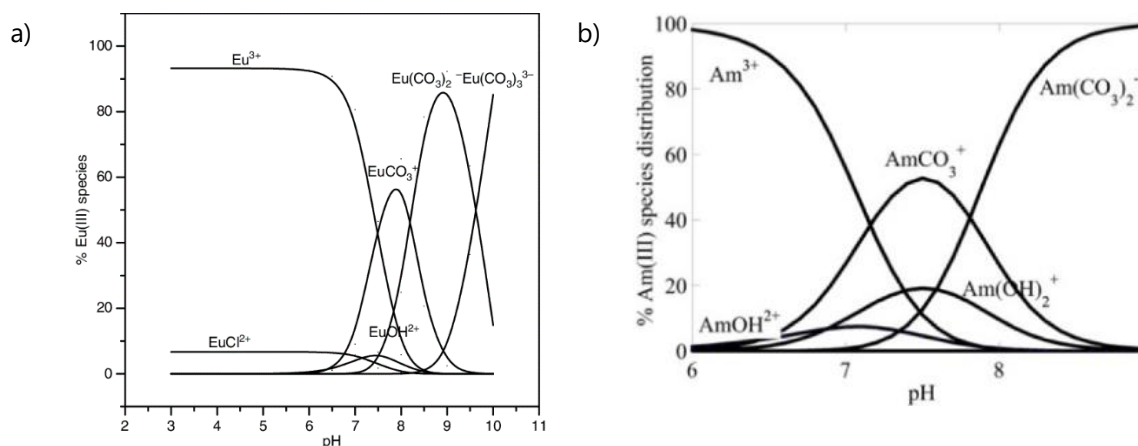


Figure 18: Relative species distribution (%) diagrams for a) Eu(III) (Plancque et al., 2003) and b) Am(III) as a function of pH in aqueous solution containing carbonates under ambient conditions (Ioannidis et al., 2023)

In Figure 18, both speciation diagrams reveal a similar behavior between Eu and Am. Given their analogous chemistry, this research initially began with ^{152}Eu , and once the optimization studies were complete, the production of sources involving Am was performed.

2 APPROACH OF THE STUDY: SURFACE MODIFICATION

This section investigates the possible approaches to achieve surface modification on the chosen substrates.

Two predominant methodologies exist for the introduction of functional groups onto surfaces (Neouze and Schubert, 2008). The first approach consists in introducing a bifunctional organic compound in a single step (Figure 19.a). The bifunctional organic molecule contains one functional group (denoted as "X") that attaches to the surface, while the secondary group ("Z") is the group that the surface is functionalized with. If the interaction between the surface and the "X" group is through covalent bonding, the process is called "grafting". Coating can also be described with this one-step approach, if more than one monolayer of the bifunctional molecule is deposited onto the substrate.

The modification by two steps (Figure 19.b) employs a sequential process, initially reacting a bifunctional compound (X-Y) with the surface. Herein, "Y" serves as a coupling site, as this Y end group can be transformed into the final functional group "Z".

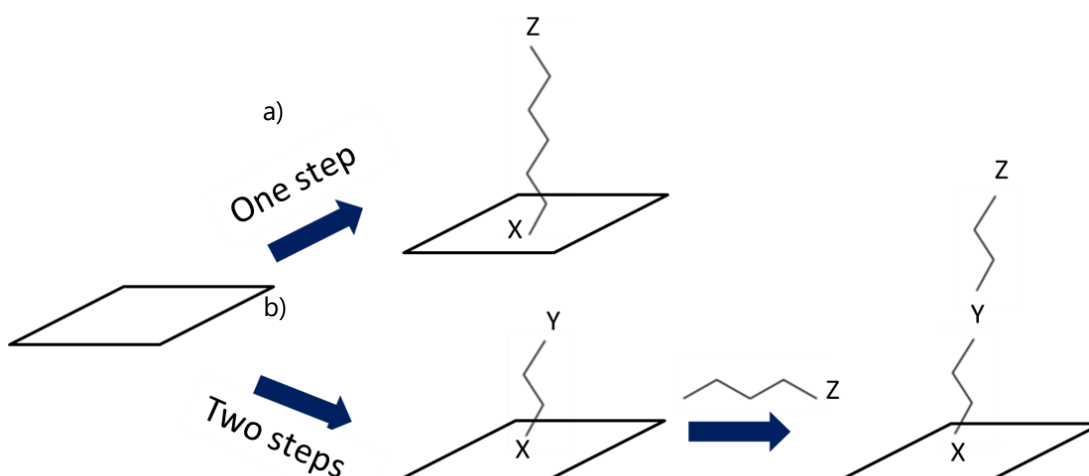


Figure 19: Possible approaches to modify the surface of a substrate a) one step, b) two steps. Both identified methods for grafting molecules onto substrates are applicable, with a notable preference for the one-step approach due to its simplicity with a single chemical, rather than modifying the terminal functionality.

The investigation detailed in the next parts began with an identification of suitable terminal groups, known as "Z", at the end of the grafting molecule, intended for binding to Europium and Americium. Afterwards, a detailed examination of the possible "X" functional groups, able to attach onto the chosen substrates, aluminum and polymer, was conducted. Eventually, suitable commercial molecules were chosen. The final selection of a suitable molecule and its application method will be determined based on comparison of these alternatives.

3 THE CHEMICAL FUNCTIONS FOR RADIONUCLIDE BINDING

This section explores the chemical functionalities that are favorable for binding trivalent RNs, especially ^{241}Am , with a focus on resin utilized to concentrate and/or separate RNs. An investigation of ion exchange resins is undertaken, assessing the conditions critical for their optimal performance, including the influence of pH levels.

3.1 THE MECHANISMS OF EXTRACTION RESINS

Ion exchange resins have different affinity values depending on the functional groups in the resin structure and on the solvent nature and concentration. In this section, this will be explained with more details.

The main mechanism of extraction resins is ion exchange. It consists in the separation of ions from a solution using solid inorganic oxides or organic ion exchange groups with negative or positive charges. The matrix of an ion exchange membrane maintains electro-neutrality through a balance of oppositely charged ions, referred to as counter-ions. These counter-ions, which are free to move within the structure of the membrane, can be stoichiometrically and reversibly exchanged with ions of the same charge from an adjacent electrolyte solution. Ion exchange resins, which comprise cross-linked polymer networks, contain insoluble phases to which ions are electrostatically bound, are significantly utilized in separation of compounds with varying electrical charges (Alexandratos, 2009). The exchange of these counter ions within the matrix is facilitated by either diffusion or the influence of an electric field (Alexandratos, 2009).

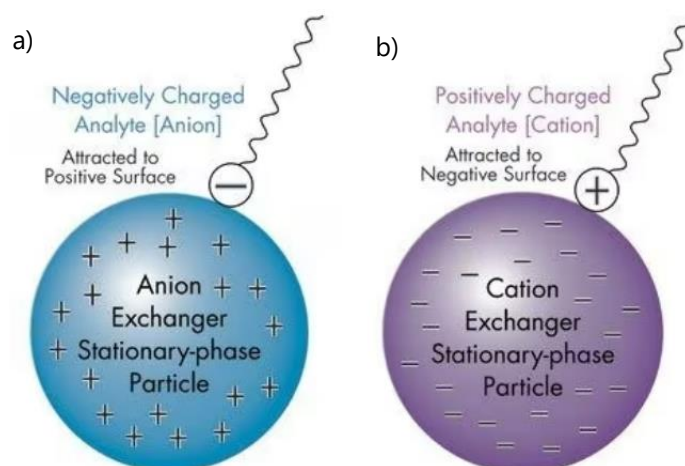


Figure 20: Principle of Ion exchange resins a) anion exchange resin, b) cation exchange resin

Upon contact with a solution containing ions of the same charge, a substitution reaction takes place with these counter ions (Martin et al., 2013). All ions, either anions or cations, are in equilibrium between the mobile phase and the stationary phase (El Ouardi et al., 2023). Depending on the charge of the groups, they are known as anionic exchangers or cationic exchangers. An anion-exchange material will be positively charged (Figure 20.a), whereas a cation-exchanger needs to be negatively charged (Figure 20.b).

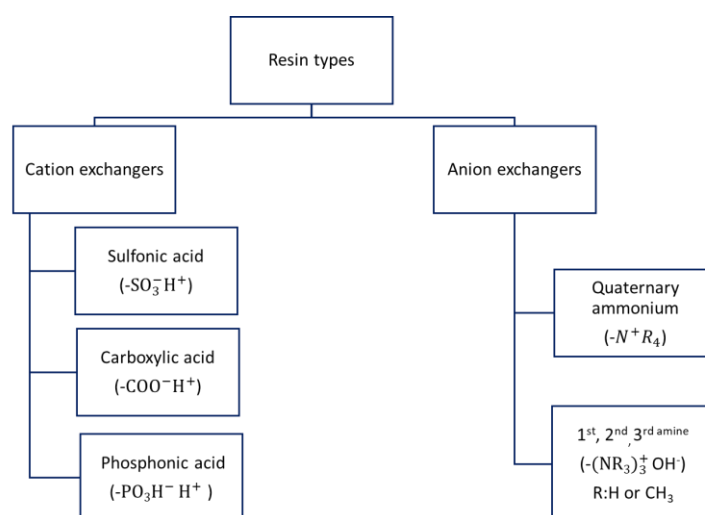


Figure 21: Functional groups found on some typical ion exchangers

There are two types of interaction occurring between these functional groups and the targeted ionic species: ion pairing or ion substitution of the counter ions in the resin, and coordination bonding or chelating interaction, where electron donor species in the ion exchange resin interact with the target species (Alexandratos and Quillen, 1990; Silva et al., 2018). The classification into strong and weak ion exchange properties relies on the pH range within which the resin is capable of ionizing. This distinction is crucial for selecting the appropriate functionalization groups, keeping in mind that the aim of this study is to attach trivalent lanthanides or actinides at low pH, see speciation diagrams as shown in Figure 18.

The most common functional groups are shown in Figure 21. Sulfonic acids are classified as strongly acidic cation exchangers, and carboxylic acids are known as weakly acidic cation exchangers. Additionally, the quaternary ammonium compounds, encompassing types 1, 2, and 3, are identified as strongly basic anion exchangers, whereas amine and polyamine groups are categorized as weakly basic anion exchangers. The chelating ion exchangers include phosphonic, phosphoric, aminophosphonic, and thiol groups (Silva et al., 2018)

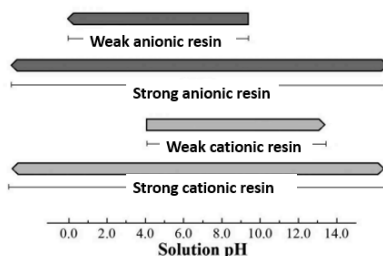
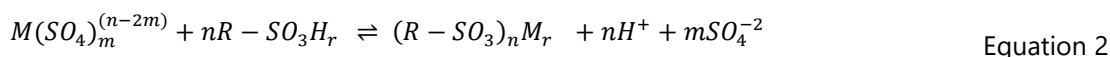


Figure 22: Operating pH range of functional groups in cationic and anionic resins (Silva et al., 2018)

Based on the information from Figure 22, the focus should be on the more functional groups that have a broader range of working conditions for example, strong cationic and strong anionic exchangers.

For example, the metal M extraction reaction with sulfonic acid groups is shown in Equation 2.



Where R-SO₃H_r represents the sulfonic acid group of the resin (Hermassi et al., 2022).

Ligands containing phosphorus groups play an important role as chelating agents for metal ions. These ligands demonstrate strong coordination abilities, leading to significant ionic complexation under highly acidic conditions (Alexandratos et al., 1998).

Inorganic ion exchangers also exist, such as alumina, silica and zirconia, collectively referred to as hydrous oxide ion exchangers. These metal hydroxide compounds exhibit both cation and anion exchange properties, impacted by pH conditions. At higher pH values, cation exchange behavior becomes more prominent, while at lower pH, conversely, anion exchange behavior becomes more significant (Ion Chromatography, 1990).

Manganese oxides, containing Mn(IV) and Mn(III) ions, have a negatively charged framework structured around exchangeable K⁺ ions. Studies focusing on ion exchanges in MnO₂ suggest that following the exchange of K⁺ ions, MnO₂ layer exhibits a “memory effect” for the cation size (Bartoś et al., 1997). Cations with an ionic radii close to that of K⁺ should show a better affinity compared to others.

3.2 COMMON EXTRACTION RESINS FOR ACTINIDES

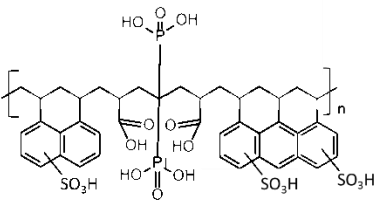
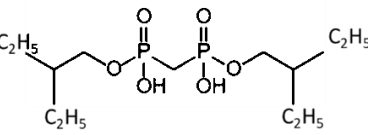
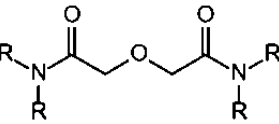
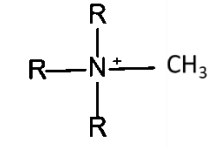
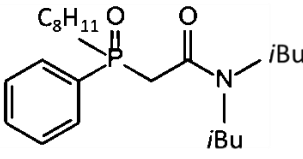
Extraction chromatography resins play a crucial role in radiochemical separations by employing a similar mechanism to solvent extraction. In this process, reagents typically used in solvent extraction and functioning as the stationary phase, are impregnated into a porous, inert matrix, such as silica gel or an organic polymer. These resins are notably useful in the separation of actinides and lanthanides (Lehto and Hou, 2011). A detailed overview of various resins and their properties is presented in Table 5.

The weight distribution coefficient D_w value (mL/g) is a key parameter in separation processes that indicates the retention property of an element on a resin in a specific medium (such as HCl, H₂SO₄, HNO₃) (Marinov et al., 2016). This value can be calculated as shown in Equation 3. In this context, C_{eq1} represents the equilibrium concentration in the organic phase, while C_{eq2} denotes the equilibrium concentration in the aqueous phase. A_0 (Bq) refers to the activity of the initial solution, and A_{eq} (Bq) to the activity of the equilibrium solution.

$$D_w = \frac{(C_0 - C_{eq})}{C_{eq}} \quad \text{Equation 3}$$

From Table 5, a comparison can be drawn among the ion exchange resins, ranking them from the highest to the lowest selectivity for americium. The order is as follows: Dipex, Diphonix, DGA, TRU, and TEVA Resin. Through the literature review, phosphonic acid and sulfonic acid stand out as favorable ligand candidates for RN binding, particularly for trivalent actinides or lanthanides. Quaternary ammonium groups are also tested due to their commercially available options, even though they are less favorable.

Table 5: Examples of resin types

Resin type	Elements affinity K_d max value [solvent concentration]	Functional group	Usage of separation
 <p>Diphonix Resin (Kim et al., 2000)</p>	Am(III): 10^8 [0.1 M HCl] An (III), An(IV) and An(VI) oxidation states	Diphosphonic acid, sulfonic and carboxylic acid	Ion exchange
 <p>AC Resin (Dipex Resin) (Horwitz et al., 1997)</p>	Am (III) : 2×10^8 [1 M HCl] Pu(IV): 2×10^7 [0.2 M HCl] Th(IV): 1.5×10^7 [0.02 M HCl] Np(IV): 10^7 [0.1 M HCl] U(VI) : 4×10^6 [0.03 M HCl]	Phosphonic acid groups	Extraction
 <p>DGA Resin (Horwitz et al., 2005)</p>	Am (III) : 7×10^3 [5 M HCl] An(III) and Ln(III) Pu: 1.5×10^5 [4 M HCl] Th: 8×10^3 [8 M HCl] U: 2×10^3 [5 M HCl]	Diglycolamide	Extraction
 <p>TEVA Resin (Horwitz et al., 1995)</p>	Am(III): 1×10^{-1} [10 M HCl] Pu(IV): 8×10^4 [1 M HCl] Tc (VII): 7×10^4 [0.1 M HCl] U(VI) : 2×10^3 [7 M HCl] Np(IV) : 1×10^3 [10 M HCl] Th (IV) : 1×10^{-1} [10 M HCl]	Aliphatic quaternary amine (Aliquat® 336)	Extraction / Ion exchange
 <p>TRU Resin (CMPO) (Horwitz et al., 1995)</p>	Am(III): 1.5×10^1 [8 M HCl] Transuranium elements, An(IV) or An(VI) Pu(IV): 10^6 [3 M HCl] Np(IV): 2×10^5 [8 M HCl] Th(IV): 6×10^4 [6 M HCl] U(VI): 4×10^3 [3 M HCl]	Phosphine oxide	Extraction
MnO ₂ coated Resin: impregnated on diphonix resin (Surbeck, 2000)	pH: 2-3 for U(VI) pH: 4-8 for Ra(II)	MnO ₂	Ion exchange

Moreover, the literature indicates that MnO₂ thin films possess selective adsorption properties for certain divalent RNs such as Ra(II), UO₂²⁺ as was explained in the previous section. These films are used to extract RNs from wastewater and measured directly as a radioactive source with alpha spectrometry.

Furthermore, in the application of Mn oxide coatings, numerous studies have elucidated the mechanism underlying the binding process of RN on such coatings. The oxidation process applied to the substrate is believed to involve the adsorption of low-valent metal ions onto Mn oxides, followed by electron transfer (Li et al., 2024).

This insight is pivotal in guiding the selection of functional groups for subsequent exploration and potential application in RN binding, linking back to the central theme of investigating suitable chemical functionalization approaches.

4 ATTACHMENT OF CHEMICALS ON THE SURFACE

Now that the functions to be placed on the surfaces are identified, the different possibilities to modify the substrates chosen will be described. Polymeric surfaces will be treated first, then aluminum will be considered.

4.1 POLYMERIC SURFACES

Polymer-based materials have widespread use across various sectors, including adhesives, biomaterials, protective coatings, composites, fibers, and thin films. These applications often demand specific properties such as chemical composition, hydrophilicity, surface roughness, crystallinity, electrical conductivity, and lubricity. Standard polymers, however, typically lack the necessary surface characteristics required for specialized uses. Consequently, surface modification techniques have gained significance within the plastics industry to convert economical synthetic polymers into high-value products. The modification of a polymer surface can be achieved through a range of chemical and physical methods. In the following section, the structure of the polymeric substrates and the methods to modify their surfaces are given in detail.

4.1.1 The structure of PET

PET is the most commonly used thermoplastic polymer, renowned for its good mechanical strength, versatility, corrosion resistance, toughness and fatigue resistance especially at elevated temperature (Chen et al., 2010; Mui et al., 2018). However, due to its low surface energy, it exhibits from poor adhesion, wettability and biocompatibility. Consequently, there have been numerous attempts in the literature to improve the surface properties of PET through modification. In this section, the investigation regarding the possible modification methods for PET surfaces are described.

A fundamental challenge with PET is its lack of inherent reactive functional groups on the surface, making direct covalent attachment difficult. To initiate surface modifications on PET, it is essential

to introduce free chemical reactive species onto the surface (N. Bui et al., 1993). Using wet chemistry techniques, organic synthesis can be conducted at the solid-liquid interface. Hydrolysis can be used to cut the ester groups of the polymer chains, liberating carboxylic acids and hydroxyl groups. The, through selective activating reactions, it is possible to either increase the number of carboxyl groups or hydroxyl groups at the chain ends of PET (Boxus et al., 1996).

4.1.2 The structure of epoxy resin

The composition of epoxy resins usually involves multiple components, engaging in cross-linking processes through either homopolymerization or a combination of different monomers (Gonzalez et al., 2012). The key element in these reactions is the epoxy monomer, distinct for its oxirane functional group comprising a three-member ring formed between two carbon atoms and one oxygen, as shown in Figure 23. This unique structure, characterized by high strain and electronegativity of carbon and oxygen, makes the oxirane group more reactive compared to standard ethers. This reactivity is pivotal in enabling the ring-opening reactions for the curing process of epoxy resins.

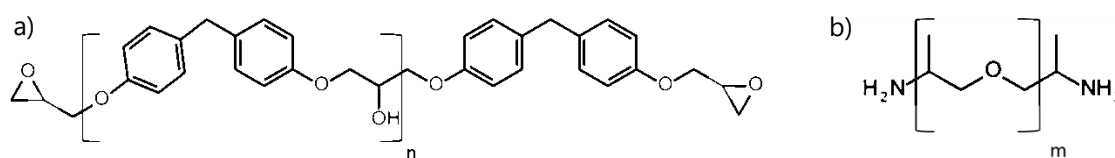


Figure 23: Chemical structure of the epoxy resin a) Part A: Epoxy polymer, b) Part B: Amine oligomer

Epoxy resins, a family of thermosetting materials, are extensively used as adhesives, coatings and matrices in polymer composites. Their popularity stems from the low viscosity of formulations, good insulating properties even at high temperatures and robust chemical and thermal resistance (Gonzalez et al., 2012). These resins can be described as 3D polymer networks, created through the curing process, a chemical reaction between monomers. In this study, by taking advantage of the low viscosity of epoxy resins, complex geometries can be molded. Once these monomers undergo the curing process, they solidify, effectively maintaining the intricate shapes they have been formed into.

In forming an epoxy resin network, two critical stages are gelation and vitrification. During gelation, primary amino groups (R₂) undergo sequential transformations into secondary and tertiary amino groups. When R₁ (Epoxy polymer part A) and R₂ (amine oligomer) blocks in the molecular structure contain a second reactive group, such as oxirane or amino groups, more molecules are added at both the branched ends and with new monomers (as shown in Figure 24). This reaction causes an increase in both the molecular weight and the polydispersity of the compound until a single macromolecule is formed. If the temperature is high enough, the state of the system irreversibly shifts from a liquid-like to a rubber-like form, signaling the formation of a gel. For epoxy/amine, the chemical process that leads to network formation can be showed according to the scheme in Figure 24:

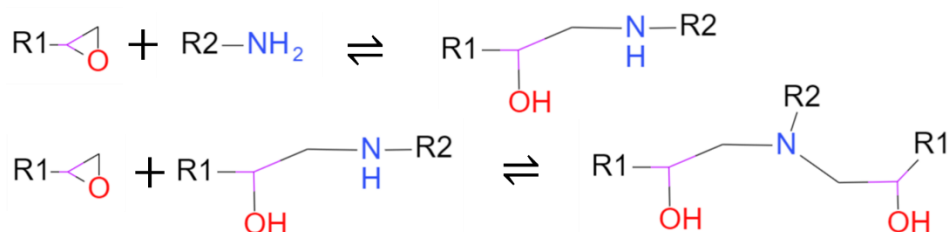


Figure 24: Epoxy/amine reaction scheme (Gonzalez et al., 2012)

In the subsequent section, an investigation regarding existing chemical grafting methods aimed at enhancing the surface properties of PET or epoxy resins is conducted. In particular, attention is given to studies involving the formation of hydroxyl bonds, which is a convenient anchoring group for functionalization on the surface.

4.1.3 Chemical methods for forming hydroxyl bonds (-OH)

Various techniques have been used to modify polymeric surfaces for different purposes, e.g. improving biocompatibility, facilitate drug loading, clothing, furnishings and packaging (Boxus et al., 1996; N. Bui et al., 1993; Xu et al., 2015). In all studies, polymeric surfaces were first activated to form reactive functions such as hydroxyl groups, carboxylic acids, amino groups. To increase the reactive functions on the surface, the focus was on the formation of hydroxyl groups both for PET and epoxy resin.

4.1.3.1 Formation of hydroxyl bonds on PET substrates

In one study, the goal was reactivating polymer-end groups of PET, such as carboxyl and hydroxyl functions, to serve as an anchor for bioactive molecules (Boxus et al., 1996). In our study, the method used for activating the ends of the PET will be employed to bind RNs instead of bioactive molecules.

For the PET substrate, forming hydroxyl bonds on the surface was performed sequential steps of treatments as shown in Figure 25, which is including hydrolysis and reduction of the hydrolyzed groups on the PET surface. Through reductive reactions, carboxylic acid end groups on the PET are converted into benzyl alcohol which aimed to obtain to graft the chemical molecules onto the surface of the PET.

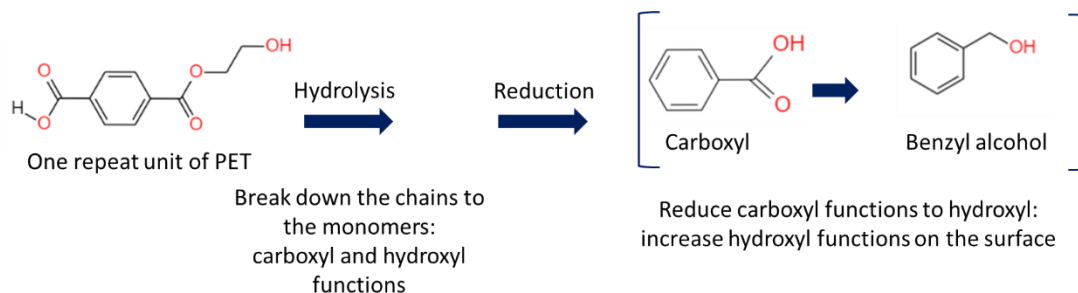


Figure 25: The pathway of the hydrolysis and reduction reactions

The hydrolysis and reduction method, as investigated by Boxus, is applied to increase the hydroxyl groups on the PET surface to serve as a grafting function for sulfonation (Boxus et al., 1996). Initially, the PET surface undergoes hydrolysis to break down its first layer into constituent monomers using a strong alkaline solution of NaOH and acetonitrile, after one night of immersion at room temperature. The basic conditions and water initiate the depolymerization process through hydrolysis, with acetonitrile acting as a co-solvent to enhance the reaction. This basic hydrolysis with NaOH (at 0.88 mol/L) in aqueous acetonitrile creates new chain ends through ester cleavage.

An alternative approach to hydrolysis also involves immersing PET samples in a mixture NaOH solution and ACN for one night at 60 °C. For this method the concentration of NaOH is slightly higher (0.12 mol/L).

The hydrolyzed PET is then converted into a chemically stable and reduced form using sodium borohydride (NaBH_4) as the reducing agent, with catechol and anhydrous THF acting as stabilizers and solvents. The mixture of NaBH_4 (0.5 mol/L) in dry THF is stirred for one night at room temperature.

In another publication (Mougenot et al., 1996), this team was interested in the functional characterization and the tailored-made derivatization PET surfaces to enhance carboxylic chain ends. They also quantified the number of chain ends per unit surface to be up to dozens of picomol per cm^2 , corresponding to a derivatization of a few percent of the polymer repeat units.

4.1.3.2 Formation of hydroxyl bonds on epoxy resin substrates

A useful research aimed to enhance the adhesive properties between copper and polymer structures using surface functionalization on epoxy-novolak resin (Siau et al., 2004a). For this study, the surface was oxidized with a KMnO_4 or a $\text{K}_2\text{Cr}_2\text{O}_7$ treatment.

The effect of the reaction temperature and the use of swelling agents were tested. They immersed the samples at 40 °C and 80 °C for 10 min in KMnO_4 and $\text{K}_2\text{Cr}_2\text{O}_7$ solutions for oxidation purposes, which means here forming hydroxyl bonds. Therefore, the protocol described in this article was followed and improved upon, to obtain KMnO_4 -treated epoxy resins, then sulfonated resins for RN binding.

Findings of Siau revealed that the oxidation treatment led to an increase in roughness. They observed that $K_2Cr_2O_7$ resulted in less roughness compared to $KMnO_4$. Furthermore, they found that increasing the temperature also increased the roughness of the surface.

Basic $KMnO_4$ solution is frequently used as an oxidizing agent in organic chemistry, due to capability to oxidize primary and secondary alcoholic functions. In the context of epoxy resin, this solution effectively breaks the R-O-R bonds, causing certain parts of the cured polymer surface to dissolve into the solution, and resulting in a rougher surface (Siau et al., 2004a). The treatment also renders the surface more hydrophilic.

The cured epoxy-novalac resin used by Siau contains functional groups such as secondary alcohols and ether functions, which undergo oxidation, leading to formation of ketones, aromatic and primary alcohols, as depicted in Figure 26.

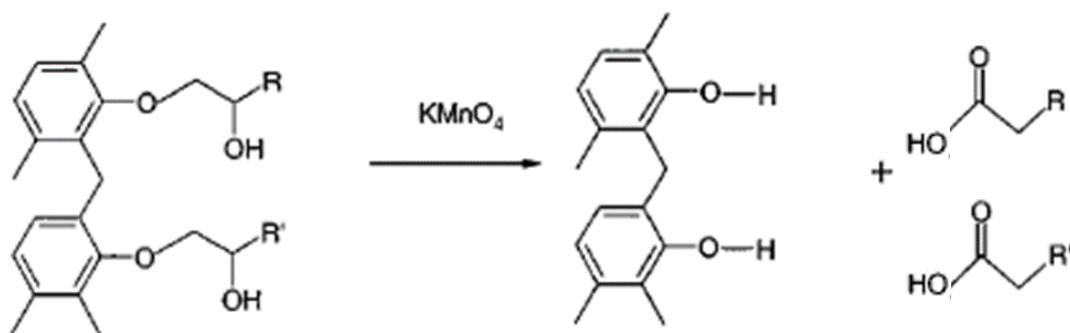


Figure 26: Oxidation of functional groups in the polymer chain (Siau et al., 2004a)

The primary alcohols can further oxidize into carboxylic acid functions, or, given the basic nature of the solution, be transformed into carboxylate ions. As these surface groups react, they take part of the polymer with them, causing continuous evaluation both of the surface and its functional groups. This oxidation process replaces functionalities with more polar ones, resulting in increased hydrophilicity of the surface.

This breakdown reaction occurs in four steps, with each step involving the degradation of a part of the polymer chain at the polymer-liquid interface due to reactions with the oxidizer. The active group on the epoxy is progressively transmitted down the chain, and after oxidation, some parts are being dissolved into the liquid, reducing the thickness of the polymer. Only the groups located on the surface are active and can react with the oxidizing agent. The groups deeper in the polymer temporarily remain inactive or "frozen" due to the steric hindrance from neighboring polymer molecules. Swelling agents function by increasing the polar groups on the surface, allowing them to react with the oxidizing agents and increasing the number of the polymer breakdown groups at the surface.

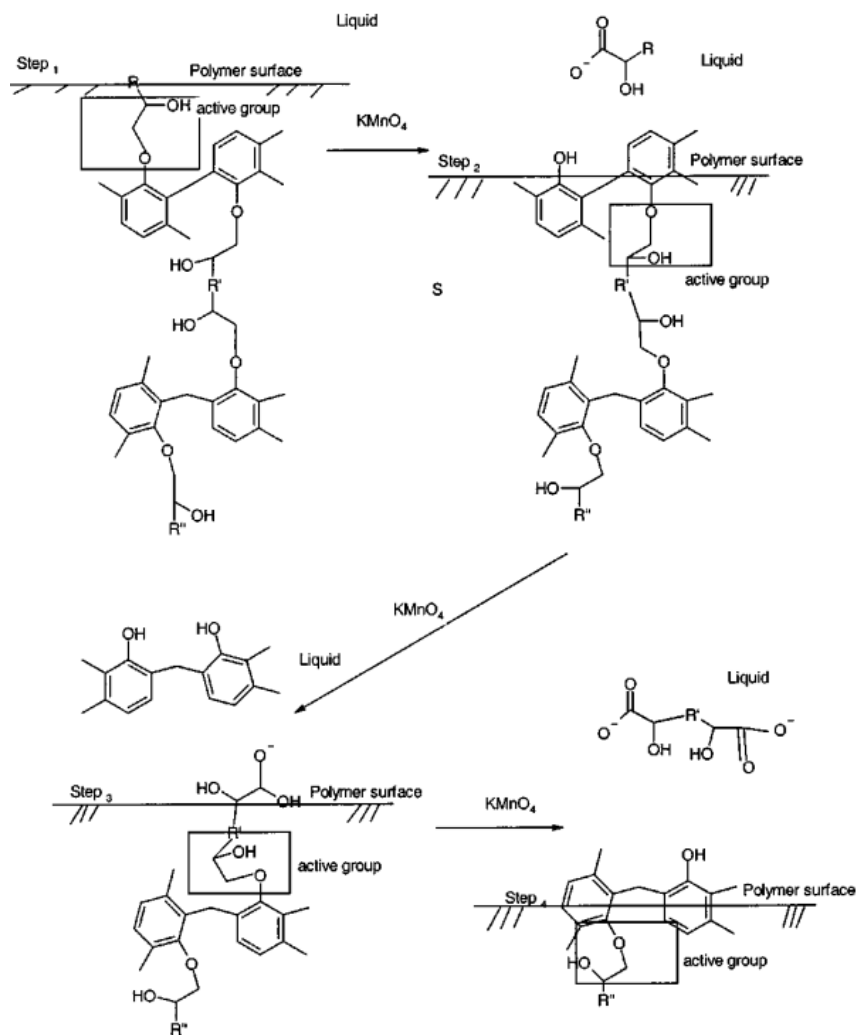


Figure 27: The order of the polymer chain breakdown (Siau et al., 2004a)

4.1.4 Sulfonation of polymeric substrates

As mentioned earlier, sulfonic acid groups have been found to be highly effective in binding RNs, based on investigations into ion exchange resins. Therefore, this particular investigation focuses on the grafting of polymer surfaces with sulfonic acid groups and thoroughly examines the techniques employed for their grafting.

Recent literature has explored the application of sulfonation grafting techniques on a variety of materials, such as polyether ether ketone (PEEK), Proton Exchange Membranes (PEM), polyethylene terephthalate (PET), and epoxy resins. These studies often utilize chemicals containing sulfonic acid groups to enhance surface properties. The improvements include hydrophilicity, enhanced adhesion, improved biocompatibility, conductivity, and anti-fogging capabilities (Uyama et al., 1998). Such studies are invaluable for understanding the process

and implications of sulfonating polymeric surfaces.

One notable study aimed to create a polyphosphazene grafted butylphenoxy membrane for proton exchange (Ouadah et al., 2018). In this research, 1, 4-butane sultone played a crucial role to graft on the proton exchange membrane. The process typically involves the use of aliphatic sulfonated groups, such as 1, 4-butane sultone, a compound known for its commercial availability and ability for nucleophilic attacks, particularly reacting with the nitrogen in amino groups. Furthermore, sultones are utilized to quaternize nitrogen in tertiary amines, facilitating the formation of zwitterion polymers. This is particularly relevant when considering the NH_2 groups in Part B of the epoxy resin structure.

The experimental procedure involved stirring a DMSO solution and NaH with a butylphenoxy membrane at 45 °C for 12 hours. Following that 1, 4-butane sultone was added dropwise, and the mixture was stirred at 100 °C for 24 hours before being precipitated in isopropanol. The final polymer was then dried at 50 °C for 12 hours under vacuum. A key finding of this study was that they obtained an increased concentration of acid groups in the polymer, which also led to a higher conductivity than Nafion membrane (Ouadah et al., 2018). This suggests that the technique could be effective for surface source production. Additionally, the study offers an opportunity to compare Nafion membranes with modified polymeric surfaces as Nafion membranes were previously used in surface source production.

Sulfonation reactions involving an alcohol group and 1,4-butane sultone have been reported in the literature (Berti et al., 2008; Ma et al., 2016). The first step of the mechanism is the activation of OH groups by deprotonation with sodium hydride (NaH). Sodium hydride functions dually as a base and a hydride source (Hesek et al., 2009). It is used commonly to deprotonate alcohols, phenols, amides, ketones, esters, and other functional groups to promote their nucleophilic substitution. The alkoxide anion attacks the carbon close to the sultone group of 1,4-butanediol, leading to the ring opening which is illustrated in Figure 28. The process of deprotonation of an alcohol with a base transforms it into an alkoxide anion (Figure 28.b), which is basic and nucleophilic, enabling its participation in diverse chemical reactions, including both substitution and elimination reactions (Figure 28.c).

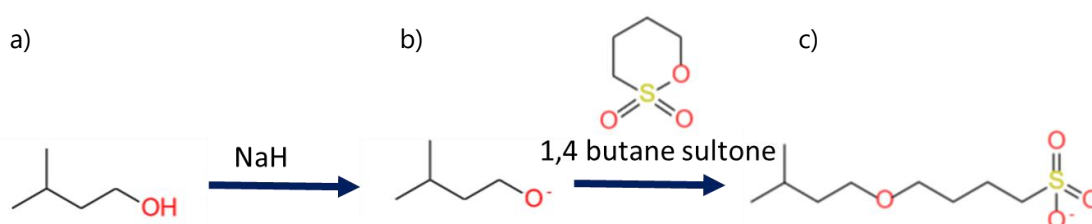


Figure 28: Williamson ether synthesis ($\text{S}_\text{N}2$ mechanism) with 1,4 butane sultone a) alcohol chain ends, b) deprotonation of alcohol and formation of alkoxide anion, c) substitution and elimination reaction

Another study that focused on modifying poly(butylene terephthalate) (PBT) with 1,4-butane sultone has also been investigated. Unlike the previous study, which applied modifications to the surface of the resin, this method was performed during the polymerization of a non cross-linked polymer.

The polymerization method (as shown in Figure 29), involving the simultaneous mixing of all reagents – butane diol, Dimethyl terephthalate, and 1,4-butane sultone – in the presence of a strong base like Na_2CO_3 at 215 °C for 1 hour and the addition of a catalyst like tetrabutyl titanate (TBT) at 180 °C. The reaction then completes at 215 °C for 30 minutes (Berti et al., 2008).

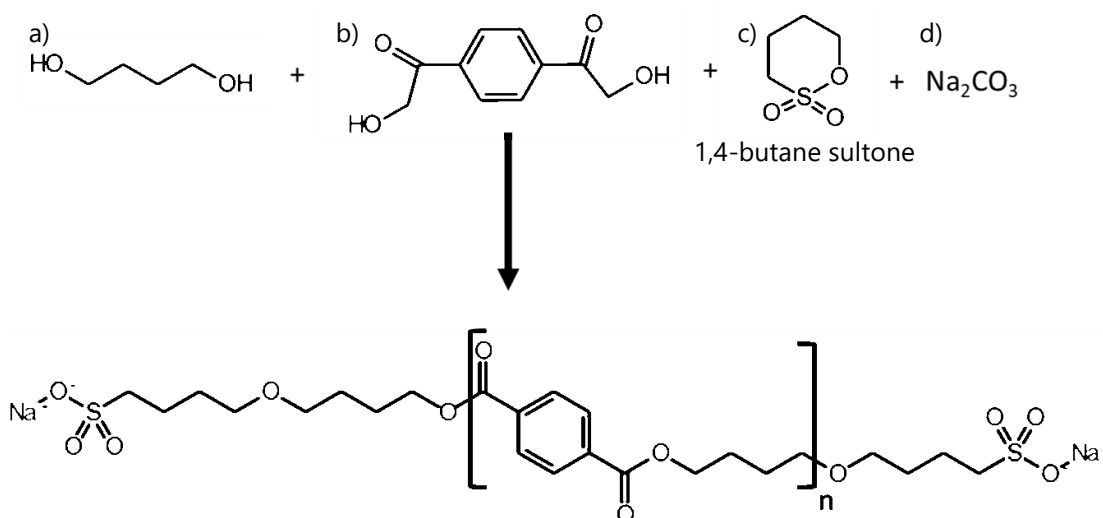


Figure 29: One step method to produce sulfonic acid group grafted on polybutylene terephthalate a) Butane diol (BD), b) Dimethyl terephthalate, c) 1, 4-butane sultone, d) Sodium carbonate

4.2 ALUMINUM SURFACES

This section describes various methods to achieve modification on aluminum substrates. In the literature, the modification treatments aim at improving the properties of aluminum substrates, particularly in terms of corrosion resistance, wettability enhancement, and other relevant aspects, such as color resistance. It is crucial to note that while specific molecules identified in these studies may not be directly applicable, they serve as valuable examples of the possible grafting functions for aluminum modification. These examples will be adapted and modified to align with the specific objectives of our research.

In aluminum substrate modification, two primary methodologies have been explored: conversion coating techniques and grafting chemical functions onto the substrate. The literature mentions the presence of traditional inorganic pre-treatment coatings, such as chromium-based solutions (Luschinetz et al., 2007). Nevertheless, in light of their potential risks, there is a growing demand for alternative approaches. One potential alternative, as evidenced by various references, covers

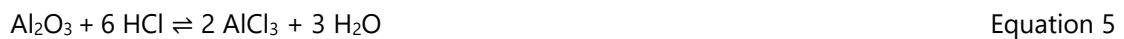
the utilization of solutions containing potassium permanganate (Danilidis et al., 2007; Kharitonov et al., 2020; Siau et al., 2004a; Song et al., 2022). Another alternative is the grafting technique, which utilizes hybrid materials comprising organic and inorganic components (Hubert Mutin et al., 2005). Grafting, in particular, necessitates a series of pre-treatment steps to prepare the surface for subsequent modifications.

4.2.1 Forming Al-OH bonds by etching

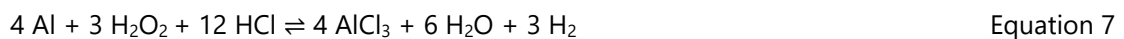
Increasing the number of hydroxyl groups is necessary for grafting on aluminum surfaces. Therefore, some pre-treatments, such as etching, should be applied on the aluminum surface beforehand. The investigation regarding these pre-treatments is detailed in this section.

One research group described a process involving a 0.1 M NaOH solution treatment for 2 minutes, followed by rinsing in deionized water, immersing in 20% v/v solution HNO₃ for 2 minutes, and completing it with another rinse (Muñoz et al., 2018).

Another research group suggested a chemical etching at room temperature for 5 minutes using a 1:1 molar ratio mixture of HCl (1 mol/L) and H₂O₂ (1 mol/L) (Peng et al., 2019). Then, samples were cleaned in ultrasonic bath in deionized water. The selected 1:1 ratio, deemed most effective in the study, will be used in this work, although the strong oxidation effect of hydrogen peroxide in acidic conditions is noted as a potential concern. The oxidizing action of hydrogen peroxide transforms aluminum into aluminum oxide (Al₂O₃), as represented in Equation 4. This oxide layer is unstable in HCl-containing solutions, leading to the formation of AlCl₃, as shown in Equation 5.

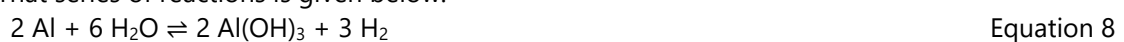


Aluminum, being an active metal, can also react directly with HCl, forming AlCl₃ rapidly (Equation 6), which enhances etching speed and results in a multiscale hierarchical structure. All balance equation can be represented by Equation 7.



Chemical etchants primarily target and dissolve aluminium on higher-energy facets, leading to anisotropic or selective corrosion behaviour.

Another approach involves immersing aluminum in boiling deionized water for an extended period, followed by upright drying. This method results in the formation of a pseudo-boehmite oxide layer (AlOOH.H₂O), a thick aluminum hydroxide layer with excess water (Özkanat et al., 2012). That series of reactions is given below.





Equation 8 forms the aluminum hydroxide bayerite and hydrogen, the second reaction (Equation 9) forms the aluminum hydroxide boehmite and hydrogen, and the last one (Equation 10) formed aluminum oxide and hydrogen (Petrovic and Thomas, 2008). All these reactions are thermodynamically favorable and highly exothermic.

An experimental investigation of the influence of the etching step will be described in Chapter 4.

4.2.2 The investigation of potential grafting molecules

4.2.2.1 Grafting molecules containing silanol groups

In the field of aluminum substrate modification, organoalkoxysilanes and organochlorosilanes, generally represented by the formula $\text{R}_n\text{SiX}_{3-n}$ (where X = Cl, alkoxy), are widely recognized as the most effective coupling molecules (Hubert Mutin et al., 2005). These molecules react with aluminum oxide to form Al-O-Si bonds (Plueddemann, 1991). Recognized as common modifiers for metal oxide surfaces, silanes offer a range of functionalities, such as amino, carboxylic acid, epoxy groups and more. In addition to these advantages, they are also commercially available.

The interaction of alkoxy silanes and chlorosilanes with metal oxide surfaces occurs through condensation reactions. Remarkably, the reactivity of chlorosilanes, like R_2SiCl_2 or RSiCl_3 , is so high that neither water nor catalysts are required to facilitate the reaction. However, modification with silanes can lead to byproducts such as HCl or alcohol, which may alter the properties of the grafted surfaces.

In an alkoxy silane solution, two primary reactions occur: hydrolysis and condensation. First, in the presence of water, the alkoxy groups are sequentially hydrolyzed, forming silanol species as shown in Figure 30. Subsequently, these silanols condense to form oligomers, eventually growing into larger molecules. Organofunctional trialkoxy silanes in aqueous media rapidly hydrolyze under mildly acidic conditions to form monomeric silanol but condense slowly into oligomeric forms. However, this condensation reaction tends to accelerate at pH values above 7 (Abel et al., 2006). Continuous condensation reaction would lead to the elimination of silanol groups, which are crucial for reacting with surface hydroxyls to create covalent bonds on the aluminum surface. The formation of more covalent bonds across the interface increases the durability of the bond. Therefore, it is essential to enhance silane hydrolysis while minimizing silanol condensation.

Surface modification involved heterocondensation between the organosilicon coupling molecule and the inorganic part leads to the formation of Si-O-M bonds (M=metal or Si), while homocondensation between two coupling molecules leads to the formation of Si-O-Si bonds. Accordingly, the structure of the modified surface is governed by the competition between heterocondensation and homocondensation reactions (Hubert Mutin et al., 2005).

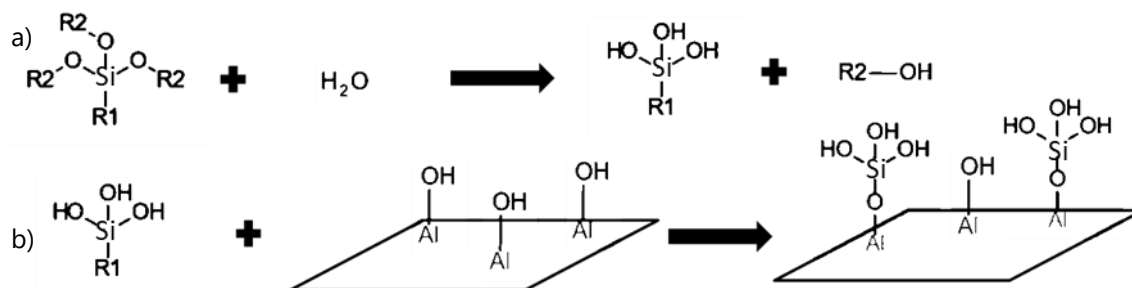


Figure 30: Hydrolysis (a) and condensation (b) reaction of aluminum surface (adapted from (Abel et al., 2006))

In surface modification using organotrialkoxysilanes or organotrichlorosilanes, the balance between hetero and homocondensation depends on the support nature and the water content. Complete monolayer formation requires water presence, yet increasing water content risks forming multilayers through the polymerization of multifunctional organosilicon molecules. Therefore, the quality of surface modification is highly sensitive to the water content of the solvent or to the water adsorbed on the surface of the aluminum oxide.

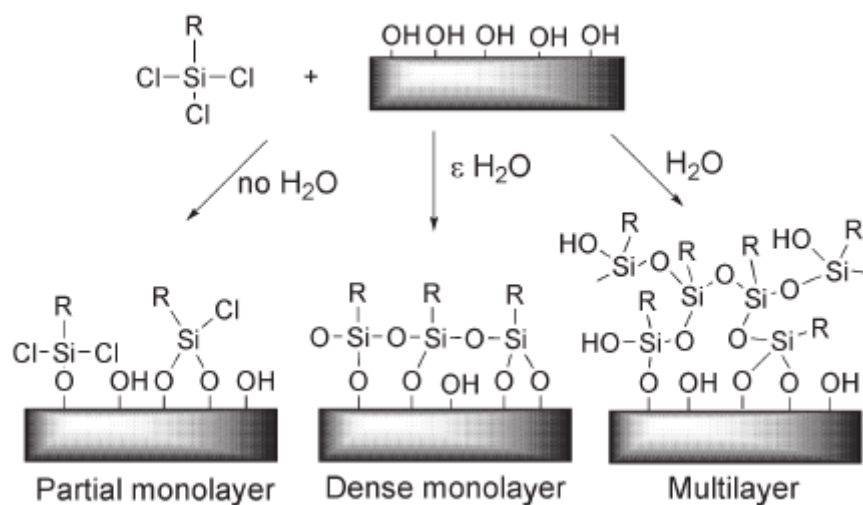


Figure 31: Schematic illustration of the influence of water content on the surface modification (Hubert Mutin et al., 2005)

In Table 6, the grafting groups containing silane functions are listed with their experimental methods

Table 6: Silanol grafting chemicals and their experimental parameters

Aluminum type	Grafting group containing silane (chemical name)	Experimental method
Alumina monolithic columns (Nayak et al., 2019)	3-aminopropyltetraethoxysilane (APTES)	Silanization APTES: CTAB: EtOH:H ₂ SO ₄ 1:0.1:9:0.004 (molar ratios) Drying: room T
8011A aluminum 0.3 mm thick 1.5 x 1.5 cm ² (Rahimi et al., 2014)	1H,1H,2H,2H-perfluorooctyltrichlorosilane (PFO) Surface activator: Methoxide Solvent : Toluene	In a solution of 250 µL PFO and 750 µL toluene heated up to 110 °C
6082-T6 3 x 2.4 x 0.2 cm ³ (Khaskhoussi et al., 2020)	Octadecyl trimethoxysilane (OTMS)	Immersed in 1 v.% OTMS / Toluene for 10 min at room T Drying: oven at 100 °C
2.6 × 2.6 × 0.15 cm ³ Aluminum plates, specifications not given (Yin et al., 2012)	Perfluoroalkyl triethoxysilane (PFO) Solvent : Methanol	0.5 wt.% PFO, 88 wt.% methanol and 10 wt.% DI water, 1.5 wt.% HCl Dipped 4 times, cured at 100 °C

The study of surface modification methods for aluminum monolithic columns with silanes has been a subject of interest in recent research due its straightforwardness and the use of non-toxic solvents. Nayak detailed the mechanism of functionalization via sol-gel synthesis, using a molar ratio of APTES: CTAB: EtOH: H₂SO₄ (1:0.1:9:0.004), incubated at 60 °C for 90 minutes (Nayak et al., 2019).

Yin et al. (2012) employed a grafting method with a long carbon chain chemical that also contains alkoxy silane moieties, to achieve superhydrophobic surfaces on aluminum alloy. The method involved immersing etched samples in a mixture containing 0.5 wt.% perfluoroalkyl triethoxysilane (PFO), methanol (88 wt.%), ultrapure water (10 wt.%), and HCl (0.1 mol/L 1.5 wt.%) by dipping four times, and then curing at 100 °C for 6 h (Yin et al., 2012). This approach was selected due to its chemical efficiency and ease of application.

In contrast, Khaskhoussi proposed another approach, using octa-decyltrimethoxysilane in toluene to form self-assembled monolayers. This method utilized the apolarity nature of toluene to dissolve molecules, aligning and concentrating them on the surface. The reactivity between Si-OH silanol groups and Al-OH aluminum hydroxyl groups was crucial for forming monolayers with long alkyl chains (Khaskhoussi et al., 2020). However, this study and the one of Rahimi et al. (2014) were excluded from consideration for our work, due to their use of toxic chemicals like toluene in the modification process.

From these literature investigations, several commercial silane molecules were chosen and described. Some could be grafted in a single step to yield the desired RN binding functionality, while others required a secondary step to transform the end group of the grafted molecule. One of the example of this two steps grafting method is illustrated in Figure 32 with the transformation of thiol into sulfonic acid groups on the aluminum surface in the second step.

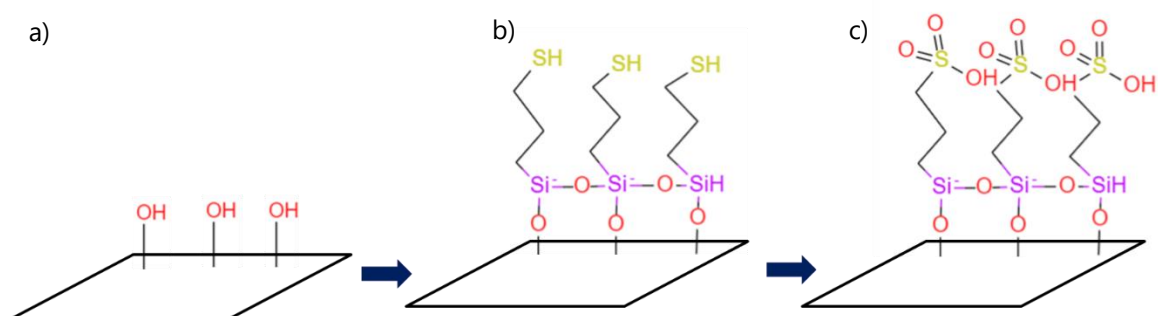


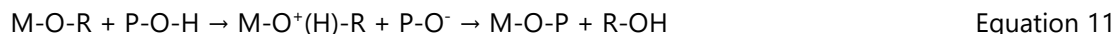
Figure 32: The modification of the end functions on the hydrolysed aluminum surface

a) Hydroxyl functions on the aluminum surface, b) grafting of the silanol groups onto the aluminum surface by silanization, c) transformation of the grafted thiol groups to the sulfonic acid functions by oxidation (Chen et al., 2010)

4.2.2.2 Grafting molecule containing phosphonic acid groups

In surface modification strategies, organophosphorus acids are emerging as complementary alternatives to organosilicon compounds due to their excellent affinity towards metal and transition metal-containing supports such as oxides, hydroxides, and carbonates. Despite being less widespread than their organosilicon counterparts, organophosphorus molecules, are notably less sensitive to nucleophilic substitution, making P-O-C bonds quite stable against hydrolysis (Hubert Mutin et al., 2005).

An important aspect of organophosphorus compounds is their ability to form robust M-O-P bonds, without the competition between hetero and homocondensation reactions seen in organosilicon compounds, which means that can only undergo homocondensation to form P-O-P (Neouze and Schubert, 2008). This characteristic makes them suitable for creating monolayers on metal oxide surfaces, regardless of water content, and enhances their stability, especially in multidentate attachments.



A study suggests that the adsorption of alkyl phosphonic acid on aluminum surfaces proceeds via an acid-base condensation reaction mechanism, forming tridentate complexes with the phosphonic acid head group bound to the oxide film through symmetric P-O-Al bonds (Luschinetz et al., 2007). This method, inspired by earlier studies, was adapted with pre-conditioned surfaces through etching methods, ensuring consistent pre-treatment across all samples. Furthermore, the anchorage of phosphonate groups onto the metal oxide surface can be mono-, bi-, or tridentate. This variability in bonding modes introduces some complexity in

surface modification. Each type of attachment – mono, bi, or tridentate – presents distinct implications for the stability of the resulting bond. The multidentate attachment, in particular, is a critical stabilizing factor for surface modifications, as it can potentially offer enhanced robustness and durability to the modified surfaces (Neouze and Schubert, 2008).

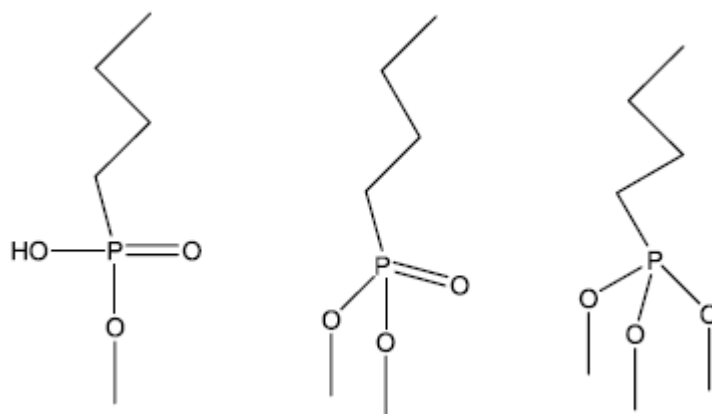


Figure 33: Possible binding modes of phosphonate ligand on the aluminum surface (Neouze and Schubert, 2008)

Table 7: Phosphonic acid grafting with some experimental parameters

Aluminum type	Phosphonic acid molecule	Experimental method
(α -Al ₂ O ₃) (Lushtinetz et al., 2007)	Octadecylphosphonic acid, ODPA	Room T Immersed in 1 mmol ethanolic solution for 1 h.
None (Lubelli and Hees, 2007)	Diethylenetriaminepentakis(methylphosphonic acid)	10 wt.% Na ₂ SO ₄ solution in DTPMP (0.001 M) at pH 8

The application of phosphonic acid grafting, as detailed in Lushtinetz's work, was adapted and enhanced through methodologies described in Lubelli's study, for potential improvements. This research was also directed towards enhancing the protective coating on aluminum surfaces, particularly to increase durability under wet and humid conditions (Lushtinetz et al., 2007).

The adsorption of alkylphosphonic acids on the aluminum surface occurs by an acid-base condensation reaction mechanism. The grafting process is conducted at room temperature, involving the immersion of etched samples in a 1 mmol ethanolic solution of ODPA for one hour. Computational FTIR analysis of this reaction suggested that the absence of a P=O mode in the spectra is indicative of the adsorption process favoring tridentate complexes, wherein the acid binds to the surface via three symmetric P-O-Al bonds.

Another group investigated the inhibition of salt crystallization in porous materials using phosphonic acid molecules like DTPMP combined with Na₂SO₄ salt. We were looking forward to

finding an appropriate method for grafting DTPMP. It focused specifically on the application process setup. It is important to note that the article itself did not involve functionalization onto aluminum. DTPMP (0.001 mol/L) was dissolved in a 10 wt.% Na₂SO₄ solution at pH 8 (Lubelli and Hees, 2007).

4.2.3 Conversion coating techniques

In the literature, several studies focused on the application of conversion coatings to aluminum surfaces, primarily with the goal of improving corrosion resistance on aluminum surfaces. This section provides a thorough examination of these investigations.

The term “conversion coating” refers to the chemical or electrochemical treatment applied to metal surfaces to create a superficial layer consisting of metal oxides, chromates, phosphates, or other compounds that form a chemical bond with the surface. In the metal finishing industry, this term typically signifies transforming a metal surface into a material that more readily accepts applied primers or paints while also providing corrosion resistance in case the outer layer is compromised (Kulinich and Akhtar, 2012).

Chemical conversion coatings in particular, comprise chemical bonds between the coating and its underlying metal which serve as an intermediate layer that is highly adherent due to the presence of these chemical bonds (Song et al., 2022). The conversion coating of metallic substrate in a chemical conversion solution, results in a reaction at the interface, which is given in below.



Where A represents the metal reacting with the medium, B refers to the anion of the medium, and x denotes the electron valence.

The objective of our investigation into conversion coatings and their application methods is to identify some methods for achieving stable coatings capable of binding RNs from acidic solutions. This necessitates the stability of the coating in acidic environments.

In this research, special attention was given to the production conditions of manganese conversion coatings, due to their ability to act as a cation exchanger. In addition, chromium oxide is also a cation exchanger, and therefore was also investigated. Most of the manganese coatings are performed under basic conditions, while chromate coatings are mostly applied in acidic conditions. A significant drawback of chromate coatings is their toxicity and potential environmental harm, especially in large-scale applications, which is not our case (Danilidis et al., 2007; Kharitonov et al., 2020). Despite these concerns, our study will briefly consider chromate coatings to understand the impact of acidic conditions on their application and to compare their radionuclide binding abilities with those of manganese oxide coatings.

This research is organized into three main sections: the application of manganese oxide coatings under acidic and basic conditions, the exploration of chromate coatings as a possible alternative, and the comparison of these coatings.

4.2.3.1 Manganese oxide (MnOx) coating

The structural diversity of manganese oxide makes them suitable candidate for various applications, such as energy storage systems, biosensors, coatings, environmental science, and nuclear science. Our aim is to understand their formation mechanism onto aluminum surfaces.

Manganese oxides exhibit a wide range of oxidation states, from +II to +IV, leading to the formation of minerals with mixed valence states. Known for their significant oxidative capacity, manganese oxides also possess high redox potentials in two redox couples: Mn(IV)/Mn(II) and Mn(III)/Mn(II). The high valence redox couple (Mn(IV)/Mn(II)), with a standard reduction potential of approximately 1.2 V, is comparable to oxygen, enabling the oxidation of a wide range of reduced metal and metalloid species in environment. These include, but are not limited to, Cr, U, As, Se, Tc, Np, Pu, Co, Sb, Tl, and V (Lafferty et al., 2010; Wang and Giammar, 2015; Li et al., 2024). Additionally, manganese oxide is characterized by high sorption, limited crystallinity, substantial surface area, and highly reactive vacancy sites (Szlankowicz et al., 2023). Moreover, the redox capability of Mn oxide particles is affected by various factors. The redox reaction between metals and Mn oxides typically involves three fundamental stages: firstly, metal ions adsorb onto the edge or interlayer of Mn oxides, forming coordination complexes through either inner or outer-sphere coordination; subsequently, electron transfer occurs; finally, the coordination complexes dissociate (Li et al., 2024).

The fundamental structure of manganese oxide, based on the MnO_6 unit, enables the formation of various structural forms. This unit consists of octahedrally coordinated O^{2-} ions around a central Mn^{4+} ion, as depicted in Figure 34. The structural arrangement can occur through edge and corner sharing, leading to the formation of tunnel or chain structures, and layered structures, each capable of accommodating protons and cations. Chain structure is formed by corner-sharing arrangement while tunnel resulted from the combination of single, double or triple chains of MnO_6 . Layer structure is constructed by the sheets or layers stacking of MnO_6 octahedral. As a transition metal, manganese oxide presents various valence states, resulting in a diversity of minerals with distinct physical and chemical properties.

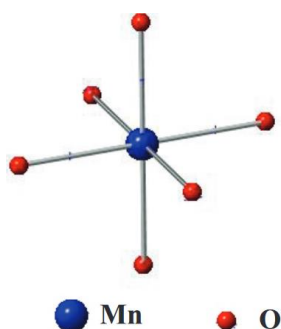


Figure 34: Schematic illustration of MnO_6

Despite the presence of over 30 types of manganese oxides, often intermixed, they are generally referred to as MnO_x due to the challenge of distinguishing individual mineral phases. Pyrolusite (β - $Mn^{4+}O_2$) is among the most abundant and stable, featuring a crystal structure composed of single chains of $Mn(IV)O_6$ octahedra that share edges and corners, forming a framework structure. Birnessite (δ - MnO_2), the predominant manganese oxide phase, is integral to oxidation-reduction and cation exchange reactions. It exhibits a layered structure with significant interlayer distance filled with cations and water, providing accessible active sites.

The Mn conversion coating process involves reducing Mn(VII) in solution to a lower oxidation state, followed by precipitating as an oxide which coats and passivates the substrate (Madden and Scully, 2014). Recent studies have emphasized the importance of pH in the consistency of coating layers, particularly in manganese oxide applications where pH influences the stability of the coating. Investigations have covered a range of pH conditions, to assess their impact on the quality and durability of the coatings. Other important factors influence the success of the coating such as the temperature of the coating treatment and its duration. The correlation between these parameters was studied by a research team (Eikenberg et al., 2001). Figure 35 shows the relationship between MnO_2 coating density on polyamide discs and the duration of the coating treatment. It was observed that treatment duration and temperature were directly related. This result was supported by another study about manganese oxide coating on aluminum, stating that a 1-minute treatment at 68 °C produced similar outcomes as a 60-minute treatment at a temperature of 25°C (Kulinich and Akhtar, 2012).

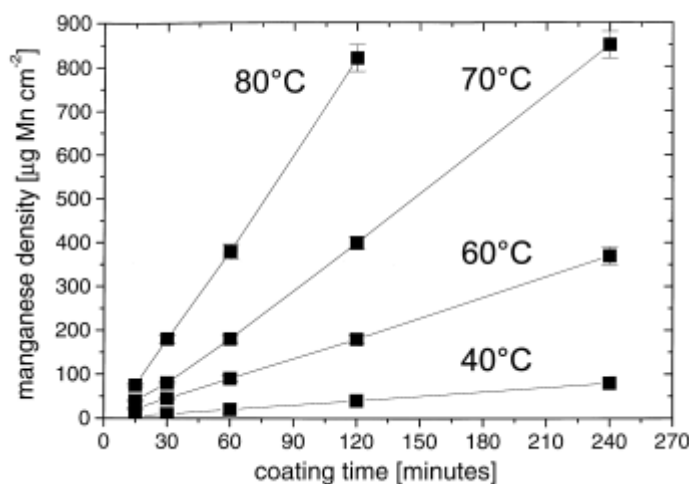


Figure 35: Correlation between the surface density of MnO_2 coating on polyamide discs as a function of the coating treatment duration (Eikenberg et al., 2001)

In addition, this section addresses the reaction mechanism when surfaces interact with permanganate to produce the manganese coating. As a strong oxidizer, permanganate has a high oxidation potential, reducing MnO_4^- ions to Mn^{2+} ions in a pH range of 0 to 8. This characteristic, primarily due to high valence state of manganese Mn(VII) in the permanganate ion (MnO_4^-), is illustrated in Figure 36 showing the Pourbaix diagram of Mn.

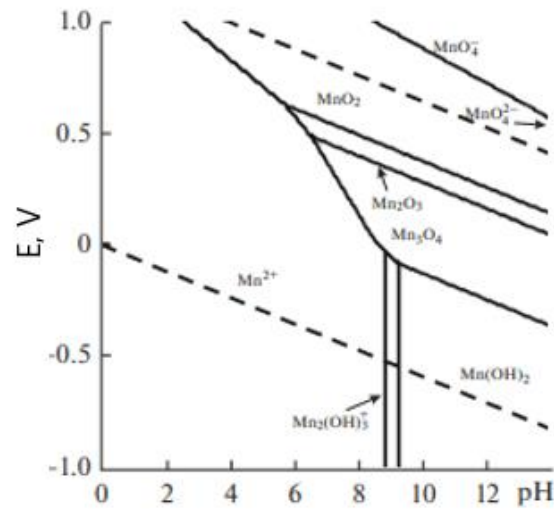


Figure 36: E-pH diagram for aqueous manganese compounds in the solution containing 5 mmol/L KMnO_4 (Kharitonov et al., 2020)

The initial reaction involves the reduction of Mn(VII) to manganese (IV) dioxide, represented as follows:



Several reactions can occur, further reducing manganese (IV) oxide to manganese (III) oxide, a mixed-valence oxide:



This series of reductions finalizes the formation of manganese in the +II state, as represented below:



At low pH and low potentials, manganese oxides tend to dissolve as Mn(II) ions, reflecting their sensitivity to acidic conditions. On the contrary, the situation changes markedly at pH above 8. In these conditions, a stable form of insoluble manganese hydroxide (Mn(OH)_2) is obtained (Madden and Scully, 2014).

Eikenberg and colleagues provided evidence supporting the impact of pH on surface complexation reactions (Eikenberg et al., 2001). Their study explored the effect of different pH levels on reactions occurring on coated surfaces, ranging from a pH range of 3 to 8. Nevertheless, for U-NucfilmDisc the recommended pH of use is stated between 2 to 3. At lower pH the MnO_2 layer might be less stable.

4.2.3.2 Acidic conversion coating with potassium permanganate

A practical disadvantage of manganese oxide-based conversion coatings is that they require high temperatures and involve more complex procedures than traditional chromate conversion coatings (Danilidis et al., 2007).

In another article by Kharatonov, acidic conditions were used at a lower temperature. The sample was then immersed in a 0.005 mol/L KMnO_4 solution at pH adjusted to 3 using HNO_3 (Kharitonov et al., 2020)

Umehra worked at neutral pH using a buffer solution. We modified this method for aluminum (Umehara et al., 2003). This alternative method utilized HCl in combination with KMnO_4 and sodium tetraborate ($\text{Na}_2\text{B}_4\text{O}_7$). The advantage of this method is its ability to maintain a stable pH around 7 through all the reaction thanks to the buffering action of HCl and borax. In the publication, the final results indicated that the coating consisted of manganese oxide (or hydroxide) and boron oxide on the surface.

These diverse studies collectively contribute to the understanding and development of manganese oxide-based conversion coatings, highlighting the various approaches and conditions under which these coatings can be effectively utilized.

4.2.3.3 Basic conversion coating with potassium permanganate

Studies have investigated the application of borax- KMnO_4 baths at around pH 9, focusing on the formation and stability of coatings under these conditions. The chemicals used include reactive species like LiCl, NaCl, NaNO_3 , borax ($\text{Na}_2\text{B}_4\text{O}_7$), and silicate with KMnO_4 (Kulinich and Akhtar, 2012). As mentioned earlier, in such basic environments above pH 8, the aluminum oxide is unstable, dissolving in the aqueous solution. The dissolution process in an alkaline medium (pH 9) follows the reaction:



Furthermore, the oxidation of aluminum and reduction of Mn(VII) to Mn(IV) is represented as:



Our study adapted this method by using similar concentrations as the article of Kulinich, : 0.1 mol/L KMnO_4 and 0.05 mol/L borax, achieving a solution with a pH around 9 (Kulinich and Akhtar, 2012).

In another basic condition application of potassium permanganate coating, by Danilidis, they test a no-rinse treatment (Danilidis et al., 2007). By this way the process time and the volume of the effluents from the reaction are decreased but reactions with the substrate must occur rapidly. The conversion treatment with 0.1 M KMnO_4 was applied by spin coating for 10 seconds at 600 rotations per minute, then dried immediately at 100°C for 1 minute.

In an article from Siau, the manganese coating was applied for improving adhesion properties between the epoxy resin and aluminum surface (Siau et al., 2004a). The treatment was based on 55 g/L KMnO_4 and 1.2 mol/L NaOH. Experiments were conducted for 10 minutes at 40 and 80 °C. In our work, the coating solution is aimed to be applied on aluminum foil, in contrary to the reference article, the concentration of the solution was decreased to avoid the destruction of the aluminum foils.

Another research group tested a temperature range from 38 °C to 82°C and a pH between 9 to 10 for the manganese coating applications. At low temperatures around 25 °C, the reaction can take up to 60 minutes, a parameter worth considering in future studies. At 68 °C, coatings can be produced in 1 minute (Song et al., 2022).

4.2.3.4 Chromium oxide (CrOx) coating

In the presence of aluminum, Cr(VI) reduces to various Cr(III) compounds, forming a soft gel-like mixture. Remaining traces of Cr(VI) in the conversion coating create a yellow to dark brown shades to the chromium oxide coating (CrOx). ..

The protective mechanism of the coating involves forming a mixed chromium/metal oxide film, typically 0.1-3 μm thick, on the metal surface, mainly in acidic conditions with a pH around 1 to 2. This coating is composed of Cr(III)-Cr(VI) oxides and hydrated Al oxide, with its thickness being dependent on the duration and chemical composition of the coating solution.

The formation of CrOx involves the electrochemical reduction of Cr(VI) and inorganic polymerization to form a conversion film. This process involves formation of Cr(VI) in the solution to form hydrated $\text{Cr}(\text{H}_2\text{O})_6^{3+}$, which hydrolyzes at the locally alkaline region near the aluminum-solution interface to form hydrated Cr hydroxide, $\text{Cr}(\text{OH})_3(\text{H}_2\text{O})_3$. This structure polymerizes, creating Cr(III)-O-Cr(III) linkages, constituting the polymer backbone. Simultaneously, Cr(VI) binds through oxygen ligands, creating Cr(III)-O-Cr(VI) linkages characteristic of CrOx.

A key distinction between chromate and manganese coatings is observed. While chromate coatings, consisting of organic polymers, tend to lose properties above 70 °C, manganese oxide coatings, which are non-polymeric, demonstrate superior heat resistance (Kulinich and Akhtar, 2012).

A 0.5 mol/L $\text{K}_2\text{Cr}_2\text{O}_7$ and 1 mol/L H_2SO_4 solution, as suggested in the literature, was used to immerse the samples for 10 minutes at 40 and 80 °C. This experiment was compared with the potassium permanganate treatment revealing that introduced more surface roughness compared to $\text{K}_2\text{Cr}_2\text{O}_7$.

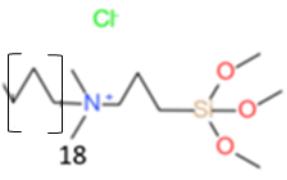
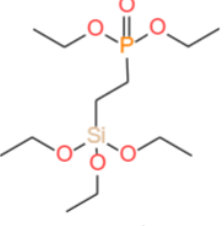
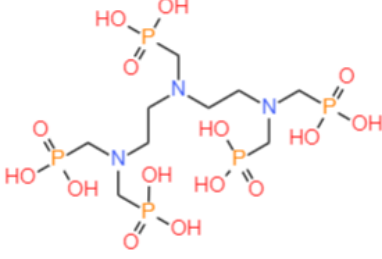
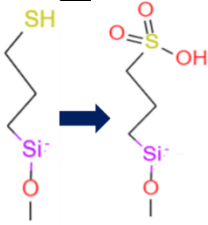
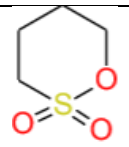
The formation process of chromate conversion coatings is thought to originate from the dissolution of metal surface (Gray and Luan, 2002). This dissolution is accompanied by the reduction of water or oxygen to form hydroxyl ions, and consequently increasing the pH at the liquid-metal interface. Such increase in the pH level leads to precipitation of a thin complex chromium-metal gel on the surface that contains both hexavalent and trivalent chromium compounds. The pH level plays a crucial role in controlling the formation of these chromate films.

Furthermore, temperature is another important parameter in the stability of the coatings, they should not be subjected to temperatures close to 70 °C.

5 CONCLUSION OF CHAPTER 2

After reviewing the literature, different methods were assessed to allow two substrates, aluminum and polymer, to bind to Europium and Americium. For polymeric surfaces, the emphasis was placed on sulfonic acid groups to bind to the RN, and 1,4-butane sultone was chosen to graft to pre-treated PET and epoxy surfaces. For aluminum, the use of silanes and phosphonic acids were considered for grafting, and for attaching radionuclides (RNs), quaternary ammonium, sulfonic acid, and phosphonic acid were identified as potential options. Additionally, conversion coatings (MnOx and CrOx) were also selected for the aluminum substrate, due to their ability to both attach onto the Al surface to create strong layers, and to exchange cations such as Eu^{3+} and Am^{3+} . The commercial availability of the possible chemicals was checked and led to define the following list of selected chemicals (Table 8).

Table 8: Chosen chemicals for the experimental procedures

		Aluminum substrate	
Grafting molecule			3-(Trimethoxysilyl)propyl- <i>N,N,N</i> -trimethylammonium- ¹⁵ N chloride (DMOAC) Grafting function: Silanes RN binding function: Quaternary ammonium
			(2-Diethylphosphatoethyl) Triethoxysilane (DPTES) Grafting function: Silanes or phosphonic acid RN binding function: Phosphonic acid
			Diethylene triaminepentakis(methylphosphonic acid) solution (DTPMP) Grafting function: Phosphonic acid RN binding function: Phosphonic acid
			(3-Mercaptopropyl)trimethoxysilane (MPTMS) Grafting function: Silanes RN binding function: Sulfonic acid
Coating method	Manganese coating		KMnO ₄ Both acidic and basic conditions trials were performed
	Chromate coating		K ₂ Cr ₂ O ₇ Under acidic conditions
		Polymeric substrates	
Grafting method			RN binding function: Sulfonic acid
	1,4 butane sultone		

CHAPTER 3: PRODUCTION AND CHARACTERIZATION OF POLYMERIC SURFACE SOURCES

The objective of this study was to modify polymeric surfaces to introduce chemical functionalities capable of binding radionuclides (RN) onto the surface. In this chapter, the studies conducted focused on two distinct substrates, namely Polyethylene terephthalate (PET) and epoxy resin.

PET was selected due to its availability as thin foils. It should allow to provide flexible sources that can be calibrated flat and then bent to mimic cylindrical shapes, such as pipes. In addition, PET sources could be placed on rigid aluminum plates to yield sources that comply with ISO 8769 (ISO 8769, 2020). In order to obtain PET surface sources, two methods: sulfonation and KMnO_4 treatment, were performed. The sulfonation method involved three steps, while the second method was a one-step KMnO_4 treatment.

Epoxy resin provides the opportunity to tune the roughness of surface sources by incorporating particles into the liquid formulation and by using non-flat molds, allowing for the replication of real surfaces (as shown in Figure 37). Epoxy resin surface sources were produced using a functionalization method, sulfonation, with a preliminary oxidation step.

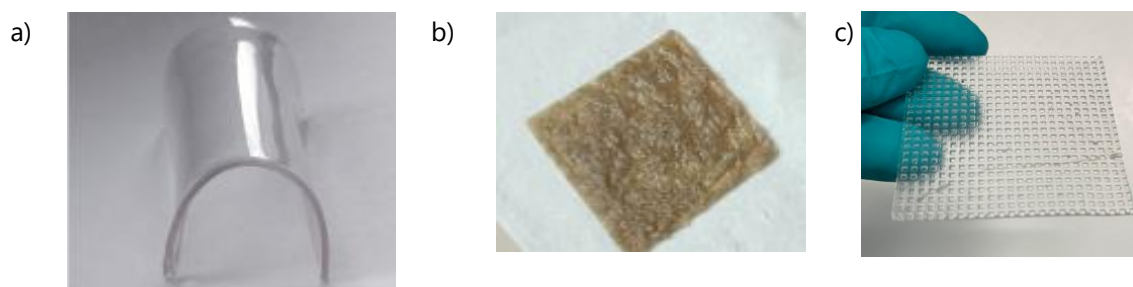


Figure 37: Examples of epoxy resin surface sources, mimicking a) a curved surface, b) a cement-like surface, c) a rough surface created with a rough mold

The efficiency of each step in both methods was evaluated with chemical techniques. After the completion of the chemical characterization, optimized parameters were chosen for the surface modification methods. Following the modification of both substrates (PET and epoxy resin), RN attachment experiments were performed for all the produced samples. This was achieved by immersing the substrates in solutions containing the desired RN (^{152}Eu or ^{241}Am), to fix it on the substrate. The ability of the modified surfaces to bind to the RN was assessed with radiometric characterization.

1 MATERIALS AND METHODS

1.1 MATERIALS

In these experiments, PET samples measuring 5x5 cm² and 18 μm thick were utilized. For the first step, hydrolysis sodium hydroxide (1 M NaOH, Sigma-Aldrich) was used with acetonitrile (ACN, ≥99.9%, VWR). The subsequent reduction step involved the use of sodium borohydride (NaBH₄, Merck), anhydrous tetrahydrofuran (THF, >99%, Merck), and catechol (Merck). The final sulfonation step was conducted with NaH (Merck), 1,4-butane sultone (≥99.0%, Sigma-Aldrich), acetonitrile (ACN, ≥99.9%, VWR) and Dimethyl sulfoxide (DMSO, anhydrous, ≥99.9%, Sigma Aldrich).

Epoxy resin pieces measuring 5x5 cm² and 11x16 cm² were prepared by mixing part A (epoxy) and part B (amine hardener) from Stycast 1264 bicomponent resin (Ellsworth Adhesives). The casting process involved the use of three types of molds: a rigid, white polytetrafluoroethylene (PTFE) mold (5x5 cm²), a flexible, yellow mold (5x5 cm²) and a rigid, blue metal mold (11x16 cm²) (as shown in Figure 38). The flexible molds were produced using a 3D printer Form 3B (Formlabs) with the Flexible 80A resin, obtained from Formlabs. The blue metal and the white PTFE molds were made by machining. The thickness of the epoxy resin for the white mold, flexible yellow molds and the blue metal mold was 3 mm, 3 mm, and 1.5 mm, respectively. With the yellow flexible molds, a HNO₃ (3 M) solution was added to the mixture of part A and part B. In the casting process, an unmolding agent (Robsil) was employed, for the flexible molds and the blue metal mold.

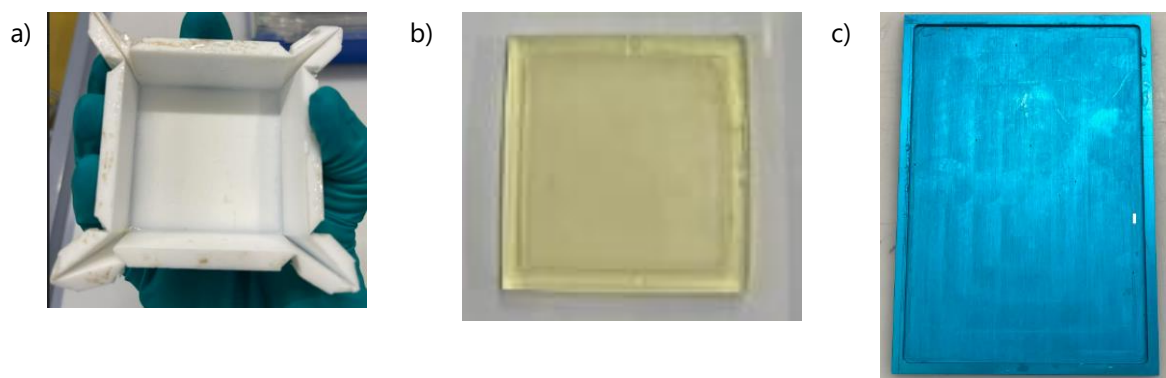


Figure 38: The molds used in the casting of epoxy resin samples a) Rigid white PTFE mold (5x5 cm²), b) Flexible yellow mold (5x5 cm²), and c) Blue metal mold (11x16 cm²)

The cleaning process of the polymeric surface sources was performed with isopropanol (≥99.5%, Sigma-Aldrich) and acetone (≥99.5%, Sigma-Aldrich).

The KMnO₄ treatment process involved potassium permanganate (≥99.0%, KMnO₄, Prolabo) and sodium hydroxide solution (1 M NaOH, Sigma-Aldrich) followed by a cleaning step with an acetic

acid solution (10%, Prolabo). For the sulfonation process, NaH (Sigma-Aldrich), 1,4-butane sultone ($\geq 99.0\%$, Sigma-Aldrich), acetonitrile (ACN, $\geq 99.9\%$, VWR) and Dimethyl sulfoxide (DMSO, anhydrous, $\geq 99.9\%$, Sigma Aldrich) were employed.

The ^{152}Eu solution used in the RN binding experiments had an activity of (22.01 ± 0.07) kBq/g ($k = 1$), reference date: 28/11/2022). This solution was in 1 mol/L hydrochloric acid (HCl) with $0.2 \mu\text{g/g}$ of stable Eu. In addition, a solution of ^{241}Am in 1 mol/L HCl was used without any carrier. The ^{241}Am solution had an activity of (31.06 ± 0.14) kBq/g ($k = 1$) at the same reference date.

1.2 METHODS

1.2.1 Modification of the PET surfaces

Two methods were selected for the modification of the surface of the PET samples: sulfonation and coating. The first method involved a series of sequential steps, to sulfonate the PET surface. This process started with the hydrolysis of PET samples, thereby increasing the quantity of carboxyl and hydroxyl chain ends present on the surface. The subsequent step is the reduction of carboxylic acid functional groups into hydroxyl (OH), enabling the attachment of sulfonic acid groups to these hydroxyl groups in the 3rd step. The SO_3^- groups have the ability to bind the chosen RNs (^{152}Eu and ^{241}Am) onto the PET sample.

The second method, KMnO_4 treatment, was employed to facilitate a comparison with other substrates, as this technique was utilized for both aluminum and epoxy resin. The methods used for functionalizing the PET samples are illustrated in Figure 39.

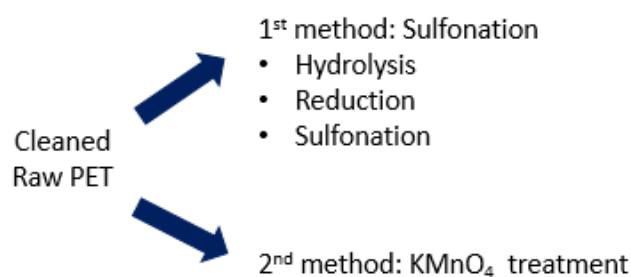


Figure 39: The methods for the PET modification

1.2.1.1 The steps of the PET sulfonation

In this section, detailed information on the methods that lead to sulfonation is provided.

1.2.1.1.1 Hydrolysis of PET

First, the samples were cleaned with isopropanol and acetone in the ultrasonic bath for 10 minutes. The main goal of the cleaning step was to eliminate any remaining residues on the surface. For the hydrolysis of PET, the samples were immersed in 2.5 mL of a 1 mol/L NaOH solution, 7.5 mL of ultrapure water and 10 mL of ACN. The reaction was conducted for 17 hours at 60°C . Following

hydrolysis, the samples were rinsed with ultrapure water and ethanol. Out of four samples one particular sample was chosen to be treated with RN, which sample is referenced as E5.

1.2.1.1.2 Reduction of hydrolyzed PET

To enable the functionalization of PET with compounds that react with hydroxyl groups, it is important to increase the number of these groups on the surface. To achieve this goal, NaBH₄ was used to reduce the carboxylic acid groups formed by hydrolysis in the presence of catechol.

NaBH₄ was dissolved in THF (10 mL) with continuous stirring, until complete dissolution. Simultaneously, a mixture of catechol and THF (10 mL) was prepared in a separate beaker. Subsequently, these two solutions were combined into a single beaker, and the hydrolyzed PET sample was immersed in the final solution while stirring for 18 h at room temperature (22 °C). To prevent evaporation during the reaction, the beaker was covered with parafilm®.

After the treatment, the reaction medium was neutralized by the addition of DI water, and the sample was subsequently rinsed with DI water and ethanol. Finally, the sample was dried at room temperature (22 °C). This treated sample is referenced as E6.

1.2.1.1.3 Sulfonation of reduced PET

First, NaH was dissolved in the selected solvent, ACN. The solution was kept under continuous stirring at a temperature of 45 °C for a period of 1 h until complete dissolution. Subsequently, 1,4-butane sultone was introduced into the NaH solution, then the final solution was kept under agitation at 70 °C for 5 min to achieve its complete dissolution.

The reduced PET sample was subsequently immersed in this final solution, and kept under agitation for 16 h at 70 °C, to enable the sulfonation reaction. Notably, rapid evaporation was observed during the sulfonation process, necessitating the addition of solvent to maintain the reaction. This evaporation also resulted in changes in the concentration of the solution. However, the solution was evaporated during the night for the first series of experiments (E series). Finally, the sample was rinsed with ultrapure water to complete the reaction and remove any excess chemicals from their surfaces. This sample is referenced as E7.

1.2.1.2 KMnO₄ treatment of PET

The second method is the KMnO₄ treatment of PET samples, which was conducted using the same method used for the epoxy and aluminum substrates.

First, the samples were cleaned with isopropanol and acetone in the ultrasonic bath for 10 min, to eliminate any remaining residues on the surface. The treatment was carried out using a 0.30 mol/L KMnO₄ solution, prepared by using 30 mL of 1 mol/L NaOH. This sample is referenced as H5.

To ensure the complete dissolution of KMnO₄, the solution was agitated using a magnetic stirrer for 5 min. The PET samples were then immersed in the solution. To prevent evaporation, the reaction vessel was closed with a watch glass throughout the treatment duration. The samples

were kept in the reaction medium at an approximate temperature of 50 °C for an hour.

When the reaction was complete, the samples were rinsed with ultrapure water until no remaining permanganate color was observed in the washing water. Subsequently, the prepared samples were cleaned using 10% acetic acid solution in an ultrasonic bath for 1 h. Finally, the samples were rinsed again with DI water and left to dry completely at room temperature (22 °C). The experimental conditions and chemicals utilized in each step are summarized for both methods in Table 9.

Table 9: The experimental conditions for the PET functionalization methods

Method	Sample code	Chemicals	Experimental conditions
1	E5 (Hydrolyzed sample)	2.5 mL of 1 mol/L NaOH 7.5 mL DI water 2.5 mL acetonitrile	17 h (at 60 °C)
1	E6 (Reduced sample)	0.38 g of NaBH ₄ (19 g/L) 1.13 g of catechol (56.5 g/L) 20 mL of anhydrous THF	18 h (at 22 °C)
1	E7 (Sulfonated sample)	0.10 g of NaH 0.32 g of 1,4 butane sultone 20 mL ACN	16 h (at 70 °C)
2	H5 (KMnO ₄ treated sample)	2.25 g KMnO ₄ 30 mL of 1 mol/L NaOH	1 h (at 50 °C)

1.2.2 Functionalization of Epoxy Resin

The functionalization of epoxy resin started with an oxidation reaction with KMnO₄, used to release hydroxyl bonds (-OH) from the surface. Afterwards, a sulfonation reaction led to the attachment of sulfonic acid groups onto the surface of the resin. These steps are shown in Figure 40.

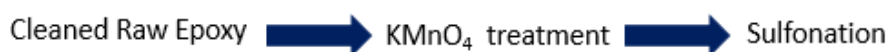


Figure 40: The functionalization method planned for epoxy resin

1.2.2.1 Casting and cleaning of the epoxy resin

When the white PTFE and the blue metallic molds were used, the resin was prepared by mixing part A (69 wt.%) and part B (31 wt.%) for 2 minutes in a beaker. Subsequently, the mixture was poured into the mold and left to cure at a temperature of 60 °C for a duration of 6 hours.

Before pouring the required amount of resin mixture into the molds, the blue metallic molds were prepared by applying an unmolding agent. This pre-treatment was not required when using the white PTFE molds.

When a flexible mold was used with the same procedure, the epoxy resin stuck to the mold, even with the use of an unmolding agent. This is probably due to a reaction between the mold, made of 3D printed polymer, and the epoxy resin. Consequently, 2.2 wt.% of 3 mol/L HNO₃ were added as a catalyst, when mixing part A and part B of the epoxy resin. The unmolding agent was also applied on the molds before casting. By implementing this method, the epoxy resins were solid in approximately 2 h at 22 °C, enabling their easy removal from the molds. The epoxy resin samples were subsequently placed in an oven at 60 °C to finish curing. After complete curing, a cleaning procedure was conducted for all epoxy samples. The samples were cleaned with isopropanol and acetone in an ultrasonic bath for a duration of 10 min.

1.2.2.2 KMnO₄ treatment of epoxy resin

The pre-step of sulfonation, an oxidation process with KMnO₄, was carried out using a concentration of KMnO₄ within the range of 0.27-0.36 mol/L in 30 mL of 1 mol/L NaOH. The samples were designated alphabetically to maintain a systematic order. However, it is important to note that the progression of letters does not strictly follow consecutive order for each step of the treatment. This deviation occurred because all the steps of the procedures were conducted at the same time. Detailed information regarding the samples and their corresponding experimental conditions is presented in Table 10.

Table 10: Experimental conditions of the oxidation of epoxy resin

Sample code	KMnO ₄ concentration (mol/L)	NaOH solution concentration (mol/L)	Duration (min)	Temperature (°C)
E2	0.36	1	30	80
F2, G2, J1, K1, K2, K3	0.27 - 0.34	1	60	80

To ensure the complete dissolution of KMnO₄, the solution was stirred using a magnetic stirrer for 5 min. Then, the cleaned epoxy resin samples were immersed in the aforementioned solution. In order to prevent evaporation, the reaction vessel was closed with a watch glass throughout the treatment procedure. The samples were kept in the oxidation solution at an approximate temperature of 80 °C.

The initial reaction duration for the E2 sample was set at 30 min. This sample was prepared with a solution of 0.36 mol/L of KMnO₄ in 40 mL of 1 mol/L NaOH.

The impact of longer duration on the KMnO₄ treatment was studied. Therefore, after the production of the E2 sample, the duration of the oxidation process was increased to 60 min and this parameter was kept constant for the rest of the samples.

Each solution was prepared separately and subsequently immersed in a hot water bath, as illustrated in Figure 41.a.



Figure 41: a) Experimental set up for the oxidation of epoxy samples, b) an oxidized sample before washing for 1 h, c) an oxidized sample after washing with acetic acid and DI water

Once the reaction was complete (Figure 41.b), the samples were rinsed with ultrapure water. Subsequently, the prepared samples were cleaned using a 10% acetic acid solution in an ultrasonic bath for 1 h. Finally, the samples were rinsed again with ultrapure water (Figure 41.c) and subsequently left to dry completely at 22 °C.

1.2.2.3 Sulfonation of the epoxy resin

The methods employed for the sulfonation process, alongside their corresponding experimental parameters are presented in Table 11.

Table 11: Experimental conditions for sulfonation of epoxy resin

Sample code	Solvent	Experimental conditions
E3	ACN	16 h @70 °C
F3	ACN	3 h @70 °C + 16 h @22 °C
G3	ACN	3 h @70 °C + 16 h @22 °C
H6	DMSO	3 h @70 °C + 16 h @22 °C
L1-L2-L3	ACN	3 h @70 °C + 16 h @22 °C

The sulfonation process was similar to the one described for PET: it was initiated by dissolving NaH (0.10 g) in the selected solvent (10 mL), which could be either ACN or DMSO. The solution was kept under continuous stirring at a temperature of 45 °C for 1 h (Figure 42.a). Subsequently, 1,4-butane sultone (0.30 g) was introduced into the NaH solution, to obtain two times stoichiometric molar ratio of NaH (Figure 42.b). This final solution was kept under agitation at 70 °C for 3 hours and 16 hours at 22 °C can be seen in Figure 42.c.

The applied sulfonation process was similar to the one described in the literature (Ouadah et al., 2018), but NaH was mixed with ACN, instead of DMSO. Additionally, a shorter reaction time is chosen for the initiation of the reaction between NaH and acetonitrile.

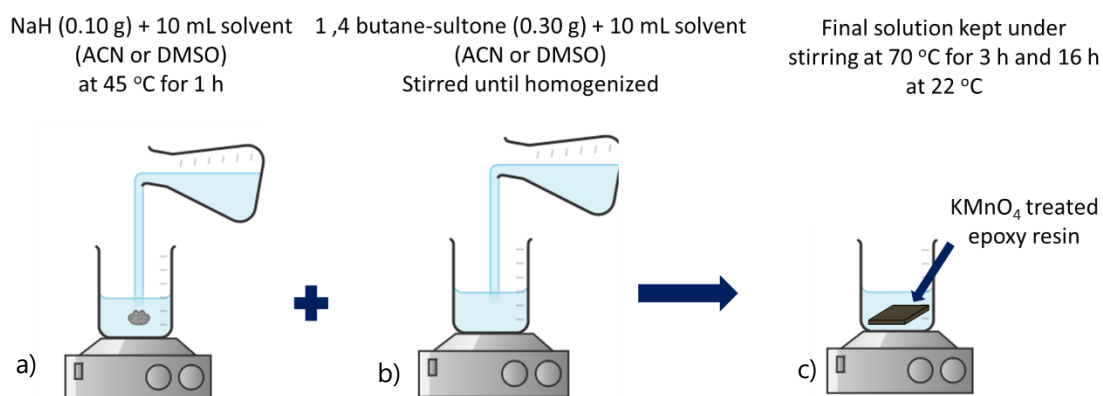


Figure 42: Experimental set up of the sulfonation treatment a) dissolution of NaH (presented in a grey stone like substance) in solvent, b) mixing of 1,4-butane sultone with solvent, c) immersion of the pre-treated epoxy surface

The first test of the sulfonation treatment was performed by immersing in the prepared solution and stirred for a period of 16 h at 70 °C. Notably, a rapid evaporation was observed during the sulfonation process, necessitating the addition of solvent (10 mL ACN) to maintain the reaction volume. To control the reaction conditions overnight and prevent excessive solvent evaporation, the reaction vessel was kept at room temperature (22 °C) overnight. Finally, the samples were rinsed with ultrapure water to remove any excess chemicals from their surfaces.

1.2.3 Surface characterization

Attenuated total reflection Fourier transform infrared spectroscopy (ATR-FTIR) was used to characterize the samples before RN binding experiments, to identify the chemical functionalities present on the surfaces of the samples. A Q Platinum-ATR device from Bruker was utilized, and the spectra were acquired by conducting 128 scans within the range of 600 to 4000 cm^{-1} at a scan rate of 2.0 $\text{cm}^{-1}\cdot\text{s}^{-1}$.

Before each analysis, a background spectrum was acquired to compensate for any potential baseline noise or interference that might arise during the actual measurements. The baseline should be relatively flat, indicating the absence of residues on the crystal.

To maintain consistency and minimize variations in the obtained spectra, analyses of the same sets of experiments were performed on the same day. The equipment used in these analyses eliminates water and CO_2 peaks originating from the atmosphere. However, for some measurements, complete elimination could not be achieved. Additional information about this technique is given in Appendix-3, at the end of the manuscript.

1.2.4 Radionuclide binding experiments for polymeric surface sources

In all experiments, gravimetric dilutions were performed to keep the traceability and the uncertainties values compare to volumetric dilutions. The radionuclide binding medium was prepared by mixing ultrapure water, 1 mol/L HCl (to reach pH 2), and a stock solution of radionuclide. The ultrapure water and HCl solutions were weighed using a Mettler-Toledo XPE504 balance (500 g range, 0.1 mg resolution). The radioactive solution was weighed using the pycnometer method (Lourenço and Bobin, 2015) and a Mettler-Toledo MT5 microbalance (5 g range, 1 μg resolution). The beakers were agitated and homogenized after the addition of each component. Following this, the polymeric samples were immersed in the RN binding medium for a certain amount of time ranged from 1 h to 144 h which depends on the substrates of the source, production condition, the chemical functions used in the modification method. During the immersion period, each beaker was sealed with parafilm®, to minimize the evaporation. In order to ensure the comparability of fixation yields, the total amount of elements present in the solution, including both stable and active isotopes, was chosen as outlined in Table 12. A reference solution was also prepared for each experiment, employing the same components as the sample solutions, without immersing any samples.

The experiments started with an isotope of Eu, which is a chemical analog of Am and therefore is expected to have similar interactions with the modified surfaces. ^{152}Eu and ^{241}Am were the isotopes chosen for the two elements. ^{152}Eu decays mostly by electron capture and β^- emission and it is a well-known multi-gamma emitter mostly between 21.78 and 1408.01 keV, whereas ^{241}Am is an alpha emitter with a low energy gamma emission at 59.54 keV. Using europium allows easier radiation protection measures and easier waste management. For this reason, the optimization tests were performed with ^{152}Eu to determine the optimal parameters of each step for all surface modification methods. Following this, a series of experiments were conducted using ^{241}Am to evaluate the intermediate precision of the source preparation as a whole.

Table 12: Parameters of the RN binding experiments for polymeric surface sources

RN	Stable/Active isotope ratio	Total amount of elements in solution (picomol)	Epoxy resin	PET
^{152}Eu	~ 57	~ 65	Raw KMnO_4 treated Sulfonated	Method 1 : Raw Hydrolyzed Reduced Sulfonated
				Method 2 : KMnO_4 treated
^{241}Am	0 (No carrier)	~ 35	KMnO_4 treated Sulfonated	/

1.2.5 Radiometric characterizations

Liquid scintillation counting (LSC) analysis was performed using a TRICARB 2900TR (PerkinElmer) and 300 SL Automatic TDCR counter (HIDEX). Information about these techniques is given in Appendix-2 under the title of "Radiological characterization methods".

The treated polymeric samples were immersed in the RN solution to allow the binding of RN to the surface of the sample, as illustrated in Figure 43. To observe the kinetics of this attachment during the immersion period, several aliquots were sampled. The liquid scintillation samples were prepared by taking 1 mL from the solution in contact with the sample. That solution was mixed with 10 mL of LSC cocktail (Ultima Gold LLT, Perkin Elmer) in a 20 mL high purity, low potassium glass vial and each sample was measured for 15 min.

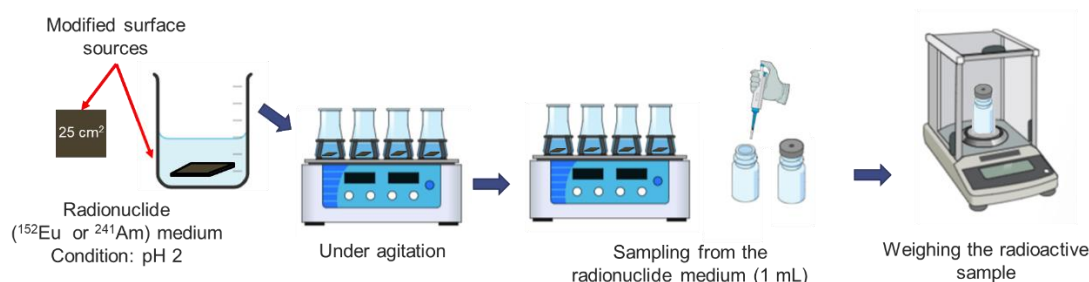


Figure 43: Experimental setup of the RN binding experiment

At the beginning of the experiment, the maximum activity for the reference LSC samples were approximately 20 Bq for the ^{152}Eu binding medium, and 20-30 Bq for the ^{241}Am binding medium. For each RNs different blank samples were prepared to correct the LSC data. For Eu sources a blank sample, prepared with Eu carrier solution, while for Am sources; HCl (pH 2) was used to prepare the blank sample.

The maximum fixation yield (Y) was calculated using Equation 19, at the time when the fixation yield was maximum. $(\text{CPS}/\text{g})_{\text{sample}}$ and $(\text{CPS}/\text{g})_{\text{ref}}$ represent the count per second per gram of the sample and of the reference solution (without any sample), respectively.

$$Y = \frac{\left(\frac{\text{CPS}}{\text{g}}\right)_{\text{sample}} - \left(\frac{\text{CPS}}{\text{g}}\right)_{\text{ref}}}{\left(\frac{\text{CPS}}{\text{g}}\right)_{\text{ref}}} \quad \text{Equation 19}$$

The calculations were performed assuming that all RN atoms were attached to the surface of the sample. This assumption was verified by ensuring that the RN in solution did not attach to the walls of the glass beakers.

Following the RN binding experiments, one source from each step of the modification of the epoxy surface (K1, oxidized and bound to ^{241}Am and L1, sulfonated and bound to ^{241}Am) underwent a swab test to assess the strength of the link between the surface and the attached RN, and thus to estimate the surface contamination of the sources.

The determination of removable contamination from the sources was conducted by dry or humid swab tests. The experiments were performed on both sides of the sources, ensuring that the area of one side (25 cm^2) of the source was covered. While one side of the source was tested using a dry swab, the other side was tested with a humid swab. In total, four sets of analyses were carried out. The measurements were conducted by the SPR laboratory of Saclay using an alpha-beta low-level counter with a counting time of 15 min (Berthold/ LB 790 model).

The uniformity of the polymeric sources was analyzed using photosensitive BAS-MS Fujifilm imaging plates and a GE Healthcare Amersham Typhoon scanner, with a resolution of $100 \mu\text{m}$. The sources were placed on an autoradiography imaging screen for 72 h (Figure 44.a), and the screen was imaged with the scanner after exposure (Figure 44.b). The image (Figure 44.c) obtained was analyzed using the OptiQuant software. Information about this technique is given in

Appendix-2 in the title of "Phosphor autoradiography imaging".



Figure 44: Illustration of the autoradiography: a) exposure of a source (grey) on the imaging plate (white) b) autoradiography imaging system c) reading step in the scanner, d) signal of the source

Each pixel of an autoradiography image has a numerical value that is proportional to the amount of radiation detected in that area during exposure. To follow the recommendations of the ISO 8769 standard (ISO 8769, 2020) for the measurement of the source uniformity, the sources should be divided into equally shaped portions, which are about 10 cm² or less. For this reason, the samples (25 cm²) were divided into 9 square portions (3x3, 2.7 cm² each) and 4 square portions (2x2, 6.25 cm² each). The uniformity of a sample is expressed as 1 minus the standard deviation of the surface emission rates (σ_n) of each individual portion of the entire reference measurement standard divided by the mean value of these emission rates (n) as shown in Equation 1.

$$\left(1 - \frac{\sigma_n}{n}\right) \times 100 (\%) \quad \text{Equation 1}$$

¹⁵²Eu disintegrates 72.1% by electron capture, about 0.027% by emission of positrons (beta plus) to ¹⁵²Sm and 27.9% by beta minus emission to ¹⁵²Gd. ²⁴¹Am decays 100% by alpha transitions to ²³⁷Np. Following this decay, the excited ²³⁷Np returns to the ground state by emitting 59.54 keV gamma rays or conversion electrons.

Due to the dual alpha and gamma emissions of ²⁴¹Am and the dual beta and gamma emissions of ¹⁵²Eu, the obtained images show the sum of the distribution of all types of radiation. Therefore, an additional exposure experiment was performed, using a masking plate between the source and detector screen. For the ¹⁵²Eu sources, an Al foil (0.03 mm thick) was placed to attenuate most of the beta particles emitted by the source, while for the ²⁴¹Am source, a sheet of paper was used to stop the alpha particles.

2 RESULTS AND DISCUSSION

In this section, a comprehensive overview of the chemical and radiometric analyses conducted on PET and epoxy resin samples is provided. The analyses of the PET samples were investigated first, followed by those of the epoxy resin samples. Two methods, sulfonation and KMnO₄ treatment were performed to obtain modified PET samples, and epoxy resin samples underwent modification by sulfonation with a pre-treatment using KMnO₄.

2.1 CHEMICAL CHARACTERIZATION

2.1.1 Chemical changes in the PET structure

The schematic views of the sulfonation and KMnO_4 treatment are shown in Figure 45.a-e.

PET is a polyester, which comprises terephthalic acid groups and ethylene glycol moieties and it is characterized by the presence of both terminal carboxylic acid and terminal hydroxyl functional groups (as illustrated in Figure 45.a). These end-groups are not expected to be significantly present on the surface of PET, because this commercially available polymer has a high molecular weight. Therefore, PET is chemically stable, but also presents a challenge for surface functionalization, as the scarcity of reactive end-groups limits the opportunities for modification.

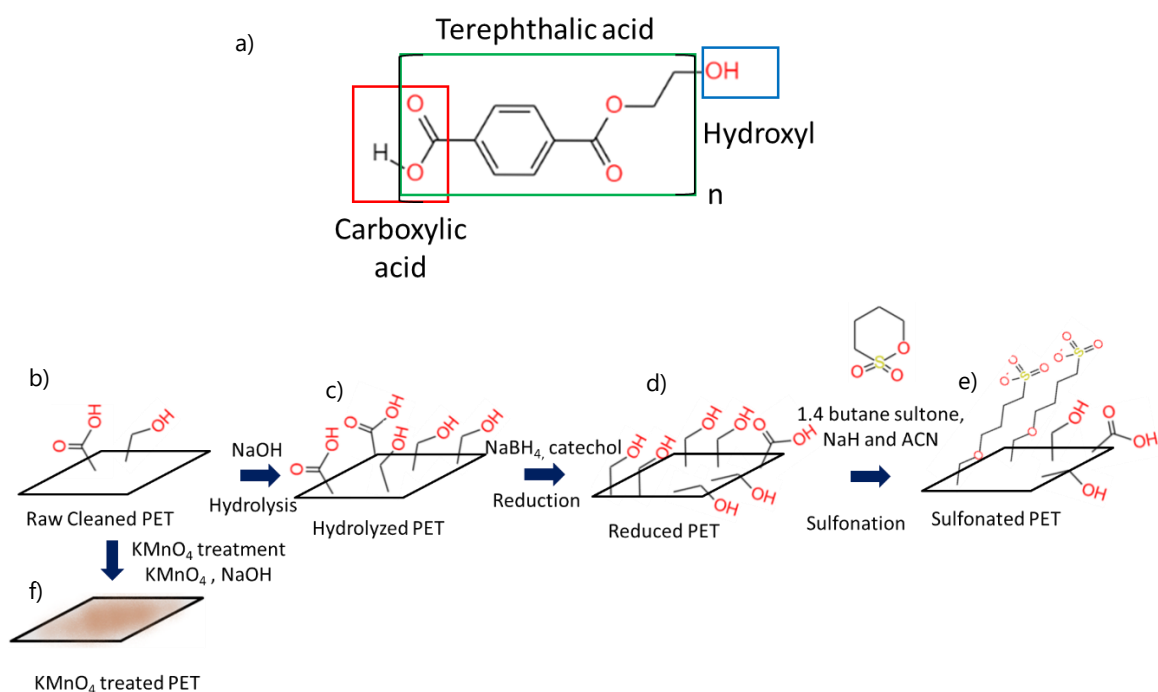


Figure 45: a) Chemical structure of PET, schematic view of: b) raw PET, c) hydrolyzed PET, d) reduced PET, e) sulfonated PET, f) KMnO_4 treated PET

In order to attach sulfonic acid groups onto the surface of PET, grafting with 1,4-butane sultone can be considered (Ouadah et al., 2018). However, this reaction requires a significant amount of hydroxyl groups on the surface. The surface of PET should thus be pre-treated to create more groups on it.

The protocol chosen was a basic hydrolysis of PET films with NaOH in acetonitrile. New hydroxyl groups and carboxylic acid chain ends were formed by cleavage of the ester groups present in the backbone of PET (as seen in Figure 45.c and Figure 46).



Figure 46: Ester cleavage reaction of PET

Following this step, a reduction reaction was carried out to transform the carboxylic acid end groups into alcohol moieties (Figure 45.d). This process increases the number of hydroxyl bonds on the surface. Finally, the hydroxyl groups reacted with 1,4-butane sultone (Figure 45.e). The details about the mechanism of sulfonation are given in Chapter 2, in section 4.1.4.

The second method is a treatment with KMnO_4 in basic conditions. For this method, PET was used without any pre-treatment. In the literature, a KMnO_4 treatment in acidic conditions was used to oxidize PET samples, to create more carboxylic acid groups. The PET samples used had been subjected to a first hydrolysis step, where the carboxylic acid and hydroxyl chain ends of PET were increased (Boxus et al., 1996). In the case reported here, without any hydrolysis step, it is unclear if the KMnO_4 treatment leads to oxidation of the hydroxyl bonds into carboxylic bonds, because less functional groups are present on the surface. However, a MnO_2 coating might be formed on the surface during the treatment, through the reduction of Mn(VII) derived from the KMnO_4 solution to a lower oxidation state, similarly to the reaction on aluminum (Ren et al., 2020). The formation of a precipitated layer of manganese oxide on the surface should not depend on specific functional groups to be present on the surface of PET.

2.1.2 Infrared spectroscopy of PET

This present study on PET was focused on the production of sulfonated PET, and the examination of each step involved in this method. The produced all PET samples were prepared specifically for ATR-FTIR analysis, which provides qualitative information on the chemical bonds at the surface of the samples. It is important to clarify that the spacing between spectra in the ATR-FTIR spectrum was artificially adjusted to allow easier comparison of the spectra.

In order to identify the chemical functions of PET samples, ATR-FTIR analysis was employed on raw, hydrolyzed, reduced, and sulfonated PET samples. The intensity of the peaks of raw PET is lower when compared to the other samples; therefore, the raw PET graph is shown separately on top of the spectra of the modified samples, in Figure 47. The full spectra from 4000 to 600 cm^{-1} are given in Appendix 3

The raw PET displayed peaks at 1247 , 1093 , 1010 , 865 , 725 and 668 cm^{-1} . The spectra of the treated PET samples displayed common peaks with the raw PET with some slight shifts and intensity variations. All these shifts were observed after the surface hydrolysis and were consistent in all treated samples. After hydrolysis, the peak at 1247 cm^{-1} was sharper, with a higher intensity, and was shifted to 1258 cm^{-1} . This shift and the changes in peak characteristics can be attributed to modifications in the terephthalate group, which forms the backbone of the PET structure. These observations might indicate that the hydrolysis process has induced significant changes in the PET

material, particularly involving the ester cleavage reaction. The peaks at 1093 and 1010 cm^{-1} exhibited a notably higher intensity after hydrolysis. Furthermore, these peaks displayed a distinctive shoulder-like structure, along with a slight shift in their positions when compared to the raw PET spectrum. These changes might be attributed to the alteration in the methylene group and vibrations of the ester C-O bond and O-C=O stretching. The peaks at 865, 725, and 668 cm^{-1} remained consistent throughout all treated samples.

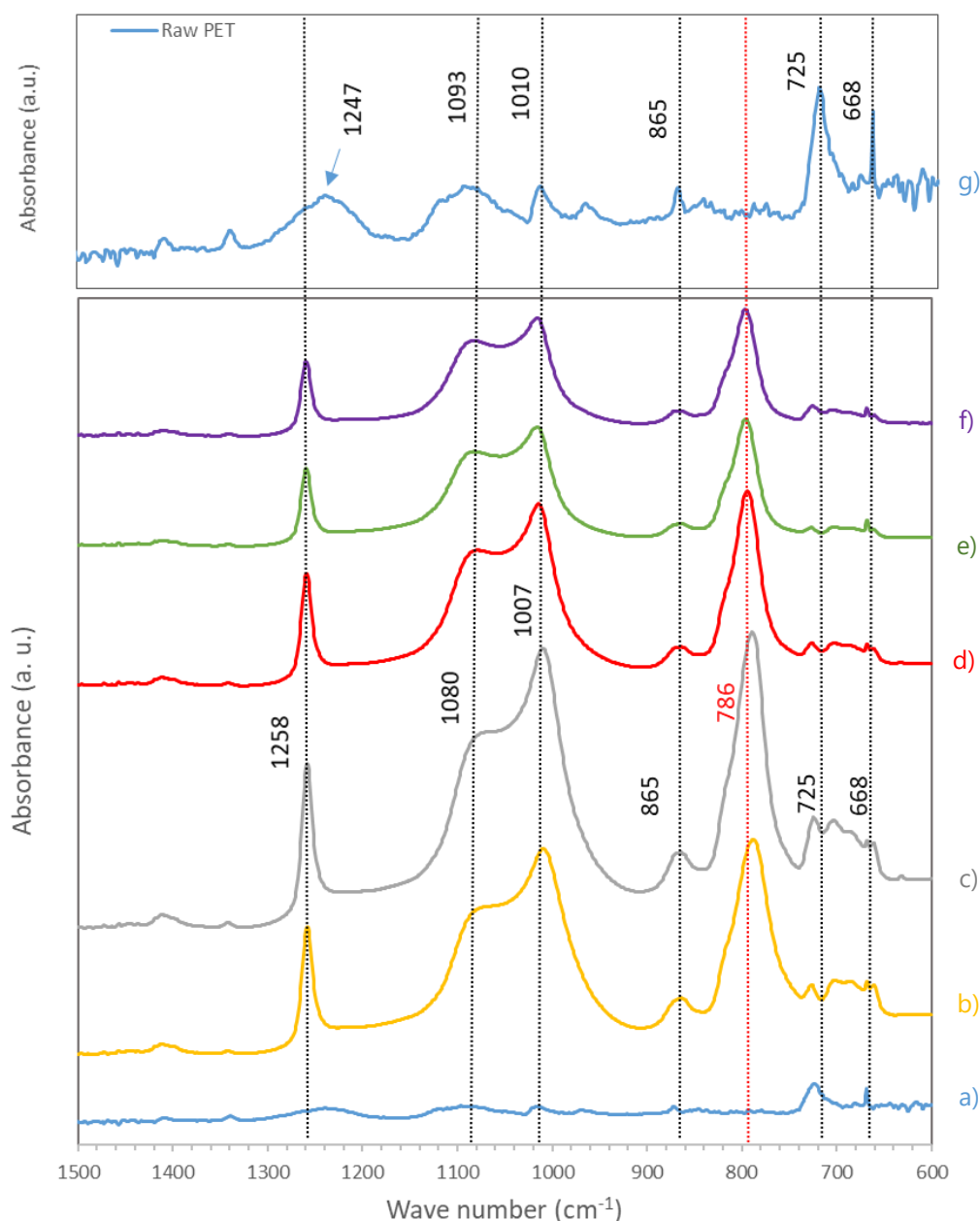


Figure 47: ATR-FTIR spectrum of the PET samples a) raw PET, b) white part of hydrolyzed PET, c) transparent part of hydrolyzed PET, d) transparent part of reduced PET, e) white part of reduced

PET, f) sulfonated PET, g) close up version of the raw PET spectrum

Additionally, after the hydrolysis treatment a new high intensity peak appeared on the spectrum at 786 cm^{-1} , which was observed for all treated samples. This might indicate that a reaction happened on the terephthalic acid on the PET structure. The vibrational bands observed in the PET samples, along with their assignments, are provided in Table 13.

Table 13: Vibrational bands of raw PET samples (Pereira et al., 2017; Torres-Huerta et al., 2016)

Wave number of the band (cm^{-1})	Assignment
1247	Terephthalate Group ($\text{OOC}_6\text{H}_4\text{-COO}$)
1190-1080	O-C=O stretching
1093	Vibrations of the ester C-O bond
725	Interaction of the polar ester groups and the benzene ring
668	C-H out of plane bending wagging vibration of aromatic ring

Furthermore, the hydrolyzed and reduced samples displayed noticeable physical disparities on their surfaces, including white traces. As a result, various analyses were conducted on different areas of the samples to assess their impact. The transparent region of the samples exhibited peaks at the same wavenumbers with varying intensity, making it challenging to draw conclusions about potential differences in chemical composition (Figure 47.c and d).

The spectra of the reduced and sulfonated samples did not present additional peaks from the hydrolyzed one. One possible reason is that the high-intensity groups produced during PET hydrolysis may mask or obscure the appearance of other lower intensity peaks, making them challenging to detect. This might be explained by the limitations of the FTIR analysis. To obtain a confirmation on the presence of specific chemical bonds, a technique with better detection capability is required, for the upcoming studies, possibly such as Raman and X-ray photoelectron spectroscopy (XPS).

In conclusion, the FTIR analysis of PET samples showed certain limitations in providing conclusive evidence of surface modification after hydrolysis. As a result, the modified samples were tested with radionuclides to assess their ability to attach to the RN. The presence of radioactivity following the modification was confirmed through LSC analysis in the following section.

2.1.3 Chemical changes in the epoxy resin structure

The chemical structures of the two components of the epoxy resin used are shown in Figure 48.a and Figure 48.b. The modification of the surface of the epoxy resin samples was conducted through two steps: KMnO_4 oxidation treatment and sulfonation (as displayed in Figure 48.c). In the oxidation step, the epoxy resin was treated in a basic KMnO_4 solution, which is an oxidizing agent that can break R-O-R bonds to form primary and secondary alcoholic functions (in Figure 48.a), causing certain parts of cured epoxy to dissolve into the solution (Siau et al., 2004a).

The cured epoxy resin contains functions like secondary alcohol and ether functions, these can be oxidized into ketones, aromatic and primary alcohols. This reaction also resulted in the release of secondary and/ or tertiary amines. A detailed explanation can be found in Chapter 2, section 4.1.2. The sulfonation step incorporated sulfonic acid groups into the epoxy resin by chemical bonding with the hydroxyl groups previously obtained on the surface (Figure 48.c).

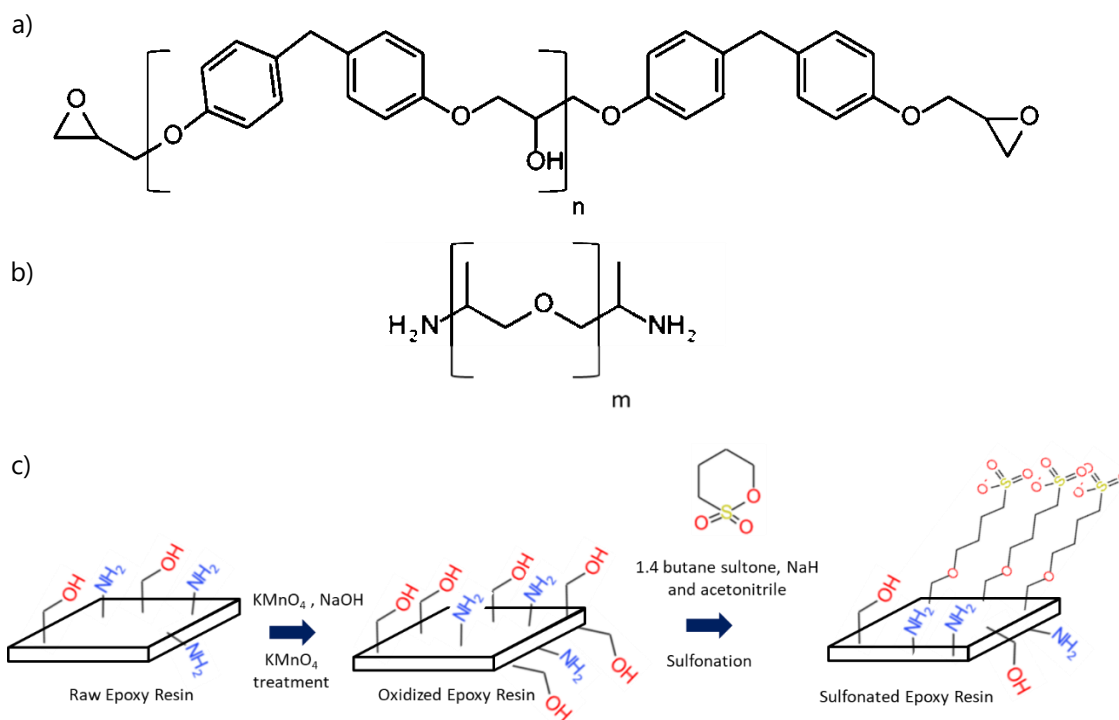


Figure 48: Chemical structure of epoxy resin a) component A, b) component B, c) a possible modification mechanism of epoxy resin

Sodium hydride (NaH) is used to activate the nucleophilic substitution reaction (Hesek et al., 2009). A possible reaction mechanism is illustrated in Figure 49, following a $\text{S}_{\text{N}}2$ substitution of the SO_3 group by the activated hydroxyl group. Both steps were investigated by chemical and radiometric characterization analyses.

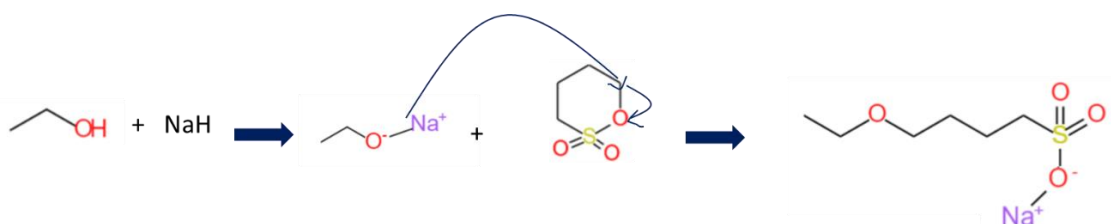


Figure 49: A possible mechanism on the hydroxyl end of the oxidized epoxy resin samples

2.1.4 Infrared spectroscopy of the epoxy resin

The chemical characterization of epoxy resin samples was accomplished through ATR-FTIR analysis, which allowed the identification of the functional groups present on the surface. The spectra of the samples are presented in this section. These samples were prepared specifically for ATR-FTIR analysis, which provide qualitative information on the chemical bonds present on the surface of the samples. Again, the spacing between the spectra in the figures was artificially adjusted to compare them more easily. The results were analyzed in two spectral regions. The first region includes a range from 4000 to 1800 cm^{-1} (as presented in Figure 50), while the second region, which is particularly relevant to epoxy resin, focuses on the fingerprint, ranging from 1800 to 600 cm^{-1} (as shown in Figure 51).

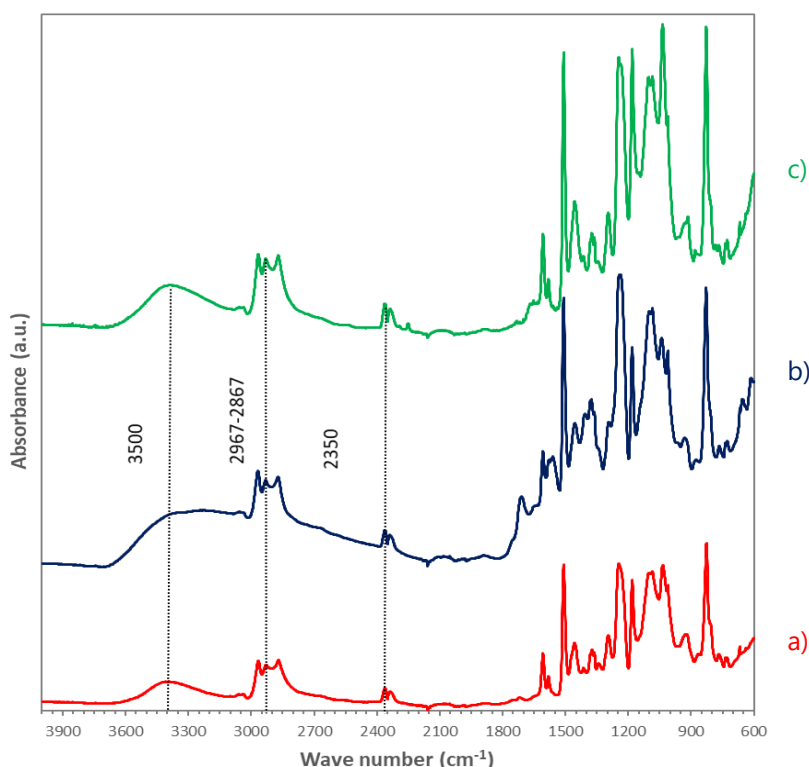


Figure 50: The ATR-FTIR Spectrum of the epoxy sample from 4000 to 600 cm^{-1} a) raw cleaned

epoxy resin, b) oxidized epoxy resin, c) sulfonated epoxy resin

Raw epoxy exhibited a band from 3500 to 3300 cm^{-1} , three peaks from 2967 to 2867 cm^{-1} , and a group of peaks around 2350 to 2330 cm^{-1} . The broad band between 3500-3300 cm^{-1} might indicate the -NH stretching bond of aromatic primary amine or heterocyclic secondary amine, and/or the vibration of the -OH bonds of alcohols in the epoxy resin (Cherian et al., 2016). Primary amines typically exhibit a doublet (reflecting asymmetric and symmetric stretching modes), whereas secondary amines show a single band (Gonzalez et al., 2012) indicating the presence of secondary amine groups in the epoxy resin. The region from 2967 to 2867 cm^{-1} was likely associated with -CH group stretching of the epoxy backbone. The group of peaks that were present around 2350 to 2330 cm^{-1} were attributed to CO_2 peaks due to the noise.

The treatment with the KMnO_4 oxidizing solution introduced a wide broad band in the region from 3500 to 3000 cm^{-1} (Figure 50.b). It can be attributed to the -OH stretching and bending modes of the adsorbed water (Durmus et al., 2009; Siau et al., 2004b), or to an increase in the quantity of hydroxyl groups within the resin due to the KMnO_4 treatment.

With the sulfonation treatment (Figure 50.c), the band located around 3500 cm^{-1} narrows compared to the KMnO_4 treated sample. As this band already exist in the raw epoxy resin (Figure 50.a), it might be attributed to adsorbed water and OH groups in the epoxy structure. Additionally, this may be attributed to the O-H vibration of sulfonic acid groups interacting with molecular water and adsorbed water from the surface, due to the sulfonation treatment (Çalı, 2019; Gao et al., 2017) In the spectral region between 2967-2867 cm^{-1} , no notable changes were observed for any of the samples, as depicted in Figure 50.b and c.

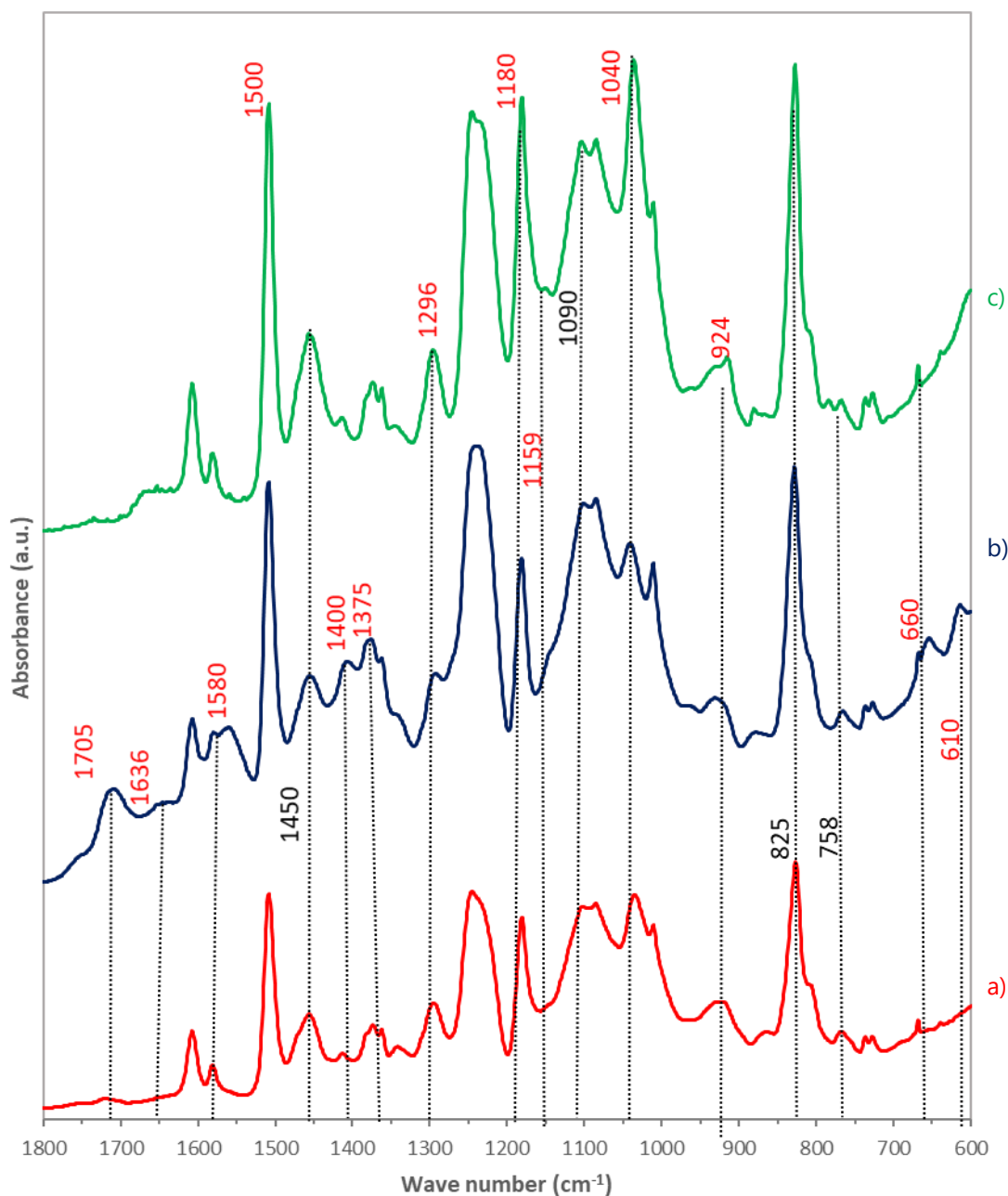


Figure 51: Fingerprint region of the epoxy resin a) raw epoxy, b) oxidized epoxy resin, c) sulfonated epoxy resin

The peaks observed in the fingerprint region (1800 to 600 cm^{-1}) for raw, oxidized and sulfonated epoxy resins with their corresponding wavenumbers, are depicted in Figure 51. The peaks that changed or appeared after the treatments were highlighted with red wave numbers. Between 1800 cm^{-1} to 600 cm^{-1} , the vibrational frequencies and the attributions of the characteristic peaks of the raw epoxy resin are given in Table 14.

Table 14: The vibrational frequencies of the raw epoxy resin (Çalı, 2019; Gao et al., 2017; Gonzalez et al., 2012; Han et al., 2011; Kallingal et al., 2023; Ouadah et al., 2018)

Band (cm ⁻¹)	Assignment
1370	Deformation CH ₃ of C-(CH ₃) ₂
1090	Stretching C-O-C of ethers
924	C-O deformation of the oxirane group
825	Stretching C-O-C of oxirane group
758	Rocking of -CH and CH ₂

After the oxidation (Figure 51.b), a series of new peaks appeared in the spectrum at 1705, 1636, 1580, 1400, 1373, 660 and 610 cm⁻¹. The peak around 1700 cm⁻¹ potentially indicates the -OH and C=O stretching of carboxylic acid bonds, supporting the formation of -OH and C=O bonds on the epoxy surface (Siau et al., 2004b). Furthermore, the bands located at 1636, 1580 and 1400 correspond to stretching vibrations of C-O (hydroxyl, ester or ether) and -OH bending vibrations (Zheng et al., 2013). These results may indicate the KMnO₄ treatment introduced hydroxyl and carboxyl groups onto the epoxy surface, supporting the idea of surface oxidation. The two other peaks that appeared within the range of 660 to 610 cm⁻¹, might arise from the stretching vibration of the Mn-O and Mn-O-Mn bonds (Kang et al., 2007; Zheng et al., 2013), which indicated the formation of manganese oxide, due to the KMnO₄ treatment.

Since the ATR-FTIR is not a quantitative technique, to observe the changes between each treatment, a reference peak, which is not expected to change with surface modification, was chosen on the spectrum of the raw epoxy. The peak at 1090 cm⁻¹, indicating the presence of ether bonds in the backbone, was chosen as a reference, because it was similar for all samples.

The intensities of several peaks changed after sulfonation (Figure 51.c), particularly the peaks at 1500, 1450, 1296, 1040, and 924 cm⁻¹. The peak at 1296 cm⁻¹ is attributed to the asymmetric and symmetric O=S=O stretching vibrations (Çalı, 2019; Gao et al., 2017). This peak was observed in the raw and oxidized epoxy, but in the sulfonated sample, its intensity increased compared to the reference peak at 1090 cm⁻¹, which might suggest a change induced by sulfonation, likely associated with the stretching vibrations of the sulfonic acid groups. Furthermore, the peak at 1180 cm⁻¹ displays a significantly higher intensity following sulfonation, compared to the reference peak at 1090 cm⁻¹, probably indicating the stretching vibrations of sulfonic acid groups. At 1159 cm⁻¹, a low intensity peak appeared, assigned to the asymmetric and symmetric SO₂ stretching mode (Zhou et al., 2019). The ratio of the peak at 1040 cm⁻¹ to the reference peak at 1090 cm⁻¹ has also increased, potentially attributed to incorporating S=O peaks, close to the C-O and C-O-C absorption signals. All these peaks support the presence of the sulfonic acid groups on the surface.

The peak at 924 cm^{-1} exhibits an additional low intensity shoulder compared to raw and oxidized epoxy resin, which can correspond to the absorbance of the butane sultone molecule (Wang et al., 2022). This might indicate the presence of unreacted butane sultone on the surface. The persistence of these groups even after cleaning may imply that they are embedded within the porous structure of the epoxy resin (created by the oxidation treatment), and have not undergone the sulfonation reaction. The peaks that appeared or displayed changes after the chemical modifications are given in Table 15.

Table 15: The vibrational frequencies indicating oxidation and sulfonation (Çalı, 2019; Gao et al., 2017; Gonzalez et al., 2012; Han et al., 2011; Ouadah et al., 2018; Zhou et al., 2019)

Band (cm^{-1})	Assignment
1252-96	Asymmetrical and symmetrical O=S=O stretching vibrations
1180 and 1159	Stretching vibrations of sulfonic acid groups
1180 and 1040	S=O stretching vibrations
1025	Asymmetrical/symmetrical bonds of S=O
625	Mn-O stretching modes

2.2 RADIOMETRIC CHARACTERIZATION

2.2.1 Liquid Scintillation Counting analysis

This section presents the results of LSC analysis for polymeric surface sources immersed in ^{152}Eu or ^{241}Am solutions. While the PET samples were tested with ^{152}Eu solution, epoxy samples underwent the RN attachment experiments with first ^{152}Eu and then ^{241}Am . The results are categorized and presented in two sections; the first focuses on the PET samples, and the second on epoxy samples. During the PET and epoxy studies, the ability to attach RNs to modified epoxy surfaces was evaluated after each surface modification step. Then, for epoxy, the optimum conditions of surface modification were identified with ^{152}Eu attachment studies. Eventually, the intermediate precision of the best method was assessed with ^{241}Am binding studies. The fixation yield of each sample was calculated using Equation 19. The uncertainty values of the each samples were calculated with the equation given in the Appendix-2.

The sources for LSC analysis are prepared following the method outlined in Figure 43. The fixation yield of the RN on the source, at a sampling time, is equal to the activity difference between the solution in contact with the modified sample and the reference solution without any sample. The activities calculated from the maximum fixation yield of the sources were given under the assumption of a uniform distribution of RN over the entire surface. This will be checked with autoradiography analyses in the next section.

2.2.1.1 LSC analysis of the PET samples

The production of PET modified samples was performed using two different methods (as shown in Figure 39). To bind RN, the modified samples were immersed in a ^{152}Eu solution of around 20 Bq/g, at pH 2.

Figure 52 presents the kinetic behavior of ^{152}Eu attachment onto the samples during the immersion. The maximum activities on the surfaces, calculated from the decrease in the radioactivity level of each source are given in Table 16. The black interval data shown for each data point are related with the interval of the uncertainty range for each measurement. The total amount of elements (active and stable isotopes) in the solution at the beginning of the experiment is also given in the tables in picomol to compare the ability of the samples to bind RNs.

The LSC allows to follow the amount of free RN remaining in solution. When the radioactivity decreases, it signifies that some RN have bound to the surface immersed in the solution. The maximum fixation yield is reached at the lowest point of the curve.

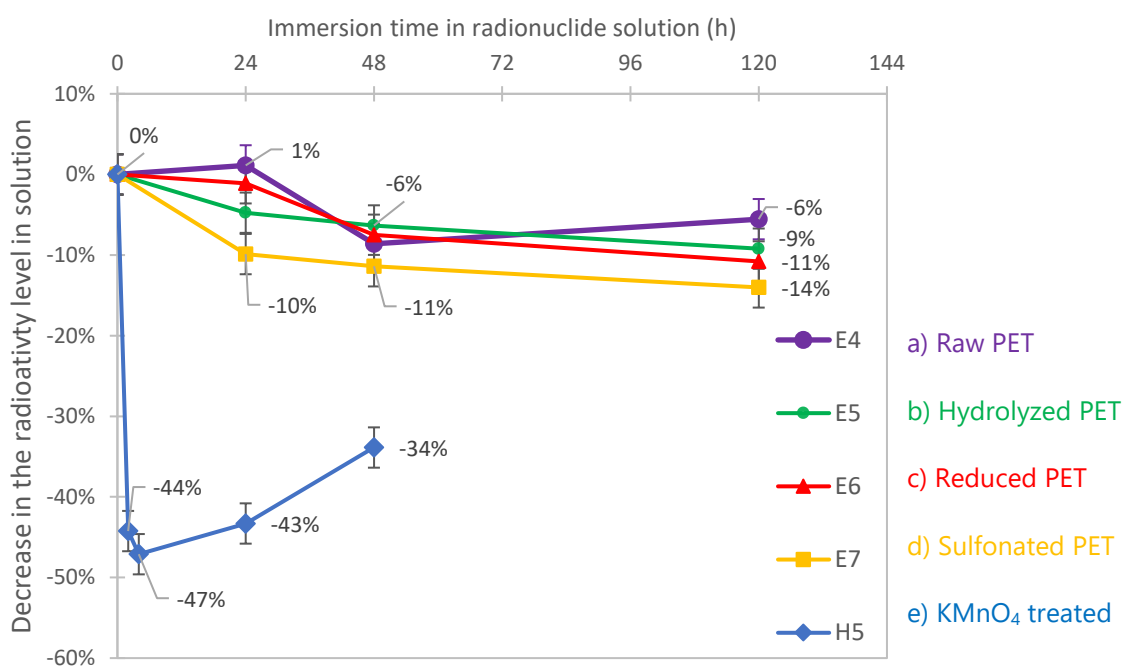


Figure 52: The attachment of ^{152}Eu on the PET samples a) E4 (raw PET), b) E5 (hydrolyzed PET), c) E6 (reduced PET), d) E7 (sulfonated PET), e) H5 (KMnO_4 treated PET)

Table 16: Maximum activity of the PET surface sources immersed in a ^{152}Eu solution

Sample name	Applied treatment	Total amount of Eu in solution (picomol)	Maximum fixation yield, standard uncertainty ($k = 1$)	A_{max} (Bq), standard uncertainty ($k = 1$)
E4	Raw PET	65	$-(8.6 \pm 2.8)\%$	(95 ± 30)
E5	Hydrolyzed PET	70	$-(9.2 \pm 2.8)\%$	(108 ± 32)
E6	Reduced PET	63	$-(10.8 \pm 2.7)\%$	(114 ± 29)
E7	Sulfonated PET	70	$-(14.0 \pm 2.7)\%$	(165 ± 32)
H5	KMnO_4 treated PET	68	$-(47.1 \pm 2.5)\%$	(517 ± 27)

Sample E4 (raw PET) showed the lowest fixation yield (around 6%) at the end of the RN binding experiment. Since this sample was not modified, it is expected that this low amount of radionuclides is only physisorbed onto the surface. The samples E5, E6 and E7, produced with the first method, sulfonation, exhibited a similar kinetic behavior: their fixation yield increased slightly up to 48 h (Figure 52.b, c and d). The value of the maximum fixation yield increases from E5 to E7, from 9% to 14%, (Table 16). The sulfonation step (Figure 52.d) increased RN binding compared with the other steps of the method. This seems to indicate that the sulfonation reaction was successful and that ^{152}Eu attached to those groups on the surface.

The E sample H5 was produced by the second method, a one-step treatment with KMnO_4 . This particular sample reached the highest fixation yield among all the PET samples, around 47% (Figure 52.e). Furthermore, the ^{152}Eu fixation displayed a different kinetic behavior, achieving its maximum fixation after only 4 h. However, the yield decreased from 47% to 34% at the end of the immersion (48 h). This could indicate a loss of the coating during the immersion period or a detachment of some of the fixated RN from the surface.

After the KMnO_4 treatment, the PET sample could have undergone oxidation, transforming the hydroxyl end-groups of the polymer into carboxylic acids groups, or could have been coated with MnOx , or both (as discussed in section 2.1.1 of this chapter). However, MnOx was reported to be a better ion exchanger than carboxylic acid groups at acidic pH. Therefore, the higher fixation yield for this sample seems to indicate that the KMnO_4 treatment led to a MnOx coating.

Following the results from LSC analysis, the decision was made to renounce further improvement of the PET samples and instead concentrate on improving the epoxy resin samples. The main reason for this decision is the limited number of functional groups available even after the pre-treatment steps for PET, which constrains its potential for further enhancements. In contrast, epoxy resin, with its more abundant functional groups, presented a more promising option for development and optimization.

2.2.1.2 LSC analysis of the epoxy resin samples

The functionalization of epoxy resin with sulfonic acid groups follows two steps, a pre-treatment performed with KMnO_4 to oxidize the surface, then, the reaction of $-\text{OH}$ bonds on the surface to yield sulfonic acid groups. First, our purpose was to assess the impact of each step on the ability of the surface to bind the RN. The functionalization steps were then optimized by placing the samples in contact with a ^{152}Eu solution, while intermediate precision assessments were carried out with ^{241}Am . The LSC analysis were compared for oxidation and sulfonation treatments for each RN.

2.2.1.2.1 Epoxy resin samples spiked with ^{152}Eu

2.2.1.2.1.1 Assessment of the binding ability of the epoxy resin after each modification step

This section presents the RN binding experiments conducted with the oxidized and sulfonated epoxy resins, as illustrated in Figure 53. The figure provides a comprehensive assessment conducted for each step, starting from the raw epoxy substrate and progressing through the oxidized and sulfonated epoxy substrates.

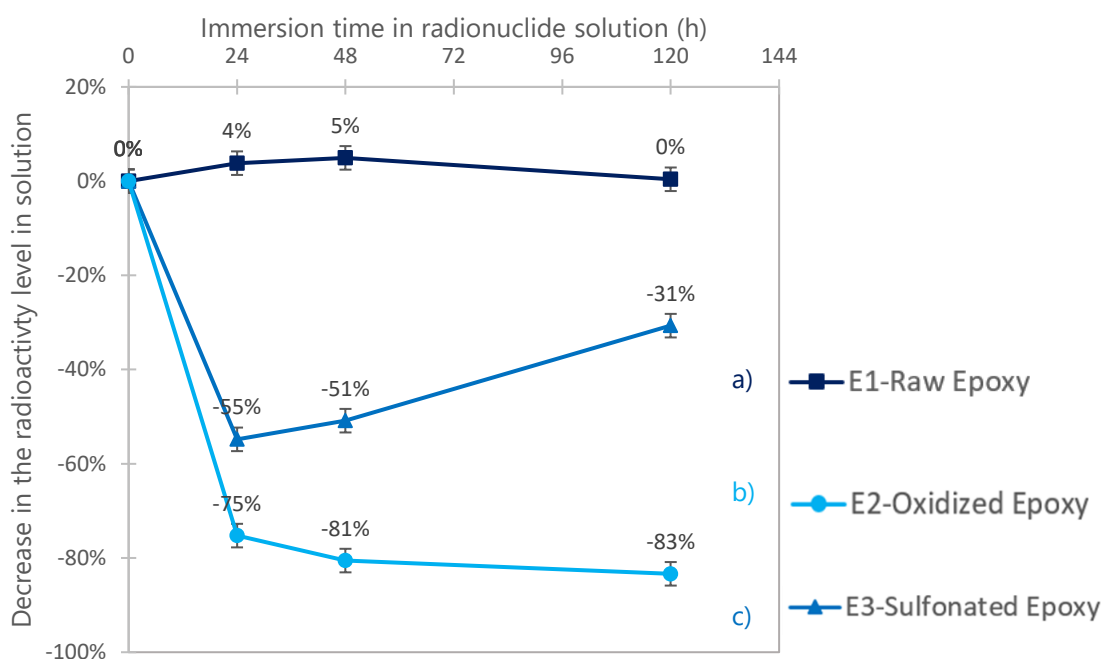


Figure 53: Kinetic behavior of the fixation of ^{152}Eu onto epoxy samples a) raw epoxy (E1), b) oxidized epoxy (E2), c) sulfonated epoxy (E3)

The raw epoxy resin exhibited negligible RN fixation at the end of the immersion, with value falling within the measurement uncertainty range (Figure 53.a). The oxidation and sulfonation treatments (Figure 53.b and c) resulted in higher fixation yields throughout all sampling intervals. After 24 h,

the best fixation was achieved by the oxidized sample with 75% fixation and only 55% for the sulfonated one. After 48 h, the oxidized sample remained stable, while the fixation yield of the sulfonated sample decreased, which might indicate that the RN detached from the surface. The interaction of the RN with the sulfonated surface seems weaker than with the oxidized surface.

It is reasonable to hypothesize that sulfonation occurred on the oxidized regions, driven by the presence of hydroxyl (-OH) bonds created by the KMnO_4 treatment. This process may lead, in turn, to RN binding via sulfonic acid functional groups. On the other hand, the oxidized surface, is only supposed to possess -OH and COOH bonds. The sulfonated groups are expected to display a superior binding behavior compared to those. Therefore, the higher fixation yield obtained for oxidized surfaces rather than sulfonated surfaces is unexpected.

However, the oxidation treatment is conducted using KMnO_4 , which is a known precursor of manganese oxide (MnOx), also reported as an inorganic cation exchanger (as explained in Chapter 2). MnOx layers were used previously in the literature to concentrate divalent radionuclides, especially Ra^{2+} and UO_2^{2+} , to purify water samples ("NucFilm Discs"). Furthermore, a black coating was observed on the epoxy surfaces after oxidation, which might indicate the formation of a MnOx coating. Furthermore, the ATR-FTIR spectrum showed that some bands that could be attributed to MnOx appeared after the KMnO_4 treatment (Figure 51.b), which supports the presence of manganese oxide groups on the surface.

Therefore, it might be possible that the high fixation yield of oxidized epoxy surfaces is primarily due to a MnOx coating. With the sulfonation method, a noteworthy occurrence is the removal of the black coating. The sulfonation process, may then convert the OH groups of the surface into sulfonic acid groups, as was evidenced with ATR-FTIR, but it also removes most of the MnOx layer from the surface, which may account for the observed lower fixation yields. Furthermore, it is also possible that the presence of a MnOx layer prevents some of the -OH bonds from being converted into sulfonated groups, which lowers the amount of sulfonic acid binding groups on the surface, also leading to a lower fixation yield.

It is worth mentioning that binding of RN onto the MnOx coating appears to be a more facile process. In contrast, sulfonation should result in a more stable structure due to the formation of strong chemical bonds on the surface of the epoxy. However, the stability also depends on binding the RN to the sulfonic acid groups through strong interactions. This will be discussed in the coming sections about the non-contamination test and autoradiography images.

These results were followed by the optimization of the KMnO_4 treatment and the sulfonation of the epoxy resin.

2.2.1.2.1.2 Optimization of the KMnO_4 treatment of epoxy resin samples using ^{152}Eu binding experiments

Several parameters can influence the fixation yield of radionuclides on oxidized epoxy samples. These include parameters from the KMnO_4 treatment, such as the molar ratio of the chemicals used in the oxidization solution, the oxidation duration, or the immersion duration in the RN solution. In this section, the impact of the oxidation duration was investigated.

E2 was the first trial of the KMnO_4 treatment with 0.36 mol/L of KMnO_4 and an oxidation duration of 30 min. Subsequently, the F2 and G2 samples were treated for 60 min, with a similar KMnO_4 concentration, to evaluate the influence of the longer oxidation duration.

Figure 54 provides the kinetic behavior of ^{152}Eu on the E2, F2 and G2 samples, and Table 17 provides the maximum fixation yields and activity of the oxidized epoxy samples spiked with ^{152}Eu .

The E2 sample had the lowest fixation yield among this series, which could be attributed to the duration of the oxidation reaction. By increasing the oxidation duration, the amount of the MnOx coated on the surface increased, which seems to improve the attachment of the RNs on the sample. Sample E2 displayed an increase in the fixation yield after 48 h, but continued to increase slowly up to 120 h, when the binding experiment was stopped.

Samples F2 and G2, subjected to identical experimental conditions, displayed the same fixation yield (within uncertainties), and kinetic behavior. Both samples reached the maximum fixation yield, around 98%, after 24 h (Table 17). After 48 h, their fixation yield seemed to decrease slightly (G2 from 97% to 91%, and F2 from 98% to 93%) (Figure 54.b and c). This observation underscores the intermediate precision of the samples obtained using the optimized oxidation protocol. Furthermore, the fixation yield of the F2 sample stayed constant after 48 h, which demonstrated that the stability of these sources in an aqueous medium was successfully maintained for up to 144 h (6 days).

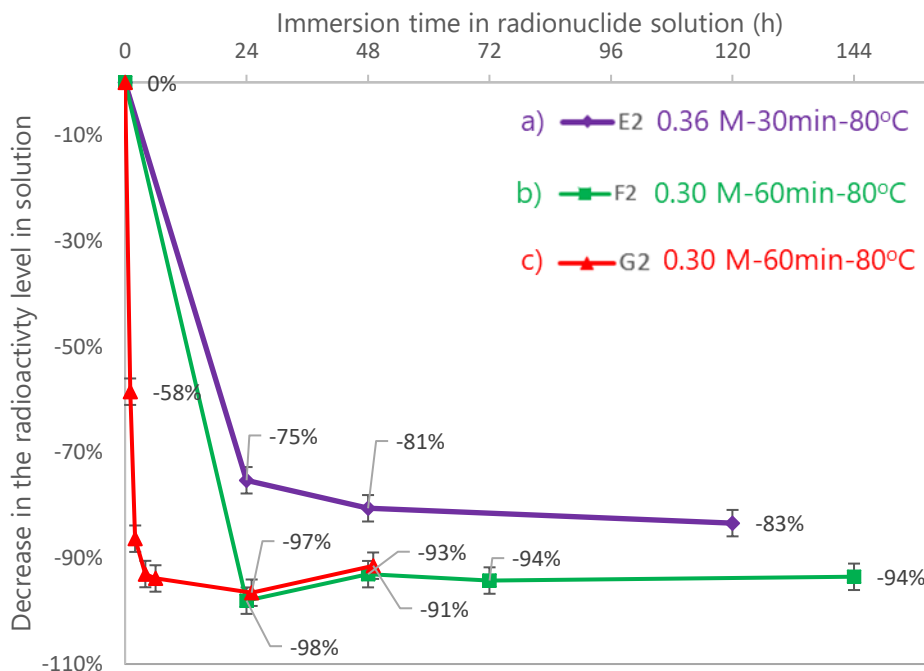
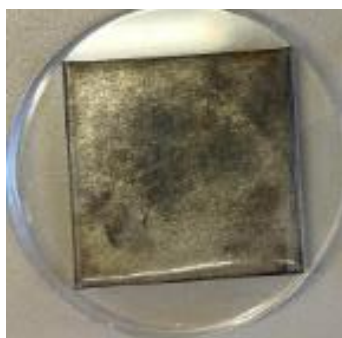


Figure 54: Kinetic behavior of the fixation of ^{152}Eu onto oxidized epoxy samples, a) E2, b) F2 and

c) G2 samples

Table 17: Maximum radioactivity levels of the oxidized epoxy samples immersed in a ^{152}Eu solution

Epoxy samples	Experimental conditions of oxidation (Concentration of KMnO_4 (mol/L)- duration- temperature)	Total amount of Eu in solution (picomol)	Maximum fixation yield, standard uncertainty ($k = 1$)	A_{max} (Bq), standard uncertainty ($k = 1$)	t_{max} (h)
Oxidized (E2)	~0.36 M-30min-80°C	70	(83.4 \pm 2.7)%	(978 \pm 32)	120
Oxidized (F2)	~0.30 M-60min-80°C	52	(98.0 \pm 2.9)%	(860 \pm 25)	24
Oxidized (G2)	~0.30 M-60min-80°C	77	(96.5 \pm 2.8)%	(1248 \pm 30)	24

a) E2 (~0.30M- 30 min-80°C)
 ^{152}Eu b) F2 (~0.30M-60 min-80°C)
 ^{152}Eu c) G2 (~0.30M-60 min-80°C)
 ^{152}Eu Figure 55: Pictures of the oxidized samples treated with ^{152}Eu a) E2, b) F2, and c) G2

During the optimization studies, the experimental set up was improved and optimized. From the pictures of the sources, an improvement of the coating distribution is observed after each trial; E being the first, followed by F, and finally, G2 (Figure 55).

2.2.1.2.1.3 Optimization of the sulfonation of epoxy resin samples using ^{152}Eu binding experiments

In this section, the impact of the selected parameters, the sulfonation duration and the reaction temperature, on the attachment of RN to the surface was investigated, and optimized.

The sulfonation reaction was performed on samples that were previously oxidized with KMnO_4 . Sample E3 was subjected to a shorter 30 min KMnO_4 treatment than the others (H6, G3 and F3) that were treated for 60 min.

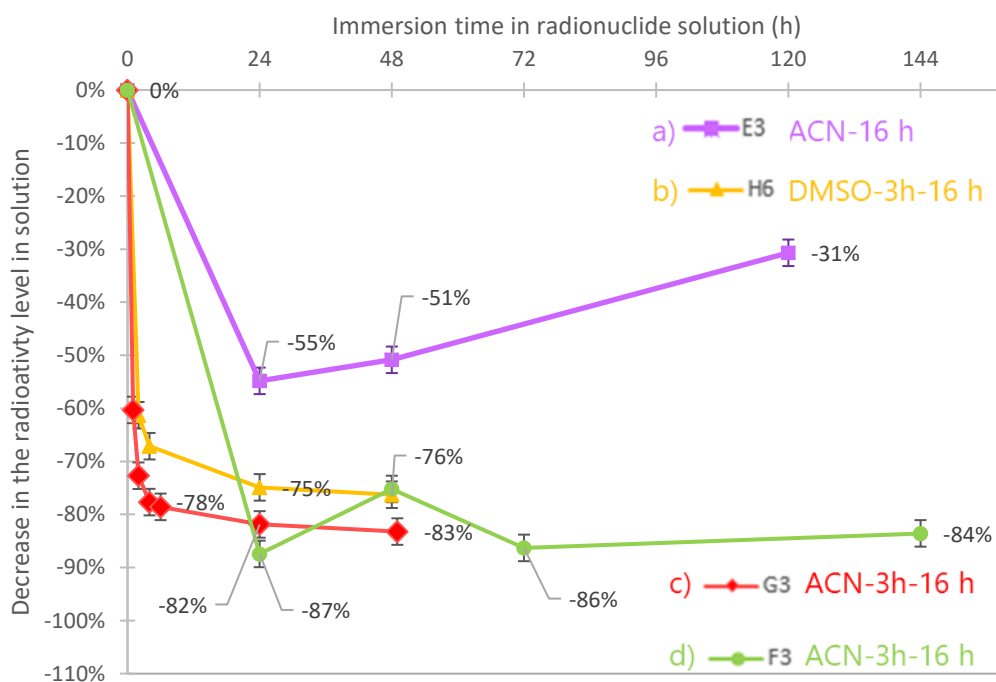


Figure 56: Kinetic behavior of the fixation of ^{152}Eu onto sulfonated epoxy samples a) E3 (ACN-16h-70°C), b) H6 (DMSO-3h@70°C+16 h@22°C), c) G3 (ACN-3h@70°C+16h@22°C), d) F3 (ACN-3h@70°C+16h@22°C)

Figure 56 illustrates the kinetic behavior of the sulfonated samples in contact with ^{152}Eu , and Table 18 presents the maximum fixation yields of those samples. The E3 sample exhibited the lowest maximum fixation yield among the samples, around 55% (Table 18). Furthermore, this sample exhibited a decrease of the fixation yield after 24 h, indicating a possible detachment of the RN, or a loss of the grafted layer (Figure 56.a) The fixation yield of the other samples stayed constant after reaching their maximum (Figure 56.b, c and d).

Table 18: Maximum radioactivity levels of sulfonated epoxy samples immersed in a ^{152}Eu solution

Sulfonated epoxy samples and their experimental conditions (Solvent-duration-temperature)	Total amount of Eu in solution (picomol)	Maximum fixation yield ($k = 1$)	A_{max} (Bq) ($k = 1$)	t_{max} (h)
E3 (ACN-16 h-70°C)	63	$-(54.8 \pm 2.5)\%$	(583 ± 27)	24
F3 (ACN-3h@70°C+16h@22°C)	53	$-(87.4 \pm 2.7)\%$	(786 ± 25)	24
G3 (ACN-3h@70°C+16h@22°C)	61	$-(81.9 \pm 2.7)\%$	(845 ± 28)	48
H6 (DMSO-3h@70°C+16h@22°C)	61	$-(76.3 \pm 2.6)\%$	(783 ± 27)	48

Two parameters could have contributed to this difference for E3: the shorter KMnO_4 pre-treatment, and/or the difficulty to control a high temperature for overnight during the sulfonation reaction. The improvements in the oxidation treatment may lead to more sulfonated groups. Another factor that could play a role in the success of the sulfonation treatment is the high temperature of the solvent during the sulfonation reaction. When E3 was subjected to the temperature treatment (70 °C) for 16 h, the solvent completely evaporated. It is possible that when the solvent evaporated, the reaction stopped and did not proceed overnight. For the other samples, when evaporation occurred, ACN was added to the reaction vessel to prevent the reaction from stopping. Additionally, they were kept at room temperature (22 °C) for 16 h instead of 70 °C. An alternative hypothesis is that the high-temperature treatment may have damaged the coating formed during the oxidation treatment.

The H6 sample (DMSO-3h@70°C+16h@22°C) was produced with DMSO as solvent instead of ACN. The selection of DMSO was driven by its superior solubility capacity for NaH compared to acetonitrile. The H6 sample seemed to display lower maximum fixation yield than the F3 and G3 samples (Table 18), furthermore, the epoxy resin was deformed (Figure 57), probably due to the swelling effect of DMSO.



Figure 57: Appearance of the sulfonated sample using DMSO solvent (H6)

Among the samples spiked with ^{152}Eu , samples F3 and G3 demonstrated the highest fixation yield, and those samples were not deformed by the treatment, therefore their production protocol was kept as optimal (ACN-3h@70°C+16h@22°C).

2.2.1.2.2 Epoxy resin samples immersed in a ^{241}Am solution

2.2.1.2.2.1 Intermediate precision studies of the oxidized epoxy resin with ^{241}Am

Following the determination of optimal oxidation parameters ($\sim 0.30\text{M KMnO}_4$ -60 min- 80°C), a series of intermediate precision tests were carried out using ^{241}Am , to evaluate whether separately prepared samples could attach RN in a similar way. The J1 sample was prepared first, and K1, K2, and K3 samples were prepared simultaneously, in different beakers.

Figure 58 shows the kinetic behavior of the samples J1, K1, K2, and K3, and the maximum fixation yield of the oxidized epoxy resin sources spiked with ^{241}Am are given in Table 19. After the J1 series, the amount of added Am was reduced from 60 picomol to 30 picomol to achieve lower levels of radioactivity on the product.

All samples displayed a similar behavior, with a maximum fixation yield of approximately 98% (Table 19). For the first trial of ^{241}Am sources, the J1 sample was produced. Previous experiments with Eu sources indicated that the maximum fixation yield in epoxy sample is typically achieved after 24 h of immersion. Based on this information, an initial immersion duration of 24 h was chosen for the J1 sample.

The J1 sample (Figure 58 .a) achieved its maximum fixation yield at 24 h when the immersion was stopped, as expected from previous analysis. From this experiment, it is challenging to predict definitively whether the attachment of ^{241}Am will continue. For the next experimental analysis K samples were produced and they immersed in the RN binding solution for 144 h. The samples K1, K2, and K3 were kept longer in the RN solution, but the maximum fixation yield was also reached within 48 h and stayed constant throughout the duration of immersion in the RN medium (Figure 58b, c, d). Nonetheless, the kinetic shows a similar trend as the other samples until the end of the immersion duration.

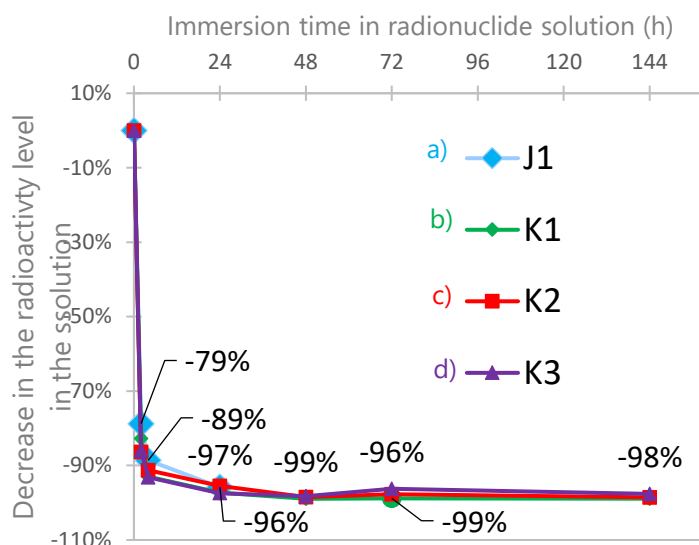


Figure 58: The kinetic behavior of ²⁴¹Am onto the oxidized epoxy resin samples a) J1, b) K1, c) K2 and d) K3.

Furthermore, the K1, K2, and K3 samples, displayed very similar fixation yields and analogous kinetic behaviors. These observations suggested that the oxidation method applied to these samples was intermediate precision condition. Moreover, these samples demonstrated the ability to maintain fixation yields at a consistent level up to 144 h, or 6 days, with no apparent removal of the fixated RNs.

Table 19: Maximum activities of the oxidized epoxy sources immersed in a ²⁴¹Am solution

Epoxy samples	Experimental conditions (Concentration of KMnO ₄ -t _{rxn} -T)	Total amount of ²⁴¹ Am in solution (picomol)	Maximum fixation yield (k = 1)	A _{max} (Bq) (k = 1)	t _{max} (h)
Oxidized (J1)	~0.3M-60min-80°C	60	-(95.8 ± 2.8)%	(1610 ± 48)	24 h
Oxidized (K1)	~0.3M-60min-80°C	32	-(98.9 ± 2.9)%	(953 ± 28)	48 h
Oxidized (K2)	~0.3M-60min-80°C	33	-(98.6 ± 2.9)%	(993 ± 29)	48 h
Oxidized (K3)	~0.3M-60min-80°C	37	-(97.7 ± 2.9)%	(1110 ± 33)	48 h

2.2.1.2.2.2 The sulfonated epoxy resin spiked with ²⁴¹Am

Following the determination of the optimal sulfonation treatment (ACN-3h@70°C+16h@22°C), a series of intermediate precision tests were carried out using ²⁴¹Am. All samples were prepared under identical conditions.

The kinetic behavior of the samples is displayed in Figure 59 and summarized in Table 20. L2 and L3 samples exhibited identical kinetic behavior (fixation yield about 92%), while L1 reaching a lower fixation yield (around 80%).

Table 20: Maximum activities of the sulfonated epoxy sources immersed in ^{241}Am

Epoxy samples	Experimental conditions of sulfonation (Molar ratio of 1,4-butane sultone/NaH- t_{rxn} -T)	Total amount of ^{241}Am in solution (picomol)	Maximum fixation yield ($k = 1$)	A_{max} (Bq) ($k = 1$)
Sulfonated (L1)	ACN-3 h@70°C+16h@22°C	37	-(80.1 ± 2.6)%	(914 ± 30)
Sulfonated (L2)	ACN-3h@70°C+16h@22°C	38	-(92.4 ± 2.8)%	(1076 ± 30)
Sulfonated (L3)	ACN-3h@70°C+16h@22°C	36	-(92.8 ± 2.8)%	(1016 ± 30)

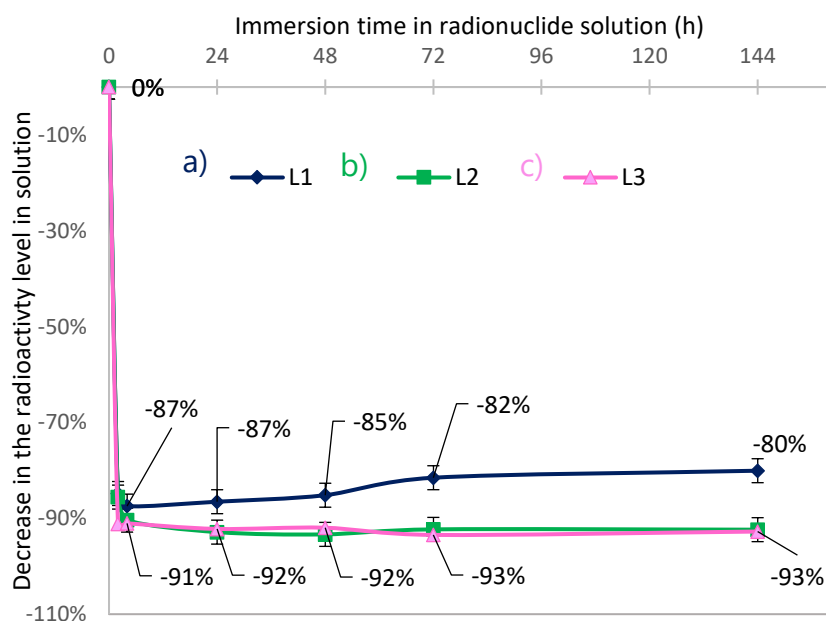


Figure 59: The kinetic behavior of the sulfonated samples immersed in ^{241}Am solution

All of these samples were prepared separately. The L1 sample encountered some experimental challenges during the sulfonation. The crystallizer got broken, after 30 minutes, and as a result, a new solution was prepared. The pre-step of the sulfonation, mixing NaH and ACN (Figure 42.a), was completed quickly instead of mixing for 1 h at 45 °C. It is possible that the mixing could not be completed properly and NaH cannot play its role of starting the nucleophilic substitution correctly. Another hypothesis could be the occurrence of some complications during the oxidation treatment of the L1 sample. Sample L1 was notably less black than the others (Figure 60). If the oxidation step could not be achieved, the release of the hydroxyl bonds from the surface would not be successful, which might have an impact on the efficiency of the sulfonation treatment. The

color of the epoxy after the oxidation could be a physical indicator signifying a successful MnOx coating.

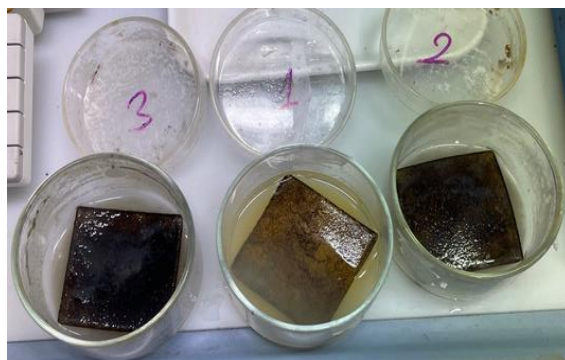


Figure 60: Appearances of samples of the L series after the sulfonation treatment

In the case of the L1 sample, the maximum fixation yield is not as high as other samples but still it exhibited an acceptable value, 80% (Figure 59.a). On the other hand, when considering the L2 and L3 samples, the maximum yield was reached after 24 h and remained stable until the end of the immersion duration (Figure 59.b and c). These observations suggested that experimental problems may lead to a 10% difference in fixation yield. However, if the experimental conditions can be controlled, the production of the sources is intermediate precision on two samples (L2 and L3). Moreover, these samples demonstrated the ability to maintain fixation yields at a consistent level even after a 48 h duration, with no apparent detachment of the RNs.

2.2.1.2.2.3 Comparison between oxidized and sulfonated epoxy resin immersed in a ^{241}Am solution

After optimization of the experimental protocols of KMnO_4 treatment and sulfonation, it was observed that fixation yields were slightly lower for the sulfonated samples than those achieved with the oxidized counterparts (Table 21). This observation was similar before optimization, and for ^{152}Eu .

This difference can be attributed to several factors. Firstly, the manganese dioxide coating present in the oxidized samples might have a stronger affinity for retaining radionuclides compared to the sulfonic acid groups in the sulfonated samples. Furthermore, since sulfonation is a second step applied to oxidized samples, the reduced fixation in these samples could be linked to the partial removal of the manganese oxide coating that coated during the oxidation process. This loss of coating likely results in lower fixation efficiency of RNs in the sulfonated samples. Thus, the key factor influencing the fixation yield appears to be the presence or absence of the manganese dioxide coating, which is compromised during the sulfonation process.

Table 21: Maximum fixation yields of the best samples that oxidized and sulfonated in ^{241}Am

Epoxy samples	Experimental conditions of sulfonation	Total amount of ^{241}Am in solution (picomol)	Maximum fixation yield ($k = 1$)	A_{max} (Bq), ($k = 1$)	t_{max} (h)
Oxidized (K1)	~0.3M-60min-80°C	32	-(98.9 ± 2.9)%	(953 ± 28)	48 h
Sulfonated (L3)	ACN-3h@70°C+16h@22°C	36	-(92.8 ± 2.8)%	(1016 ± 30)	72 h

2.2.1.2.3 Comparison between ^{152}Eu and ^{241}Am binding

In this part, from the optimized KMnO_4 treatment and sulfonation methods, two best samples were chosen to underline the different behaviors with Eu and Am solutions. In the Table 22 and Table 23, the total number of atoms (stable and active) is also given. For ^{241}Am solution does not contain have any stable Eu atoms, contrary to the ^{152}Eu solution.

Table 22: Maximum fixation yields and activities of ^{152}Eu and ^{241}Am onto KMnO_4 treated epoxy samples

KMnO_4 treated samples immersed in ^{152}Eu solution	0.30 M KMnO_4 - 60 min-80°C	Total amount of element in solution (picomol)	Maximum fixation yield ($k = 1$)	A_{max} (Bq) ($k = 1$)
	F2	52	-(98.0 ± 2.9)%	(860 ± 25)
G2	77	-(96.5 ± 2.8)%	(1248 ± 30)	
KMnO_4 treated samples immersed in ^{241}Am solution	J1	60	-(95.8 ± 2.8)%	(1610 ± 50)
	K1-K2-K3	~ 34	-(98.9 ± 2.9)%	(953 ± 30)

For the samples that treated with KMnO_4 samples, there was no significant difference observed in the fixation yield (Table 22). However, when considering sulfonated samples (Table 23), the fixation yield of the samples immersed in a Eu solution was around 5% to 8% lower than the fixation yield of the samples immersed in an Am solution.

Nevertheless, the total amount of element in solution was around 1.5 times higher for the Eu solutions than for the Am ones. It is then possible that, for the Eu solutions, the number of atoms was higher than the available binding sites on the modified epoxy resin, resulting in a fixation yield lower than 100%. On another hand, the amount of ^{241}Am being lower, the number of atoms might not exceed the number on binding sites on the surface, leading to a fixation yield close to 100%.

Table 23: Maximum fixation yields and activities of ^{152}Eu and ^{241}Am onto sulfonated epoxy samples

Sulfonated samples immersed in	ACN-3h@70°C+16 h@22°C	Total amount of element in solution (picomol)	Maximum fixation yield ($k = 1$)	A_{max} (Bq) ($k = 1$)
^{152}Eu solution	F3	53	-(87.4 ± 2.7)%	(786 ± 25)
	G3	61	-(81.9 ± 2.7)%	(845 ± 28)
^{241}Am solution	L2	38	-(92.4 ± 2.8)%	(1076 ± 30)
	L3	36	-(92.8 ± 2.8)%	(1016 ± 30)

2.2.1.2.4 Comparison between polymeric substrates

A comparison between the epoxy and PET substrates, immersed in a ^{152}Eu solution, is presented in Table 24. This allows for a direct comparison of the substrates when subjected to the same chemical treatment.

Table 24: Comparison of PET and epoxy resin substrates with the best oxidized and sulfonated samples that were immersed in a ^{152}Eu solution

Sample name	Applied method	Total amount of Eu in solution (picomol)	Maximum fixation yield, standard uncertainty ($k = 1$)	A_{max} (Bq) ($k = 1$)
KMnO ₄ treated PET H5	~0.30 M-60min-80°C	68	-(47.1 ± 2.5)%	(520 ± 30)
Sulfonated PET E7	ACN-3h@70°C+16h@22°C	70	-(14.0 ± 2.7)%	(165 ± 30)
KMnO ₄ treated epoxy resin F2	~0.30 M-60min-80°C	52	-(98.0 ± 2.9)%	(860 ± 25)
Sulfonated epoxy resin F3	ACN-3h@70°C+16h@22°C	53	-(87.4 ± 2.7)%	(786 ± 25)

It was observed that the epoxy resin samples generally exhibited higher fixation values compared to the PET samples. This disparity can likely be attributed to the number of functional groups present on the surface of each material. PET is reported to have less surface functional groups than epoxy, and breaking the ester bonds of PET to create new reactive groups is more difficult than breaking the ether and amine bonds of the epoxy resin.

Furthermore, since the structure of epoxy is a 3D cross-linked network and the one of PET is aligned polymer chains, chemical attacks on the surface of epoxy result more easily in the formation of pores, compared to the PET (Crawford and Quinn, 2017). This increase in surface roughness in turns increases the number of functional groups able to attach the RN. However, this roughness may have an impact on the emission of alpha particles from the produced source, and it would be beneficial to quantify this impact in future work.

Another potential factor influencing the lower fixation yield of PET compared to epoxy resin could be related to the physical interaction of PET with the beaker during the treatments. It was noted that PET tends to adhere to the bottom of the beaker, meaning that one side of the PET sample may not be fully functionalized or exposed to the solution, thus not uptaking RNs effectively.

2.2.2 Phosphor imaging Autoradiography analysis

In this section, the confirmation of RN presence on the surfaces and the assessment of RN distribution uniformity were investigated through phosphor imaging autoradiography analysis.

The main assumption underlying the LSC analysis is that the observed decrease in radioactivity levels in the solution during the RN binding experiments is due to the attachment of the RN on the immersed surface. Autoradiography allowed verifying if activity is actually present on the surfaces.

The radioactivity level of each source can be calculated with the fixation yield at the last sampling time and the radioactivity initially present in the RN binding medium. Equation 20 describes the calculation of the source activity (Bq).

$$A_{\text{sample}} = |Y_{\text{at the sampling time}}| \% \times A_{\text{initial}} \times m_{\text{total}} \quad \text{Equation 20}$$

In Equation 20 where “ $|Y_{\text{at the sampling time}}| \%$ ” equals to “ $|Y_{\text{end}}| \%$ ” is the absolute value of the fixation yield at the end of the immersion time, A_{initial} is the mass activity of the RN solution (in Bq/g) and m_{total} the mass of RN solution (in g) that was added in the beaker. Only the samples with a high yield at the end of the RN binding experiment could be analyzed with autoradiography. The activity of the surfaces with a low fixation yield was not high enough to create an image on the film.

Furthermore, autoradiography can give an indication of the uniformity of the sources. This is important because when the activity per unit surface (A_s) is calculated for some sources, it implies that the radionuclides are distributed uniformly across the entire surface area of the source Equation 21.

$$A_s = \left(\frac{A_{\text{end}}}{\text{Total surface area of the source}} \right) \quad \text{Equation 21}$$

Autoradiography images were used to measure this uniformity, according to ISO 8769 (ISO 8769, 2020). This standard defines uniformity as the standard deviation of the surface emission rates from individual portions of the entire source area Equation 1. This document also recommends that these sources be flat and have uniformity values exceeding 90%.

In this section, uniformity measurements that were conducted on polymeric surface sources are presented. The 25 cm² sources were divided into 4 portions of 6.25 cm², the values are chosen to follow the same size of the subareas are stated in the ISO standard. Generally, the duration of the exposures was about 3 days.

All the measurements that were performed with autoradiography imaging system come with a 10% standard uncertainty in the uniformity values. These calculations are explained in Appendix-2.

In the figures presented in this section, "U" represents the uniformity of the source, "A_{end}" denotes the activity on the source at the conclusion of the immersion experiment. "A_s" signifies the surface activity of the source, also measured at the end of the immersion process. The scale bar added next to the autoradiography images refers to the radioactivity level according to the value of the color of the signal. Red signifies the highest activity values, blue shows the lower values, while grey is the background. For comparisons, all images presented together in a figure were recorded during the same exposure.

The scanner within the autoradiography device translates the scanned data into Digital Light Units (DLU) for each pixel. The results are then visually represented as a two-dimensional image in the OptiQuant software.

Moreover, for all the samples, the uniformity calculations performed for 3x3 grids are given in Appendix-2 in the title of "Phosphor autoradiography imaging". Compared to the 2x2 grids, they generally give a lower uniformity. Each sub-area of the 2x2 grids measure 6.25 cm², while the ones of the 3x3 grids measure 2.8 cm². 2x2 grids give a uniformity value that is averaged over a larger surface, which can cover the fact that a sub-area is not entirely homogeneous. Furthermore, the measurement of uniformity is affected by the edges of the source, usually resulting in higher DLU values close to the edges. With a 2x2 grid, all the cells contain two edges of the source, while with a 3 x 3 grid, this is not the case. This might realistically decrease the uniformity calculated with 3x3 grids.

2.2.2.1 Autoradiography analysis of PET samples

In Figure 61, the calculated total activity from LSC measurements of the PET sources at the end of the immersion and their uniformity are given.

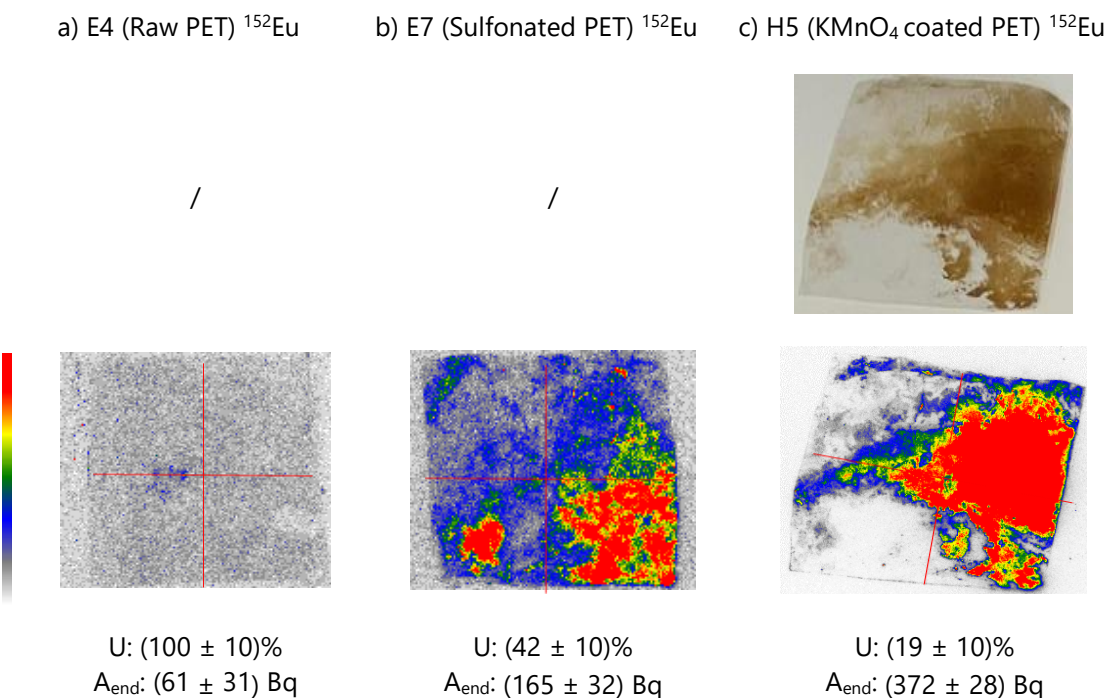


Figure 61: Pictures of samples, phosphor imaging autoradiography images, uniformity and radioactivity levels of PET samples treated with ^{152}Eu a) E4, b) E7, c) H5

The E4 sample (Figure 61.a) showed a very low level of radioactivity (only about 16%). This was expected because this sample was raw PET and was not supposed to bind RN significantly. As the radioactivity level was close to the background, it exhibited a high uniformity close to 100%. The observed small blue spots localized at the center of the sample might be related with RN physically attached on the surface through weak bonds.

The E7 sample (Figure 61.b) exhibited a two times lower radioactivity level than the KMnO₄ treated H5 sample (Figure 61.c), based on the fixation yield from LSC analysis. However, the differences in radioactivity levels within the subareas of E7 were not excessively large, while for the H5 sample, the activity was mainly located in the top right corner. As a result, the uniformity of E7 was higher compared to the H5 sample.

The image of H5 (Figure 61.c) revealed a notable correlation between the existence of the brownish coating and the regions that displayed radioactivity. This implied that the brownish layer indicates where the RNs were attached to the surface. These images showed that while the modification of PET surfaces led to some attachment of radioactivity, further optimization is needed to reach surfaces that are more uniform. However, this optimization was not performed, because epoxy resins showed more promising results.

2.2.2.2 *Autoradiography analysis of epoxy resin samples*

2.2.2.2.1 Epoxy resin samples in contact with ^{152}Eu

2.2.2.2.1.1 Oxidized epoxy resin samples uptaking ^{152}Eu

The activities and uniformities of the oxidized samples with KMnO_4 are shown in Figure 62.

The KMnO_4 treatment applied to the cleaned epoxy resin covered the epoxy surface with a black coating, which exhibited a powdery texture. After the immersion of the samples in the RN binding medium, the autoradiography images showed that there is a correlation between the coated black areas and the areas where the RN is attached (Figure 62). This also suggests that if the uniformity of the coating is enhanced, the uniformity of the sources may improve as well.

E2 (Figure 62.a) had the highest radioactivity level, and uniformity. However, the uniformity values of all the samples are similar, with a mean value of 86%.

For samples G2 and F2, the radioactivity seems to accumulate on the edges of the sample (Figure 62.b and c). This pattern suggests that the binding process may initiate at the edges of the samples and gradually progress toward the center. Both F2 and G2 were produced under identical conditions. However, G2 was immersed in the RN binding solution for 24 h, while F2 was kept for as long as 6 days.

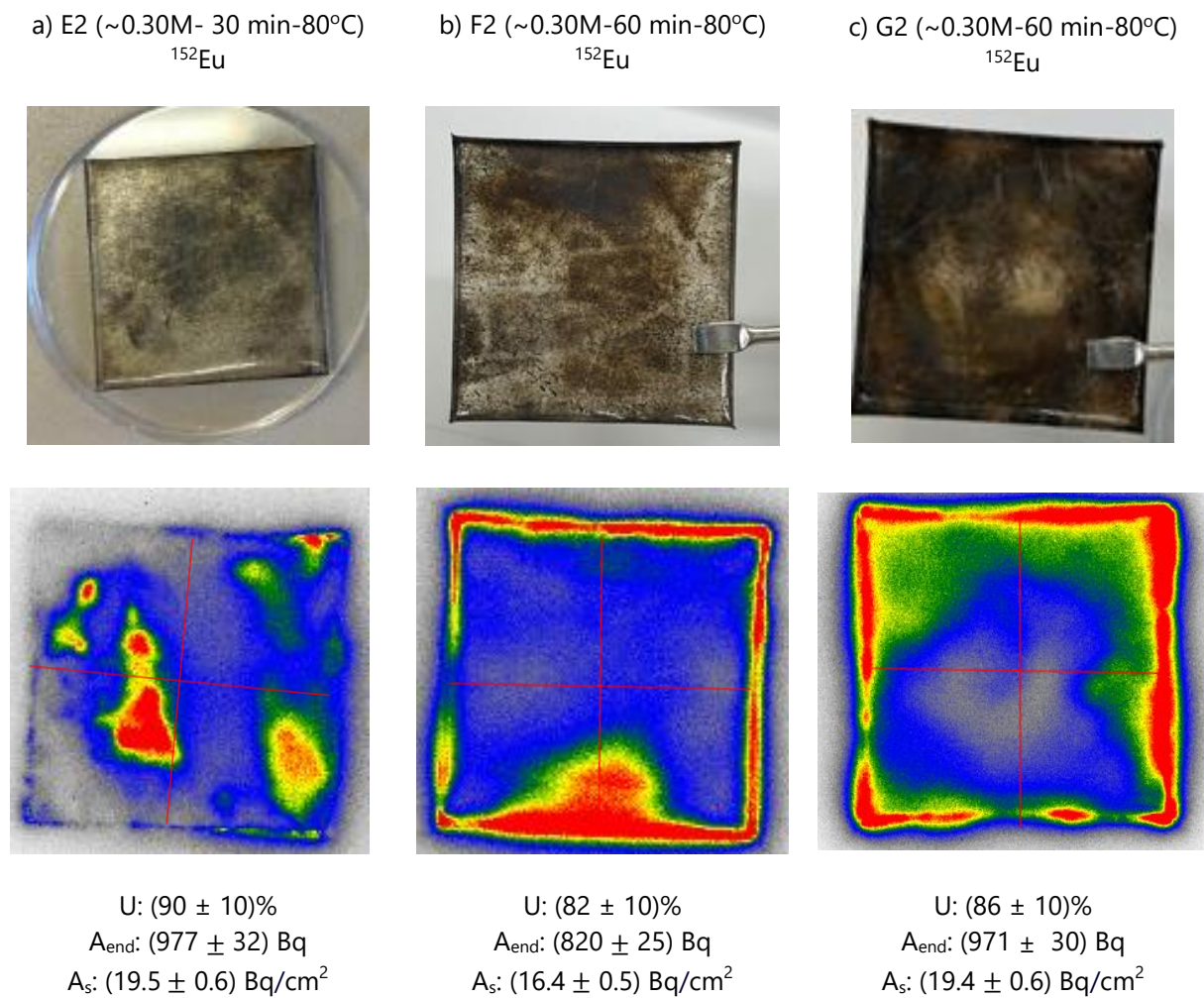


Figure 62: Pictures of samples, phosphor imaging autoradiography images, uniformity and radioactivity levels of the oxidized samples treated with ¹⁵²Eu a) E2, b) F2 and c) G2

2.2.2.2.1.2 Sulfonated epoxy resin samples uptaking ¹⁵²Eu

The autoradiography images of all the sulfonated samples are given in this section except for H6. The usage of DMSO as a solvent led to deformation of the H6 sample (as seen in Figure 57) for this reason, that sample could not be imaged properly.

The autoradiography images of the sulfonated samples are shown in Figure 63. Within this set of samples, F3 and G3 samples have the highest uniformity, with a value of 80% (Figure 63.b and c).

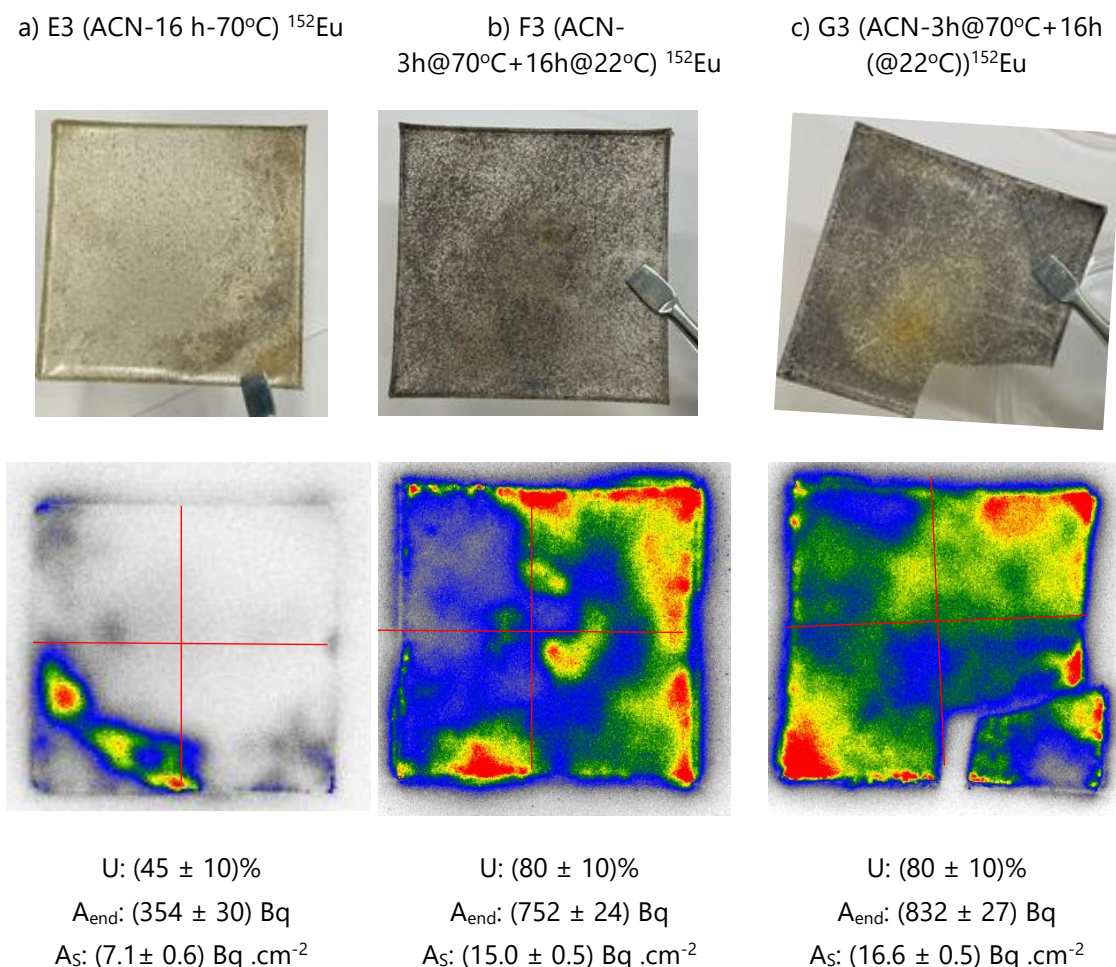


Figure 63: Pictures, phosphor imaging autoradiography images, uniformity and activity of sulfonated epoxy samples treated with ¹⁵²Eu, a) E3, b) F3 and c) G3

In the case of E3 there was a motif at one edge. Similarly to KMnO₄ treated samples, these sulfonated samples still have black areas on the surface, which also correlated with their autoradiography images. That might indicate that the RN attachment occurred preferentially on the region where the MnOx coating remains. However, the oxidation might also impact the success of sulfonation, since the OH groups needed for the sulfonation reaction are formed during the oxidation. Thus, it is possible that the improvement of the oxidation with KMnO₄ from E series to F series resulted in a more efficient oxidation of the epoxy surfaces, leading, in turn, to more sulfonated groups.

2.2.2.2 Epoxy resin samples in contact with ²⁴¹Am

In this section, the autoradiography images of the oxidized and the sulfonated epoxy samples after immersion in a ²⁴¹Am solution are discussed (Figure 64).

Generally, all oxidized samples exhibit a circular pattern with a lower activity in the center of the sources. That can be related with their oxidation procedure, as the RNs tend to attach to the

oxidized areas. The oxidation reactions were carried out in round crystallizers with slightly domed bottoms, which may have caused this pattern on oxidized or MnO_x-coated areas on the samples. There was possibly less contact between the solution and the sample at the center, as the samples were into direct contact with the beaker bottom, which may also have caused friction on the surfaces, leading to partial removal of the coating.

K1 has a slightly lower uniformity value of 75% (Figure 64.a), while K2 and K3 have a similar high uniformity value of 90% (Figure 64.b and c).

The sulfonated samples exhibited structures resembling "hotspots" on the surface. The L2 sample (Figure 64.e), among the sulfonated samples, exhibited both the highest radioactivity level and the highest uniformity.

In contrast to the oxidized sources, the sulfonated ones do not display a central pattern. That distinctive appearance can indicate that these two techniques employed different bonding mechanism of the RN on the surface. Another cause for this difference in the appearance could be that during the sulfonation treatment, the previously formed MnO_x coating might have been partly removed. Eventually, due to the loss of some coating on the surface, the RN fixation is lower compared to the sulfonated samples. This would imply that the manganese oxide coating plays a more important part in the RN fixation, even for sulfonated samples.

The sources obtained with oxidized epoxy resin were more uniform than the ones obtained with PET, with uniformity values from 75% to 90%.

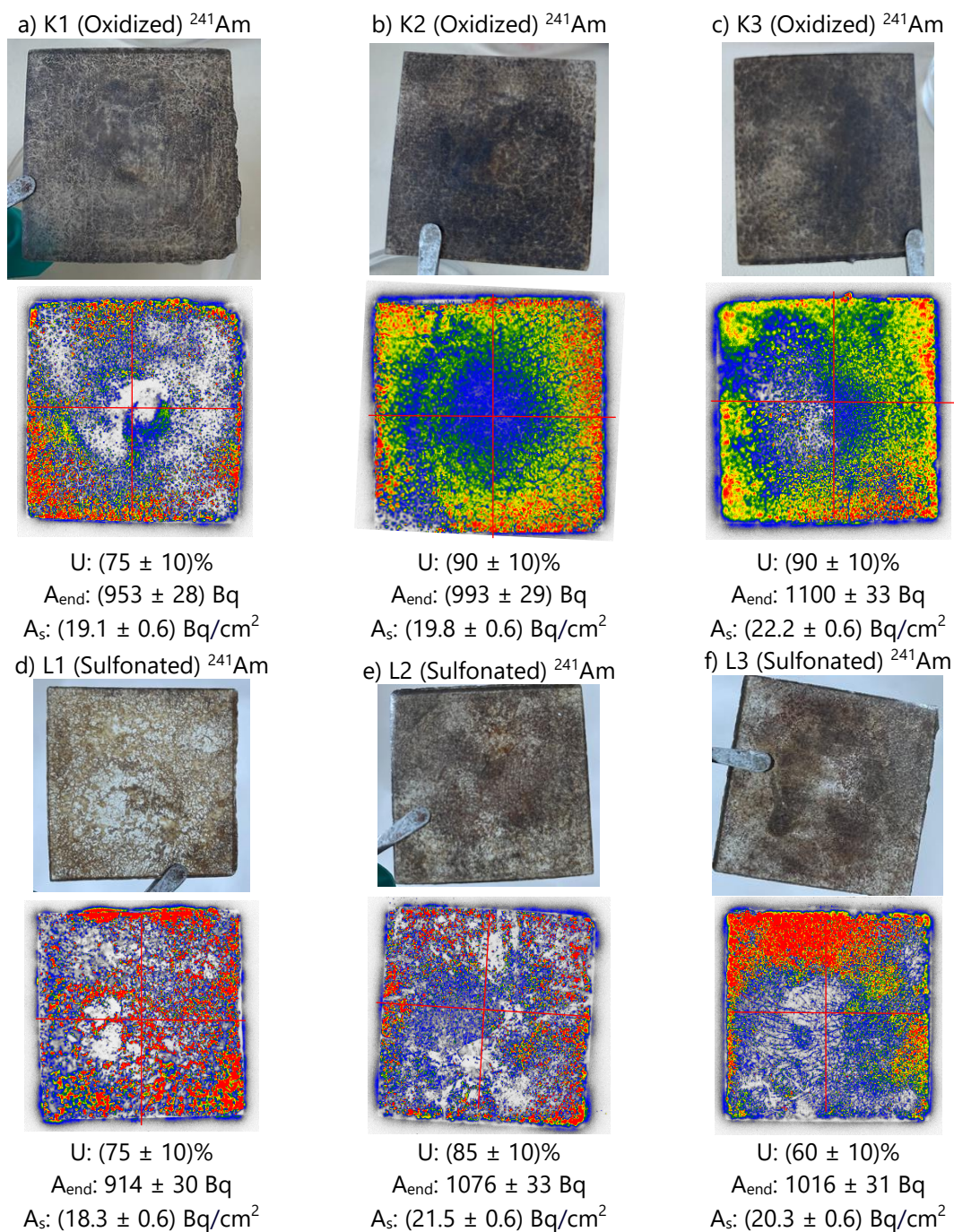


Figure 64: Pictures, phosphor imaging autoradiography images, uniformity, and activity of ^{241}Am epoxy surface sources a) K1 (Oxidized), b) K2 (Oxidized), c) K3 (Oxidized), d) L1 (Sulfonated), e) L2 (Sulfonated), f) L3 (Sulfonated)

2.2.2.2.3 Uniformity as a function of the emission type on oxidized and sulfonated epoxy samples with ^{241}Am

All samples have one porous and one smooth side resulting from the molding of the epoxy resin. The smooth side of the sources was checked during the masking experiments. The sources were exposed to two phosphor imaging films to de-couple the signal generated by both the alpha and the gamma emissions of ^{241}Am . The first screen recorded both alpha and gamma emissions but it also acted as a mask that stopped all alpha emissions so that the second film recorded only gamma photons (Figure 65).

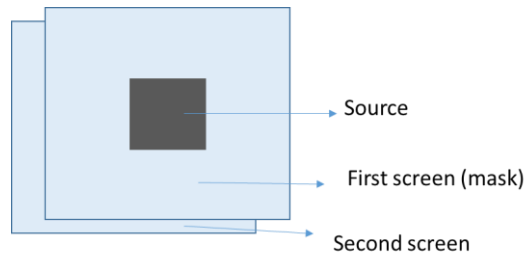


Figure 65: Experimental set up for the exposure with two screens

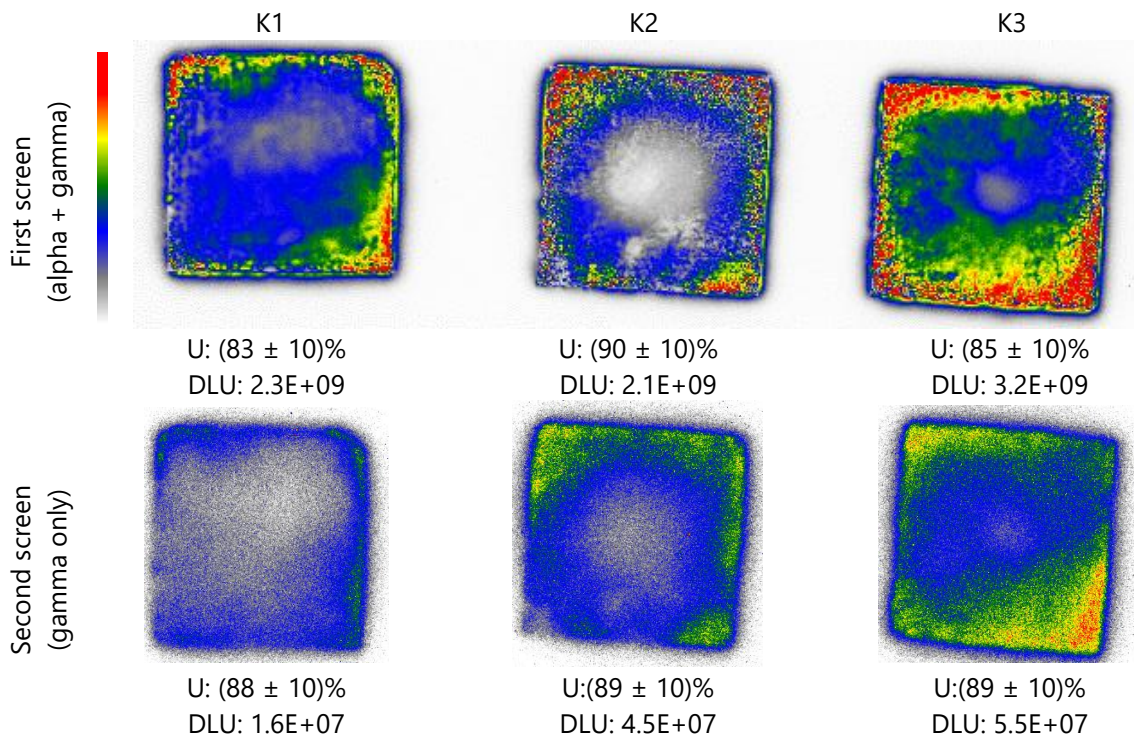


Figure 66: Phosphor imaging autoradiography images, and uniformity values of the K series (^{241}Am) with and without the alpha emissions from the smooth side of the sources, using 2 x 2 grids

The phosphor imaging autoradiography images of the K and L samples are given in Figure 66 and Figure 67 respectively. For all the samples, as the alpha emission and the gamma emission are in coincidence, as expected. On both screens, a similar radioactivity distribution can be identified. Consequently, the values of the uniformity are very similar too from the first screen to the other. The images from the second screen seems more blurry, possibly due to the gamma emission scattering. Even though, two different screens were used in the experiment, the DLU values from the second screen only represented a few percent of the DLU values from the first screen.

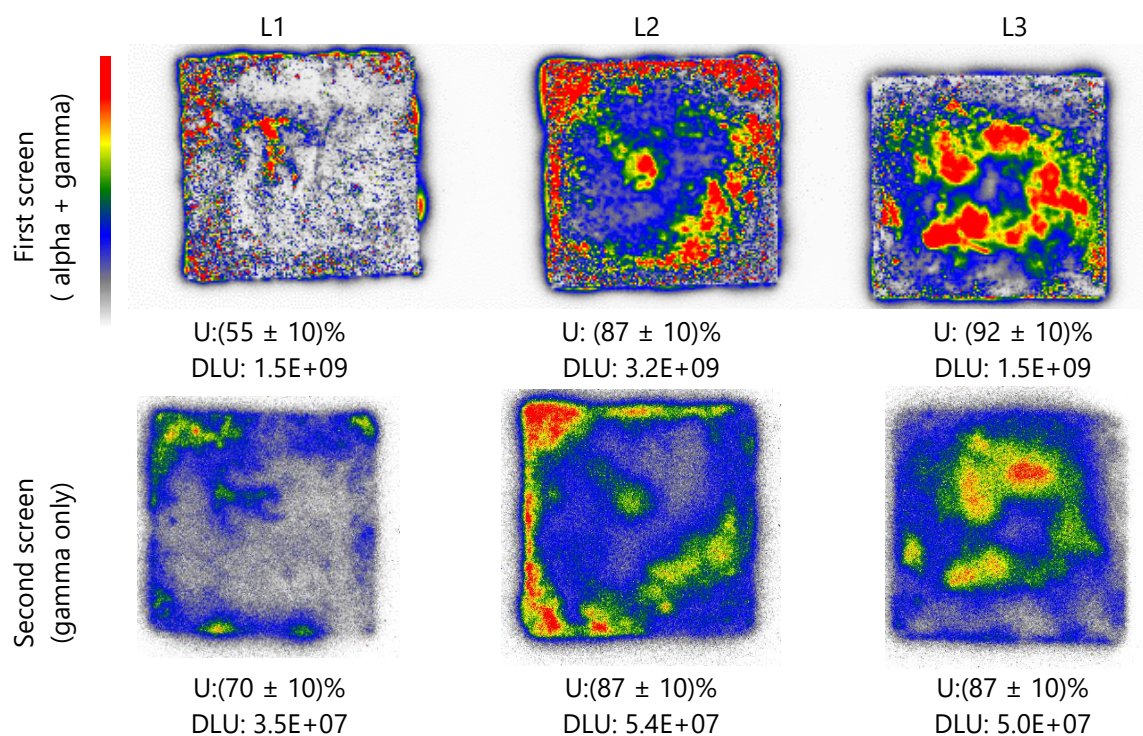


Figure 67: Phosphor imaging autoradiography images, and uniformity values of the L series (^{241}Am) with and without the alpha emissions from the smooth side of the sources, using 2 x 2 grids

2.2.3 Non-contamination test for oxidized and sulfonated epoxy samples with ^{241}Am

A non-contamination test was performed to estimate the removable contamination from the surface of selected sources according to ISO 7503-2 (ISO 7503-2, 2016). All samples have one porous and one smooth side resulting from the molding of the epoxy resin.

Dry wipes and humid wipes were employed in the non-contamination tests. Each experiment was performed one time. DI water was used to humidify the wipes to observe the impact of water on the RN removing efficiency from the surface. The smooth side of the sources was systematically checked with a dry swipe and the porous one with a humid one.

The values that were obtained from the non-contamination tests are presented in Table 25.

Table 25: Results of the dry and wet non-contamination tests on epoxy resin K1 and L1 samples spiked with ^{241}Am

Sample name	Radioactivity on the source (Bq) ($k = 1$)	Non-contamination test result ($k = 1$)
K1, Oxidized epoxy (^{241}Am)	955 ± 30	K1-smooth-dry: (29 ± 1) Bq K1-porous-humid: (17 ± 1) Bq
L1, Sulfonated epoxy (^{241}Am)	915 ± 30	L1-smooth-dry: (11 ± 1) Bq L1-porous-humid: (29 ± 1) Bq

For the KMnO_4 -treated sample K1, a higher activity was observed on the dry wipe (29 Bq), than on the humid one (17 Bq). This behavior was opposite for the sulfonated samples L1, for which the removed activity was higher on humid wipes (29 Bq) than on dry wipes (11 Bq).

For the oxidized sample (K1), the higher radioactivity level measured on the dry wipe compared to the humid one may be due to electrostatic forces. Dry wipes could potentially interact more effectively with the black dusty coating on the oxidized epoxy.

The disparity between oxidized and sulfonated sources may arise from the characteristics of the surface. The sulfonated sample could have a surface that is less prone to moisture, leading to better stability of the fixed radioactivity during humid wipe tests.

In both cases, the activity removed through wiping, either dry or wet, was similar and was about 30 Bq, which represents about 3% of the total activity. In any case, the activity removed was higher than 1 Bq, which is the limit for non-contamination described in (ISO 9978, 2020).

In the subsequent section, autoradiography images of the samples subjected to non-contamination tests are presented. The smooth sides of the samples were wiped with dry wipes, while the porous sides were treated with wet wipes. Before discussing the impact of the non-contamination test it might be meaningful to state the different physical appearance of the oxidized and sulfonated samples. Especially, a powder-like structure is observed on the surfaces of the coated samples. However, this feature observed differently on the sulfonated sample, where the powdery texture was less pronounced. This variation could be attributed to the effects of the sulfonation reaction following the oxidation treatment, which may alter the structural properties of the MnOx particles formed on the surface of the epoxy resin. On the other hand, despite no visible changes on the sample surfaces after wiping. As the wipes are white still some of the powdery particles can be observed on the wipes. This observation suggests subtle removal of the MnOx that are not discernible to the naked eye.

There was no difference in the uniformity values of the samples before and after the non-contamination test. For the oxidized samples, uniformity values increased, whereas for the sulfonated samples, uniformity decreased following the wipe test. However, a comparison of the autoradiography images of the samples does not accurately indicate whether radioactivity was

lost from the surfaces. This is attributed to the significant uncertainty inherent in each exposure, which affected the reliability of this assessment.

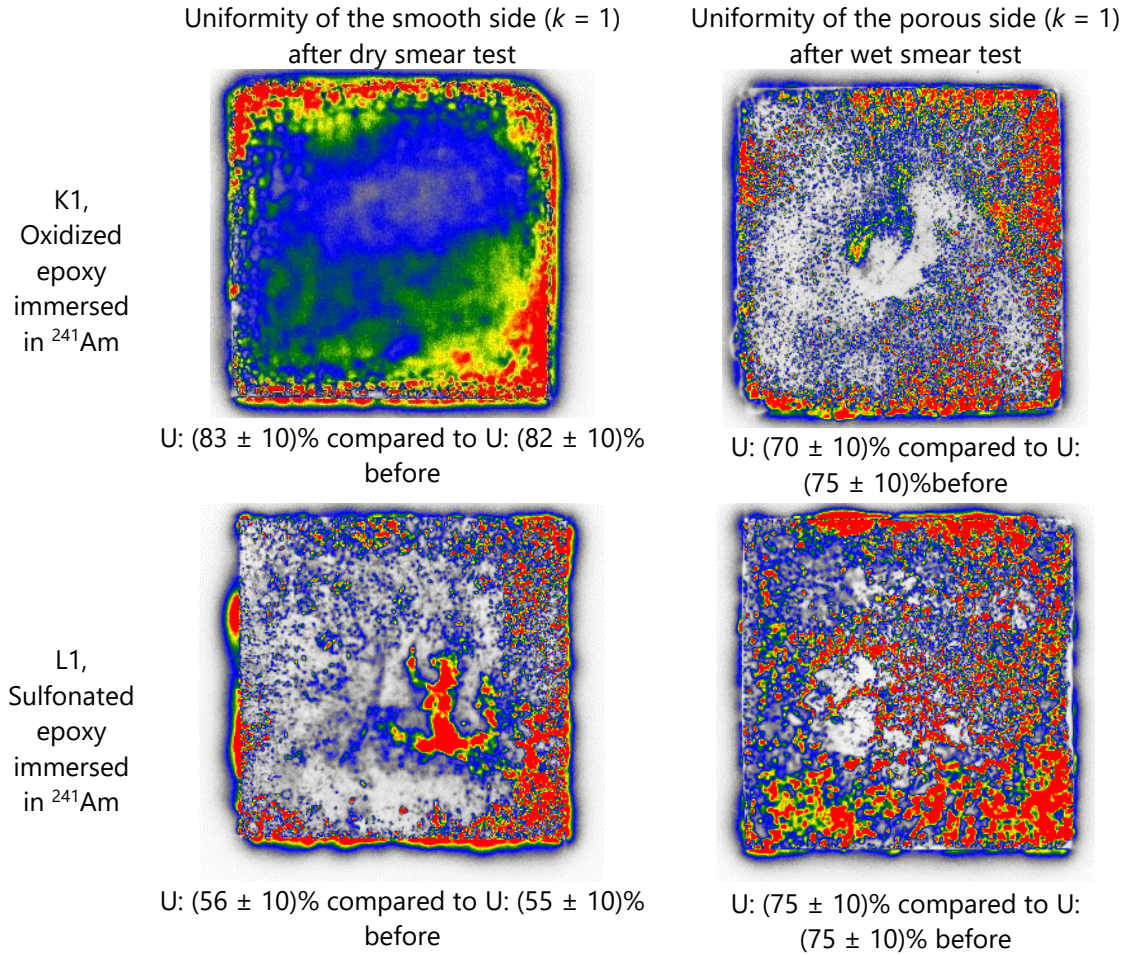


Figure 68: Autoradiography images of the samples after the non-contamination tests

In conclusion, it can be asserted that neither of the methods, whether using dry or humid wipes, demonstrated the characteristic of a non-contaminating surface for sources close to 1 kBq. Nevertheless, the goal of the future studies regarding these surface sources could be have a decrease in the non-contamination values of the sources or obtaining non-contaminating surfaces. Nevertheless, it is also possible that most of the removable activity was transferred onto the swipes and that further wiping tests would have removed less or no activity. Also, for D&D needs, the overall activity on such sources will be much lower, thus the removable activity will be very likely below the 1 Bq limit stated in ISO (ISO 9978, 2020).

3 CONCLUSION OF CHAPTER 3

This chapter presented a comprehensive overview of the methods and parameters involved in producing polymeric surface sources, utilizing PET and epoxy resin as substrates. Both substrates underwent two types of chemical treatments: KMnO_4 treatment and sulfonation, using different protocols. The effectiveness of each treatment was assessed through a combination of chemical and radiological characterization methods, including ATR-FTIR, Liquid Scintillation Counting (LSC), and digital autoradiography imaging. The PET samples were tested with ^{152}Eu , while the epoxy resin samples were tested with both ^{152}Eu and ^{241}Am .

For PET, the sulfonated surfaces were obtained after a 3-step process, and the KMnO_4 -treated surfaces were obtained in one step. For the epoxy resin, the KMnO_4 treatment was used before sulfonation, to oxidize the surfaces.

For PET samples, sulfonation involved preliminary steps of hydrolysis and reduction, to increase the number of hydroxyl functions on the surface. ATR-FTIR analysis confirmed that the PET was successfully modified after the hydrolysis reaction. LSC analysis demonstrated that each treatment step enhanced the fixation of ^{152}Eu on the surfaces, with sulfonated samples achieving a maximum fixation yield around 14%. KMnO_4 modified samples, treated under basic conditions, reached a higher fixation yield of 47%. This high fixation yield was probably due to the formation of a MnOx layer on the surface of PET, possibly with additional surface oxidation. However, the exact mechanism of the formation of the coating is not precisely known. The comparison between pictures of the samples and autoradiography images of PET samples treated with KMnO_4 , indicated a surface coating correlated with the attached RNs, supporting the hypothesis of a MnOx coating. However, the uniformity values for these samples were around 20%, in contrast to the sulfonated sample, which exhibited a highest uniformity of approximately 40%. The best sample among all the PET sources was the KMnO_4 treated (H5). However, the results were not promising enough, and the improvement of the PET functionalization was abandoned.

Epoxy resin samples underwent a similar treatment with KMnO_4 and subsequently, a sulfonation reaction with 1,4-butane sultone. ATR-FTIR analysis of these samples indicated that surface modification was achieved in both treatments. Additionally, the presence of MnOx was observed in the FTIR analysis, which implies that a manganese oxide coating was formed during KMnO_4 oxidation on epoxy surfaces. When immersed in RN solutions, oxidized samples yielded higher fixation rates compared to sulfonated samples for both ^{152}Eu and ^{241}Am . The maximum fixation yield for the oxidized epoxy sample immersed in ^{152}Eu solution was reached with sample F2, with approximately 100% of RN fixation, corresponding to about 860 Bq. Sulfonated samples also demonstrated significant fixation yields, slightly lower than oxidized samples tested with ^{152}Eu , with approximately 85% of fixation yield for the best sample among this series (F3), with a maximum activity of 785 Bq. The uniformity of the ^{152}Eu sources reached around 80% for both oxidized and sulfonated samples. Moreover, the comparison between pictures of the samples and autoradiography images showed a correlation between the coated black areas and the locations where RNs are attached. This suggests that to increase the uniformity the coating must be improved. In the case of ^{241}Am treated epoxy samples, consistent results were obtained, with fixation yields around 100% for oxidized samples, and around higher than 90% for sulfonated

samples. Oxidized samples exhibited uniformity values of about 90%, while sulfonated samples reached 85%.

In conclusion, the optimal parameters for both KMnO_4 treatment (0.36M-60min-80°C) and sulfonation (using twice the molar ratio of 1,4-butane sultone in ACN for 3 hours at 70°C, followed by 16 hours at 22°C) were successfully identified. These findings not only demonstrate the potential of these treatments in enhancing polymeric surface sources but also provide valuable insights for future research in this domain.

CHAPTER 4: PRODUCTION AND CHARACTERIZATION OF ALUMINUM SURFACE SOURCES

In this chapter, the focus is on the modification of aluminum surfaces to introduce chemical functionalities capable of binding radionuclides (RNs) to the surface. The choice of utilizing aluminum foils as a substrate is based their flexibility allowing to mimic pipes and complex shapes, while be complying with the demanding specifications outlined in ISO 8769.

In order to obtain these sources, two methods have been employed: grafting and coating. The first method consists in a set of pre-treatments, followed by four different grafting methods with four chemicals. These chemicals were carefully chosen based on specific groups that chemically bind to the aluminum surface, silanol and phosphonic acid groups, and groups for radionuclide attachment, phosphonic acid, quaternary amine and sulfonic acid. Optimization studies were conducted for every chemical, by testing several parameters, including the reaction duration of the grafting, the temperature, and the pH.

On the other hand, the second method involves a manganese oxide or a chromium oxide coating. These coating techniques are frequently used in the industry to obtain coatings on aluminum surfaces to avoid corrosion. Various parameters of the processes used to form these coatings were optimized, such as the reaction temperature, its duration, and the concentration of the chemicals.

The last step of the experimental procedure for obtaining radioactive sources, which consist in fixing radioactivity on the modified surfaces, was only performed on selected samples that passed the optimization test by chemical characterization analysis for the samples prepared by the first method. For the second method, all the samples underwent RN binding experiments. These RN fixation experiments were performed by immersing the substrates in solutions containing the desired RNs, namely ^{152}Eu and ^{241}Am , similarly to what was presented in the previous chapter.

Each step of these methods was evaluated through chemical and radiometric characterization techniques; the order of the characterization techniques was identified according to the need of the experiments. For the first method, the focus was on the chemical characterization followed by radiometric analysis, while for the second method; the analysis was initiated by radiometric characterization. Then, the chemical characterization of the chosen samples was performed after the radiometric analysis on inactive samples.

1 MATERIALS AND METHODS

1.1 MATERIALS

Surface sources were prepared using 3x3 cm² or 5x5 cm² squares cut from Al foil. Several foil types were used: 0.03 mm thick foils finish unknown (99.5%, Neyco), 0.3 mm thick half-hard finish foil (99.5%, Goodfellow) and 0.3 mm thick hard finish foils (99.5%, Goodfellow). For polishing, 600 grit grinding paper was used. For chemical etching, sodium hydroxide (0.1 M NaOH, Sigma-Aldrich), nitric acid (20% v/v HNO₃, Merck), hydrochloric acid (37 wt% HCl, Merck), hydrogen peroxide (30% v/v H₂O₂, Merck), and copper chloride (1 M CuCl₂, Sigma Aldrich) were used.

The DMOAC (CAS number: 27668-52-6) and DPTES (CAS Number: 757-44-8) grafting method involved dimethyloctadecyl [3-(trimethoxysilyl) propyl] ammonium chloride solution (42 wt.% in methanol, Sigma-Aldrich), and (2-Diethylphosphatoethyl) triethoxysilane (92%, Gelest), methanol (99.8%, Merck) and hydrochloric acid (37 wt.% HCl, Merck).

The DTPMP (CAS number: 15827-60-8) grafting method involved diethylenetriaminepentakis (methylphosphonic acid) solution (50%, DTPMP, Sigma-Aldrich), DI water, and sodium sulfate (Na₂SO₄, Merck).

The MPTMS (CAS number: 4420-74-0) grafting method comprised 3-mercaptopropyl trimethoxysilane (95%, MPTMS, Sigma-Aldrich), hydrogen peroxide (31%, BASF), and acetone (99.5%, Carlo Erba).

The manganese oxide treatment involved potassium permanganate (≥99.0%, KMnO₄, Prolabo) and sodium hydroxide (1 M NaOH, Sigma-Aldrich). Manganese oxide coating in acidic conditions was adjusted with H₂SO₄ (98%, VWR), HNO₃ (0.1 mol/L, VWR) and HCl (0.1 mol/L, VWR). The chromium oxide method involved potassium dichromate (≥99.0% K₂Cr₂O₇, Merck) and sulfuric acid (98%, H₂SO₄, Merck).

The ¹⁵²Eu solution used in the RN binding experiments had an activity of (22.01 ± 0.07) kBq/g (*k* = 1), reference date: 28/11/2022). This solution was in 1 mol/L hydrochloric acid (HCl) with 0.2 µg/g of stable Eu. For the samples produced in D series the RN binding experiments had an activity of (21.08 ± 0.07) kBq/g (*k* = 1) at the same reference date. This solution was in 1 mol/L HCl with 3 µg/g 1 of stable Eu. In B series the RN binding experiments had an activity of (2.3 ± 0.1) kBq/g (*k* = 1) at the same reference date. This solution was in 1 mol/L HCl with 2 µg/g 1 of stable Eu. In addition, a solution of ²⁴¹Am in 1 mol/L HCl was used without any carrier. The ²⁴¹Am solution had an activity of (31.06 ± 0.14) kBq/g (*k* = 1) at the same reference date.

1.2 METHODS

In order to modify the aluminum surface, two methods (grafting and coating) were followed. An overview of both approaches used is illustrated in Figure 69.

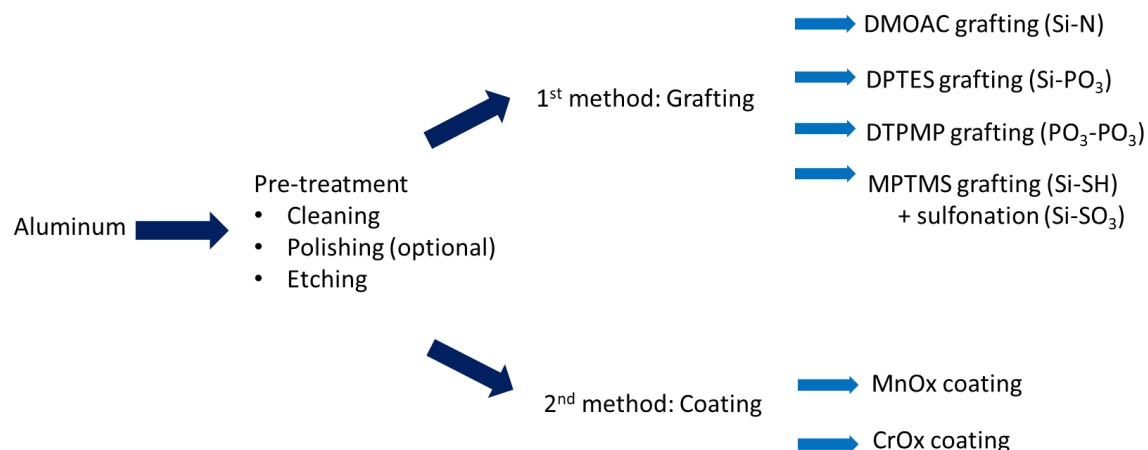


Figure 69: Aluminum modification approaches (grafting and coating)

In the grafting method, four different modifications were tested, each designed with a short nomenclature derived from the chemical structure of the chemicals used in the process. As shown in Figure 69, this shortcut name is composed of the chemical group that attaches to the aluminum foil (either Si or PO_3) and the chemical group for RN binding (either N, or PO_3 , or SO_3).

The Si-N method (Figure 70.a) comprises DMOAC to modify the aluminum, using the reaction between the silanol groups and the surface of the aluminum. The quaternary ammonium groups should bind the RN.

The modification of aluminum surfaces with DPTES (Si- PO_3) (Figure 70.b) also uses silanol groups to attach to the surface. The phosphonic acid groups facilitate the RN binding.

The PO_3 - PO_3 method (Figure 70.c) involves DTPMP chemical, which comprises phosphonic acid groups capable of grafting onto the Al surface and binding to RNs. This chemical configuration might bring different binding modes, which is discussed in detail within this chapter.

For the Si- SO_3 method (Figure 70.d) the modification of aluminum surfaces is achieved by utilizing MPTMS. Silanol groups react with the surface, leading to the attachment of thiol groups (SH), which are then converted to sulfonic acid for RN binding (SO_3).

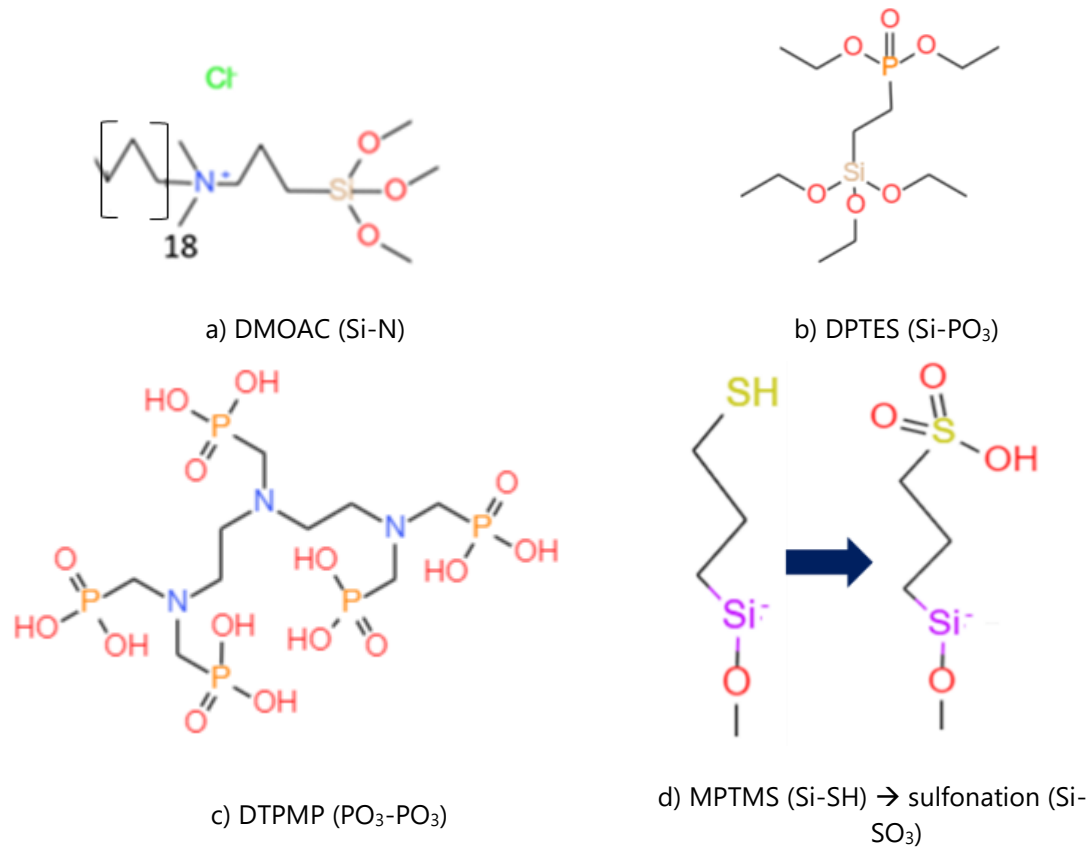


Figure 70: The chemical structure of the chemicals used in the grafting methods

Coating methods rely on two chemicals, each resulting in a different coating on the aluminum surface. The utilization of KMnO_4 results in a manganese oxide coating on the aluminum substrate and is denoted as MnO_x in the study. The utilization of $\text{K}_2\text{Cr}_2\text{O}_7$ leads to the formation of a chromium layer on the aluminum surface, referred to as CrO_x , in the study.

1.2.1 Al surface modification methods

This section outlines the experimental procedures that lead to the modification of the Al foils. First, pre-treatment steps, including cleaning, polishing, and etching, are presented in detail. Following this, different grafting procedures tailored to the particular chemical utilized in the modification methods are given with their parameters. Then, the two different coating methods that were performed are described.

1.2.1.1 Pre-treatments

Several pre-treatments were carried out to remove residues, increase the roughness, and release hydroxyl bonds to allow grafting or coating of the Al substrates

1.2.1.1.1 Polishing

At the beginning of the study, the impact of polishing was explored. Cut aluminum samples were mechanically polished with 600 grit grinding paper to remove the native oxide layer from the aluminum surface and increase its surface area.

1.2.1.1.2 Cleaning

The aluminum foils prepared for the grafting underwent a sequential cleaning process in an ultrasonic bath involving ultrapure water, acetone, and ethanol, each lasting 5 minutes. The samples were left to air-dry at room temperature (22 °C).

The cleaning of the aluminum foils used in the coating process involved the same chemicals as the cleaning procedure for the grafted samples. However, the cleaning was performed by rinsing, without sonication. Subsequently, the samples were left to air-dry at room temperature (22 °C).

1.2.1.1.3 Chemical etching

Chemical etching methods were performed to release hydroxide bonds from the surfaces. Within this study, four sets of chemical etching were employed.

The NaOH-HNO₃ etching involved immersing the cleaned aluminum foil samples in a 0.1 M NaOH solution (5 mL) for 2 minutes. Following this, the samples were rinsed with ultrapure water. Then, the samples were immersed in a 20% v/v HNO₃ (5 mL) solution for 2 minutes, followed by a final rinse with DI water (Muñoz et al., 2018). This method is visually represented in Figure 71.a.

The HCl-H₂O₂ etching method (Figure 71.b) involved immersing cleaned aluminum foil samples in a solution consisting of 5 mL of HCl (1 mol/L) and 5 mL of H₂O₂ (1 mol/L) at room temperature (22 °C) for 5 minutes (Peng et al., 2019). The samples were immersed in this solution and cleaned in an ultrasonic bath with ultrapure water for 1 min.

The boiling water (BW) treatment (Figure 71.c) was applied by immersion of the aluminum samples in boiling DI water for 5 minutes (Khaskhoussi et al., 2020).

The CuCl₂ treatment (Figure 71.d) involves immersion of cleaned samples in 5 mL of a 1 mol/L CuCl₂ aqueous solution at room temperature (22°C) for 1 min. In order to remove excess copper residues from the surface, the samples were subsequently rinsed and washed for 10 minutes with DI water in an ultrasonic bath (Khodaei and Shadmani, 2019).

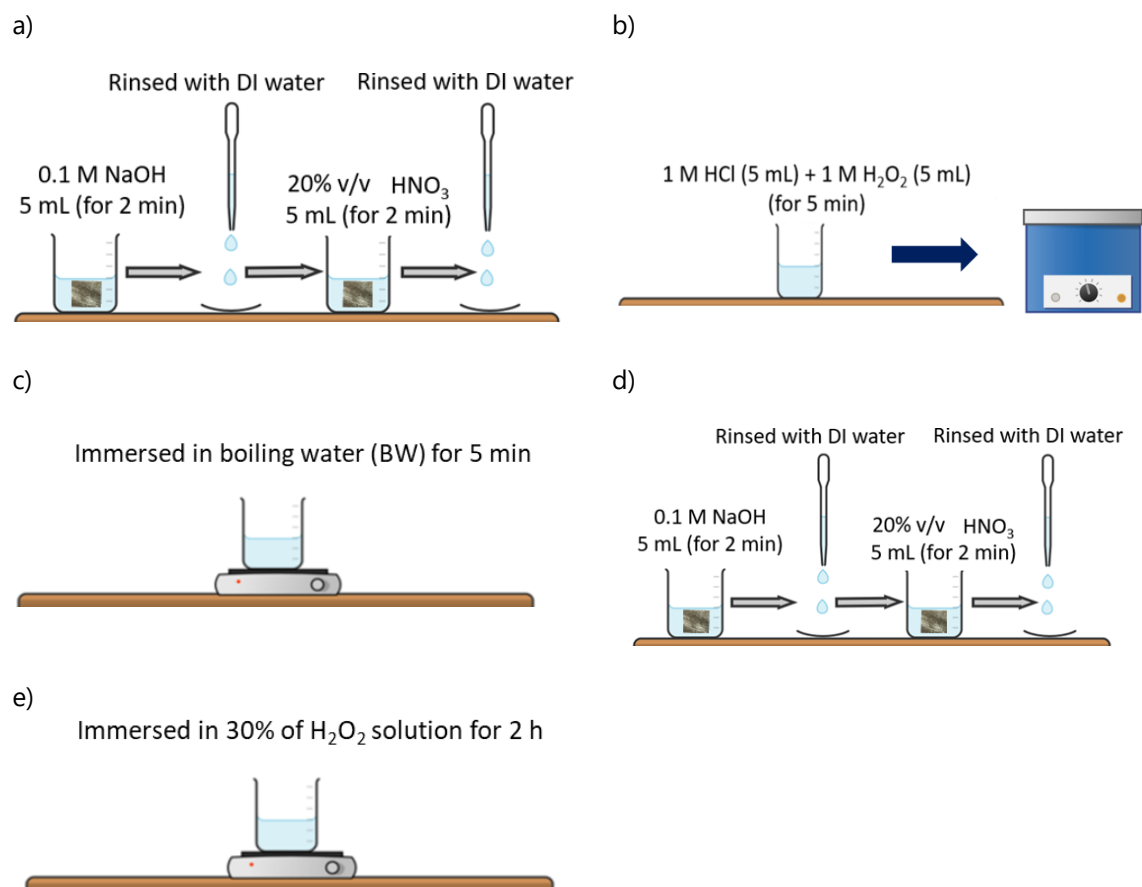


Figure 71: Illustration of the etching methods a) NaOH-HNO₃ b) HCl-H₂O₂ c) Boiling water (BW) d) CuCl₂ e) H₂O₂ treatment

For the aluminum foil samples that underwent sulfonation grafting (Si-SO₃), an additional pre-treatment step was performed by placing the samples in a 30% hydrogen peroxide (H₂O₂) solution for 2 h, after boiling water etching treatment. Then, the samples were washed with ultrapure water and left to dry in an oven at 100 °C.

1.2.1.2 Grafting methods

The grafting methods and their corresponding parameters are presented in this section. The cleaned and etched samples were subjected to selected grafting solutions. The etched samples have undergone a cleaning step; therefore, referring to "etched samples" implies that they have already been cleaned.

1.2.1.2.1.1 Grafting with DMOAC (Si-N)

In the following grafting method with silanol groups, the same protocol was applied from an article from Yin and colleagues with adjusted parameters. In the reference article (Yin et al., 2012) the method applied was dipping four times in the grafting solution, but in our study we also tested the impact of longer durations on the grafting success so this parameters was changed.

The cleaned or etched samples were immersed in a mixture of (0.5 wt.%) DMOAC, methanol (88 wt.%), ultrapure water (10 wt.%), and HCl (0.1 M, 1.5 wt.%). The impact of the immersion durations were tested for dipping, 1 h, 2.5 h, 6 h, and 12 h. After the samples were removed from the solution, they were cured at 100 °C overnight.

1.2.1.2.1.2 Grafting with DPTES (Si-PO₃)

The same grafting protocol used for the Si-N chemical was applied to the Si-PO₃, as the aluminum grafting would occur through the Si group. The cleaned or etched samples underwent grafting with a mixture of DPTES (Si-PO₃), methanol, deionized (DI) water, and HCl (0.1 M, 1.5 wt.%) by immersing in the solution. After immersion, the samples were left in the oven at 100°C for assigned durations.

The optimal reaction duration was assessed by subjecting the samples to 5 minutes, 60 minutes, 2.5 h and 12 h immersion durations.

1.2.1.2.1.3 Grafting with DTPMP (PO₃-PO₃)

In this method, the cleaned or cleaned and etched samples were immersed in 20 mL of DI water solution containing 1 mmol DTPMP for the chosen immersion duration (1 h, 2.5 h, 6 h, 12 h). Following this, the samples were placed in an oven overnight at 100 °C.

In addition to this method, an alternative method using Na₂SO₄ salt at pH 8 (adjusted using NaOH) was incorporated into the study (Lubelli and Hees, 2007), by keeping the mol number of the DTPMP constant compared to the reference article. These samples were produced at room temperature, with different reaction durations (1 h, 2.5 h, and 12 h), followed by drying in an oven at 100 °C. Additionally, one sample obtained through a 1 h reaction time at room temperature and it was not subjected to the 100 °C oven treatment.

Inspired by the idea of changing the pH of the reaction was applied to the samples by adjusting their pH to 8 and produced with reaction durations of 2.5 hours and 6 hours.

1.2.1.2.1.4 Grafting with MPTMS (Si-SO₃)

Two sequential steps were employed to immobilize sulfonic acid groups onto the surface of the aluminum foil. The aluminum foil was first submerged in a solution of 0.2 mL of MPTMS in acetone (V/V,1:100) for 3 or 20 hours. The sample was then rinsed with acetone and dried in an oven at 100 °C. Following this, the aluminum foil was immersed in a 30% v/v hydrogen peroxide solution

for about 24 hours to oxidize the thiol end groups into sulfonic acid groups. Subsequently, the foil was dried at 23 °C.

The grafting methods are presented with their selected parameters and the names of the samples in Table 26.

Table 26 : Chemicals used in the grafting methods and their parameters

Type of grafting	Chemicals	Parameters and sample names
Grafting with DMOAC (Si-N)	0.25 g DMOAC (0.01 mol/kg) 2.5 mL ultrapure water 17.5 mL MeOH 0.3 g HCl (0.1 mol/L)	Impact of etching : Si-N-Ref, Si-N-BW, Si-N-NaOH-HNO ₃ Duration of the grafting reaction (BW etched samples): Si-N-1h, Si-N-2.5h, Si-N- 6h, Si-N - 12h
Grafting with DPTES (Si-PO ₃)	0.07 g DPTES (0.01 mol/kg) 3 mL ultrapure water 17.5 g EtOH 0.03 g HCl (0.1 mol/L)	Different grafting durations on BW etched samples: Si-PO ₃ , Si-PO ₃ -2.5h, Si-PO ₃ -6h, Si-PO ₃ -12h
Grafting with DTPMP (PO ₃ -PO ₃)	0.35 g DTPMP (1 mmol/L) 15 mL ultrapure water 2 g Na ₂ SO ₄ pH: 8 (NaOH)	Grafting on BW etched samples: PO ₃ -PO ₃ -1h-T _{room} PO ₃ -PO ₃ -Na ₂ SO ₄ -2.5h, PO ₃ -PO ₃ -Na ₂ SO ₄ -10h PO ₃ -PO ₃ -pH:8-2.5h, PO ₃ -PO ₃ - pH:8-6h
Grafting with MPTMS and sulfonation (Si-SO ₃)	0.2 mL MPTMS (1 mmol/L) 20 mL acetone	Grafting on BW etched samples: Si-SO ₃ -3h, Si-SO ₃ -20h

1.2.1.3 Coating Methods

These methods were performed using two different chemicals: either KMnO₄ or K₂Cr₂O₇. The coating with manganese oxide is referred to as MnOx. The cleaned samples were immersed in solutions of varying concentrations of KMnO₄ solution (ranging from 0.27 to 1 mol/L). The KMnO₄ was dissolved in approximately 30 mL of 1 mol/L NaOH. Following this, the samples were removed from the solution, rinsed with ultrapure water, and left to dry in room temperature overnight. The study investigated different concentrations of KMnO₄, various reaction durations, and temperatures.

In the study of manganese oxide coating methods, various approaches were employed, each with adjusted from the given references according to the goal of the study. The acidic attempts, namely samples I1, I4, and I5, were prepared following distinct protocols. The I1 sample, modified from Boxus et. al, was produced using a 0.27 mol/L KMnO₄ solution in 98% H₂SO₄ and the sample was immersed for 60 min at 60 °C (Boxus et al., 1996). The I4 sample adhered to a method from Kharitinov, involving a 5 mmol/L KMnO₄ solution at 20 °C and pH 3 adjusted by 0.1 mol/L HNO₃ for 24 hours . For the I5 sample, the method employed involved a 20 mL solution containing

0.02 mol/L KMnO_4 , 0.1 mol/L $\text{Na}_2\text{B}_4\text{O}_7$ (borax), and 0.1 mol/L HCl, with an immersion time of 24 hours at 23 °C (Umehara et al., 2003).

In contrast, the basic condition samples, identified as H1, H2, H3, H4, and J3, were produced under varying basic conditions. The H1 sample, following Kulinich's protocol, involved a 0.1 mol/L KMnO_4 and 0.05 mol/L $\text{Na}_2\text{B}_4\text{O}_7$ solution at pH 9, for 60-minute immersion at 23°C (Kulinich and Akhtar, 2012). The H2 sample, adapted from a study from Danilidis used a 0.1 mol/L KMnO_4 solution in 1 mol/L NaOH, with the application performed by dipping for a minute. Samples H3 and H4, inspired by the study from Siau et.al, involved immersion in a 0.34 mol/L KMnO_4 and 30 mL of 1 mol/L NaOH solution, where H3 was dipped for ten minutes and H4 for one hour, both at 50°C (Siau et al., 2004a). The J3 sample has followed the same preparation method as sample H3.

Additionally, for intermediate precision checks, R, T, and Y series were prepared using a 0.28 M KMnO_4 solution and the following conditions: 50°C for 15 minutes, 80°C for 15 minutes, and 80°C for 40 minutes respectively. These experiments aimed to assess the intermediate precision of the manganese coating methods under identical conditions. The experimental conditions are listed in Table 27. Unless the pH is mentioned, the reaction medium was NaOH 1 M (pH around 14).

The samples were assigned specific codes with corresponding explanations to facilitate easy reference. The initial part of each code indicated the method and the concentration of the MnOx solution in 1 M NaOH, followed by the chemical used to adjust the pH of the solution (such as borax $\text{Na}_2\text{B}_4\text{O}_7$, or sulfuric acid H_2SO_4), and followed by the reaction duration and temperature.

Three types of aluminum foils were employed in these tests, including regular aluminum foil with a thickness of 0.03 mm for initial experiments. Subsequent tests, conducted towards the end, utilized thicker aluminum foil (hard and half-hard finish) with a thickness of 0.3 mm. The details regarding the aluminum foil types were given in Chapter 2.

Table 27: Parameters of manganese oxide coating methodologies (MnOx) and aluminum foils finish and thickness

Code	Method KMnO ₄ Concentration (mol/L) –pH- t_{rxn} -T	Aluminum foil finish and thickness (mm)	Solvent Concentration (mol/L)
I1	0.27M-pH1-60min-50°C	Regular (0.03)	18 M H ₂ SO ₄
I4	0.005M-pH3-24h-22°C	Regular (0.03)	18 M H ₂ SO ₄
I5	0.02M-pH7-24h-22°C	Regular (0.03)	Borax buffer solution
H1	0.10M-pH9-60min-22°C	Regular (0.03)	1 M NaOH
H2	0.10M-Dipped-22°C	Regular (0.03)	1 M NaOH
H4	0.30M-Dipped-50°C	Regular (0.03)	1 M NaOH
J3	0.27M-15min-50°C	Regular (0.03)	1 M NaOH
H3	0.30M-60min-50°C	Regular (0.03)	1 M NaOH
Y1 – Y3	0.28M-15min-50°C	Hard (0.3)	1 M NaOH
T1	0.28M-15min-80°C	Half-hard (0.3)	1 M NaOH
R2	0.28M-40min-80°C	Half-hard (0.3)	1 M NaOH

The chromium oxide coating methods were performed in acidic conditions, and different reaction durations were tested. The cleaned Al foil was immersed in a solution of 0.5 M K₂Cr₂O₇ and 18 M H₂SO₄ for durations of 10 or 60 minutes. After coating, the samples were removed from the solution, washed with ultrapure water, and left to dry overnight at room temperature. In terms of chromium coating, the experimental conditions from Siau (Siau et al., 2004) was followed in this study. Due to the potential hazards of chromium solutions at larger scales, the treatment was limited to three samples, with the concentration being ten times lower than what was suggested in the literature.

Table 28: Parameters of the K₂Cr₂O₇ treatment

Code	Method Chromium Coating- t_{rxn} - T	Aluminum foil finish and thickness (mm)	Chemical Concentration (mol/L)	Duration	T
I3	CrOx –pH1-10 min-50°C	Regular (0.03)	0.5 M K ₂ Cr ₂ O ₇ 18 M H ₂ SO ₄	10 min	50 °C
I2	CrOx – pH1-60 min-50°C	Regular (0.03)	0.5 M K ₂ Cr ₂ O ₇ 18 M H ₂ SO ₄	60 min	50 °C

1.2.2 Surface Characterization

Surface characterization of the samples was carried out before the radionuclide binding experiments, with the aim of checking and optimizing the modification methods. The morphology of the modified aluminum surfaces was analyzed using an OLYMPUS optical microscope and scanning electron microscope (SEM) XL40 (Thermo Fisher). Secondary electrons detector was utilized to acquire the images (detector in the chamber, the vacuum conditions is usually around 5.10^{-6} mbar). The observations were performed between 8-10 kV (2 spot size). The samples underwent observation without priori preparation steps.

Following that, the chemical functionalities present on the surface of the aluminum sample were identified using Attenuated Total Reflection Fourier Transform Infrared spectroscopy (ATR-FTIR). For the first set of analysis (Figure 74 and Figure 77) was performed with the Golden Gate-Diamond ATR device and for the rest of the analysis Q platinum-ATR device (Bruker) were utilized. The spectra were recorded using 128 scans from 600 to 4000 cm^{-1} , with a scan rate of 2.0 cm^{-1} per min.

1.2.3 Radionuclide binding experiments for aluminum foil surface sources

Gravimetric dilutions were performed to ensure traceability in all the experimental studies. The radionuclide binding medium was prepared by mixing ultrapure water, 1 M HCl (to reach pH 2), and a stock solution of the radionuclide. The ultrapure water and HCl solutions were weighed using a Mettler-Toledo XPE504 balance. The radioactive solution was weighed using the pycnometer method (Lourenço and Bobin, 2015) and a Mettler-Toledo MT5 microbalance. The beakers underwent agitation and homogenization following the addition of each component. Subsequently, the aluminum samples were immersed in the RN binding medium and kept agitating for a certain amount of time. The beakers covered with Parafilm® to prevent evaporation.

In order to compare the fixation yields of the different experiments, the total amount of elements present in the solution, including both stable and active elements, was kept relatively constant, as outlined in Table 12.

The experiments were initiated using ^{152}Eu (chemical analog of Am). The optimization tests were performed with ^{152}Eu to determine the parameters of each production method. Following this, the intermediate precision tests were carried out using ^{241}Am .

Table 29: Parameters of the RN binding experiments for aluminum surface sources

RN	Stable/active isotope ratio	Approximate total amount of element in solution (picomol)	Grafted aluminum	Coated aluminum
^{152}Eu	~ 5600	160	5 samples (B series)	/
^{152}Eu	~ 920	400	9 samples (D series)	/
^{152}Eu	~ 57	60	20 samples	8 samples
^{241}Am	0	60	3 samples	7 samples

1.2.4 Radiometric characterization

In order to calculate the activity attached on the sources, Liquid Scintillation Counting (LSC) analysis was performed using a TRICARB 2900 TR (PerkinElmer) and HIDEX (300 SL Automatic TDCR counter) (For the series of K, L, P,R,T, Y). The LSC samples were prepared by mixing 1 mL of the solution in contact with the Al samples with 10 mL of scintillator (Ultima Gold LLT, Perkin Elmer) and measured for 15 min each.

The modified aluminum samples were immersed in the radionuclide solution to allow the binding of RN as shown in Figure 72. The kinetic of this binding step during the immersion period was followed by several samplings. The details of the calculation were given in Radiometric characterizations in Chapter 3.

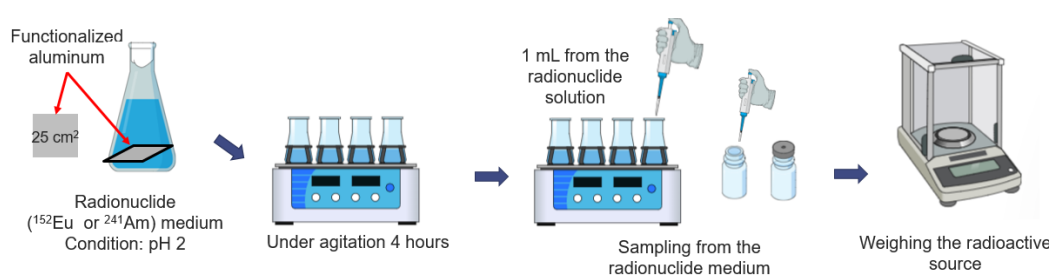


Figure 72: Experimental setup of the RN binding experiments

The uniformity of the sources was analyzed using BAS-MS Fujifilm imaging plates and a GE Healthcare Amersham Typhoon scanner. After immersion in the radionuclide solution, rinsing and drying, the sources were placed on the screen for 72 h and imaged with the scanner. The images obtained were analyzed using the software OptiQuant.

2 RESULTS AND DISCUSSION

In the following, the most promising methods for surface modification of Al were determined using SEM and ATR-FTIR, and the grafting and coating methods were then tuned. Further experiments to attach RN on the modified samples were conducted. Liquid scintillation counting (LSC) analysis was employed to quantify the radioactivity levels of the sources and ensure traceability, as a part of radiometric characterization. In addition, a phosphor autoradiography imaging system was used to visualize the distribution of the RN on the samples and facilitate a discussion on their uniformity.

2.1 SURFACE CHARACTERIZATION

Surface characterization was conducted for all the samples before RN binding experiments and analysis.

The surface topography evaluation was based on observations made with optical microscopy and is further supported by scanning electron microscopy (SEM) images, which allows a more detailed view of surface features and morphology. In addition to these visual assessments, Attenuated Total Reflection Fourier-transform infrared spectroscopy (ATR-FTIR) analysis was used to identify the chemical bonds present on the surface.

Several key parameters were addressed during surface characterization for the grafted aluminum foil samples, including the comparison between the two sides of the aluminum foils, the impact of the polishing treatment, the efficiency of various etching methods along with the polishing, and the impact of each grafting method. For the coating methods, three different methods in acidic and basic solutions were tested with KMnO_4 and only one acidic $\text{K}_2\text{Cr}_2\text{O}_7$ treatment was performed.

2.1.1 Observable differences between the two faces of aluminum foils

The aluminum foil used, of thickness 0.03 mm, has two different faces: one shiny and the other matte. This different appearance depends mainly on the surface roughness, and there should be no significant chemical differences between the two sides, as was demonstrated with X-ray Photoelectron Spectroscopy (XPS) (Li et al., 1997).

The shiny side is formed during the final rolling pass of the aluminum, which is accomplished by simultaneously rolling two sheets. Following the separation process, one surface (the one on the inner side of the rolling pass) exhibits a matte appearance, whereas the other surface displays a shiny feature.

In this section, optical microscopy and ATR-FTIR analyses were employed to examine the possible disparities between the two faces of the aluminum.

The decision-making process regarding which side of the aluminum foil should be placed on top, thereby having more contact with the grafting solution, was determined from the beginning of the study. The initial surface analysis with optical microscopy, simultaneously investigating both sides of the cleaned aluminum foil, denoted as the shiny and matte sides, is illustrated in Figure 73. On both sides of the aluminum foil, lines were observed on the optical microscopy images. Moreover, these lines are consistently present all over the surface. That might imply that the pattern observed is due to the topography of the aluminum surface. No residue was detected on the surface of the cleaned aluminum foil, proving the success of the cleaning. The shiny side (Figure 73.a) displayed only those straight lines while the matte side (Figure 73.b) exhibited more porosity or roughness. This characteristic feature is confirmed through SEM images on the matte side of the aluminum (Figure 73.c).

A parallel analysis was undertaken with ATR-FTIR analysis in order to ascertain the side of the aluminum foil that would result in more an efficient grafting or coating (Figure 74).

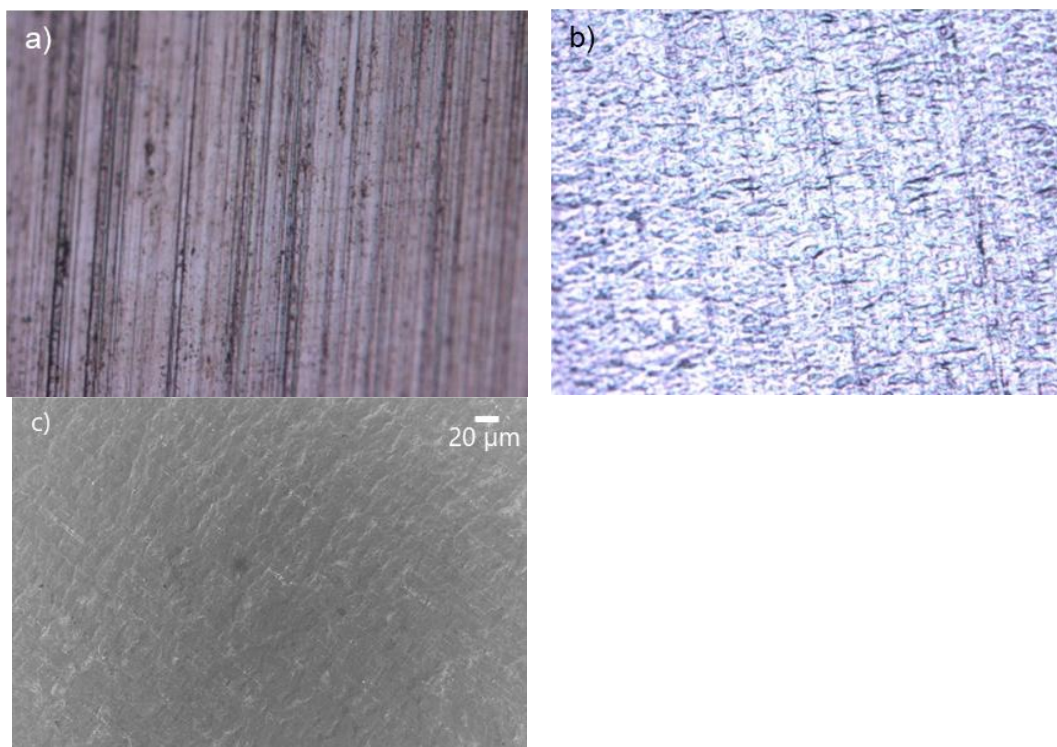


Figure 73: Images of the cleaned aluminum foil a) optical microscope image of cleaned Al foil shiny side (x50 magnification) b) optical microscope image of cleaned Al foil matte side (x50 magnification) c) top view SEM image of the cleaned Al foil matte side

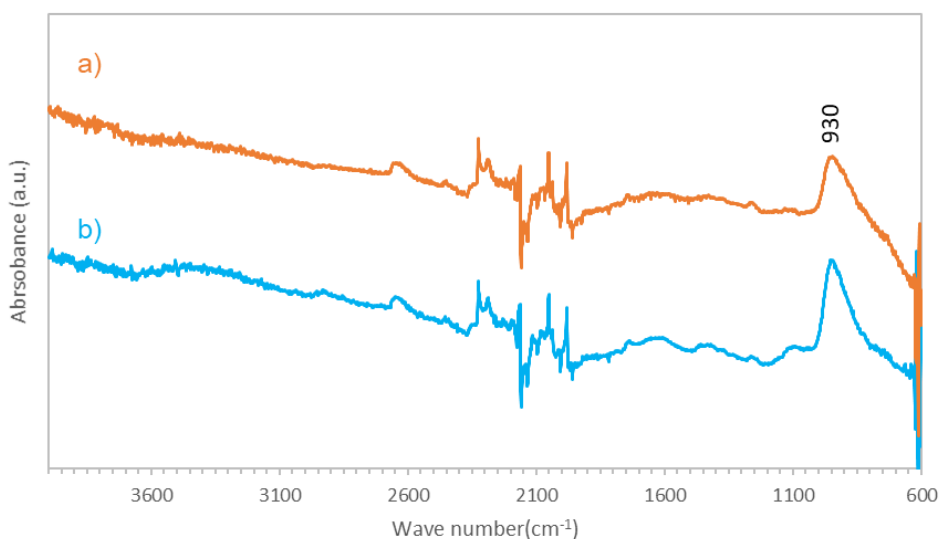


Figure 74: ATR-FTIR spectra of Al samples a) clean matte side b) clean shiny side

The Figure 74 compares the two sides of the cleaned aluminum foils. In the cleaned samples, a broad band around $3400\text{-}3000\text{ cm}^{-1}$ and a higher intensity peak at 930 cm^{-1} were detected. The peaks in the $2320\text{-}1980\text{ cm}^{-1}$ range were attributed to the CO_2 noise coming from the device. The band around $3400\text{-}3000\text{ cm}^{-1}$, which was more significant on the shiny side (Figure 74.b) than on the matte one, was assigned to the presence of -OH groups on the aluminum surface and to water adsorbed on this surface. In addition, the band observed around 930 cm^{-1} was attributed to Al-O stretching vibration due to Al_2O_3 (Özkanat et al., 2012). Aside from the band at $3400\text{-}3000\text{ cm}^{-1}$, both sides of the aluminum exhibited the same peaks. These results confirm that no organic residues are present on the surfaces after cleaning. Furthermore, the two sides are not chemically different, keeping in mind that there might be differences that ATR-FTIR does not detect.

The matte side of the aluminum foil was chosen for further surface analyses due to its greater surface roughness, which should result in a higher number of grafted groups. However, it should be noted that the methods applied in the experiments were not designed to modify just one side of the aluminum, and should result in both sides being modified.

2.1.2 The effect of polishing and etching

In this section, the necessity of polishing and the impact of three etching methods (NaOH-HNO_3 , $\text{HCl-H}_2\text{O}_2$, and boiling water (BW)) on the matte side of the aluminum foil of thickness 0.03 mm were investigated. Optical microscopy was used to examine the topographical differences (Figure 75). The images of the shiny side are provided in Appendix-3. A method using CuCl_2 was also applied to aluminum samples during the etching process investigation. However, it was observed that the use of CuCl_2 altered significantly the surface thickness, and holes were formed on the surface. The severity of the surface damage rendered the samples unsuitable for evaluation by SEM, thus highlighting a critical limitation of the CuCl_2 method in the context of aluminum surface treatment.

The etching process aims to release the -OH bonds from the surface while concurrently achieving a micro-nano scale hierarchical structure on the surface through chemical or thermal treatments (Rodič and Milošev, 2019).

The polished matte surface (Figure 75.a) exhibited linear arrangements, due to the polishing treatment. The sample etched with NaOH-HNO_3 (Figure 75.b) exhibited a grid patterned structure after this treatment, but looked similar to the sample without etching. The absence of pits and holes indicated that this treatment did not damage the surface of the foil, and could be a proper method among etching treatments. The sample etched with $\text{HCl-H}_2\text{O}_2$ solution exhibited the formation of pits and holes on the surface as depicted in Figure 75.c. This observation implies the presence of surface damage as a consequence of this treatment. Surface damage might affect the foil overall mechanical stability during the intended grafting steps, leading to the production of fragile sources. In contrast to alternative etching methods, the boiling water (BW) treatment (Figure 75.d) revealed the formation of small black spots alongside the rough structure on the polished matte sample. The presence of small dots may indicate the occurrence of surface oxidation, likely as a result of etching.

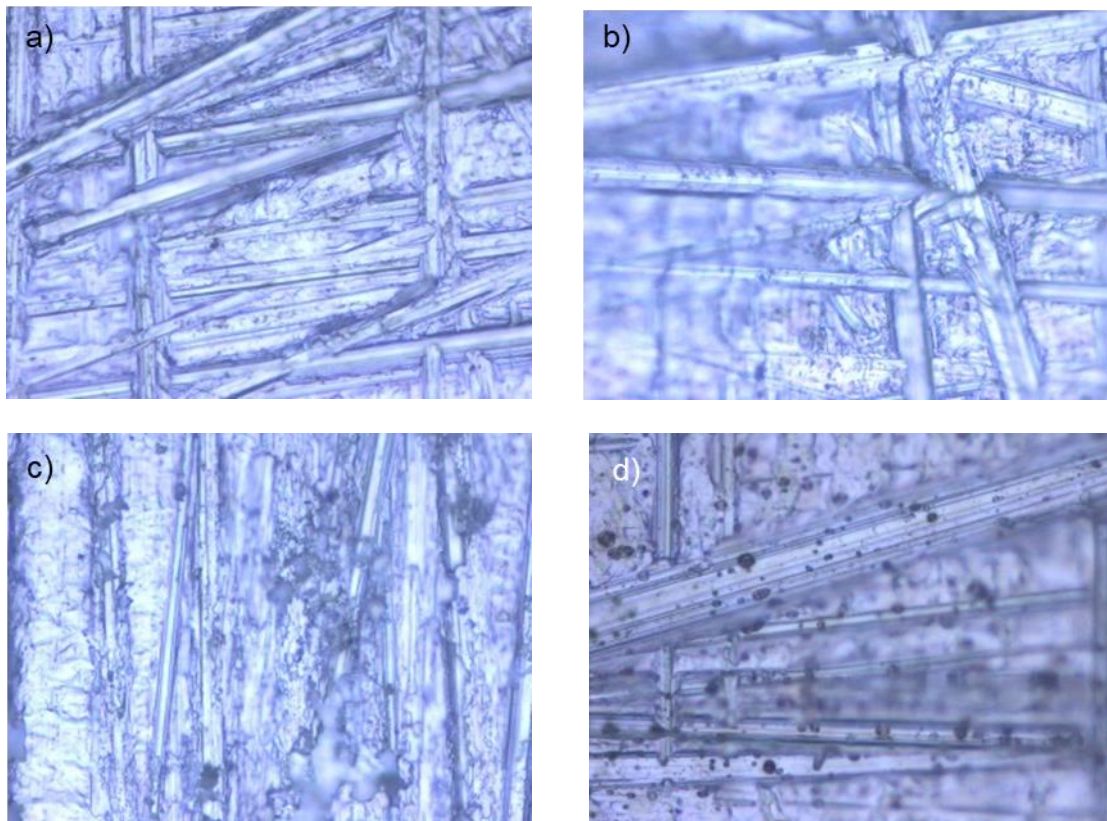


Figure 75: Optical microscopy images of matte side of the polished samples before etching and after an etching step a) Polished without etching (magnified x50), b) Polished- NaOH-HNO_3 (x50), c) Polished- $\text{HCl-H}_2\text{O}_2$ (x50), d) Polished-BW (x50)

The $\text{HCl-H}_2\text{O}_2$ etching treatment was found to be detrimental to the samples, resulting in the formation of holes or pinholes. The polishing process may enhance this damage as it removes the top layer of the foil. In some cases, even before any chemical treatment on the sample some holes were observed due to polishing step (as shown in Figure 76). When the combination of the etching and polishing the decision was made to eliminate the $\text{HCl-H}_2\text{O}_2$ etching treatment.

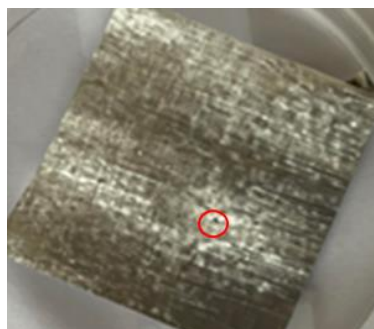


Figure 76: Appearance of the polished matte side of the regular aluminum foil (0.03 mm)

This series of analyses demonstrate that implementing polishing does not result in a specific improvement in the etching process. Additionally, the samples can be damaged even before being immersed in the grafting solution, leading to non-reproducible samples. For this reason, polishing treatment was eliminated due to its potential to damage the samples.

2.1.3 Effect of the selected etching methods

The following analysis were performed on cleaned and etched samples treated with NaOH-HNO₃ and BW on ATR-FTIR (as seen in Figure 77). Among these treatments, only the cleaned samples subjected to boiling water treatment exhibited a distinctive peak at 1068 cm⁻¹ (Figure 77.c). This peak is attributed to the –OH bond associated with the surface hydroxide of the aluminum oxide.

It has been previously reported (Khaskhoussi et al., 2020; Özkanat et al., 2012) that during the immersion of the aluminum substrate in boiling water, a reaction occurs between Al and water, represented by the Equation 22.



As a result of this reaction, the surface of aluminum transformed into Al₂O₃·xH₂O further reacted with H₂O to produce an AlO(OH) crystals known as Boehmite (Khaskhoussi et al., 2020). It is possible that the peak at 1068 cm⁻¹ corresponds to Boehmite.

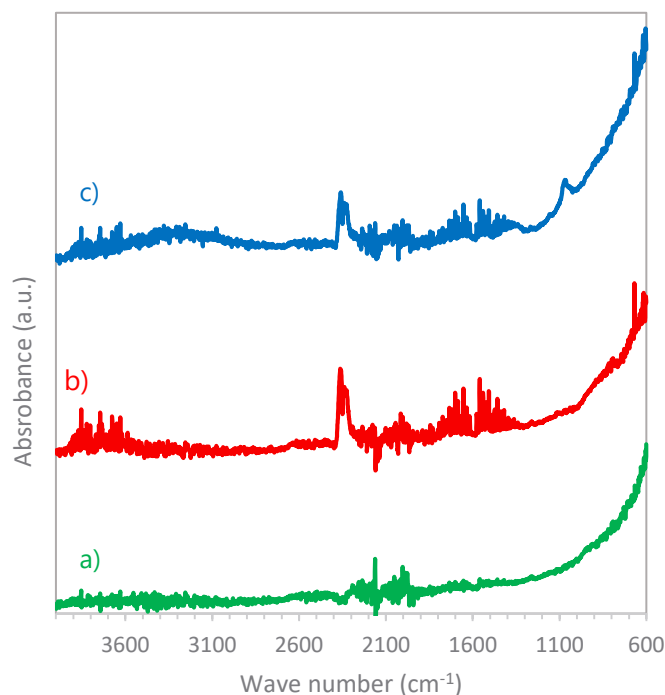


Figure 77: Impacts of the different etching methods a) cleaned sample without etching, b) sample treated with NaOH-HNO₃, c) sample treated with boiling water

Further analyses were conducted using SEM on the two samples (cleaned and etched with NaOH-HNO₃; cleaned and etched with boiling water sample (BW)) as illustrated in Figure 78.

The sample etched with NaOH-HNO₃ (Figure 78.b) displayed pits and pores of various sizes up to 10 μm on the surface. In contrast, the sample treated with boiling water (Figure 78.c) exhibited both micro- and nanostructures, combined with some dots that might be assigned to oxides on the surface.

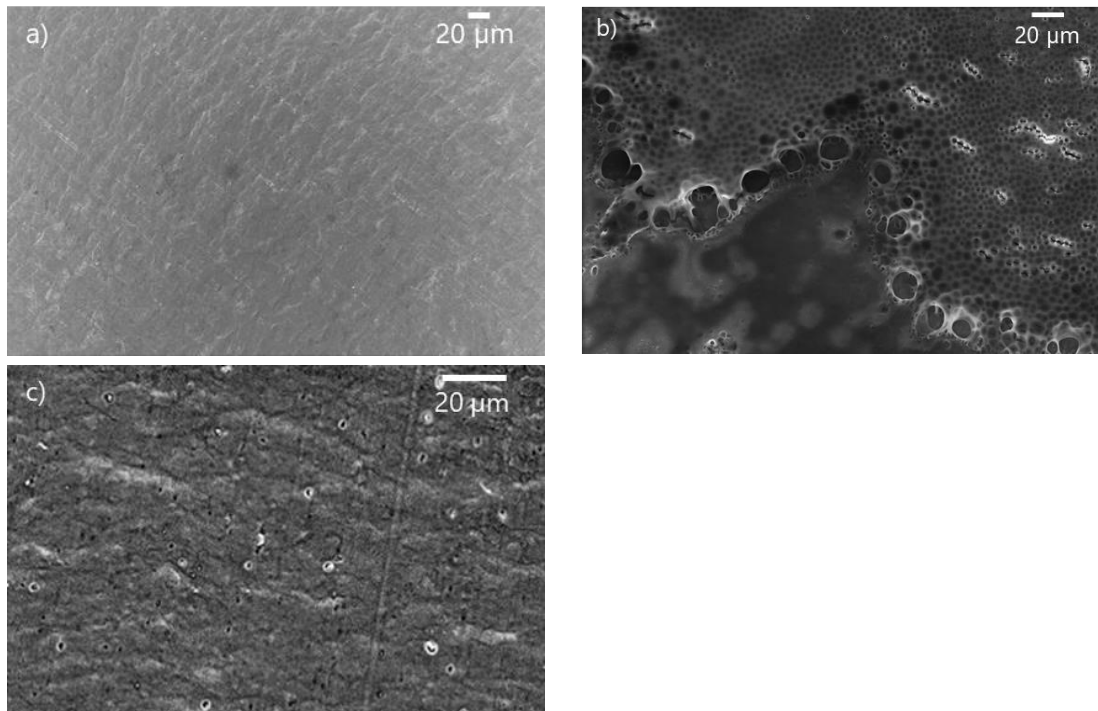


Figure 78: Top view SEM images of a) Cleaned sample b) Cleaned, etched with NaOH-HNO₃, c) Cleaned, and etched with boiling water sample (BW)

2.1.4 Impact of different grafting methods

The next analysis focused on samples subjected to the DMOAC (Si-N) grafting solution by dipping for four times. To simplify the description, a short notation of the samples is employed, for example Si-N-dipped-BW is a cleaned sample etched with a BW treatment and grafted with the Si-N approach by dipping in the grafting solution, and the Si-N-dipped sample is the cleaned sample, without etching treatment, grafted with the Si-N approach.

The surface of the Si-N-dipped sample (Figure 79.a) exhibited a honeycomb structure, with open and closed pores. The grafted region located on the surface is observable even to the naked eye. The layer observed as blurred might be related to a membrane-like structure formed by grafting on the surface. The Si-N-dipped-BW sample (Figure 79.b) displayed a random distribution of open pores with dimensions ranging from 5 up to 20 μm. In contrast, the Si-N-dipped-NaOH-HNO₃ sample (Figure 79.c) exhibited a uniform structure across its entire surface. It is important to

highlight that SEM analysis was conducted over limited surface area owing to the characteristics of the method. As a result, it does not comprehensively depict all surface features across a series of images, and does not provide insights into surface uniformity.

The Si-N treatment seemed to form a porous layer on top of the Al substrates, regardless of the etching treatment used.

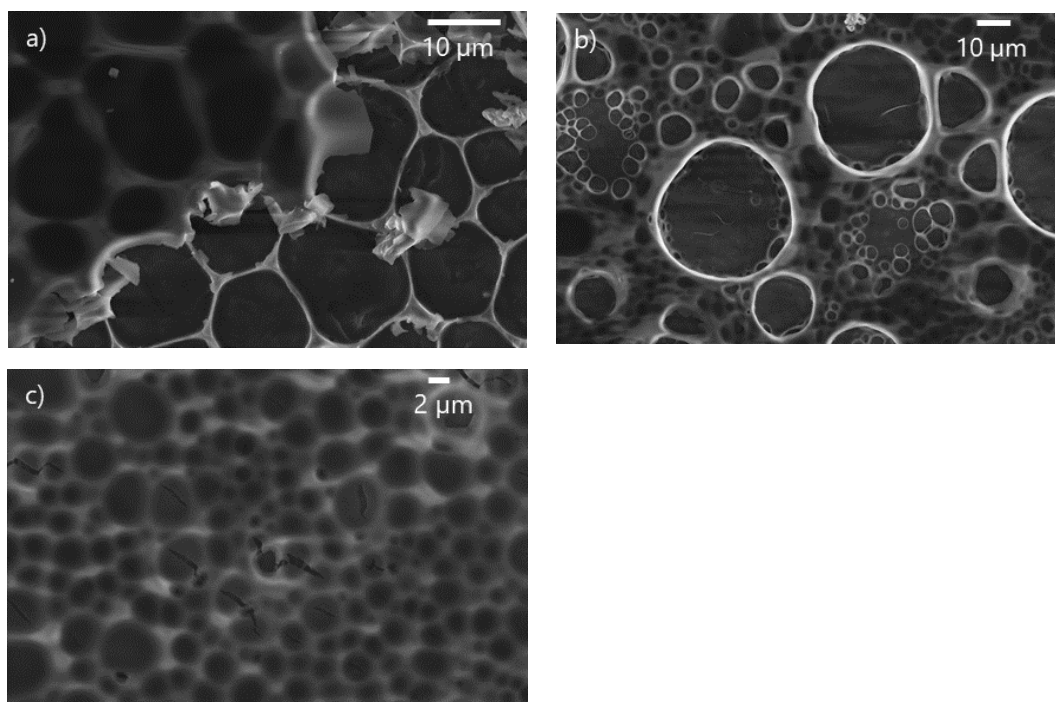


Figure 79: Top view SEM images of the Si-N grafted samples a) Si-N-dipped, b) Si-N-dipped-BW, c) Si-N-dipped-NaOH-HNO₃

In Figure 80, the PO₃-PO₃-BW and Si-PO₃-BW samples are shown, to observe the impact of different chemical groups on the surface topography. The PO₃-PO₃-BW sample (Figure 80.a) displayed needle-like structures and micrometer-sized cones homogeneously distributed over the scanned surface, similarly to the sample Si-PO₃-BW (Figure 80.b).

These images bring a discussion about the Si-PO₃ sample, which contains two distinct functional groups capable of binding to the aluminum surface, alkoxy silane groups and phosphonate groups, as seen in Figure 70.b). Determining which side of the chemical is grafted on the aluminum surface is challenging. However, the observed differences compared to Si-N grafted samples (Figure 79) may indicate that the grafted group on the surface for Si-PO₃ samples might be PO₃, rather than Si functional group. This hypothesis still needs to be proven with additional chemical characterization techniques such as X-ray photoelectron spectroscopy (XPS).

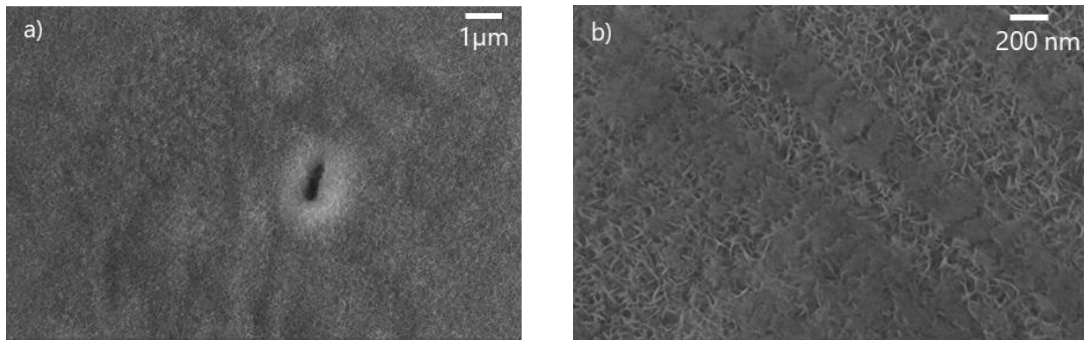


Figure 80: Top view SEM images of boiling water treated and grafted samples a) $\text{PO}_3\text{-PO}_3\text{-BW}$ b) $\text{Si-PO}_3\text{-BW}$

Figure 81 displays the SEM images of the Si-PO_3 grafted samples, illustrating the impact of reaction duration on their surface topography. The images compare two samples: one grafted for 2.5 hours (Figure 81.a) and the other for 12 hours (Figure 81.b). The 2.5-hour grafted sample, exhibits a structure similar to other grafted samples (Figure 79, Figure 80 and Figure 82). However, it is characterized by smaller needle-like particles, with sizes reaching up to 200 nm. In contrast, the sample grafted for 12 hours, referred to as $\text{Si-PO}_3\text{-12h}$, reveals a significant change. It shows the appearance of white particles on the surface, randomly distributed, with particle sizes expanding up to 10 μm.

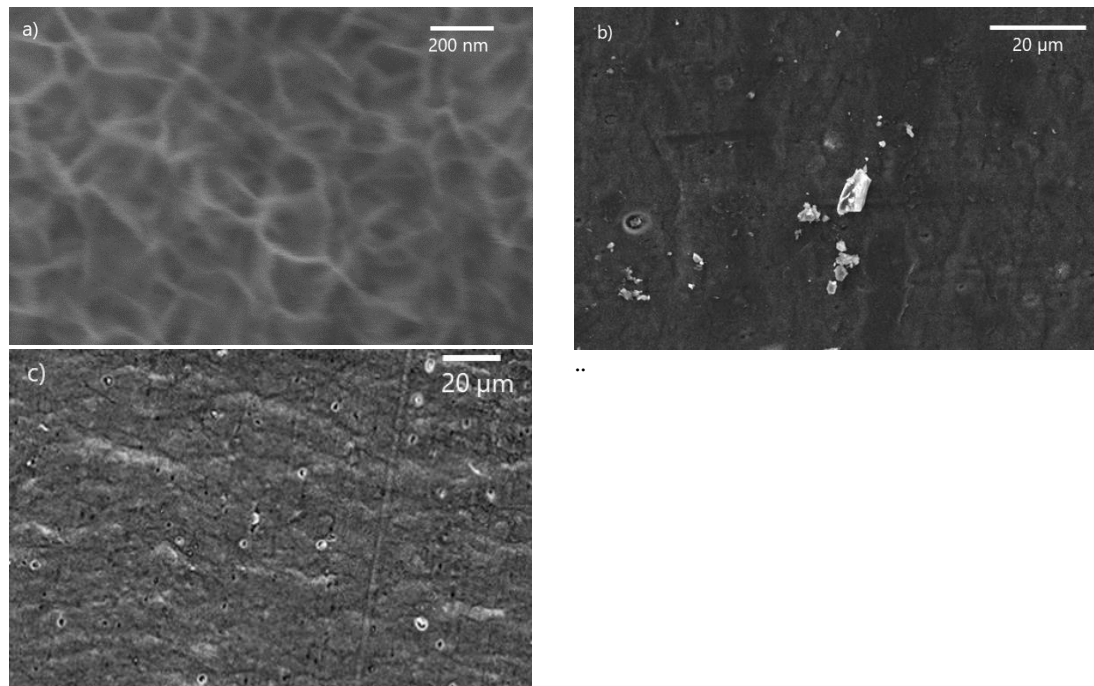


Figure 81 : Top view SEM images of the Si-PO_3 grafted samples a) $\text{Si-PO}_3\text{-2.5h}$, b) $\text{Si-PO}_3\text{-12h}$, c) $\text{Si-PO}_3\text{-12h}$

The SEM image of the Si-SO₃ grafted sample is presented in Figure 82 and compared with the one of the BW treated sample. After the grafting process with Si-SO₃, nanoscale needle-like/sub-micron rough structures were uniformly distributed across the entire surface of the aluminum, as observed in Figure 82.b.

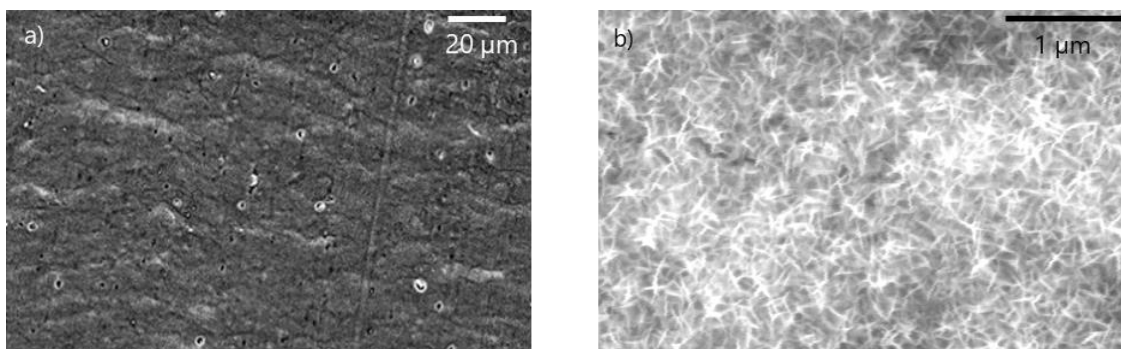


Figure 82: Top view SEM images of a) BW treated sample, b) E8 sample (Si-SO₃-3 h)

The following ATR-FTIR analysis was performed with the most promising samples from each method, as depicted in Figure 83. The cleaned and BW-treated samples were shown in the figure to compare every change that appeared on the surface. Cleaned and cleaned BW samples displayed the same peaks as observed in the previous analyses. After the BW treatment, a specific peak at 1068 cm⁻¹ appeared, which might be assigned to the -OH group released from the surface.

The peaks located between the ranges of 2355 to 1435 cm⁻¹ were observed for all the samples and were assigned to the CO₂ noise coming from the device.

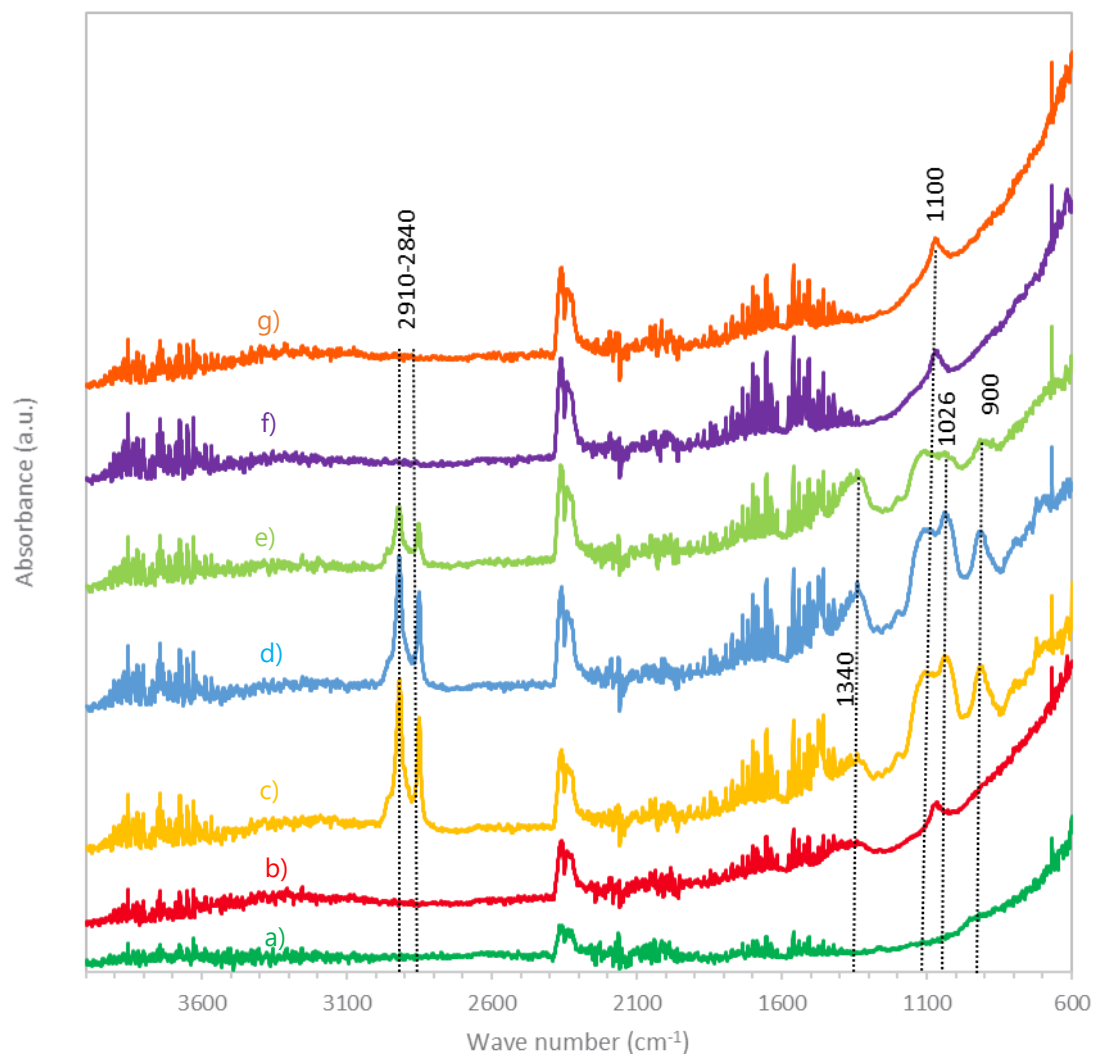


Figure 83: ATR-FTIR of Al samples: a) Cleaned, b) BW, c) Si-N-dipped, d) Si-N-dipped-BW, e) Si-N-dipped-NaOH-HNO₃, f) Si-PO₃-dipped-BW, g) PO₃-PO₃-BW

The samples that were grafted with Si-N (Si-N-dipped Figure 83.c, Si-N-dipped-BW Figure 83.d, and Si-N-dipped-NaOH-HNO₃ Figure 83.e) exhibited the same groups of peaks at 2910, 2840, 1340, 1100, 1026, 900 cm⁻¹. These peaks and their possible attributions are given in Table 30.

Table 30: Peaks of the Si-N grafted samples and their attributions

Peak wavenumber (cm ⁻¹)	Possible attribution
2910 and 2840	-CH asymmetric and symmetric vibration in propyl chain of functional organic modifiers (Das et al., 2013; Feng et al., 2013; Kang and Kim, 2020; Khaskhoussi et al., 2020)
1450	Si-CH ₂ bending vibration present in silane (Khaskhoussi et al., 2020)
1400-1100	C-N bonds (Nayak et al., 2019)
1100	Symmetric and asymmetric stretching vibrations of Si-O-Si (Khaskhoussi et al., 2020; Riaz et al., 2019)
1100-1000	Alkoxysilanes (Si-O-Al) (Kyriakou et al., 2020)
1060-1030 and 900	Stretching of siloxane (Si-O-Si)
955-830	Si-OH, involving Si-O stretch (Gong et al., 2012)
730-719	Rocking -CH ₂ / -CH (Kallingal et al., 2023)

The peaks around 2910 and 2840 cm⁻¹ might indicate the presence of long carbon chains. The low intensity peak at 1400-1100 cm⁻¹ was attributed to the C-N bond within the chemical structure of Si-N chemical and signifying the successful attachment of DMOAC. The band at 1450 cm⁻¹ was attributed to the Si-CH₂ bending vibration in the Si-N chemical and might confirm the formation of a self-assembled silane monolayer or multilayers on the surface of the aluminum (Khaskhoussi et al., 2020). The two intense peaks around 1100 cm⁻¹ might be attributed to the asymmetric siloxane bonds (Si-O-Si) of the surfaces (Khaskhoussi et al., 2020), implying that DMOAC molecules are bonding with each other and cover the surface of the aluminum foil (Figure 84).



Figure 84: Si-N chemical attaches onto the aluminum surface

The DMOAC (Si-N) chemical is able to graft onto the aluminum surface through Al-O-Si bonds, by the reaction between the Al-OH (that was obtained by the etching treatment) and Si-OH groups of the hydrolyzed DMOAC. In addition, there will be intermolecular cross-linking between adjacent silane groups, resulting in the creation of Si-O-Si bridges.

To compare the samples grafted with Si-N, a reference peak is chosen at 1340 cm⁻¹. In the spectrum from the sample Si-N-dipped-NaOH-HNO₃ (Figure 83.e), the peaks between 1100 and 900 cm⁻¹, exhibited a lower intensity than those of the Si-N grafted sample (Figure 83.c) and Si-N-dipped-BW sample (Figure 83.d), compared to the reference peak at 1340 cm⁻¹. This

observation aligns with the FTIR spectrum of the samples before grafting (Figure 77.b) indicating that the NaOH-HNO₃ treatment may not have efficiently etched the surface. This implies that the BW treatment allows for a better grafting than other etching techniques. In the following sections, all samples were only treated with BW.

After that, Si-PO₃-dipped-BW (Figure 83.f), which has the same silanol groups as the Si-N sample, was investigated. The spectrum revealed that the Si-PO₃-dipped-BW sample exhibited a single specific peak around 1100 cm⁻¹ also present in the BW sample. This observation might indicate that Si-PO₃ was not efficiently grafted, or that not enough of the molecule was grafted to be observed by ATR-FTIR analysis. This hypothesis is also applicable to the PO₃-PO₃-BW (Figure 83.g) sample, which has one peak at the same region around 1100 cm⁻¹. At this point, it is important to highlight that for the Si-PO₃ chemicals there are two possible grafting function that can bind on the aluminum surface, silanol or phosphonic acid groups. As Si-PO₃-BW (Figure 83.f) and PO₃-PO₃-BW (Figure 83.g) samples displayed the same peak around 1100 cm⁻¹, that might show that the chemicals attached on the surface through the same chemical group, phosphonic acid, thus forming P-O-Al bonds on the surface (Kyriakou et al., 2020). This aligns with the comment made on the SEM images. It might have an impact on the RN binding efficiency, as the phosphonic acid groups was aimed to bind to the RN in the Si-PO₃ chemical. That result also implies that the selectivity of the phosphonic acid group toward the Al surface is higher than that of the silanol group.

ATR-FTIR analysis was performed to identify the chemical functions of the Si-SO₃ grafted sample. The spectrum is given together with those of the cleaned and BW treated samples in Figure 85.

The Si-SO₃-3h spectrum exhibited a broad band around 3600- 3000 cm⁻¹, and peaks around 2900, 2590, 1400, 1260 cm⁻¹, high intensity peaks at 1025 cm⁻¹ and 870 cm⁻¹ and a broad band from 800 to 650 cm⁻¹. The broad band from 3600 to 3000 cm⁻¹ was attributed to the stretching vibrations of hydroxyl groups. The low intensity peak at 2900 cm⁻¹ corresponded to the C-H (CH₂ or CH₃) chemical bonds (Boxus et al., 1996). The low intensity peak at 2590 cm⁻¹ was attributed to the -SH stretching (Larkin, 2018a). This shows that the transformation of the -SH functions to sulfonic acid groups (-SO₃ groups) might not be 100% efficiently occurred on the surface. The high intensity peak around 1025 cm⁻¹ might corresponds to SO₃H stretching (Özkanat et al., 2012).

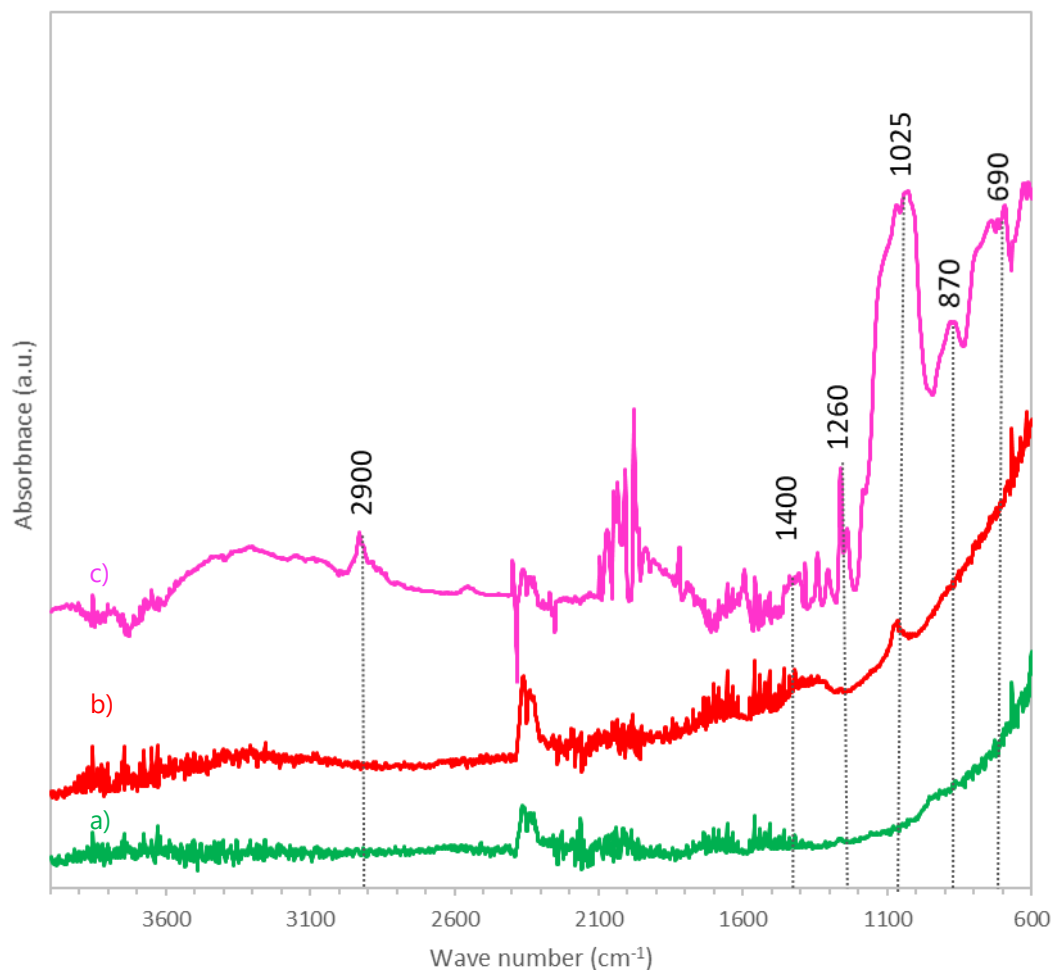


Figure 85: ATR-FTIR spectra of aluminum surface after grafting with MPTMS (Si-SH) and subsequent sulfonation, to yield Si-SO₃ groups a) Cleaned sample, b) BW treated sample, c) E8 (Si-SO₃-3h)

The possible bonds observed from the spectrum are drawn in Figure 86. The absorption band in the range 1100-1000 cm⁻¹ indicates the formation of Al-O-Si and Si-O-Si bonds with the underlying substrate and within the grafted layer, respectively. Because the molecular weights of Al and Si, are close to each other, their respective stretching vibrations can overlap in this region of the spectrum. Additionally, the bond at approximately 870 cm⁻¹ was attributed to the stretching of siloxane, indicating the presence of Si-O-Si bonds. The peak around 870 cm⁻¹ could also be related with silane-aluminum groups on the surface (Si-O-Al) that would signify the existence of a bond between aluminum and MPTMS after sulfonation (Si-SO₃). The peak at 690 cm⁻¹, might be attributed to the remaining-SH groups (Larkin, 2018a).

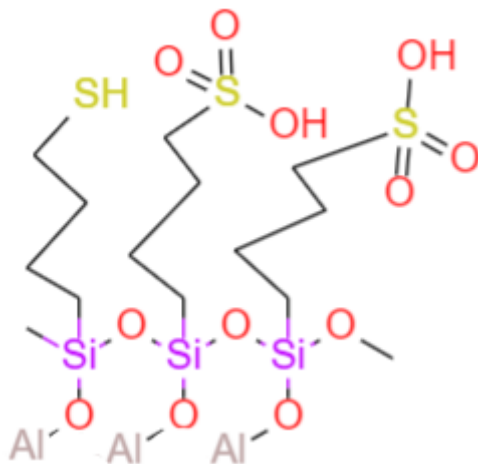


Figure 86: Possible binding modes of the Si-SO₃ chemical onto aluminum surface

2.1.4.1 Improvement of the DMOAC (Si-N) grafting method

After observing the Si-N grafted samples obtained by dipping in the grafting solution, efforts were made to improve the grafting on the surface. The immersion duration in the grafting solution increased from dipping to 1 h immersion, 2.5 h immersion, 6 h immersion, and 12 h immersion. The SEM images of these samples are presented in Figure 87.

After deciding to use BW treatment systematically as the etching method, all the samples given in the text will be denoted with just their grafting method.

Si-N-1h (Figure 87.a) sample display a honeycomb structure. However, as the immersion duration increases, this structure becomes more prominent. The lower magnification image of Si-N-12h sample (Figure 87.d) shows a well-defined 3D structure.

The Si-N-2.5h (Figure 87.b) and Si-N-6h (Figure 87.c) samples both exhibit sub-micron size roughness. These structures become more pronounced on the surface by increasing immersion duration. However, upon closer examination at various magnifications, they can also exhibit a pattern resembling a honeycomb.

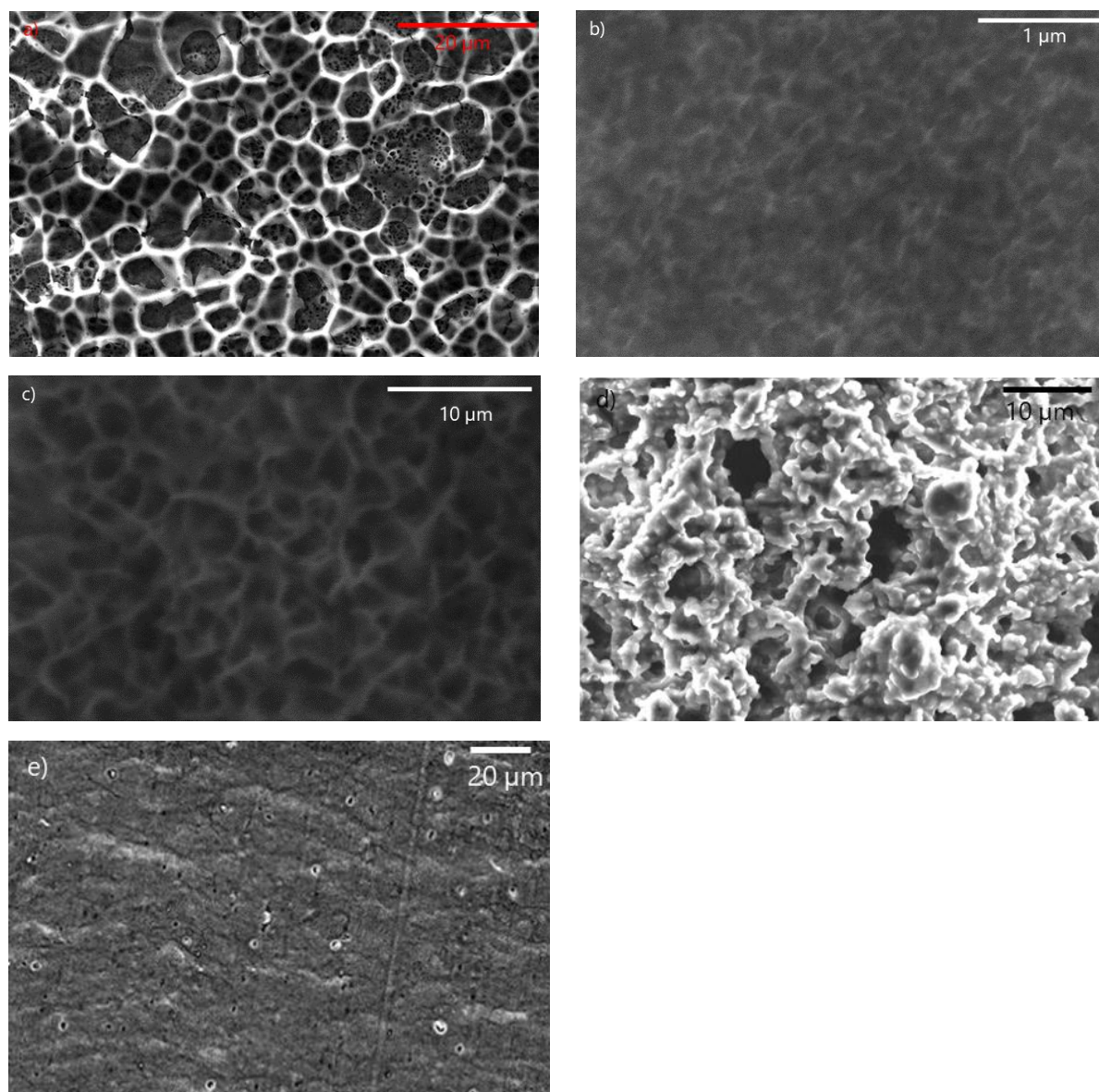


Figure 87: Top view SEM images of the Si-N grafted samples a) Si-N-1h, b) Si-N-2.5h, c) Si-N-6h, d) Si-N-12h, e) BW treated sample

The chemical characterization of the Si-N grafted samples with different immersion durations in the grafting solution were also investigated by ATR-FTIR analysis (as shown in Figure 88). This analysis was performed with the ATR-Platinum device, which has a lower detection limit than the previous device used. All the grafted samples previously underwent a BW etching process, and the spectra of the cleaned sample (Figure 88.a) and BW treated sample (Figure 88. b) are given for comparison. The detailed FTIR analysis of these samples are given in section "2.1.1.3.Effect of the selected etching methods".

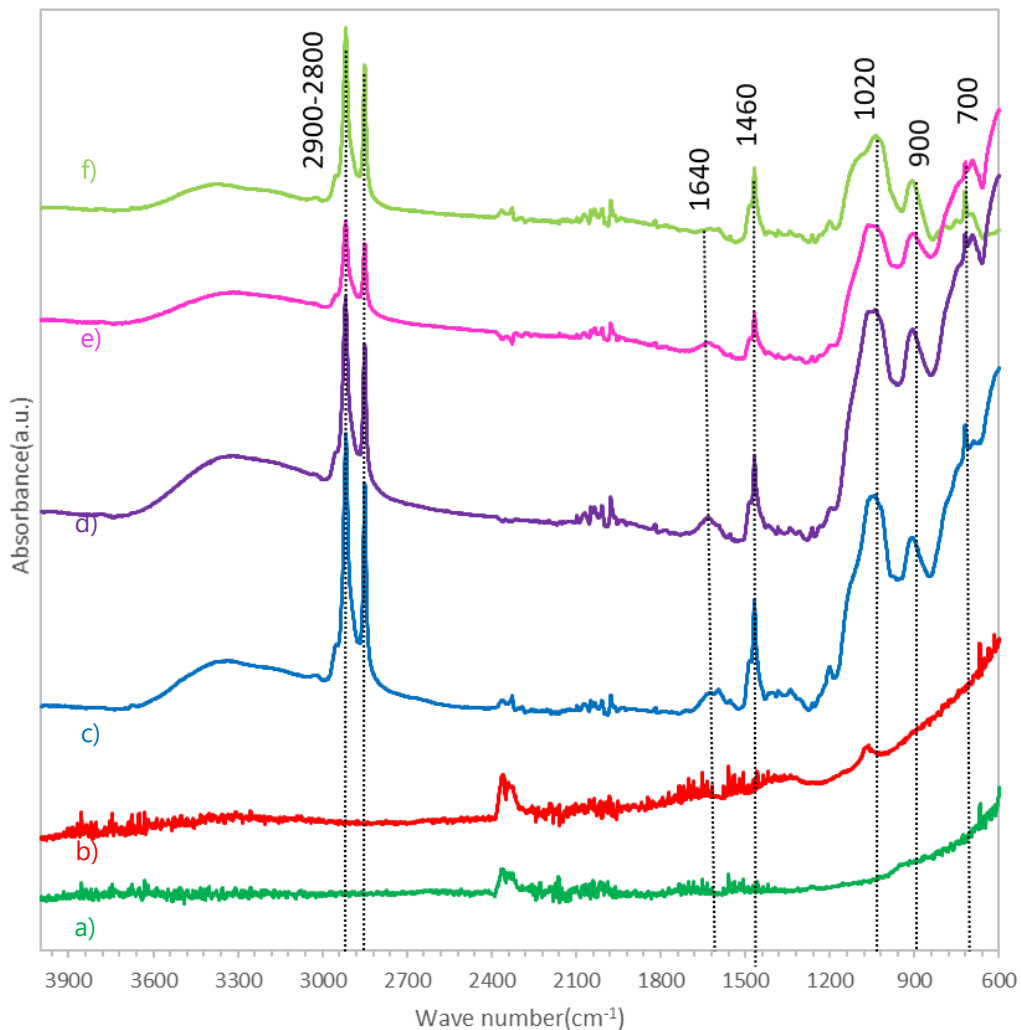


Figure 88: Si-N (DMOAC) samples grafted for different durations a) Cleaned, b) Cleaned-BW, c) Si-N-1h, d) Si-N-2.5h, e) Si-N-6h, f) Si-N-12h

After Si-N grafting, new peaks appeared on the spectra at the same wavenumbers, with varied intensities. The grafting treatment introduces a broad band around $3600\text{--}3100\text{ cm}^{-1}$ that was assigned to the -OH groups on the surface (Özkanat et al., 2012; Siau et al., 2004). In the sample that has the longest reaction duration (Si-N-10h, Figure 88.f) the intensity of the peaks around 2900 cm^{-1} , which can be attributed to the -CH bonds, is approximately the same size as that of the peaks corresponding to the siloxane groups in the spectrum (located around $1020\text{--}900\text{ cm}^{-1}$). On the contrary, in the sample with the shortest immersion duration (Figure 88.c), the intensity of the peaks around 2900 cm^{-1} is two times higher than the peaks around 1020 cm^{-1} . That phenomenon can be ascribed to the long carbon chain, which corresponds to the efficient grafting on the surface and is enhanced by increasing the immersion duration in the grafting solution. The peaks located around 1020 cm^{-1} are ascribed to alkoxy silane groups (Si-O-R) and Si-O-Al , which might indicate that the silanol group attached on the aluminum surface. Notably, a new peak appeared around 700 cm^{-1} with the grafting, suggesting the rocking of -CH_2 and -CH groups contained in the DMOAC (Si-N) structure.

SEM images of the Si-N grafted samples reveals that the longer duration seems to present thicker layer on the surface, which was supported by the FTIR-ATR analysis. These findings underscore the importance of treatment duration in influencing the material characteristics under study, from these samples the best procedure is found as the longer duration Si-N-12h grafted sample.

2.1.4.2 Improvement of the DPTES (Si-PO₃) grafting method

The Si-PO₃ grafted samples were investigated in terms of the grafting duration, 2.5 h and 12 h, by ATR-FTIR as shown in Figure 89). This analysis was performed with the device ATR-Platinum. The spectra of a cleaned sample and BW treated sample are given for comparison in Figure 89.

The broad band observed between 3400-3100 cm⁻¹ was observed in both samples (Figure 89.c and d) and was assigned to the -OH bonds on the surface. Additionally, low intensity peaks appeared at 2900-2840 cm⁻¹, that might indicate the -CH chain in the structure of the Si-PO₃ chemical. The peaks that appeared around 1050 cm⁻¹, signified the P-O-Al or Si-O-Al bonds on the surface (Kyriakou et al., 2020) (Figure 90.a and Figure 90.b). As the DPTES chemical possesses both chemical groups at its ends, identifying which group is actually grafted on the surface can be challenging. Additionally, grafting introduces a new peak on the two samples around 770 cm⁻¹ suggesting the rocking of -CH₂ and -CH groups contained in the DPTES structure.

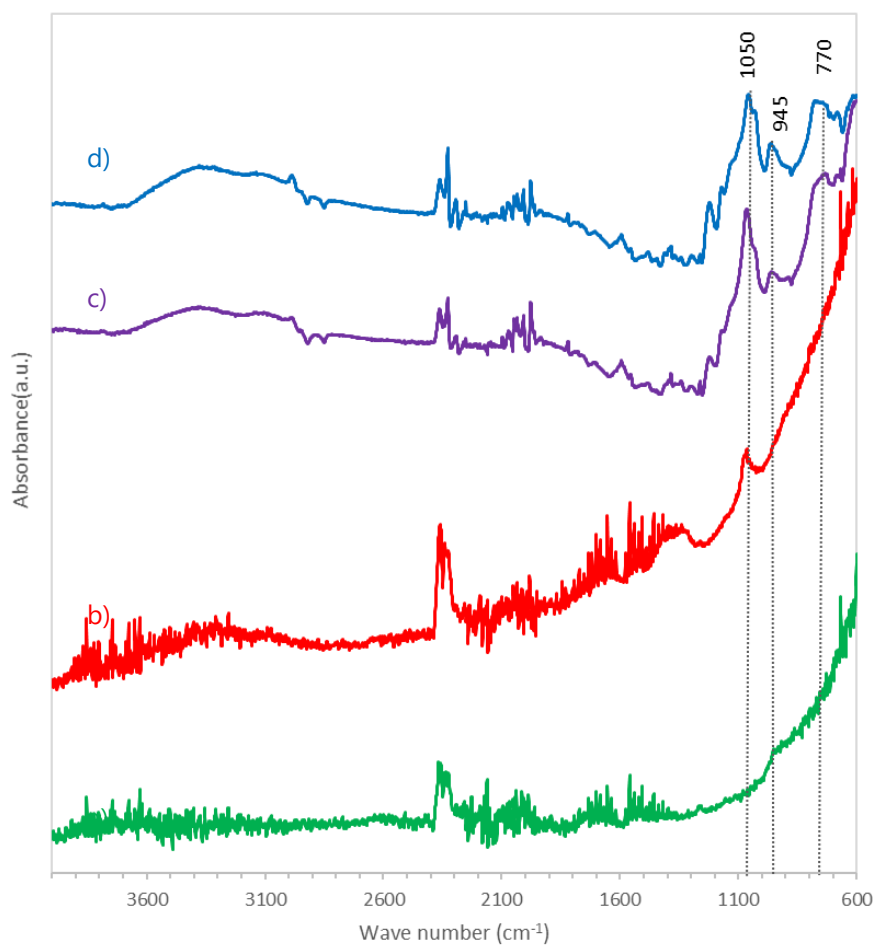


Figure 89: ATR-FTIR spectra of the Si-PO₃ grafted samples a) Cleaned, b) Cleaned-BW, c) Si-PO₃-2.5h, d) Si-PO₃-12h

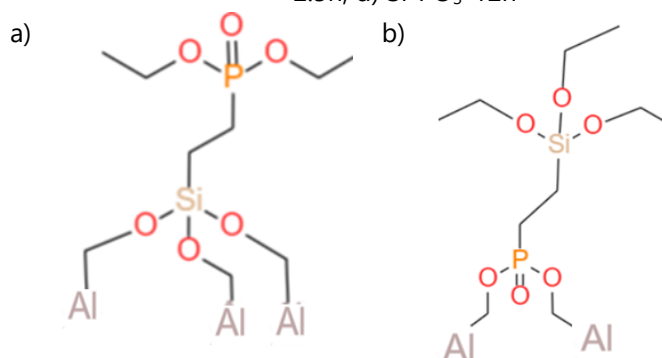


Figure 90: Possible binding modes of the Si-PO₃ chemical a) binding from silanol group, b) binding from phosphonic acid group

From ATR-FTIR spectrum the optimal reaction duration is identified for 12 h reaction which is supported by the SEM analysis. The longer the reaction duration gives bigger particles on the surface of the sample which might effect the success of the RN binding as a result.

2.1.4.3 Improvement of the DTPMP (PO_3-PO_3) grafting method

The PO_3-PO_3 grafting was performed according to two different methodologies. One method involved the use of Na_2SO_4 salt, while the other focused on the impact of the pH. These methods were tested over various grafting durations, and SEM images are presented to provide insight about the resulting topography of the surfaces.

With the exception of one sample, which was produced using the Na_2SO_4 salt method and was immersed in the grafting solution for 1 hour (denoted as $PO_3-PO_3-Na_2SO_4-1h-22^\circ C$), all samples were placed in an oven at $100^\circ C$ for overnight following their respective grafting reactions

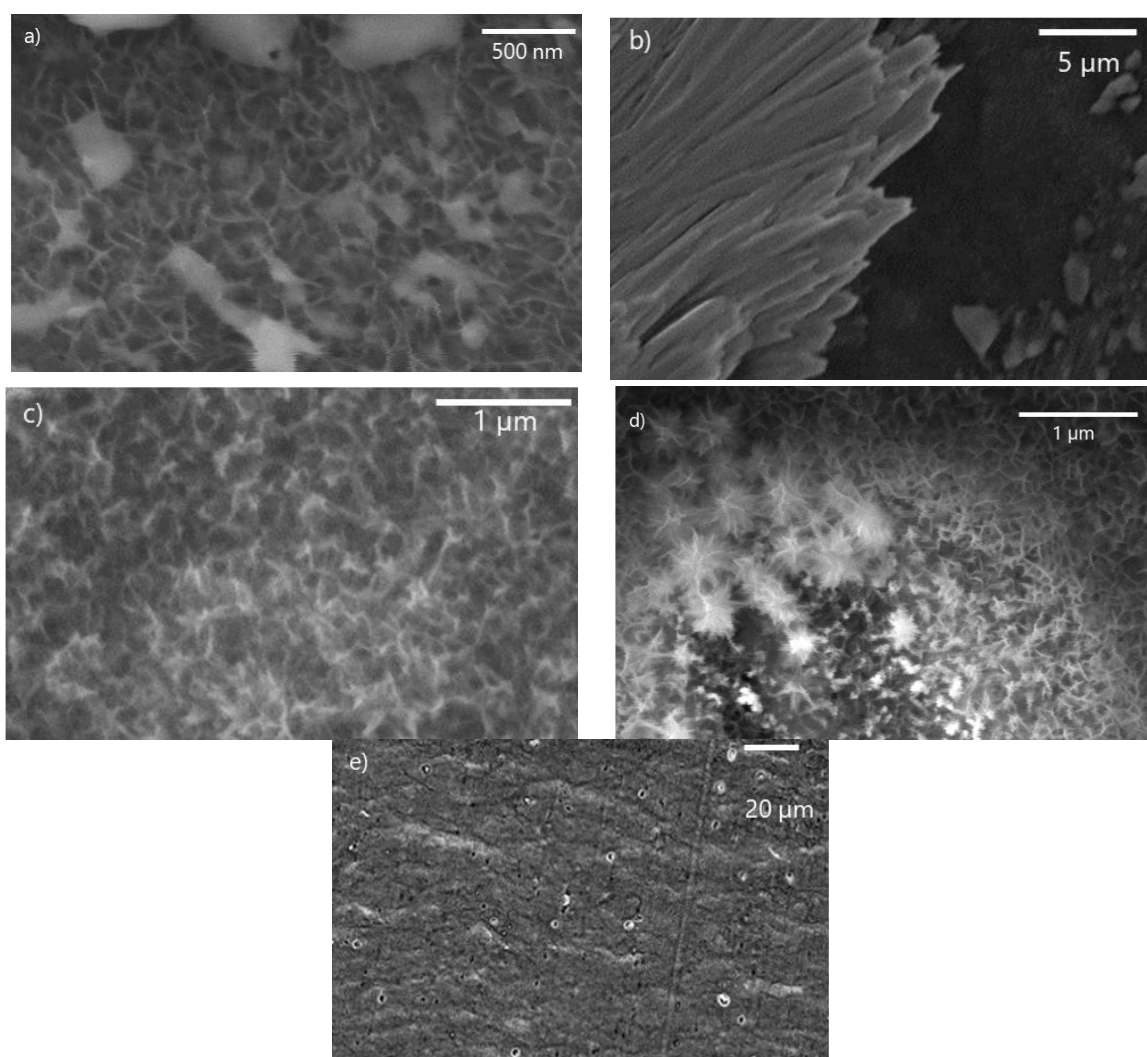


Figure 91: Top view SEM images of the PO_3-PO_3 grafted samples a) $PO_3-PO_3-Na_2SO_4-1h-22^\circ C$, b) $PO_3-PO_3-Na_2SO_4-2.5 h$, c) $PO_3-PO_3-pH8-2.5h$, d) $PO_3-PO_3-pH8-6h$, e) BW treated sample

The samples produced using the salt method $\text{PO}_3\text{-PO}_3\text{-Na}_2\text{SO}_4\text{-1h-22}^\circ\text{C}$ (Figure 91.a) and $\text{PO}_3\text{-PO}_3\text{-Na}_2\text{SO}_4\text{-2.5h}$ (Figure 91.b) exhibited persistent salt residues on the surface. These images clearly illustrate that despite the cleaning procedures, salt particles have adhered to the sample surfaces. The risk of these salt particles detaching from the surface during the RN binding experiments could become problematic for the coming parts of the study and/or result in non uniformity. Additionally, the amount of salt remaining on the surface seemed to increase with the immersion duration.

The samples produced using the pH adjustment method $\text{PO}_3\text{-PO}_3\text{-pH8-2.5h}$ (Figure 91.c) displayed sub-micron rough structure all over the surface. $\text{PO}_3\text{-PO}_3\text{-pH8-6h}$ sample is represented in Figure 91.d. As the immersion duration increased, it was observed that larger clusters resembling stars formed on the surface.

These samples underwent ATR-FTIR analysis with the addition of $\text{PO}_3\text{-PO}_3\text{-Na}_2\text{SO}_4\text{-10 h}$ sample (Figure 92). This sample could not be checked by SEM analysis due to the salt formations on the surface, which was visible to the naked eye. The vacuum system of SEM device has the capacity to draw in tiny crystal particles, which would have contaminated the device.

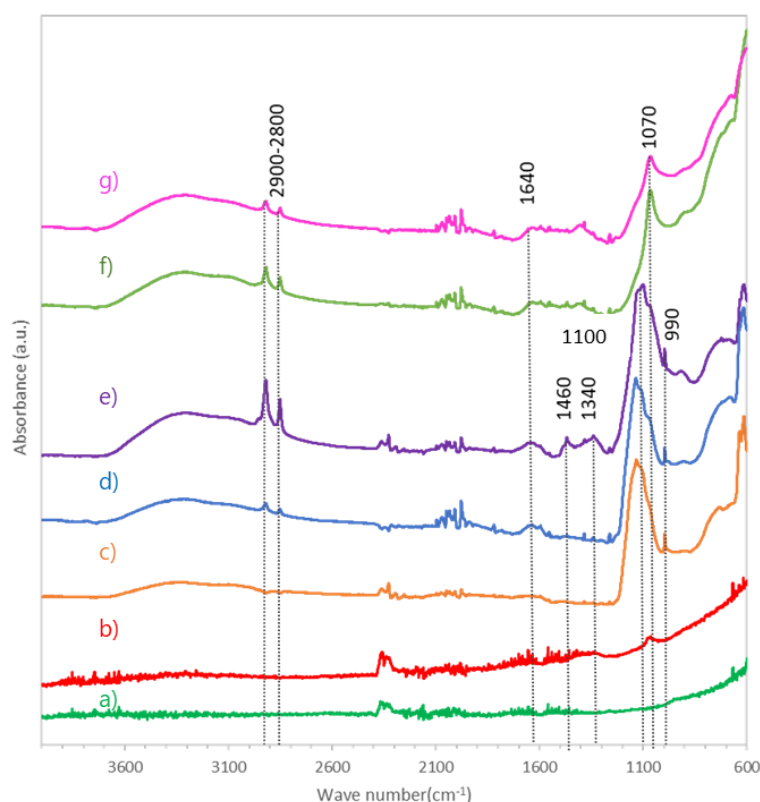


Figure 92: ATR-FTIR spectra of the $\text{PO}_3\text{-PO}_3$ grafted samples a) Cleaned, b) Cleaned-BW, c) $\text{PO}_3\text{-PO}_3\text{-Na}_2\text{SO}_4\text{-1h-22}^\circ\text{C}$, d) $\text{PO}_3\text{-PO}_3\text{-Na}_2\text{SO}_4\text{-2.5h}$, e) $\text{PO}_3\text{-PO}_3\text{-Na}_2\text{SO}_4\text{-10h}$, f) $\text{PO}_3\text{-PO}_3\text{-pH8-2.5h}$ g) $\text{PO}_3\text{-PO}_3\text{-pH8-6h}$

In all the $\text{PO}_3\text{-PO}_3$ samples produced by the Na_2SO_4 method, a specific peak appeared with a high intensity around 1160 cm^{-1} . These samples were prepared by 1 h, 2.5 h, or 10 h of immersion duration (Figure 92.c d, and e). Among these samples, the one with the longest immersion duration ($\text{PO}_3\text{-PO}_3\text{-Na}_2\text{SO}_4\text{-10h}$) displayed a broad band from 3700 to 2900 cm^{-1} , two peaks around 2900 and 2800 , peaks at 2300 , 1640 , 1460 , 1340 , 1160 cm^{-1} and a band from 880 to 600 cm^{-1} . The possible signification of these peaks is given in Table 31. The previous attributions given in Table 30 are not repeated here.

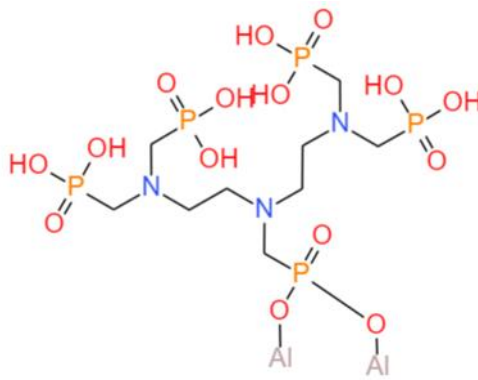


Figure 93: Possible binding mode of $\text{PO}_3\text{-PO}_3$ chemical on aluminum surface

One of the possible binding modes of $\text{PO}_3\text{-PO}_3$ is shown in Figure 93. In addition, phosphonic acid binding modes can also be mono-, or tridentate for anchorage on aluminum surface (Neouze and Schubert, 2008). The characteristic peak related to P-O-Al , located around 1100 cm^{-1} , was observed on all spectra, indicating the bond formed between the aluminum and the chemical. The sample treated at room temperature ($\text{PO}_3\text{-PO}_3\text{-Na}_2\text{SO}_4\text{-1h-22}^\circ\text{C}$, Figure 92. c) did not exhibit a peak around 1640 cm^{-1} , which could indicate -OH group deformation of the phosphonic acid functions (Eisazadeh et al., 2010). The small presence of this peak in the $\text{PO}_3\text{-PO}_3\text{-Na}_2\text{SO}_4\text{-1h-22}^\circ\text{C}$ sample implies that the reaction was not fully completed under these conditions. Moreover, the results shows that the reaction duration also have an impact on this result. Consequently, these findings indicate that the chemical grafting was less effective without a final temperature treatment under the room temperature.

Table 31: Attributions of the peaks from $\text{PO}_3\text{-PO}_3$ grafted samples (Lushtinets et al., 2007).

Peak wavenumber (cm^{-1})	Attribution
3600-3100	-OH stretches
2300	P-OH free phosphonic acid
1640	-OH deformation
1340	P=O stretching
1100	P-O-Al (Kyriakou et al., 2020)
990	P-OH

The samples treated at pH 8 ($\text{PO}_3\text{-PO}_3\text{-2.5 h}$ and $\text{PO}_3\text{-PO}_3\text{-6 h}$) displayed specific bands around $2900\text{-}2800\text{ cm}^{-1}$, from 1640 to 1340 cm^{-1} and a peak around 1100 cm^{-1} , which indicate the P-O-Al bond formation on the surface (Figure 92. f and g).

The most effective method was identified as the grafting treatment conducted at pH 8 for a duration of 6 hours, followed by an oven treatment ($\text{PO}_3\text{-PO}_3\text{-6 h}$). This finding is supported by the results of the SEM images.

2.1.5 Coating methods

The preparation of the coated samples involved only cleaning, without any etching treatments.

2.1.5.1 KMnO_4 treatment

In this section, all the substrates were treated with KMnO_4 , under acidic or basic conditions. For the chemical analysis, H3 sample ($0.30\text{M-}60\text{min-}50^\circ\text{C}$) was chosen.

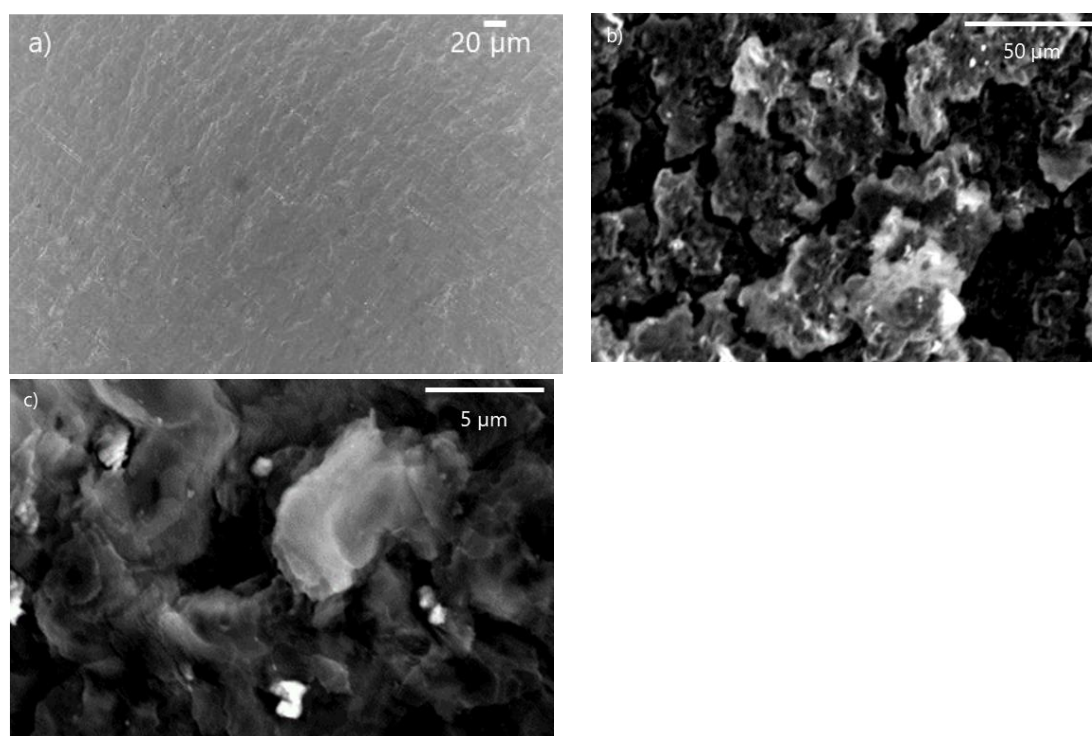


Figure 94 : Top view SEM images of a) Cleaned sample, b) H3 sample treated with KMnO_4 ($0.3\text{M-}60\text{ min-}50^\circ\text{C}$) c) zoomed area of H3 sample treated with KMnO_4

The morphology of the aluminum foil, treated with KMnO_4 , was investigated through SEM, as illustrated in Figure 94. When compared to the cleaned sample, the KMnO_4 treated sample has undergone a distinct color change. This transformation in color is characteristic of the presence of a coating. The coating creates a distinctive globular structure on the aluminum surface as observed in Figure 94.b and Figure 94.c, compared to the cleaned sample (Figure 94.a). Such an effect can be attributed to the formation of $\gamma\text{-MnO}_2$ crystallites (Kokatev et al., 2016).

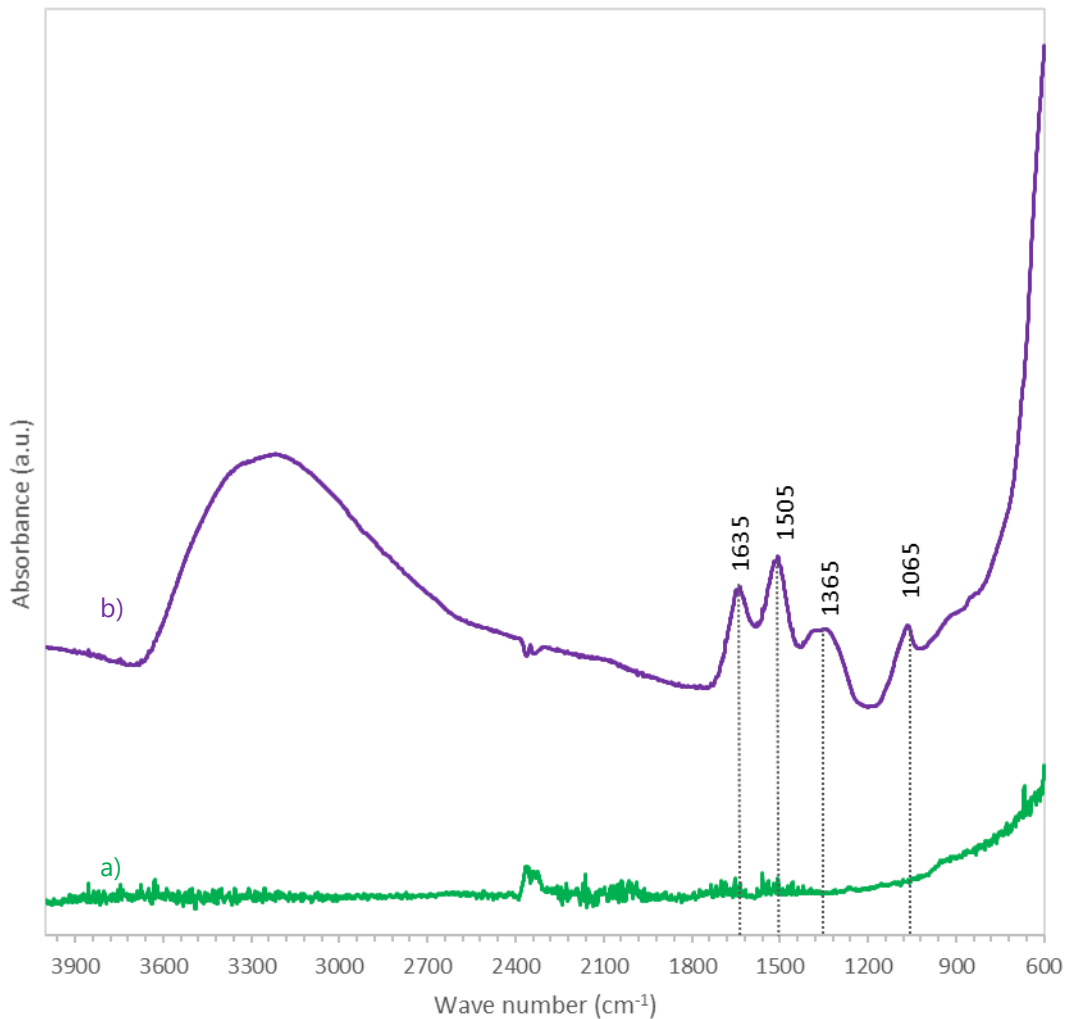


Figure 95: ATR-FTIR spectra of a KMnO_4 treated sample and references a) Cleaned sample, b) H3 sample (0.30M-60min-50°C)

The treatment with the KMnO_4 solution induces a notable change in the FTIR spectrum (Figure 95. b). In particular, a broad absorption band within the $3600\text{--}3100\text{ cm}^{-1}$ range suggested the presence of asymmetric and symmetric --OH bond stretching vibrations (Siau et al., 2005). The appearance of distinct peaks at 1635 , 1505 , and 1365 cm^{-1} were strongly indicative of --OH vibrations (Zheng et al., 2013). However, these peaks may also signify --CO stretching, potentially related to surface contamination. Additionally, the peak at 1065 cm^{-1} may suggest the presence of --OH bands on the surface, or it could be linked to the vibration of the $\text{Mn}^{3+}\text{--O}$ bond (Kang and Kim, 2020). Furthermore, the high intensity peak that appeared in 600 cm^{-1} might indicate the peaks displayed at 660 cm^{-1} . Which is attributed to the stretching vibration of the Mn--O bonds (del Olmo et al., 2022; Kang and Kim, 2020; Zheng et al., 2013) and that proved the formation of the coating on the surface of the samples. In summary, the presence of these distinct peaks strongly supports the formation of a manganese oxide coating on the aluminum surface.

2.1.5.2 $K_2Cr_2O_7$ treatment

The morphology of the aluminum foil treated with $K_2Cr_2O_7$ was investigated through SEM, as illustrated in Figure 96. The I2 sample, displayed distinctive needle-like structures on its surface (Figure 96). These structures exhibit remarkable uniformity in terms of shape, with dimensions reaching up to 50 μm .

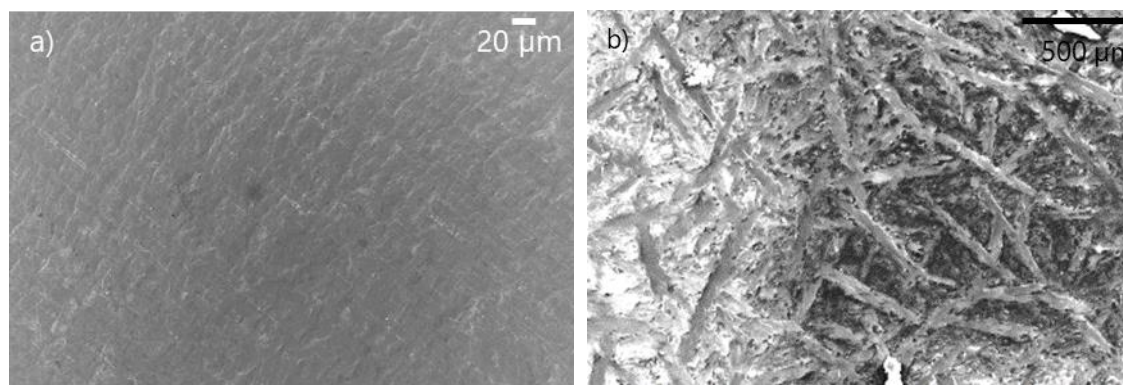


Figure 96: Top-view SEM images of the I2 sample treated with $K_2Cr_2O_7$ (0.50M- H_2SO_4 -60min-50°C) a) Cleaned sample, b) $K_2Cr_2O_7$ (0.50M- H_2SO_4 -60min-50°C)

The spectrum of the sample modified with $K_2Cr_2O_7$ (depicted in Figure 97.b) exhibited a broad absorption band within the 3600-3100 cm^{-1} region. Additionally, a peak at 1650 cm^{-1} signified the HOH bending of water molecules bound within the chromium film (Xia and McCreery, 1998). In the fingerprint region, a prominent peak at 1145 cm^{-1} stood out, attributed to the presence of Cr(V) species (Vuurman et al., 1993; Xia and McCreery, 1998). Furthermore, the presence of a shoulder around 910 cm^{-1} region suggested a Cr (VI)-O vibration. This feature can be attributed to the Al/Cr mixed oxide or Cr mixed oxide, further supporting the conclusion that a Cr (VI)-O coating is indeed present on the surface of the Al foil.(Tüzün et al., 2023).

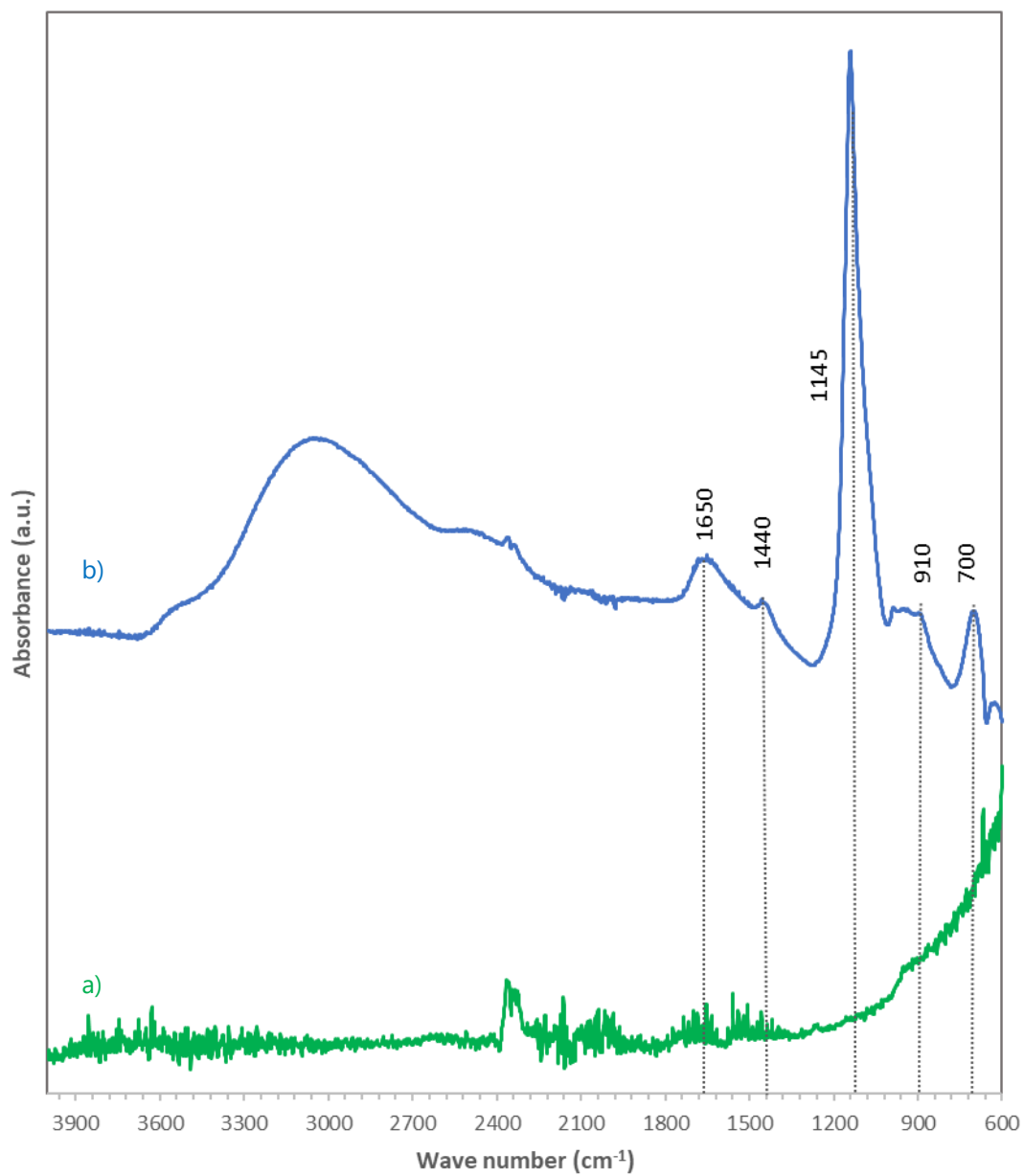


Figure 97: ATR-FTIR spectra of the CrO_x coated sample I2 and references a) Cleaned sample, b) I2 sample (0.50M-H₂SO₄-60min-50°C)

2.2 RADIOMETRIC ANALYSIS

2.2.1 Liquid scintillation analysis

The following section presents the analysis from the LSC experiments conducted on aluminum foil samples. The samples that have meaningful fixation yields are presented.

2.2.1.1 Analysis of the grafted samples (Si-N, Si-PO₃, PO₃-PO₃)

The highest fixation yield achieved during the immersion period, maximum activity level and the duration to reach the maximum yield are given in the following tables.

Table 32: Maximum radioactivity levels of some of the best aluminum foil grafted samples, tested with ¹⁵²Eu

Sample name	Experimental conditions of grafting	Stable Eu/ ¹⁵² Eu	Total amount of Eu in solution (picomol)	Maximum fixation yield ($k = 1$)	A_{\max} (Bq) ($k = 1$)	t_{\max} (h)
B6	Si-N-2.5h	5600	185	$-(20.1 \pm 6.5) \%$	(6.5 ± 2.0)	72 h
B7	Si-N-6h	5600	185	$-(19.8 \pm 6.5) \%$	(4.9 ± 1.6)	72 h
C6	Si-N-2.5h	57	19	$-(6.0 \pm 2.8) \%$	(19.7 ± 9.1)	2 h
C8	PO ₃ -PO ₃ -Na ₂ SO ₄ -pH8-10h	57	18	$-(4.5 \pm 2.8)\%$	(13.5 ± 8.5)	72 h
C9	PO ₃ -PO ₃ -Na ₂ SO ₄ -10h	57	16	$-(6.6 \pm 2.8)\%$	(18.0 ± 7.6)	2 h
D10	Si-SO ₃ -20h	910	395	$-(7.2 \pm 2.8)\%$	(28 ± 11)	72 h

Before moving forward with the grafting chemical decision, thirty samples were produced by the all-grafting methods. Only the six best samples are presented in this section. In this discussion, the RN fixation yields of various grafted samples were analyzed and selected from a set of experiments. These samples, chosen for their best fixation yields, were immersed in different radionuclide solutions labeled B, C, and D. The graphs showing the kinetic behavior of the ¹⁵²Eu attachment onto the grafted samples are given in Appendix-3.

Si-N grafted B6 and B7 samples fixation yield were almost has the same value. The fixation yield of B7 shows that by increasing the immersion duration in the grafting solution the fixation yield of the samples can have better results in a shorter period of time. This can be seen in Appendix-3.

The C6 sample, grafted with Si-N chemical for 2.5 hours, initially showed a 6% fixation yield after 2 hours. However, this yield decreased to around 1% over time, suggesting detachment of the attached RNs from the sample surface Appendix-3.

Comparatively, the method involving salt and pH adjustment used for the grafting of the C8 sample ($\text{PO}_3\text{-PO}_3\text{-Na}_2\text{SO}_4\text{-pH8-10h}$) demonstrated a better stability than the sample treated only with salt, C9 sample ($\text{PO}_3\text{-PO}_3\text{-Na}_2\text{SO}_4\text{-10h}$). For the C9 sample, the radioactivity level in the beaker unexpectedly increased after 72 hours; while the evaporation was under control. This means that the increase in the radioactivity level cannot be related to the concentration of the solution. This situation suggests an issue with the stability of the sample. On the other hand, C8 sample is maintained the fixation yield until the end of the immersion duration in the RN binding solution (up to 72 h). Due to its stability advantage of the C8 sample, this one is identified as the most effective, likely due to the pH of 8 during grafting process. This finding highlighted the importance of pH control in the grafting process, especially for the $\text{PO}_3\text{-PO}_3$ grafting.

For all the samples except D10 ($\text{Si-SO}_3\text{-20h}$), the optimal immersion time was identified to be 2 hours in the RN solution. The D10 sample production seems to be the most effective grafting method among the tests. Remarkably, the fixation yield on the sample continued to increase even after 72 hours of immersion, indicating its potential for future experiments. The following section was devoted to Si-SO_3 grafting method.

From these preliminary experiments, we only use the solution used in the C experiment with an activity of 22.01 kBq/g and excess of stable/active ratio 57, it should allow higher fixation yields and higher activity for lower stable/active ratios. In addition, the rest of the experiments that will presents in the coming sections were performed with this solution.

2.2.1.2 Sulfonated samples production (Si-SO_3) and optimization studies

The sulfonated samples were produced with a special pre-treatment, as detailed in the methods, section "1.2.1.1.3 Chemical etching". The etching method of the sulfonated samples combined boiling water and following that, a H_2O_2 treatment.

Sulfonic acid groups are obtained on the surface by a two-step process: first, the grafting of Si-SH molecule (MPTMS), followed by the transformation of the end groups SH into SO_3H functions. The samples E8 ($\text{Si-SO}_3\text{-3h}$) and G8 ($\text{Si-SO}_3\text{-20h}$) were produced using the sulfonation method. The duration written in the code of the samples indicates the duration of the grafting reaction with Si-SH (MPTMS). The second sample, that was grafted for 20 h (G8), was sampled more frequently to facilitate a more comprehensive observation of the kinetic behavior.

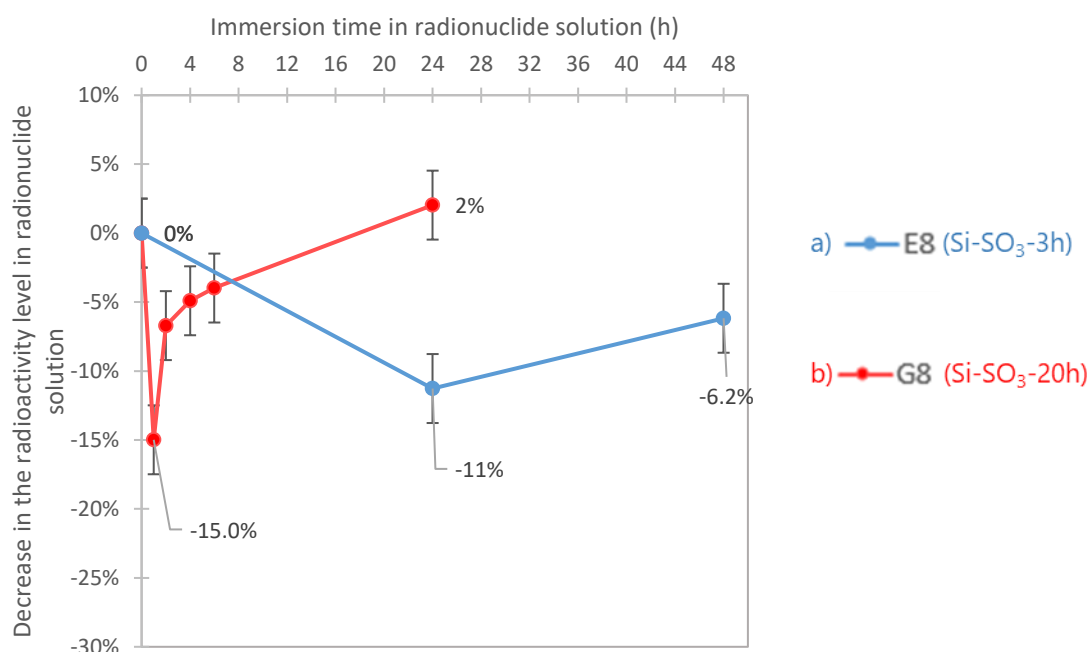


Figure 98: Kinetic behavior of the uptake of ¹⁵²Eu on sulfonated samples immersed in a ¹⁵²Eu solution (Al thickness of 0.03 mm) a) Si-SO₃-3 h b) Si-SO₃-20 h

Table 33: Maximum radioactivity levels on the sulfonated aluminum foils immersed in a ¹⁵²Eu solution

Aluminum samples	Experimental conditions of grafting	Total amount of Eu element in solution (picomol)	Maximum fixation yield, standard uncertainty ($k = 1$)	A_{\max} (Bq), standard uncertainty ($k = 1$)	t_{\max} (h)
E8	Si-SO ₃ -3 h	68	-(11.3 ± 2.7)%	129 ± 30	24 h
G8	Si-SO ₃ -20 h	65	-(15.0 ± 2.7)%	164 ± 30	1 h

Figure 98 illustrates the kinetic behavior of ¹⁵²Eu attachment onto the sulfonated samples. Both samples displayed maximum fixation yields of approximately 13%, as seen in Table 33. The corresponding graph reveals an interesting trend: for E8 (Si-SO₃-3h), the maximum activity during the immersion duration was achieved after 24 h, while for G8 (Si-SO₃-20h), it was reached after only 1 h. Subsequently, the fixation yields of the samples gradually decreased, to close to 0% for G8, and to around 6% for E8. Considering the point at which the samples reached their maximum fixation yield, a longer grafting reaction seemed to yield a coating that reached the maximum fixation yield faster.

The gradual decrease in the fixation yield of the samples could be attributed to the detachment of RNs from the surface or to the alteration of the grafted layer by the acidic conditions of the

radioactive solution. To optimize the process and prevent the detachment of RNs, it would be recommended to reduce the immersion time in the RN binding medium, terminating the RN binding reaction at approximately 4 h, at which the G8 sample has reached the maximum radioactivity level.

To evaluate the intermediate precision of the sulfonation method, with 20 hours of grafting reaction, four samples were synthesized, referred to as the "P series". Out of these, three were selected for radionuclide binding experiments. In this experiment series, aluminum foils pieces with a thickness of 0.3 mm, 10 times thicker than previously, were utilized. The kinetic behavior of RN fixation on these samples during RN binding experiments was tested with ²⁴¹Am as shown in Figure 99, and Table 34 presents the maximum fixation yields and activities of the samples

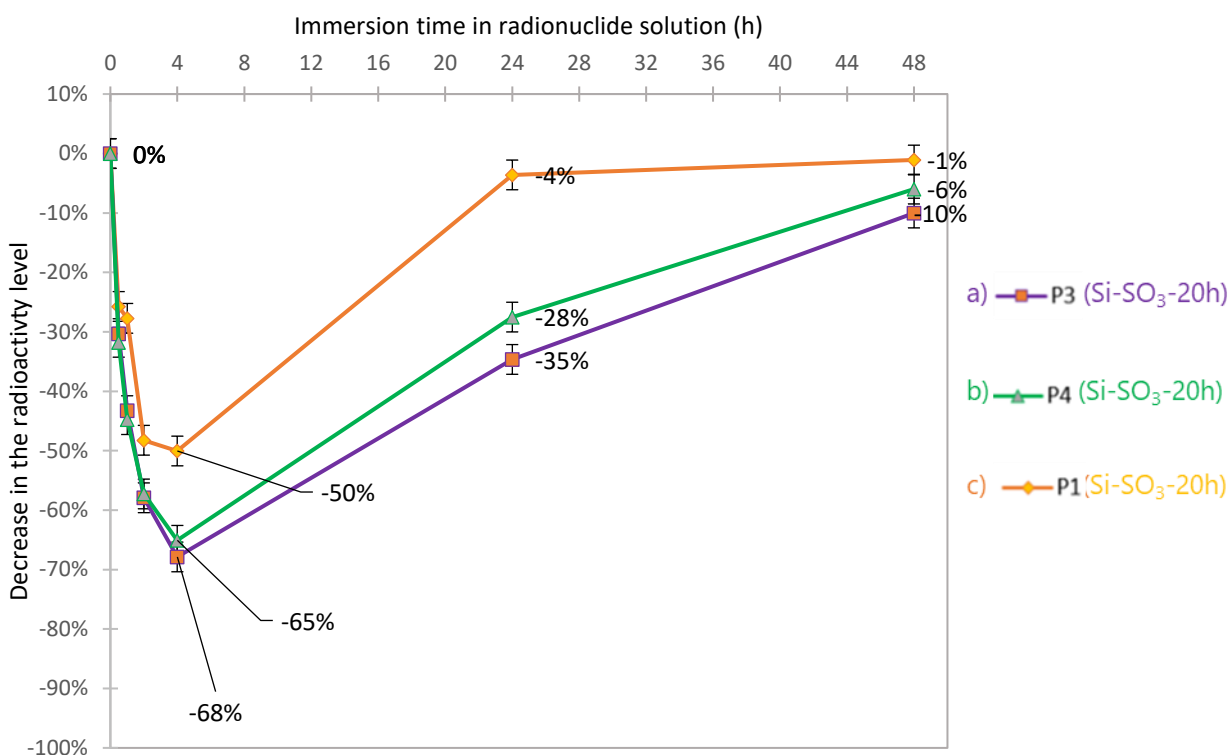


Figure 99: Kinetic behavior of ²⁴¹Am attachment onto sulfonated aluminum samples Si-SO₃-20 h with a thickness of 0.3 mm a) P3, b) P4, c) P1

Table 34: Maximum radioactivity levels of the sulfonated aluminum foil immersed in a ^{241}Am solution

Aluminum samples	Experimental conditions of grafting	Total amount of ^{241}Am element in solution (picomol)	Maximum fixation yield, standard uncertainty ($k = 1$)	A_{max} (Bq), standard uncertainty ($k = 1$)	t_{max} (h)
P3	Si-SO ₃ -20h	30	-(68.3 ± 2.5)%	610 ± 25	4 h
P4	Si-SO ₃ -20h	31	-(65.7 ± 2.5)%	635 ± 25	4 h
P1	Si-SO ₃ -20h	31	-(50.5 ± 2.5)%	470 ± 25	4 h

These samples demonstrated a consistent kinetic trend, all reaching their peak fixation yield after 4 h (Figure 99). Specifically, sample P1 exhibited a lower maximum fixation yield of 50%, while P3 and P4 attained approximately 65% fixation yield (Table 34). Over time, a gradual decrease of the fixated RN was observed, which aligns with the earlier finding with E8 and G8 samples. This also supports the previous conclusion regarding the optimal immersion time in the RN binding solution (4 h).

Upon conducting a detailed analysis, the samples P3 and P4 shared remarkably similar kinetic profiles. In contrast, the fixation yield of the P1 sample drops to 4% after 24 hours. This may be attributed to experimental variations during the pre-treatment etching step in boiling water or during the two steps of the sulfonation treatment. Identifying the precise causes of the different behavior is challenging without advanced chemical analysis techniques like X-ray photoelectron spectroscopy (XPS).

Following the earlier discussions, the impact of the nature of the radionuclide on the attachment to the treated surfaces can be investigated. For this analysis, two samples were selected, G8 and P4, both of which were subjected to immersion in different RN solutions while following comparable experimental protocols for grafting. However, the aluminum foil used in the treatments were different, the one used for ^{152}Eu binding experiment having a thickness of 0.03 mm, while the one used for ^{241}Am binding experiments had a thickness of 0.3 mm. This comparison is detailed in Table 35.

The sample immersed in the ^{241}Am solution (P4) reached a higher fixation yield of around 66%, compared to the one of the sample immersed in the ^{152}Eu solution, which was around 15% only. The amount of elements bound to the surface, is around 10 pmol for the sample immersed in the ^{152}Eu solution and about 20 pmol for the sample immersed in the ^{241}Am solution. While the excess of stable Eu over ^{152}Eu is 57 in the ^{152}Eu solution, and there is no carrier in the ^{241}Am one, it should not affect the amount of element bound, because stable Eu atoms behave the same as the radioactive ones.

Table 35: Comparison of the maximum fixation of ^{152}Eu and ^{241}Am onto Si-SO₃ treated samples

Experimental conditions	Thickness of the aluminum (mm)	Total amount of element in solution (pmol)	Maximum fixation yield, standard uncertainty ($k = 1$)	Approximate maximum amount of element attached (pmol)	t_{max} (h)
^{152}Eu solution G8 (Si-SO ₃ -20h)	0.03	65	-(15.0 ± 2.7)%	10	1 h
^{241}Am solution P4 (Si-SO ₃ -20h)	0.3	31	-(65.7 ± 2.5)%	20	4 h

The difference of fixation yield and amount of element bound could then be due to a different affinity of the grafted sulfonated layer for Eu and Am. However, another potential factor influencing the variation in fixation yields for ^{152}Eu and ^{241}Am could be the thickness of the aluminum foils utilized in the production of the sources. This thickness might alter the surface properties during grafting, leading to different properties of the grafted layer, and in turn, to different fixation yields. For example, we could assume that thicker Al foils could have led to a rougher and thus larger surface after etching, allowing the surface to be grafted with more binding functions than the thinner one. Nevertheless, it is challenging to directly compare samples produced with aluminum foils of varying thicknesses. Additionally, it is noteworthy to consider that the Eu experiments were conducted prior to the Am experiments. Over time, there were refinements in the experimental methods, including the utilization of more suitable equipment. This progression could also have significantly affected the results.

2.2.1.3 KMnO_4 and $\text{K}_2\text{Cr}_2\text{O}_7$ coated samples and their optimization studies

2.2.1.3.1 $\text{K}_2\text{Cr}_2\text{O}_7$ treated (CrOx coated) samples

In this study, two samples, I2 and I3, treated with $\text{K}_2\text{Cr}_2\text{O}_7$ coating solution for different durations, were immersed in the ^{152}Eu solution.

The sample treated for 60 minutes (I2) exhibited a higher fixation yield for ^{152}Eu than the one treated for 10 minutes (I3), as shown in Table 36. The sample labeled I2 (CrOx-pH1-60min-50°C) reached its maximum attachment after 4 hours, after which a gradual decrease was observed (Figure 100.a). The I3 sample (CrOx-pH1-10min-50°C), displayed an opposite trend, with an increase in the radioactivity level of the sampled solution (Figure 100.b). The study explored the impact of coating duration on fixation yields, revealing that longer durations resulted in higher yields (Tüzün et al., 2023). This result is not possible under realistic conditions, because this increase is not covered by the uncertainties on the measurement. This cannot be explained by the concentration of the RN binding solution, because both beakers were covered with parafilm, preventing evaporation.

It is possible that the coating initially adhered effectively, allowing RNs to concentrate on its surface. However, over time, the coating may have detached due to the acidic conditions in the

RN binding medium. Nevertheless, Eu might still be attached to the removed coating, resulting in a non-homogeneous solution. When sampling was conducted, it is possible that the aliquot contained particles of the coating, which had more Eu atoms than the average content in solution. This could explain why the aliquot at 4 h has a higher activity level than at the beginning. Furthermore, the observation that activity of the aliquots returned to the original levels (with a fixation yield close to zero) after 24 hours suggests that the coating might have completely dissolved over this period, rendering the solution homogeneous again.

The I2 sample treated for 60 minutes did not present an increase of apparent activity, which might mean that the coating was more stable, at least until 4 hours. This implies that the coating is successful in binding RNs, and that increasing the duration of the chemical coating reaction can enhance its strength and amount, and allow a more efficient immobilization of RNs on the surface. However, even this improvement did not allow the coating to be stable for more than 4 hours in pH 2 HCl solutions.

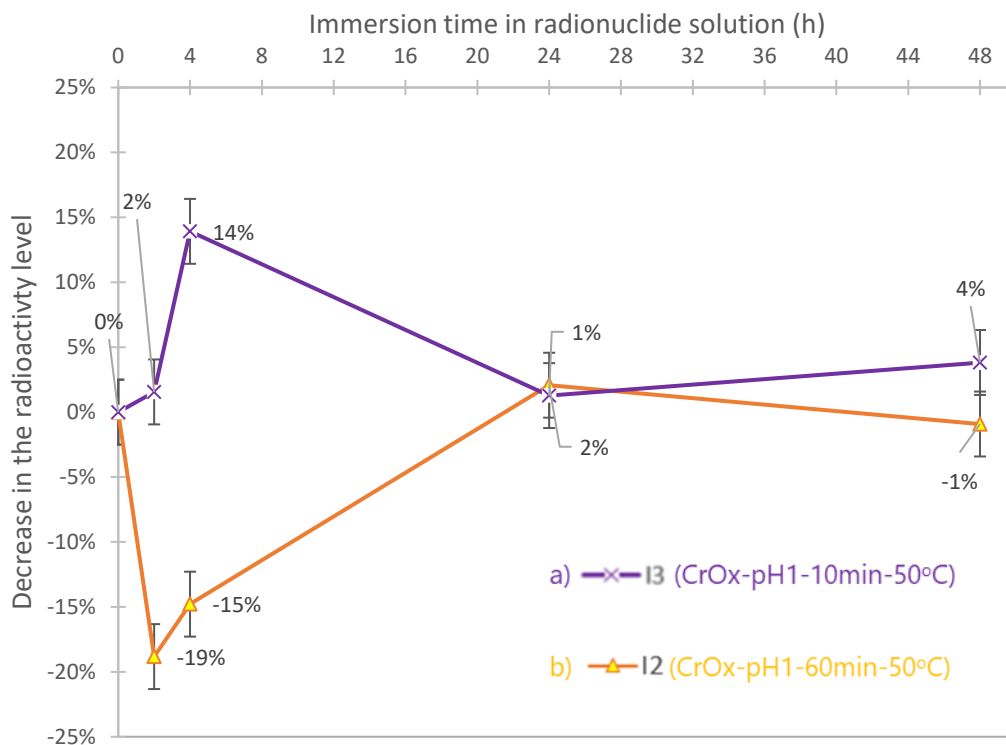


Figure 100: Kinetic behavior of ^{152}Eu attachment onto the samples treated with $\text{K}_2\text{Cr}_2\text{O}_7$ a) I2 (CrOx-10 min- 50 °C), b) I3 (CrOx-60min-50 °C)

Table 36: Maximum radioactivity levels of the $K_2Cr_2O_7$ treated aluminum foils immersed in a ^{152}Eu solution

Coated aluminum samples	Experimental conditions	Total amount of Eu in solution (picomol)	Maximum fixation yield, standard uncertainty ($k = 1$)	A_{max} (Bq), standard uncertainty ($k = 1$)
I3	CrOx-pH1-10 min-50°C	57	(1.5 ± 2.9)%	14 ± 25
I2	CrOx-pH1-60 min-50°C	58	-(18.8 ± 2.7)%	184 ± 25

In the following experiment the efficiency of the CrOx-pH1-60min-50°C treatment was evaluated by immersion in an ^{241}Am solution, shortening the experiment duration to 4 hours, which was the duration observed for the maximum fixation yield of ^{152}Eu .

With ^{241}Am , the activity of the aliquots increased after 2 hours, before returning to the initial value (fixation yield close to 0%) after 4 hours (Figure 101). The coating did not appear to be stable, even if the $K_2Cr_2O_7$ treatment was performed for 60 min.

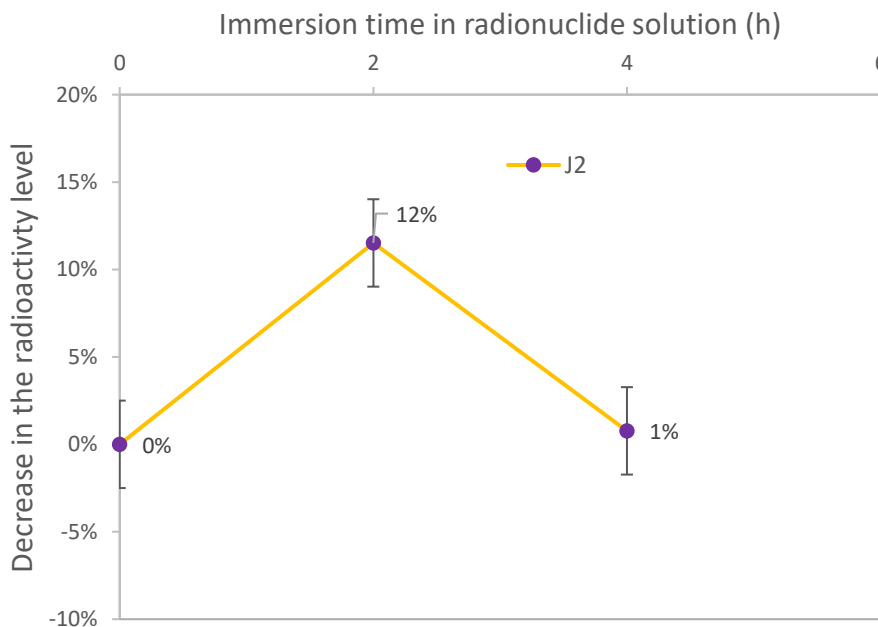


Figure 101: Kinetic behavior of ^{241}Am onto the J2 sample treated with $K_2Cr_2O_7$ (CrOx-pH1-60 min-50°C)

Given the outcomes, no further efforts weremade to enhance the performance of the CrOx treatment. Instead, the focus shifted to exploring $KMnO_4$ treatments. Since both treatments were applied simultaneously, the decision to prioritize the $KMnO_4$ method over the KCr_2O_7 treatment was based on the comparative results and observed efficiencies of the two methods.

2.2.1.3.2 KMnO₄ treated samples

2.2.1.3.2.1 KMnO₄ treated samples produced in acidic conditions

The production of the MnOx coated samples included several parameters such as the concentration of the chemicals, the immersion duration in the solution, the type of solvent, and the temperature of the reaction. In this section, the samples treated in acidic conditions are presented. The kinetics of the attachment of ¹⁵²Eu onto the surfaces are shown in *Figure 102*, and the maximum fixation yields and activities are shown in Table 37.

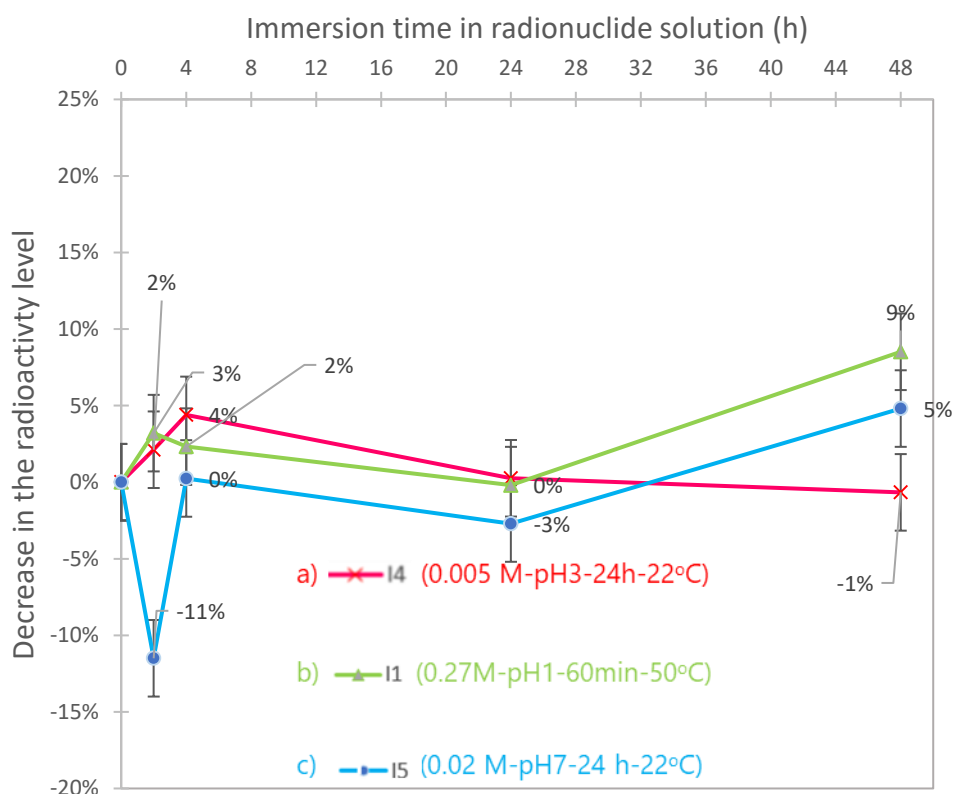


Figure 102: Kinetic behavior of ¹⁵²Eu attachment onto KMnO₄ treated samples produced in acidic conditions a) I4 (0.005 M-pH3-24h-22°C), b) I1 (0.27M-pH1-60min-50°C), and c) I5 (0.02 M-pH7-24h-22°C)

Table 37: Maximum radioactivity levels of the aluminum foils coated with MnOx produced in acidic or neutral conditions, immersed in a ^{152}Eu solution

Coated aluminum samples	Experimental conditions (Molar concentration of KMnO_4 -pH-duration-temperature)	Total amount of Eu element in solution (picomol)	Maximum fixation yield, standard uncertainty ($k = 1$)	A_{max} (Bq), standard uncertainty ($k = 1$)	t_{max} (h)
I4	0.005 M-pH3-24h-22°C	61	-	-	-
I5	0.02 M-pH7-24h-22°C	60	$-(11.5 \pm 2.7)\%$	113 ± 25	2 h
I1	0.27M-pH1-60min-50°C	61	-	-	-

In the experiments with KMnO_4 treated samples, the methods were classified according to their pH. All the samples were treated simultaneously to determine the most effective method.

A clear distinction was observed between the samples treated in acidic conditions (I1 and I4) and the one in neutral conditions (I5). Notably, the sample treated at pH 7 (I5) was the only one that demonstrated successful RN attachment, unlike the others (Table 37). This pattern reflects the similar behavior observed in $\text{K}_2\text{Cr}_2\text{O}_7$ samples treated under acidic conditions, as shown in Figure 100. This observation suggests that acidic conditions during surface modification may not result in a stable coating that can stay on the surface under the acidic RN binding conditions.

For the I4 sample (Figure 102.a), no attachment of Eu to the surface was observed, the fixation yield reaching around 1% after 48 hours, which means that there is no radioactivity on the surface of the source as the fixation yield is almost equal to zero by being within the uncertainty limit. An increase in radioactivity was observed up to 4 hours, which might be attributed to the coating removal from the surface during the immersion period. It actually means that europium atoms attach to the coated layer but this layer was not stable on Al. As particles of the manganese oxide coating are likely sampled into the liquid scintillation counter vial, an apparent increase in radioactivity is observed during the beginning of the immersion in the RN solution. I1 sample is the highest pH from the beginning of the immersion until the end have the lowest fixation yields (with the consideration of uncertainty after 24 h (Figure 102.b). After 24 h immersion I1 sample has the similar behavior as presented in I5 sample (Figure 102.c).

The fixation yield of Eu on I5 showed a decrease up to 4 hours, followed by an increase (Figure 102.c). After 48 hours, the radioactivity level of the sampled solution appeared to increase, which is theoretically not possible since the evaporation was prevented. Again, this could be due to the removal of the coating from the surface as well, due to the acidic nature of the RN binding medium. This removal seemed slower for I5 than for the other samples.

In summary, these results suggest a correlation between the pH of the coating reaction and the efficiency of RN attachment to KMnO_4 treated samples. Samples formed under acidic conditions yielding coated layers that are less stable in the acidic RN binding medium, leading to no uptake of RN by the surface.

2.2.1.3.2.2 KMnO_4 treated samples produced in basic conditions

In this part, the samples treated under basic conditions with KMnO_4 are evaluated. The kinetics of the attachment of ^{152}Eu onto the surfaces is presented in Figure 103, and the maximum fixation yields and activities are shown in Table 38. These samples underwent treatment and, based on their results, the promising experimental conditions were selected for intermediate precision tests.

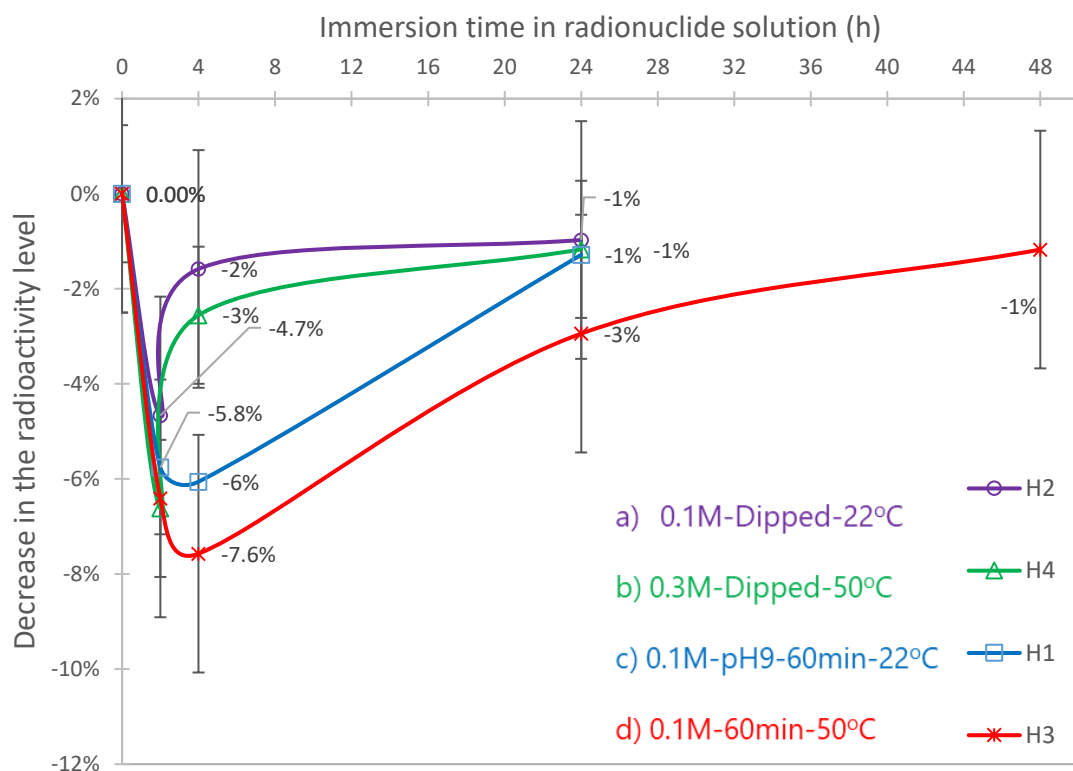


Figure 103: Kinetic behavior of ^{152}Eu onto the basic KMnO_4 treated samples a) H2 (0.1M-Dipped-22°C), b) H4 (0.3M-Dipped-50°C), c) H1 (0.1 M-pH9-60min-22°C), d) H3 (0.3M-60min-50°C)

Table 38: Maximum radioactivity levels of the aluminum foil samples coated with MnOx under basic conditions, immersed in a ^{152}Eu solution

Coated aluminum samples	Experimental conditions (Concentration of KMnO_4 - t_{rxn} -T)	Total amount of Eu element in solution (picomol)	Maximum fixation yield, standard uncertainty ($k = 1$)	A_{max} (Bq), standard uncertainty ($k = 1$)	t_{max} (h)
H1	0.1M-pH9-60min-22°C	67	$-(6.0 \pm 2.8)\%$	105 ± 45	4 h
H2	0.1M-Dipped-22°C	66	$-(4.6 \pm 2.9)\%$	55 ± 30	2 h
H4	0.3M-Dipped-50°C	66	$-(6.6 \pm 2.8)\%$	75 ± 30	2 h
H3	0.3M-60min-50°C	65	$-(7.5 \pm 2.8)\%$	85 ± 30	4 h

Upon initial observation, two behavior were observed among the samples: H2 (Figure 103.a) and H4 (Figure 103.b) exhibited comparable kinetics, while H1 (Figure 103.c) and H3 (Figure 103.d) demonstrated a different behavior. Specifically, the samples dipped in the KMnO_4 solution (H2 and H4) reached their peak fixation yield (6.5% and 4.5%, respectively) within 2 hours. In contrast, the samples treated with KMnO_4 for 60 minutes (H1 and H3) reached their maximum yields (6% and 7.5%, respectively) after 4 hours. All samples exhibited a decline in fixation after longer immersion duration, reaching nearly no fixation at all. An exception was noted for H3, which still showed a 3% fixation yield after 24 hours, and declined to about none after 48 hours.

H2 (0.1M-Dipped-22°C) and H4 (0.3M-Dipped-50°C) were produced through the immersion of the foils in KMnO_4 solutions at different concentrations and temperatures. Both H2 and H4 followed a similar kinetic pattern, achieving their maximum yields after 2 hours, suggesting that the dipping process may not create a coating stable enough in RN solutions to maintain the fixation of RN and/or of the coating beyond 2 hours. These findings imply that shorter coating reaction times may be insufficient for achieving optimal coating, especially at lower concentrations like that of H2. Enhancing the concentration to above 0.1 M and increasing immersion time could potentially improve the stability of the coating in RN binding medium and the RN binding efficiency, even at higher temperature, following the tendency observed in the article from Eikenberg (Eikenberg et al., 2001).

For H3 and H4 samples, an article related to the coating treatment to obtain adhesive bonds on the epoxy surfaces was used (Siau et al., 2004a). The article followed the experimental conditions by applying two temperatures for the coating treatment, 40 °C and 80 °C, for 10 minutes. In the first trial, a temperature of 50 °C was chosen. To examine the effect of the KMnO_4 coating duration, samples H4 (0.3M-Dipped-50°C) and H3 (0.3M-60min-50°C) can be compared. Sample H3 seemed to reach the maximum fixation yield after 4 h, while H4 reached it after 2 h. This possibly indicated that the coating duration affects the time to reach the maximum yield, suggesting that a longer coating reaction duration might lead to a more effective coating, possibly with multiple

layers, which could offer more attachment sites for RNs. This assumption would need further validation although it is also supported by the literature Eikenberg (Eikenberg et al., 2001).

The H1 (0.1M-pH9-60min-22°C) and H2 (0.1 M-Dipped-22°C) samples, which have the same molarity of KMnO_4 in the coating solution, differed in terms of pH and reaction time. Although the kinetic behavior varied between these two samples, they reached similar maximum fixation yields: H1 reached 6.0% after 4 hours, and H2 attained 4.7% after 2 hours. The H1 sample appeared more favorable; however, the parameters contributing to its higher yield could be either the reaction time or the difference in pH.

Throughout the experiment, all "H" series samples eventually experienced a reduction in fixation yield to approximately zero, indicative of a potential detachment of the initially fixated RNs, or a loss of some of the coated layer over the duration of the immersion in the RN binding medium.

Among the KMnO_4 treated samples, H3 stands out, displaying the highest fixation yield after 4 hours, indicating a promising prospect for coming studies. However, the samples produced with this method (0.3M-60min-50°C) were fragile. It was noticed that most of the aluminum foils were damaged and even had melt during the coating process. The samples that managed to be produced under these conditions had been become fragile, as seen in the H3 sample image in Figure 104.a. The image of the same sample after being immersed in the RN binding solution is presented in Figure 104.b, and indicated that the coating on this sample was lost during the 24-hour RN binding process. From 4 h after immersion the color of the coating faded away which corresponds to the time of the maximum fixation yield (Figure 103).



Figure 104: Appearance of the H3 sample a) before immersion in the RN solution b) after immersion in the RN solution

As a consequence, further studies have been initiated to fine-tune the KMnO_4 process on a ten times thicker aluminum foil (0.3 mm), particularly exploring temperature and immersion time adjustments to accommodate the fragile features of H3, as depicted in Figure 104.

2.2.1.3.2.3 KMnO_4 coated samples tested with ^{241}Am

Several options were checked, lowering the duration of the coating reaction to 15 min (J3), and using thicker aluminum foils (T and R). Under these conditions, the experimental investigations focused on the kinetic behavior of ^{241}Am binding onto KMnO_4 treated aluminum foils, providing insights into the fixation processes (as depicted in Figure 105). This section delineates the

experimental outcomes, comparing the fixation yields across different sample series, namely J3, Y, T, and R, each subjected to specific treatment conditions.

The J3 (0.27M-15min-50°C) sample was prepared following a similar procedure utilized for the H3 (0.3M-60min-50°C) sample. As the H3 sample looked weakened after this time span, the duration was decreased four times and 15 minutes was selected while keeping the temperature the same as for the H3 sample. The J3 sample achieved a 70% fixation yield after 4 hours, suggesting a rapid coating at the given conditions (Figure 105.e and Table 39).

Compared to the J3 sample, the Y series samples, which were treated at 0.28 M for 15 minutes at 50°C, reached a similar maximum fixation yield after 4 hours, but experienced a significant drop from 70% to 30% of fixation in yield at the end of immersion (Figure 105.a, c and d).

The Y series, comprising samples Y1, Y2, and Y3, demonstrated 24, 30 and 36 % of maximum fixation yield respectively after 4 hours, but only the Y2 sample was experienced a pronounced decline in fixation by the end of the immersion period. The Y series was produced simultaneously in different crystallizers while being immersed in a shared hot water bath.

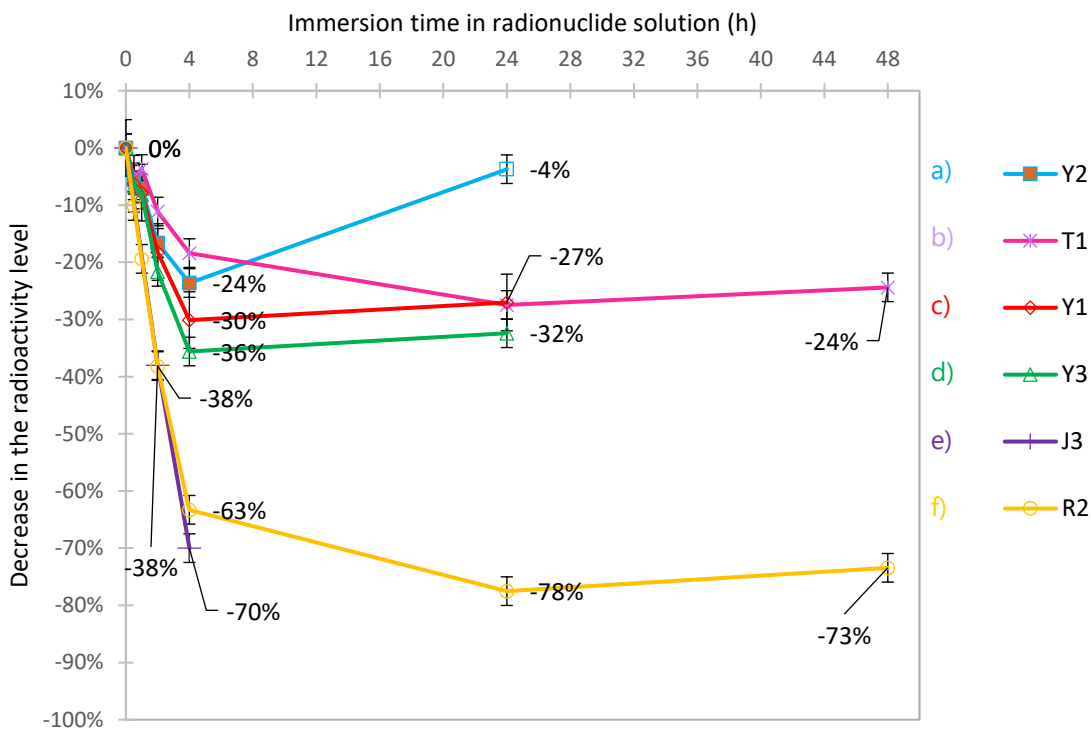


Figure 105: Kinetic behavior of ^{241}Am attachment onto KMnO_4 treated samples a) Y2 (0.28M-15 min -50°C), b) T1 (0.28M-15min-80°C), c) Y1 (0.28M-15min-50°C), d) Y3 (0.28M-15 min-50°C), e) J3* (0.27M-15min-50°C), f) R2 (0.28M-40min-80°C). Among these samples, J3 has a thickness of 0.03 mm, unlike the other samples.

Table 39: Maximum radioactivity levels of the aluminum foil samples coated with MnOx under basic conditions, immersed in a ^{241}Am solution

Coated Al samples	Experimental condition	Thickness of aluminum foil (mm)	Total amount of ^{241}Am element in solution (picomol)	Maximum fixation yield, standard uncertainty ($k = 1$)	A_{max} (Bq), standard uncertainty ($k = 1$)	t_{max} (h)
J3	0.27 M-15min-50°C	0.03	59	-(70.0 ± 2.6)%	1305 ± 45	4 h
Y1	0.28 M -15min-50°C	0.3	31	-(30.0 ± 2.6)%	290 ± 25	4 h
Y2	0.28 M-15min-50°C	0.3	30	-(25.0 ± 2.6)%	225 ± 25	4 h
Y3	0.28 M-15min-50°C	0.3	31	-(34.1 ± 2.5)%	325 ± 25	4 h
T1	0.28 M-15min-80°C	0.3	30	-(27.8 ± 2.6)%	255 ± 25	24 h
R2	0.28 M-40min-80°C	0.3	30	-(77.1 ± 2.6)%	700 ± 20	24 h

The main difference between the Y and T samples is the temperature during the coating, which was 50°C for the Y series and 80°C for the T1 sample. The time required to reach maximum fixation is 24 hours for the T1 sample. This sample investigates the effects of increased temperature during the KMnO_4 coating. It was produced using thicker aluminum foil pieces with a thickness of 0.3 mm allowing for additional optimization (similar to the Y series). This temperature was chosen due to the studies by Siau (Siau et al., 2004a). As the 80 °C could not be reached without dissolving part of the 0.03 mm aluminum foil, these trials were performed with the thicker aluminum foil to compare the results. The article stated that the samples treated at 80 °C, provided better roughness properties on the surface (Siau et al., 2004a). For the thicker aluminum, using this temperature was a good point to see the impact of the temperature on the coating properties.

In Figure 106.a, it can be seen that even with the thicker aluminum foil, it is still possible to see the destructive impact of the KMnO_4 treatment applied at 80 °C on the surface of the thicker samples. The surface roughness on the aluminum samples increased after the 80 °C treatment applied in agreement with the literature (Siau et al., 2004a).

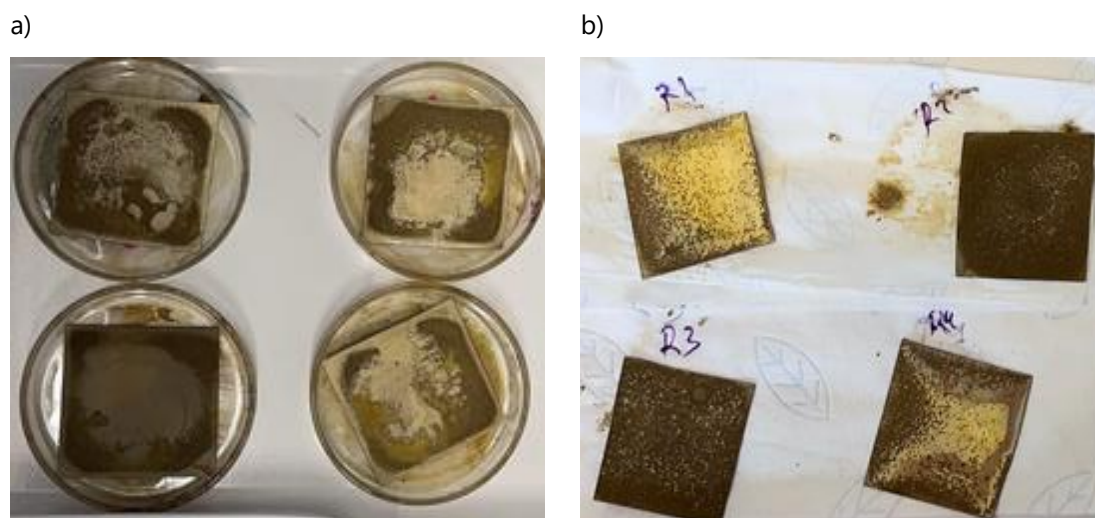


Figure 106: The appearance of the KMnO_4 treated samples a) T series samples (0.30M-15min-80°C) series, b) R series samples (0.30M-40min-80°C)

In drawing conclusions from the results of the coating experiments, it is important to consider an additional bias arising from the immersion of the coating in the radionuclide solution. This immersion process introduced variation in the results, indicating that the sensitivity of the surface to the coating solution, during the coating stage is a critical factor. To prevent the surface from becoming overly sensitive, careful consideration should be given to the coating process and the potential problems that may arise in subsequent stages. If the surface is already fragile after the coating stage, immersing it to an acidic environment for a certain period will likely increase the surface damage. Therefore, modifying the experimental parameters during immersion or using thicker substrates should be considered to avoid these issues.

Both the T1 (0.28M-15min-80°C) and R2 (0.28M-40min-80°C) samples were subjected to the same temperature but differed in the KMnO_4 treatment time for the coating process. The resulting coating was different due to the increased duration of the coating treatment, which is shown in Figure 106.b. The R2 sample achieved the best fixation yield at 78% after 24 hours, though this value slightly decreased after 48 hours, to 73%. This comparison suggests that increasing the coating duration may indeed improve the fixation yield. This may be due to a higher specific surface area following the increased roughness obtained with longer coating duration. Consequently, this could result in a higher number of functionalized groups being present on the surface, thereby requiring an extended time of 24 hours instead of the 4 hours in the RN binding medium, in order to achieve the highest fixation yield.

In conclusion, it can be inferred that the extended duration of immersion during the oxidation step, in combination with higher temperature treatment, leads to improved efficacy in terms of the fixation of RNs on the surface. Moreover, the time needed to reach the point of maximum fixation is prolonged. Longer immersion time and higher temperatures generally lead to improved fixation yields, as evidenced by the R2 sample. However, prolonged immersion times in RN binding solution can lead to a reduction in yield, suggesting that there is an optimal immersion time that maximizes fixation while minimizing subsequent losses.

In assessing the differences in attachment among the samples, we have the possibility to investigate the impact of nature of the RN on the fixation yield. Stable Eu atoms were present in the ^{152}Eu solution, and can influence the fixation yield as they occupy fixation sites onto the surface. For this purpose, samples H3 and J3 were immersed in two different RN binding solutions (Eu or Am) and underwent similar experimental procedures, and were selected for comparison. The comparative data is presented in Table 40.

Table 40: Kinetic behavior of ^{152}Eu and ^{241}Am onto KMnO_4 treated samples produced in basic conditions

Experimental conditions	Thickness (mm)	Total amount of element in solution (picomol)	Maximum fixation yield, standard uncertainty ($k = 1$)	A_{max} (Bq), standard uncertainty ($k = 1$)
^{152}Eu solution H3 (0.30M-60 min-50°C)	0.03	66	$-(7.5 \pm 2.8)\%$	75 ± 30
^{241}Am solution J3 (0.27M-15min-50°C)	0.3	59	$-(70.0 \pm 2.6)\%$	1305 ± 45

2.2.2 Phosphor imaging Autoradiography analysis

In this section, the confirmation of RN presence on the surfaces and the assessment of RN distribution uniformity were investigated through phosphor imaging autoradiography analysis.

When a result of activity per unit surface is given for the sources, there is an important underlying assumption which is that the radionuclides are distributed uniformly across the entire surface area of the source. To verify this assumption, autoradiography images were obtained.

In this section, we present the uniformity measurements that were performed on aluminum surface sources. The uniformity of the 25 cm^2 sources was calculated from 4 equal portions of 6.25 cm^2 .

The fundamental hypothesis of our study posits that the observed decrease in radioactivity levels within the solution during the RN binding experiments is attributable to RN fixated onto the surface of the substrates. To observe the distribution of the RN on the sources, digital autoradiography analysis was employed. The radioactivity level of each source was calculated based on the final fixation yield ($Y_{\text{end}}\%$) and the initial radioactivity present in the RN binding medium (A_{initial}). This calculation is given in Equation 20, where " A_{sample} " represents the source activity in Bq, and " m_{total} " denotes the total mass of solution involved during the RN binding experiment.

The radioactivity level of each source can be calculated with the fixation yield at the last sampling time and the radioactivity initially present in the RN binding medium.

$$A_{\text{sample}} = |Y_{\text{end}}| \% \times A_{\text{initial}} \times m_{\text{total}} \quad \text{Equation 20}$$

Only the samples with a high yield at the end of the RN binding experiment could be analyzed with autoradiography. The activity of the surfaces with a low fixation yield at the end of the experiment could not be used.

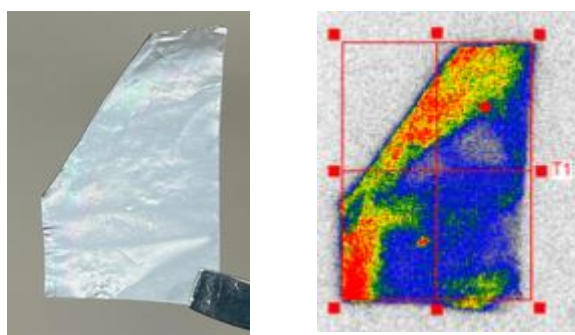
While "U" represents the uniformity of the source, "A_{end}" denotes the activity of the source at the conclusion of the immersion reaction. "A_s" signifies the surface activity of the source, also measured at the end of the immersion process. The scale bar that was added next to the autoradiography images signified the radioactivity level according to the value of the color of the signal. Red signifies high activity, blue shows the lower values, and grey is the background.

Both coated and grafted samples were imaged after the RN attachment step. Only the samples which had a meaningful radioactivity level are shown in the following autoradiography analysis.

2.2.2.1 Samples produced with grafting methods

2.2.2.1.1 Sulfonated (Si-SO₃) samples

One of the preliminary samples produced by Si-SO₃ grafting method is presented in Figure 107. The uniformity of the sources is around 70% and the radioactivity mostly accumulated at the edge of the sample.



U: (70 ± 10)%

A_{end}: (30 ± 27) Bq

Figure 107: Picture and autoradiography image of the sulfonated (Si-SO₃-20h) D10 sample immersed in ¹⁵²Eu solution

A series of analysis were conducted on sulfonated aluminum foils to study the intermediate precision of the process (denoted P series). Figure 108 displays autoradiography images of both sides of the sulfonated (Si-SO₃) 0.3 mm thick aluminum foil samples P1, P3, and P4.

The pictures of the samples show some white traces, still present after the RN binding immersion step. The photographs were deliberately taken at an angle to facilitate observation of the white traces on the samples.

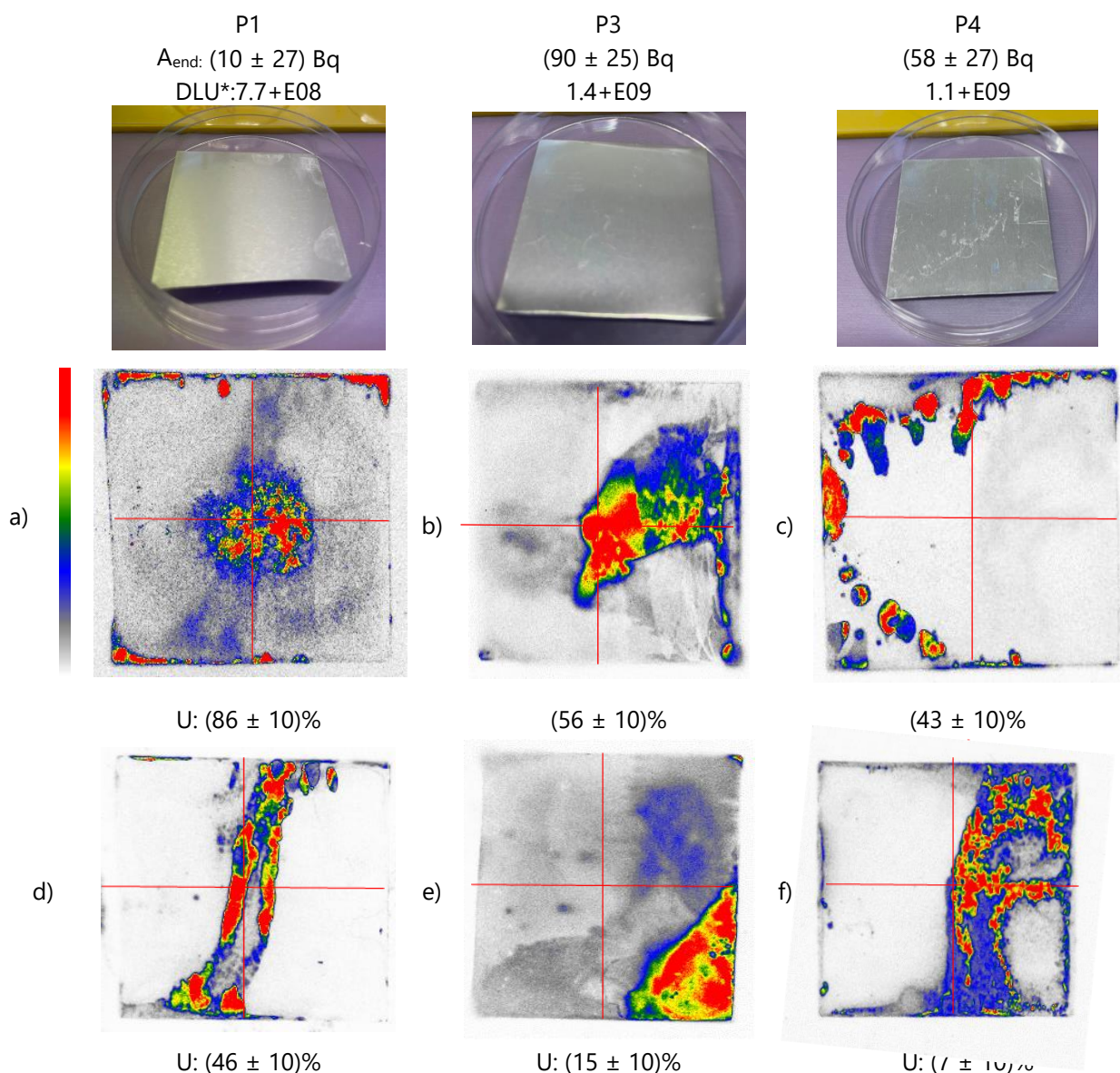


Figure 108: Pictures, autoradiography images, uniformity and activity of the sulfonated (Si-SO_3) samples immersed in ^{241}Am a) P1, b) P3, c) P4, d) Other side of P1 e) Other side of P3 f) Other side of P4. DLU*: Total digital light unit for the sample

The location of the white traces does not particularly match the RN distribution observed from the autoradiography images from either sides of the samples. Nevertheless, during the chemical characterization, binding functions were located in these white areas.

Initial observations indicated that the distribution of activity on the surfaces were not uniform. The two sides of each sample exhibited different RN distributions. Among these, the P1 sample achieved the highest uniformity on one side with a value of 86%, even though the sample is not that uniform but the activity is rather well distributed at the center.

The observed distribution of radioactivity suggested a correlation with the grafting process and where the chemical groups are attached onto the aluminum surface. It may be inferred that the grafted groups were not uniformly distributed across the surface and/or that the radionuclides did not uniformly cover the entire area. Consequently, it would be necessary to first improve the grafting step. For example, the use of an increased volume of the grafting solution could be explored, with the aim of achieving a more homogeneous distribution of the grafted groups over the entire surface of the source.

In Figure 108.a, a shadow can be seen, corresponding to the RN distribution from the other side of P1 sample (Figure 108.d). It is possible that the gamma emission from ^{241}Am can penetrate the Al thickness (0.3 mm) of the sample and deposit some of their energy on the phosphor screen. The percentage of the gamma photons that can pass through a thickness "e" of a material with a density ρ depends on the energy of the photon and on the total attenuation coefficient at this same energy (μ/ρ). The probability of interaction is one minus this percentage and is calculated according to Equation 23:

$$\text{Probability of interaction for gamma photons} = 1 - e^{-\frac{\mu}{\rho} \times \rho \times e} \quad \text{Equation 23}$$

Where μ/ρ represents the mass attenuation coefficient with units of $\text{MeV}/\text{cm}^2/\text{g}$, and ρ represents the density in g/cm^3 .

For example, in the case of ^{241}Am photons at approximately 59 keV, with μ/ρ equal to $0.284 \text{ MeV}/\text{cm}^2/\text{g}$, and the density of aluminum (ρ) being $2.7 \text{ g}/\text{cm}^3$, the probability of interaction in a 0.03 cm thick aluminum foil is calculated to be 2.3%. This implies that about 98% of the 59 keV gamma photons are left to interact with the phosphor screen placed on the opposite side of the aluminum foil.

Moreover, to attenuate 99% of the gamma radiation emitted by ^{241}Am , a thickness of 6.14 cm of aluminum foil is required. This value indicates that the thickness of the aluminum foil and the phosphor screen in the autoradiography imager is insufficient to completely block the gamma radiation. Consequently, it is expected to observe gamma emissions from both sides of the aluminum sample, leading to shadow effects in several images (Figure 108.a, c and e). These shadows typically appear in blue, indicating a relatively low signal, likely originating from gammas emitted on the opposite side of the aluminum foil.

Additionally, areas with higher signal intensity may stem from gamma emissions from both sides and/or alpha particles from the imaged side. The energy deposited by an alpha emission would likely produce a larger signal on the phosphor imaging screen compared to a gamma, as alphas transfer their energy more effectively.

The total Digital Light Unit (DLU) values from both sides of each sample show a correlation with the activity value from each sample: $P1 < P4 < P3$.

For future research aiming to produce sources with radionuclides attached only on one side, the gamma emissions from ^{241}Am can be imaged on the reverse side of the source, while another phosphor screen put in front of the activity would allow to image both the alpha and gamma emissions.

2.2.2.2 Coated samples

It was noted that the duration of immersion in the RN binding medium may have led to the removal of at least part of the surface coating for the samples produced by coating methods. Only the samples with enough activity at the end of the RN binding experiment can be imaged.

2.2.2.2.1 Autoradiography images of KMnO_4 treated samples

For the KMnO_4 treated samples immersed in a ^{152}Eu solution (H series), there is no remarkable presence of radioactivity seen on the autoradiography images. Indeed, the fixation yield was low at the end of the immersion in the RN solution; close to zero, as shown in Figure 103, and the detection limit of autoradiography may not be low enough.

An initial experiment with ^{241}Am using a KMnO_4 treated sample, known as J3 (0.27M-15min-50°C), is shown in Figure 109. In this case, only one side of the source was examined due to the thickness of the aluminum foil (initially 0.03 mm but far lower after all treatments). Also, the sample was so fragile that it could only be exposed once. The uniformity observed on this side reached 93%, which complies with the ISO 8769 standard in terms of uniformity for this 5 x 5 cm² sample (ISO 8769, 2020).

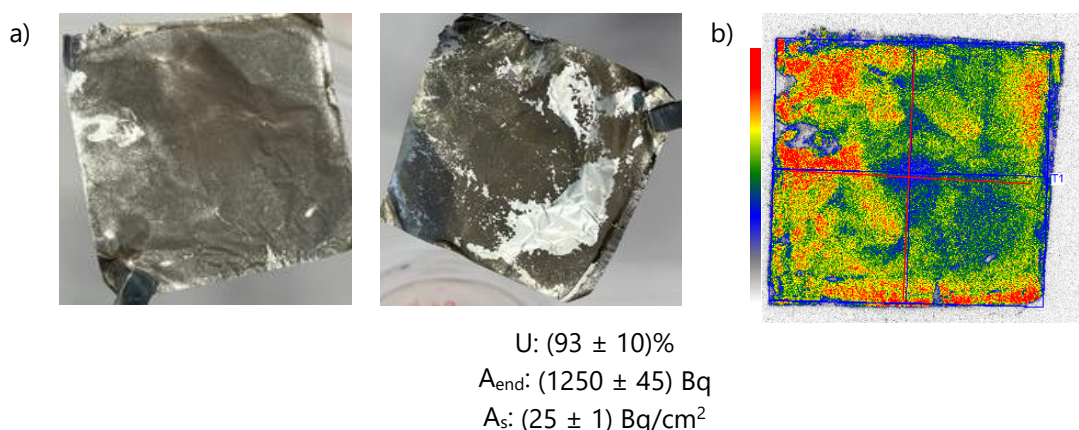


Figure 109: Pictures, autoradiography image, uniformity and activity of the KMnO_4 treated J3 sample immersed in ^{241}Am solution a) appearance of the sample after immersion in the RN solution from two sides, b) autoradiography.

The analysis of the sample image after being immersed in the RN binding medium shows a significant correlation between the emissions and the area with a brownish coating. However it can be noted that there is less activity at the center of the sample. This could be due to the domed bottom of the beaker and/or to the friction at this location during coating. This suggests that to obtain a uniform radioactive source, a uniform distribution of the brownish coating should be obtained first, which is visually practical to check.

The intermediate precision test conducted on the KMnO_4 treated samples from the Y series (0.28M-15min-50°C) showed variation within the samples, aligning with their radioactivity levels, calculated from the LSC analysis.

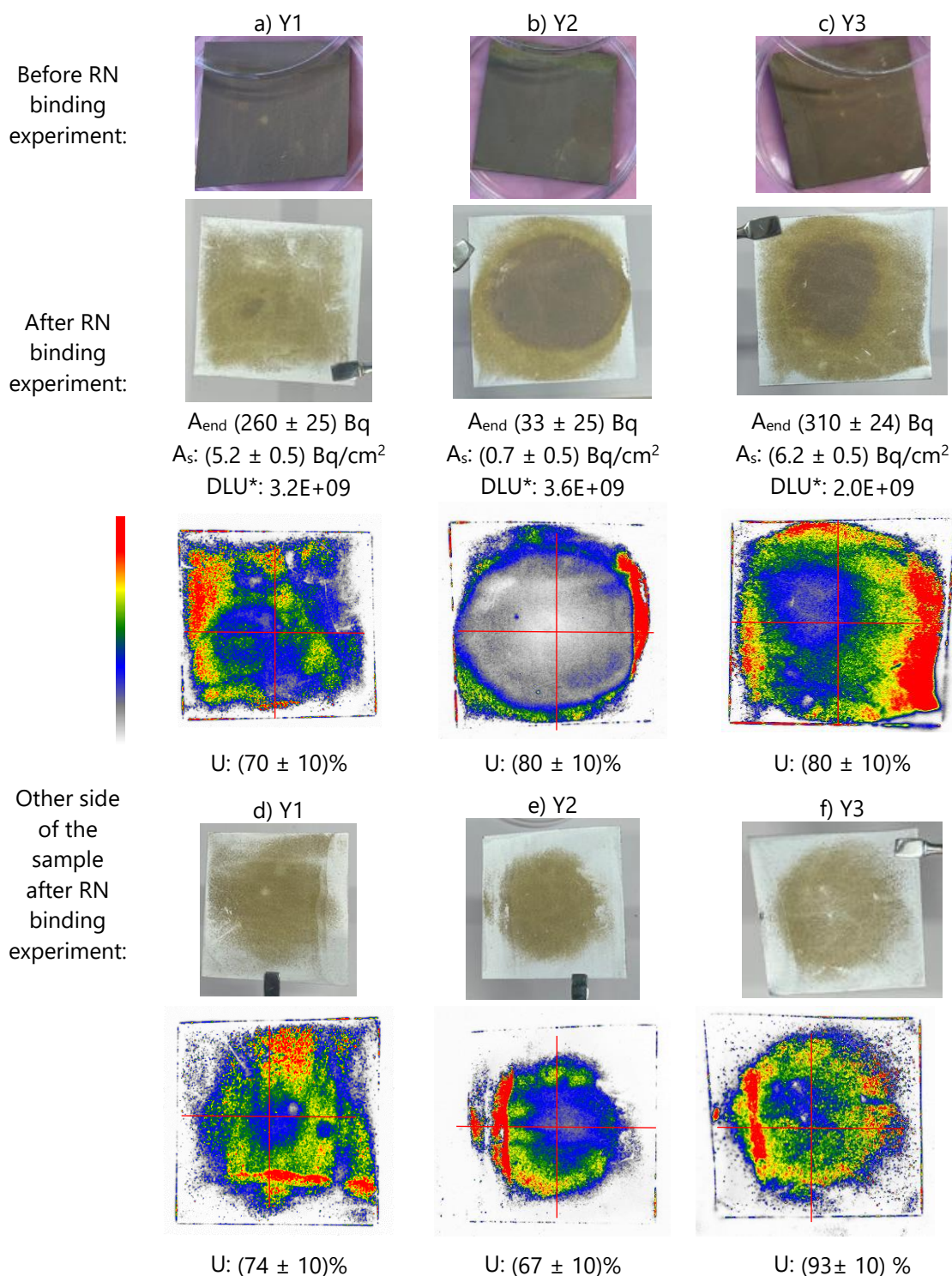


Figure 110: Pictures and two sided autoradiography images, uniformity and activity of the MnOx coated samples from Y series (0.28M-15min-50°C) with ^{241}Am a) Y1, b) Y2, c) Y3, d) Other side of Y1 e) Other side of Y2 f) Other side of Y3. DLU*: Total digital light unit for the sample

Again, a correlation is observed between the presence of the brownish manganese oxide coating, after the immersion in the RN binding medium and the locations of RN attachment (Figure 110). However, the edges of the samples appeared white after their immersion in the RN solution, suggesting that this immersion may lead to a partial removal of the coating, which in turn affects RN attachment. It can be noted that after the RN binding experiment, the areas with a dark brown color show less activity on autoradiography images. Also, it seems that red areas in the autoradiography images match locations where light brown coating is visible on the photographs. If this high signal is due to alpha emission interacting with the phosphor screen, this would indicate that these locations are coated with a layer thin enough to allow more alphas to emerge from the surface. Continuing this reasoning, if alpha particles cause more signal on the phosphor screen than gamma photons, areas with thick deposits of manganese oxide will not allow as many alpha particles to emerge, and this creates a bias in the total DLU signal measured by autoradiography. This bias could explain why the total DLUs do not correlate well with the activities calculated on the sources.

Among the Y series samples, Y3 exhibits the most uniform distribution of radioactivity, with uniformity values of 80% and 93% on either side. Y2 sample differentiated from the other samples with a lower uniformity, and this observation is in alignment with the results obtained from the LSC analysis. Y1 and Y3 exhibited a same similar uniformity on both sides.

In spite of the apparent loss of coating from samples Y1 and Y3, they still achieved to fix several hundreds of Bq. The significantly lower DLU value of Y2 implied that either it had less effective coating from the start of the experiment or it experienced a greater loss of coating, which is aligned with LSC analysis.

For further inquiry, sample Y3 (0.28M-15 min-50°C) from the Y series was compared with sample T1 (0.30M-15min-80°C), to assess the impact of the coating temperature and with sample R2 (0.30M-40min-80°C), to evaluate the influence of reaction duration in the KMnO_4 solution.

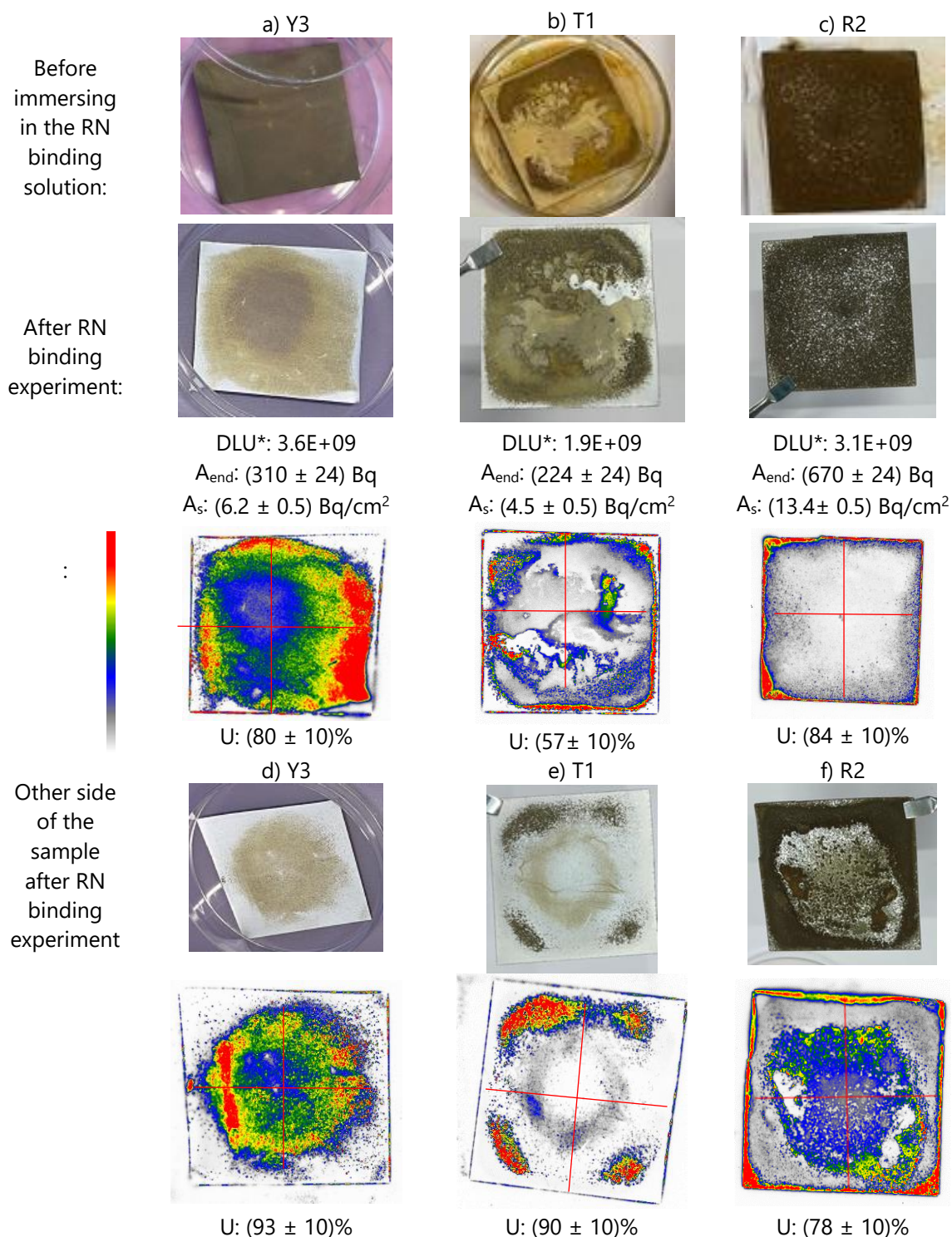


Figure 111: Pictures, two sided autoradiography images, uniformity and activity of the MnOx coated samples treated with ²⁴¹Am a) Y3 (0.28M-15 min-50°C), b) T1 (0.28M-15min-80°C), c) R2 (0.28M-40min-80°C), d) other side of Y3, f) other side of T1, e) other side of R2

When the temperature during coating was increased to 80 °C, to produce the T1 sample (0.28M-15min-80°C), the coating on the surface exhibited more roughness on some areas of the surface, as evidenced by the presence of small dots after RN binding reaction (Figure 111.b). These regions indicated a change in the physical properties of the coating under high temperatures. Comparing the pictures of the samples with the autoradiography images show that the activity is located in these regions.

For R2 sample (0.28M-40min-80°C), which was submitted to a longer coating duration at the same temperature, compared to T1 (0.28M-15min-80°C), the small dots covered most of the surface and seemed more evenly distributed (Figure 111.c). However, for this sample, the comparison of the pictures of the sample and the autoradiography images indicated that the activity was not located in all the coated areas, which is the opposite behavior of all the previous samples.

Additionally, for the R2 sample, the distributions of activity were different on the two sides. One face only had activity on the edges of the sample, while for the other, the activity was distributed both on the edges and at the center (Figure 111.c). There are several hypotheses that could explain this phenomenon. One possible explanation is the upper side of the sample had greater interaction with the coating solution, resulting in a thicker coating layer on that side. Another hypothesis could be that even though the coating was successful on both sides of the sample, the side that was at the bottom of the beaker during RN binding immersion may have been damaged by the friction caused by the agitation, resulting in a loss of RN fixation. These hypotheses highlight the complexity of the RN attachment process and the various factors that can influence it, including the orientation of the sample in the solution and the interaction between the coating and RNs. Further investigation is needed to fully understand this phenomenon.

The uniformity of samples T1 and R2 ranged between 56% and 90%, and were relatively large, even though the radionuclides were not that uniformly distributed. These high uniformity values only resulted from the symmetry of the radioactivity distribution. If more than four sub-areas were considered, the uniformity values would drop significantly.

Regarding the DLU values, T1 and Y3 seemed to be in the right order, but the DLU value for R2 was unexpectedly low. This could be due to the fact that for this sample, radioactivity was mostly distributed on the edges, which could result in an underestimation of the signal. Additionally, if ^{241}Am was located too deep in the coating, some of the emitted alpha particles would not reach the phosphor imaging screen.

Although autoradiography helped to understand where the activity attached, concluding on the effect of temperature or immersion duration during the coating step would need more experiments. So far, the results suggested complex interactions between temperature, coating properties, and radioactivity levels, necessitating a more detailed study to understand these relationships.

3 CONCLUSION OF CHAPTER 4

In this study, novel approaches were used to produce traceable surface sources for decommissioning purposes, using aluminum substrates of various thicknesses. The aluminum samples were modified using two main methods: grafting chemicals onto its surface and applying conversion coating techniques.

In the grafting studies, four chemicals were investigated for their ability to attach to the aluminum surface and to fix RNs. Silanol groups and phosphonic acids were used for grafting onto aluminum, while quaternary ammonium, phosphonic and sulfonic acids were employed for RN binding. The selected chemicals for this purpose included Si-N, Si-PO₃, PO₃-PO₃ and Si-SO₃ chosen based on literature review findings. Among all grafting methods explored, the Si-SO₃ grafting method stood out due to its remarkable fixation stability and reliability for up to 72 hours. However, most RNs detached from the surface after 48 hours. Si-SO₃ method was chosen among the grafting methods and the subsequent improvements led to fixation yields of 15% for ¹⁵²Eu and 65% for ²⁴¹Am. The comparison of sulfonated aluminum foils with those two RNs showed that ²⁴¹Am could attach to the modified aluminum surface more effectively than ¹⁵²Eu. Despite this, all fixated RNs eventually detached from the surface, indicating that the grafted sulfonic acid group might lack sufficient resistance to maintain grafting for extended periods in acidic solutions.

In terms of coating, two main methods were applied: manganese and chromium coating, under various pH and concentration conditions. The chromium coating was tested under acidic conditions, with two different coating durations. The longer duration gave better fixation yield of RN compared to the other sample. The manganese coating in basic conditions proved to be more effective, with higher fixation yields and better stability over time. Adjustments in temperature during coating were found to affect the roughness of the surface, suggesting that higher temperatures might improve coating properties.

The autoradiography analysis revealed different patterns on the surfaces, likely related to the coated surfaces. These patterns varied in uniformity from one side to the other, most of the time one side had more coating than the other, which impacted the RN fixation.

The images also indicated that before immersion in the acidic RN solution and afterward, the coating was removed. It seems that the coating close to the edges degraded first, which can be due to the agitation during radionuclide binding, causing the Al substrate to collide with the beaker walls.

Immersing the modified surfaces in an acidic solution, under agitation for several hours is definitely a tough step. To improve the RN binding step and prevent the destruction of the coating or functionalized layer, using a micro drop dispenser could be considered. This device is made of a robotic arm, which can dispense radioactive drops of a few microliters, regularly on the surface (every millimeter). Such small drops tend to dry in a few seconds, limiting the effect of the acidic solution on the surface.

In conclusion, among all the samples, the manganese oxide-coated samples under basic conditions showed the best results, with radioactivity levels ranging from 15 to 20 Bq/cm². Future studies should focus on refining grafting methods and coating conditions to enhance the stability and effectiveness of radionuclide fixation. The findings from this study offer valuable insights into developing more efficient and reliable surface sources for decommissioning purposes.

GENERAL CONCLUSION

Decommissioning and dismantling (D&D) of a nuclear facility is a time-consuming process that encompasses a characterization step where all the surfaces potentially contaminated need to be checked. This consists in identifying and locating areas where the radioactivity is above a limit. This is a challenging task especially when the activity is close to the background. The use of surface contamination monitors helps to provide some insights on these surface activities. Nevertheless, the way these devices are calibrated is not well suited for D&D needs. One of the many technical challenges is the need to measure radioactivity levels across diverse materials (e.g., concrete, metal, coating, etc.) of various shapes. This study aimed at providing a new approach to manufacture sources tailored for D&D by chemically attaching radionuclides to various substrates whose shapes can be complex.

In this study, a novel approach was proposed to produce traceable surface sources for decommissioning purposes by forming chemical bonds between the substrate and the chosen radionuclides (RNs). Three different substrates were used in the production methods, PET, epoxy and aluminum, which were chosen for their ability to mimic curved and/or rough surfaces, and are therefore closer to real D&D surfaces

PET and epoxy resin underwent similar chemical treatments, namely KMnO_4 treatment and sulfonation. For the PET samples, sulfonation was performed after two pre-treatment steps, hydrolysis and reduction, which enhanced the hydroxyl functions at the polymer chain ends. ATR-FTIR analysis confirmed the successful modification of the PET structure after hydrolysis, and LSC analysis showed that each treatment step progressively increased the fixation yield of the sources, with sulfonated samples reaching a maximum fixation yield of approximately 14%. KMnO_4 -treated samples, however, exhibited a higher fixation yield of 47%. The observed results might be attributed to manganese oxide (MnOx) coating on the PET surface potentially combined with surface oxidation, though the precise mechanism remains to be clarified. Autoradiography of KMnO_4 -treated PET samples revealed a surface coating correlated with the attached RNs, supporting the MnOx coating hypothesis. However, uniformity values for these samples were around 20%, in contrast to the sulfonated samples, which demonstrated a higher uniformity of approximately 40%. The KMnO_4 treated sample (H5) was identified as the most effective among all PET sources.

Epoxy resin samples underwent a KMnO_4 treatment and subsequent sulfonation with 1,4-butane sultone. ATR-FTIR analysis indicated successful surface modifications in both treatments. Additionally, MnOx presence was noted in the FTIR analysis, implying that a manganese oxide coating was formed following KMnO_4 oxidation on epoxy surfaces. Oxidized samples yielded higher fixation rates for both ^{152}Eu and ^{241}Am compared to sulfonated samples. The best-oxidized epoxy sample (F2) immersed in ^{152}Eu solution achieved approximately 100% fixation yield with a radioactivity level of 860 Bq. In contrast, the best sulfonated sample (F3) showed a fixation yield of approximately 85% with a maximum activity of 785 Bq. The uniformity of the ^{152}Eu sources for F2 reached 82%, while for F3, it was about 80%. For ^{241}Am -treated samples, consistent results were observed with higher fixation yields of around 100% for oxidized samples, and approximately 92% for the best sulfonated sample (L3). Oxidized samples exhibited uniformity values of around 90%,

General conclusion

while sulfonated samples reached 85%. The reason behind the higher fixation yield of the oxidized samples might be related with the the fact that MnO_x coating has a higher affinity than the sulfonic acid groups on the sulfonated samples.

In summary, the optimal parameters for KMnO₄ treatment (0.36M, 60 minutes, 80°C) and sulfonation were successfully determined (using twice the molar ratio of 1,4-butane sultone in ACN for 3 hours at 70°C, followed by 16 hours at 22°C).

Generally, modified epoxy resins were able to fix more radioactivity than their PET counterparts. As epoxy resin has 3D cross-linked network structure, pores can be formed more easily than on sheets of PET. The higher surface roughness of epoxy resins significantly increases the number of functional groups that can bind RNs, allowing more activity uptake. However, this roughness can also affect the emission of alpha particles from the produced source. The investigation of this aspect may be a valuable perspective for the coming studies.

Two main surface modification methods were employed on aluminum samples: grafting and coating. The grafting studies involved four chemicals, which could attach to the surface on one end and bind to RNs on the other end. Alkoxysilane groups and phosphonic acids were used for grafting on aluminum, while quaternary ammonium, phosphonic acid, and sulfonic acid were used for RN binding. Coating methods were performed by ranging the broad pH conditions from 1 to 13, to obtain manganese oxide coating which possesses the capability to bind RNs. Alternatively, the second coating method was applied onto aluminum substrate to obtain chromium coating.

Among all methods, the Si-SO₃ grafting method stood out for its stability and reliability up to 72 hours in an acidic solution. For this reason, the focus was given on this grafting method and an optimization was carried out. The best conditions were found to be 20 h of grafting reaction. The fixation yield for ¹⁵²Eu was about 15%, while for ²⁴¹Am, it reached 65% at maximum. Additionally, with ²⁴¹Am, the intermediate precision was successfully achieved after up to 4 hours of immersion in the RN solution. Nevertheless, by the end of the study, all fixated RNs had detached from the surface, and the fixation yield dropped close to zero. This indicated that the grafted sulfonic acid group might lack the stability to maintain the grafted molecules on the surface for 48 hours. Considering this behavior, future studies could limit the immersion in the RN binding medium to 4 hours. Various patterns were observed on both sides of the surfaces by direct observation. For autoradiography, the uniformity levels varied from one side to the other, but both sides exhibited radioactivity. Further research should focus on optimizing the grafting process and exploring alternatives to enhance the stability of RN attachment on aluminum surfaces.

Chromium oxide coating on the surface was obtained in acidic conditions and was explored as an alternative to manganese oxide coatings. The study showed that the duration of the coating process significantly affect the outcome. Longer coating durations, up to 8 hours, provided better stability.

Within the literature, manganese oxide coatings were also formed in acidic conditions. However, this study showed that samples treated under acidic conditions exhibited lower fixation yields and lower stability compared to the samples submitted to a basic KMnO₄ treatment. The most

General conclusion

successful sample was I5, which reached a maximum fixation yield of about 11% after 4 hours. This sample was treated at pH 7 using a coating solution with 0.02 M KMnO_4 for 24 hours, at room temperature (22°C).

In the case of manganese oxide coating under basic conditions, the primary results were achieved under more basic conditions, around pH 13, with an immersion duration of 60 minutes at 50°C for the H3 sample, yielding around 7% fixation for the Eu solution. After RN binding experiment, it was observed that the coating had a tendency to get removed in acidic conditions. For this reason, the experimental conditions were improved by changing parameters such as reaction duration and temperature of the reaction.

Some intermediate precision tests were performed for three different conditions by producing three samples from each method: 15 minutes at 50°C (Y series), 15 minutes at 80°C (T series), and finally 40 minutes at 80°C (R series). Among these, the best conditions were found to be 40 minutes at 80°C with the R2 sample with 77% of RN fixation yield. It was observed that maintaining a lower temperature during the coating process might lead to the loss of the coating after 4 hours (Y series). In contrast, higher temperatures appeared to enhance the coating properties and increase the success of the coating on the aluminum sample. Notably, extending the coating duration significantly improved the fixation yield, nearly doubling it (R2 (78%) compared to T1 (32%)) in the ^{241}Am solution.

For most samples, autoradiography analysis showed a clear correlation between the coated surface (visible as a brownish coating) and the emitted particles in the images. It was evident that the coating started to deteriorate at the edges, depending on the duration in the RN binding solution. The uniformity values for the Y series were around 80%. From the Y to the T series, uniformity dropped to around 60%, with a noticeable central pattern appearing, possibly reflecting the shape of the bottom of the crystallizer used during the coating process. The T1 sample, compared with R2, showed that a longer immersion duration in the coating solution improved the uniformity of the source up to 85%. However, while one side of the source had better coating, the other did not fix RNs.

Among these samples, the best results were obtained with the manganese oxide coated J3 (0.27M-15min-50°C), and R2 (0.28M-40min-80°C), samples under the basic conditions. The surface sources obtained had radioactivity levels ranging from 15 to 20 Bq/cm^2 .

These radioactivity levels can be easily tuned to obtain lower activities for the needs of D&D. With lower activities, the fixation yield for some surfaces might be enhanced but there is still the need to achieve a uniform distribution of the surface modifications in order to obtain a uniform radioactive source in the end.

In this study, efforts were directed towards producing traceable surface sources using two distinct substrates: polymeric structures and aluminum foil. Some improvements can be considered for future studies.

A critical aspect, as stated in ISO 8769, is that the reference sources should only one radioactive side (ISO 8769, 2020). This objective presents a promising direction for future research. Achieving

General conclusion

this could involve refining the production methods to facilitate RN attachment exclusively on one side of the source. This approach entails modifying only a specific side of the substrate, ensuring that RNs adhere only to this targeted area. To facilitate this process, the design and use of specialized reaction cells can be considered, similarly to the one described in a study performed at LNHB (Tsoumpko-Sitnikov et al., 2002). Such a strategy not only aligns with the standards set by ISO 8769 but also potentially simplifies the handling and application of these sources. Furthermore, by controlling the area where the modifications can be applied on a surface, it would be possible to produce purposefully non uniform sources if a hot spot is needed for example.

For RN binding, the production of pure alpha emitter sources, for example using ^{244}Cm , could be performed. This would provide a more comprehensive understanding of the binding mechanisms and the efficiency of various treatments in retaining specific types of radionuclides. It must also be recalled that the methodologies developed in this study can be applied to any element with a stable trivalent state, which covers at least all lanthanides, and most of the actinides.

In the case of epoxy samples, autoradiography images revealed a correlation between blackish areas and RN fixation locations, suggesting that improvements in the oxidation process could enhance RN fixation yields. Therefore, for polymeric sources, extending the reaction duration might improve surface coverage, potentially leading to increased porosity and a higher number of functional groups available for RN fixation. This porosity will need to be controlled if alpha emitters are to be fixed onto such sources.

An open question is whether the success of sulfonation is only due to the oxidation process or if there is a significant contribution of the sulfonic acid groups. Preliminary X-ray Photoelectron Spectroscopy (XPS) analysis could allow to identify what element is bound to the surfaces and their interactions. This analysis could clarify the differences between oxidation and sulfonation in terms of chemical bonding, allowing to understand the underlying mechanisms of KMnO_4 treatment and of the following step, sulfonation.

Another advantage of using epoxy resin as a substrate is its ability to incorporate solid fillers. In another study at LNHB, tests have been carried out to incorporate a high proportion of sand into this resin, while maintaining the cohesion of the grains thanks to the resin. Proportions of the order of 70% of relatively fine sand were successfully incorporated, making the surface naturally rough and more representative of concrete, for example. Successfully functionalizing the surface of such substrates to fix radioactivity would be an interesting step towards the production of custom sources for decommissioning.

APPENDICES

1 CHEMICAL CHARACTERIZATION METHODS

1.1 FOURIER TRANSFORM INFRARED SPECTROSCOPY

Infrared spectroscopy includes several techniques: mid-infrared (IR), near-IR, and Raman spectroscopy. For this study, our focus was the mid-IR section. Mid-IR spectroscopy offers characteristic fundamental vibrations that are employed for the elucidation of molecular structure.

Infrared spectroscopy involves the study of the interaction of radiation with molecular vibrations. IR measures transitions between molecular vibrational energy levels as a result of the absorption mid-IR radiation (Larkin, 2018b).

The IR vibrational bands are characterized by their frequency (energy), intensity (polar character or polarizability), and band shape. Since the vibrational energy levels are unique to each molecule, the IR spectrum provides a “fingerprint” of a particular molecule. The frequencies of these molecular vibrations depend on the masses of the atoms, their geometric arrangement, and the strength of their chemical bonds. In conclusion, the spectra provide valuable insights into the molecular structure, dynamics, and environmental characteristics. The main vibrational regions can be seen in Figure 112.

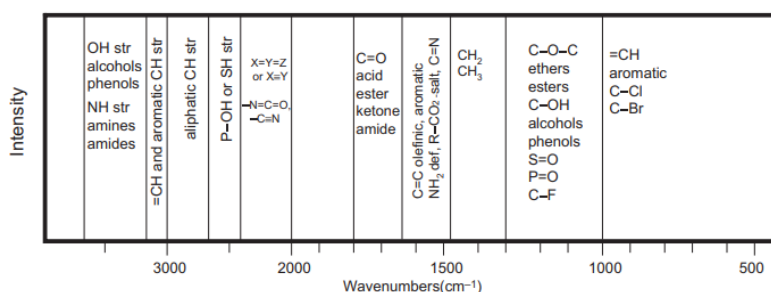


Figure 112: The fundamental vibrational regions with some characteristic group frequencies. The IR spectrum is obtained by plotting the intensity (in terms of absorbance or transmittance) versus the wavenumber, which is proportional to the energy differences between the ground and the excited vibrational states.

The radiation frequency and the molecular dipole moment are two important components of the IR absorption process. The IR absorption process involves the energy absorption by the molecule if the vibration causes a change in the dipole moment, resulting in a difference in the vibrational energy level, as seen in Figure 113.

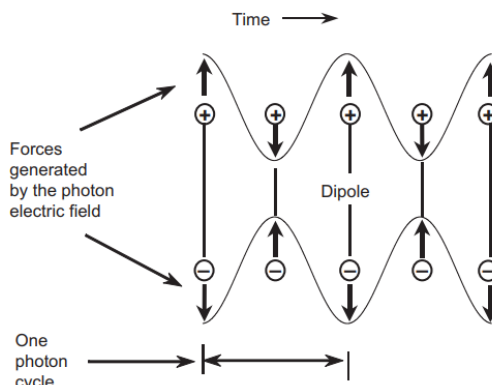


Figure 113: The oscillating electric field of the photon generates oscillating, oppositely directed forces on the positive and negative charges of the molecular dipole.

Two commonly used FTIR techniques are ATR (attenuated total reflection or internal reflection) and DRIFTS (diffuse reflectance FTIR spectroscopy). ATR technique is used to measure the IR spectra of surfaces of the materials that are too thick or strongly absorbing to be analyzed by more traditional transmission methods, which was preferred in this analysis.

The angle of incidence must be greater than the critical angle so that total internal reflectance occurs as shown in Figure 114.

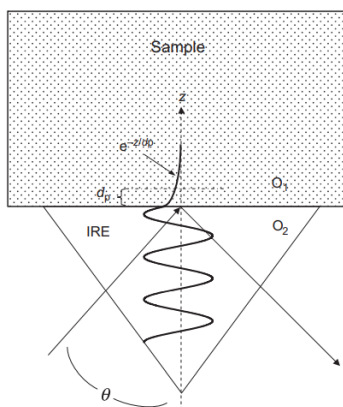


Figure 114: The diagram of a single reflection ATR crystal depicting the basic principles of the technique

The measurement was conducted using the Attenuated Total Reflectance (ATR) technique, a contact sampling method that employs a crystal with a high refractive index and IR transmitting properties. ATR always requires excellent contact between the sample and the crystal and, therefore, is a perfect method for deformed solids, liquids, or soft materials.

Quantitative analysis with FTIR requires comparing standards of known concentration and test samples. The resulting calibration plot reflects the relationship between the measured quantity and the analyte concentration. In our study, we will use this device for qualitative analysis.

1.2 SCANNING ELECTRON MICROSCOPY ANALYSES

The primary function of a scanning electron microscope is to enlarge small features or objects by scanning an electron beam of high energy on the sample surface. The SEM is, therefore, a tool used for materials characterization that provides information about the surface or near-surface structure, composition, and defects in bulk materials.

By virtue of their smaller wavelength, electrons can resolve finer features of materials to a much greater extent than optical light.

While human eye resolution is equal to 200 μm , a light microscope can typically magnify images up to 1000x to resolve the details down to 0.2 μm . Resolution in the device is defined as the smallest distinguishable distance separating two objects, i.e., minimum resolvable distance (Ul-Hamid, 2018). For a scanning electron microscope, useful magnification is typically 200,000x.

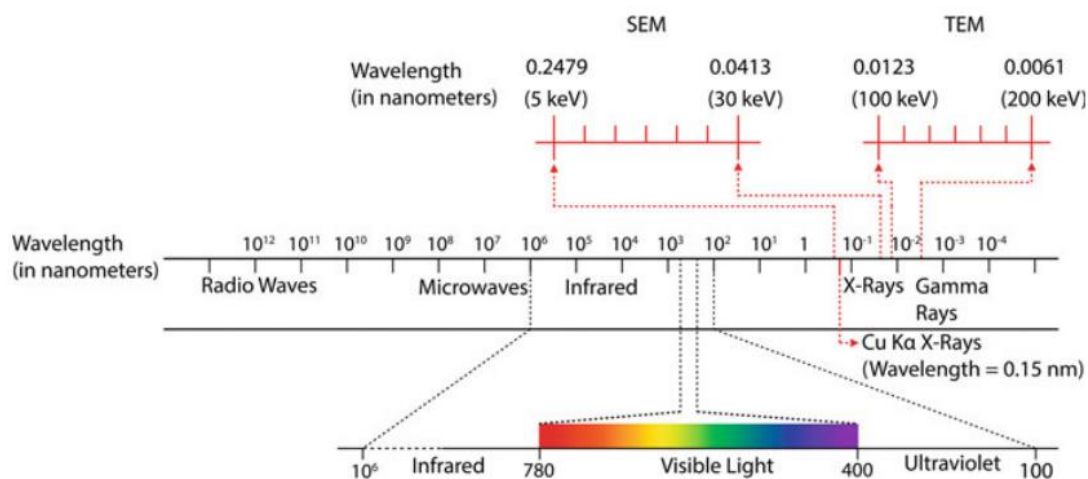


Figure 115: Electromagnetic spectrum showing the size of the wavelength used in the light, scanning electron microscope (SEM) and transmission electron microscope (TEM)(Ul-Hamid, 2018)

The SEM instrument comprises three major sections: the electron column, the specimen chamber, and the computer/electronic controls. The gun, the column, and the specimen chamber are kept under vacuum to allow electron beam generation. The electrons in the beam penetrate a few microns into the surface of a bulk sample, interact with its atoms, and generate a variety of signals such as secondary and backscattered electrons and characteristic x-rays that are collected and processed to obtain images.

When an electron beam hits and penetrates a specimen, the specimen deflects it in an elastic scattering or inelastic scattering mode. This results in generating a variety of signals, including secondary electrons, backscattered electrons, Auger electrons, etc.

The extent of each type of scattering depends on the beam energy, the atomic number of the target, and the degree of tilt used. Elastically scattered beam electrons are deflected through

large angles and eventually find their way out of the specimen, giving rise to back scattering. These electrons are called backscattered electrons (BSE), and they originally belong to the incident electron beam that strikes the surface of the specimen. Once out in the vacuum, these electrons can be captured by a detector and used to form a backscattered electron image.

2 RADIOLOGICAL CHARACTERIZATION METHODS

2.1 LIQUID SCINTILLATION COUNTING (LSC)

2.1.1 Principles of LSC

Liquid scintillation counting is a radiometric method used for measuring mostly alpha and beta-emitting RNs. This method relies on the radiation-induced formation of light and its subsequent transformation into electric pulses. The process involves mixing a liquid scintillation cocktail consisting of an organic solvent and scintillating agents with the RN-containing solution.

Liquid scintillation cocktails absorb the energy emitted by radioisotopes and re-emit it as flashes of light, to accomplish two actions, absorption and re-emission, cocktails contain at least two basic components, the solvent and the phosphor. The solvent carries out the bulk energy absorption. Dissolved in the solvent, phosphor molecules convert the absorbed energy into light. The solvent and the phosphor provide the scintillation of the mixture.

In liquid scintillation counting (LSC), the solvent is a critical component, comprising 60 to 99% of the total solution. Its primary role is to efficiently capture energy from a radioisotope undergoing decay. Since it's highly likely that an emitted particle or ray will interact predominantly with solvent molecules before its energy is depleted, the solvent needs to be adapted to collecting this energy and transferring it to the phosphor molecules without losing it through other mechanisms. It's also essential for the solvent not to quench the phosphor's scintillation and to dissolve the phosphor effectively, ensuring a stable solution.

Aromatic organic compounds have been found to be the most effective solvents for LSC. Toluene, for example, is a prototypical solvent used in this context, although safer and less toxic alternatives are now preferred in many applications. The π cloud in the aromatic ring structure of toluene acts as a target for β -particle interaction, capturing the particle's energy. This energy is typically transferred to other solvent molecules, as toluene itself has a minimal tendency to emit light or undergo other decay processes. As a result, a β -particle traveling through a toluene solution leaves behind several energized toluene molecules. The energy from these molecules is then efficiently passed among the solvent's ring systems, facilitating its capture by the dissolved phosphors.

As a β particle travels through a scintillation cocktail, it creates a sequence of energized solvent molecules in its path. These excited molecules then transfer their energy to the scintillator molecules within the cocktail. On receiving energy, each scintillator molecule emits a single

photon. The wavelength of this photon is specific to the scintillator type and does not depend on the β particle. A single β particle can activate multiple scintillator molecules, leading to the emission of several photons.

In a scintillation counter, each pulse of photons is categorized based on the number of photons it contains, which is directly related to the energy of the corresponding β emission event. These pulses are organized into distinct channels, with each channel representing a specific range of β particle energies. These channels, often referred to as counting windows, record the counts per minute (CPM) for emissions within their designated energy range. Pulses with energies outside a channel's defined limits are excluded from that channel. Typically, three channels are used to categorize the energy spectrum of emissions into low, medium, and high energy ranges. For instance, the lowest channel is set to detect the energy range of tritium (^3H) emissions, while the highest is tailored for phosphorus-32 (^{32}P) emissions.

After collecting and collating the counts, researchers gain insights into two crucial aspects: the intensity of radiation, expressed in CPM, and its energy distribution or spectrum. CPM is indicative of the isotope's quantity in the sample, while the spectrum helps in identifying the isotope.

While LSC is particularly suited for beta measurements, its use for alpha measurements is feasible, albeit with lower resolution. Many LS counters can simultaneously measure beta and alpha spectra from the same sample due to the distinct electric pulse discrimination capabilities arising from the differing pulse shapes of the emitted radiations.

In an ideal scenario, a scintillation cocktail would capture and convert all the energy from each β particle into light. This would allow for a direct interpretation of the β energy spectrum and disintegration per minute (DPM) values from the data. The highest energy emissions could be compared against the maximum emission energies (E_{max}) of known radioisotopes for isotope identification. However, in reality, scintillation cocktails are not 100% efficient in energy capture and conversion, particularly for lower energy β emissions. This inefficiency introduces complexities in data interpretation, requiring more nuanced analysis to deduce accurate results.

The path of a β particle in a scintillation cocktail is typically lower than 1 cm, and its half-life is relatively short. This means that the photons generated during an emission event are emitted from a compact area and almost simultaneously. This simultaneity allows the photomultiplier tube to detect them as a single pulse of light.

The results lie in the determination of the counting rate (in counts per second), derived from the transformation of observed energy from particles or emissions within the source into electric pulses within the detector. When the instrument counting efficiency is established, i.e. calibration is performed, for a specific RN and in fixed sample preparation conditions, this counting rate can be converted into the activity of the sample in Becquerel.

2.1.2 Normalization of LSC measurements

The preparation of liquid scintillation sources for the RN part is performed by the pycnometer weighing method to lower the uncertainties. During the immersion of the surfaces into the RN solution, all constituent were weighed (beaker, water, HCl, and the RN amount is known through the pycnometer method). To prevent evaporation during the agitating part of the RN binding experiment, the beaker were covered with parafilm®.

Where A_{beaker} represents the radioactivity level of the reaction beaker, the mass activity of the stock solution used for the RN binding experiment is multiplied by the mass of RN (m_{RN}) and then divided by the total mass of the prepared solution, comprising water, HCl acid, and the RN solution.

$$A_{\text{beaker}} = (A_m \times m_{\text{RN}}) / m_{\text{total}} \quad \text{Equation Appendix 1}$$

Where the number of moles of atoms in solution is denoted as n_{RN} , it can be calculated from the activity of the stock solution using the half-life from the RNs. In the case of ^{152}Eu , the solution contained stable isotopes that acting as carriers.

$$n_{\text{RN}} = (A_m \times t_{\text{half-life}} / \ln(2)) / \mathcal{N} \quad \text{Equation Appendix 2}$$

The counts per minute (CPM) were obtained from the LSC devices for each sampling, along with one reference for each set of experiment. This standardizes all samples according to its value, using the reference point of the RN binding experiments. These reference samples were prepared under the same conditions as other samples, without immersing any surface in them.

During the preparation of the LSC samples, an empty vial was filled with 10 mL of the chosen cocktail solution. From each beaker of interest, 1 mL of the RN solution was taken using a micropipette. The LSC glass vial was weighed before and after the addition of 1 mL of RN binding solution, and the difference determined the exact amount of RN solution added into the glass vial.

Where the CPM values from the LSC samples were correcting from the background using a blank sample. This samples were prepared using the Eu carrier solution for ^{152}Eu samples, or using only the acid in the case of ^{241}Am . The sample CPM value was subtracted from the background sample cpm value, then divided by the activity within the beaker of interest (for the sample immersed or not, in the case of the reference sample).

$$\text{Net CPM} = (\text{Gross CPM}_{\text{sample}} - \text{CPM}_{\text{background}}) \quad \text{Equation Appendix 3}$$

These values were then converted to counts/s/g. The net CPM value was divided by 60 (to convert minutes to seconds) and then divided by the mass of the solution added by the pipette for the preparation of the LSC source.

$$\text{Counts/s/g} = (\text{Net CPM} / 60) / \text{Mass of solution} \quad \text{Equation Appendix 4}$$

During the RN binding experiment, the evaporation was controlled and checked by regular weighing of the beakers.

$$\text{Evaporation percentage} = (\text{Initial mass} - \text{Final mass}) / \text{Initial mass} \quad \text{Equation Appendix 5}$$

During the preparation of each beaker, the duration between the sample immersion and the first sampling was kept constant for all samples.

2.1.3 Uncertainty calculation for LSC analysis

The uncertainty calculation for Liquid Scintillation Counting analysis follows the ISO/IEC Guide 98-1:2024 standard, also known as the GUM (Guide to the expression of Uncertainty in Measurement), which involves the application of the law of propagation of uncertainty (ISO/IEC Guide 98-1, 2024).

Where the normalized count rate defined as N , which represents the counts per second normalized by the activity in the LSC sample. It is calculated as:

$$N = \frac{CPS_{norm}}{m_{sample}} = \frac{R_{net}}{A_0 * m_{sample} * m_{sample}} \quad \text{Equation Appendix 6}$$

$$N = \text{counts per s per g normalised by the activity in the LSC sample} \quad \text{Equation Appendix 7}$$

$$R_{net} = R - R_0 \quad \text{Equation Appendix 8}$$

Here, CPS_{norm} denotes the normalized count rate, m_{sample} represents the mass of the sample, R_{net} is the net count rate (difference between total count rate R and background count rate R_0), and A_0 is the mass activity per beaker, calculated from the activity (A_{stock}) of the stock solution, the mass (m_{stock}) of solution, and the mass of the beaker (m_{beaker}).

$$A_0 = \frac{A_{stock} * m_{stock}}{m_{beaker}} \quad \text{Equation Appendix 9}$$

The fixation yield is then determined as the difference between the normalized count rates of the sample (N_{sample}) and the reference (N_{ref}) normalized by the reference count rate.

$$\text{Fixation yield} = \frac{N_{sample} - N_{ref}}{N_{ref}} \quad \text{Equation Appendix 10}$$

$$\frac{u(N)}{N} = \sqrt{\left(\frac{u(R_{net})}{R_{net}}\right)^2 + \left(\frac{u(A_0)}{A_0}\right)^2 + 2 * \left(\frac{u(m_{sample})}{m_{sample}}\right)^2} \quad \text{Equation Appendix 11}$$

Table 41: Standard uncertainty budget for LSC measurements

Uncertainty components	u_{rel} (normalized count rates)
Counting time (t kept constant)	0,01% negligible
Sample mass	0,06% negligible
Mass activity (per beaker)	0,4%
Counts or count rates	0,5%-5%
Detection efficiency variation (quenching, chemical stability/sampling, instrument stability)	2% (conservative)
Relative combined uncertainty	2%-6%

The relative combined standard uncertainty u_{rel} of the normalized count rates is calculated using the law of propagation of uncertainty. It accounts for various components, included in Table 41: . Counting time, usually maintained constant during measurements, generally introduces a negligible uncertainty contribution. Similarly, the uncertainty stemming from the sample mass is typically negligible. The uncertainty associated with the mass activity per beaker (A_0) is assessed by considering several factors. This uncertainty $\left(\frac{u(A_0)}{A_0}\right)$ is influenced by the uncertainties in the activity of the stock solution $u(A_{stock\ solution})$, mass of the stock solution $u(m_{stock\ solution})$, and the mass of the beaker $u(m_{beaker})$. Counts or count rates obtained from measurements can exhibit uncertainties ranging from 0.5% to 5%, depending on the activity measured. Detection efficiency variation, attributable to phenomena such as quenching, chemical stability/sampling, and instrument stability, typically contributes a 2% uncertainty, considered conservative. The relative combined uncertainty (u_{rel}) is expressed as a percentage and typically falls within the range of 2% to 6%.

2.2 PHOSPHOR AUTORADIOGRAPHY IMAGING

2.2.1 Principle

Autoradiography is a technique used to visualize the spatial distribution of radioactive substances in a sample (biological or non-organic). It involves the exposure of photographic film or a detector sensitive to ionizing radiations emitted by the radioactive isotopes incorporated in this sample. Radioactive isotopes emit particles (β or α) and sometimes radiation (γ or X) which interact reversibly or not with a constituent of the film or detector, producing an emission image of the radioactive substance in the sample.



Figure 116: Placing of an autoradiography plate in the device

This technique using the luminescent imaging plate is based on the interaction of particles with a photo-stimulable luminescent screen containing a fine coating of photostimulable phosphors (BaFX: Eu^{2+} , X=Cl, Br or I) that can detect and store ionizing radiation (Kanehal et al., 1995). A photo-stimulable phosphor layer containing micrometric phosphor particles with traces of bivalent europium ions is located between a protective layer and a plastic support (Sardini et al., 2015). Radiations emitted from the sources provoke the excitation of ground state Eu^{2+} to metastable state Eu^{3+} , which releases electrons into the conduction band of the luminescent crystals. These electrons are then trapped in the bromine vacancies. Laser reading stimulates the emission of photons proportional to the number of electrons trapped in the conduction band of the phosphor crystals. Once the image is obtained, the film is exposed to intense white light to return to the ground state, that is, reduce Eu^{3+} to Eu^{2+} . Thus, the screen loses the information previously stored and becomes reusable for another exposure.

In phosphor imaging, a storage phosphor screen captures the energy from the radioactive material. The storage screen contains a thin layer of crystals that absorb and store energy emitted by radioactive material. The storage screen is exposed to a radioactive sample.

Accumulated energy is released as luminescence upon excitation of the phosphors by a laser beam. The released luminescence is digitized for quantitative spatial reproduction of the radioactive specimen. The luminescence intensity from the imaging plate is proportional to the intensity of original radiation. The device has an imaging plate eraser to ensure quick and complete erasure of imaging screens to maximize data and image quality.

There are several types of films whose compositions differ to favor sensitivity or resolution, or a compromise of both. At the level of the emulsion, the fineness of the grains conditions the resolution, and their quantity determines the sensitivity [1]. Knowing that we know the emission properties of the radionuclides, it is then possible to discriminate the known energy emitted particles that we wish to study. Generally, the assembly is as follows: a plastic support topped with an emulsion layer (thickness of $5\ \mu\text{m}$) covered by a protective layer (Bourrel and Courrière, 2003). This corresponds to the "Multipurpose Standard (MS) screens" and "Super Resolution (SR) screens" held by the LNHB (GE Health Care, 2018). Other films like TR (from Perkin Elmer) are more suited to let through low-energy radiations since they do not have this protective layer.

Consequently, the TR film is ideal for detecting β particles of Tritium (average energy of 6 keV) (Haudebourg and Fichet, 2016). This is also valid for studying α particles which have a very short path in matter. However, TR films tend to be more sensitive to emissions contributing to background noise and penetrating radiations (γ) (Haudebourg and Fichet, 2016). Therefore, they are more fragile and have a shorter lifespan.

The device available at LNHB-MA for autoradiography, named "Amersham™ Typhoon™ Biomolecular Imager," was designed by GE Healthcare. Its primary use concerns molecular biology work (observation of proteins, enzymes). Thus, it has other operating modes, such as Optical Density (OD), Near-Infrared (NIR) fluorescence, and RGB fluorescence ("Amersham™ Typhoon™ Catalogs," 2018)

In the case of this study the so-called IP (for Phosphor Imaging) configuration that can perform the reading of the radioluminescent film. This is done with a 635 nm red laser, as this is the optimal wavelength for releasing electrons from the film. This results in emitting a number of photons proportional to the radiation received by the pixel read on the film. The software offers two file extensions:

$$.tif \text{ formula } pixel(DLU) = linout \times \frac{65,534}{\max(linout)} \quad \text{Equation Appendix 12}$$

$$.gel \text{ formula } pixel(DLU) = 65\,535 \times \sqrt{\frac{linout}{100\,000}} \quad \text{Equation Appendix 13}$$

Where pixel (DLU) represents the pixel value corresponding to the Digital Light Unit. In these formulas, "linout" represents the reading point of the scanners on the film (unitless). The gel format is preferred during the analysis.

This imager is provided with an "Eraser" giving the possibility to reset the film after each use. This device allows exposing the film under bright white light for a sufficient duration to reduce Eu^{3+} ions to Eu^{2+} . The erasing time of this device can extend up to 30 minutes maximum. The necessary resetting time changes depending on several factors ("Cyclone Plus Storage Phosphor System," 2011). These are listed the energy of the particle emitted by the isotope, the exposure duration, and the intensity of the white light.

Generally, during the experiments conducted, the film was erased for about ten minutes after each exposure. It is also preferable to erase a film before the next exposure. The film being very sensitive, background noise sets in quickly depending on the radiological and light ambiance of the room in which it is located.

Regarding image analysis, two software programs can be used. The first, "ImageQuant," is directly provided with the Amersham™ Typhoon™ imager. It works with both image formats (.gel and .tif) and is particularly useful for showing the radioactivity distribution of the sources. It gives statistical values of the image (median, mean, standard deviation) in intensity per pixel. However, the major disadvantage of this software lies in the use of the "grid" tool. Indeed, when we want to manually trace a matrix to study the uniformity of the source, it is not possible to rotate it to align it correctly

with the source. Therefore, in the analysis of the images the "OptiQuant" software is preferred. OptiQuant provides values in light intensity DLU. It allows entering the exact dimensions (in mm) of the cells and adding an angle. As a result, we can make more accurate quantifications.

The same film was used for all measurements. The source exposures were carried out in the imager room (in ambient light) and the sources were placed inside a cassette for 72 hours. This cassette was specially designed to protect the film from UV during exposure and its use is recommended in the imager documentation ("Amersham™ Typhoon™ Catalogs," 2018).

2.2.2 Uncertainty calculation for autoradiography analysis

In this study, the decision regarding the size of the subdivisions of the source was made based on the ISO 8769 standard, which applies to sources of at least 100 cm². It advises to use sub-areas of at least 6.25 cm², which is why the 25-cm² sources images were analyzed using 4 sub-areas rather than 9.

Repeatability experiments were performed with some commercial surface sources and a variation of DLU within the range of 2% to 10% was obtained (type A uncertainty). It was decided to keep a conservative value and the value of 10% was chosen as the standard uncertainty.

It is worth noting that it would ideally be necessary to image each individual portion of the source separately while shielding other portions to prevent uniformity bias at the edges. However, due to time constraints, such an analysis technique was not feasible; imaging each 4 sub-areas of both sides of one source would have taken about 24 days per source. Nevertheless, for ²⁴¹Am sources, as the signal on the screen is mostly due to the interaction of alpha particles, the bias due to any edge effect is expected to be low.

The Table 42 shows the effect of choosing a grid of 9 sub-areas instead of a grid of only 4 sub-areas. As expected, the 3x3 uniformity values are systematically lower (no symmetry contrary to the 4 sub-areas) but they are still less than 10% lower, which shows that the choice of a 10% standard uncertainty accounts for this bias.

Table 42: Effect of the grid size on the uniformity values

Uniformity	Size of the grid 2*2	Size of the grid 3*3
K2	90%	85%
L2	85%	77%

3 EXTRA ATR-FTIR SPECTRA, SEM OR OPTICAL MICROSCOPE IMAGES AND KINETICS OF RN FIXATION

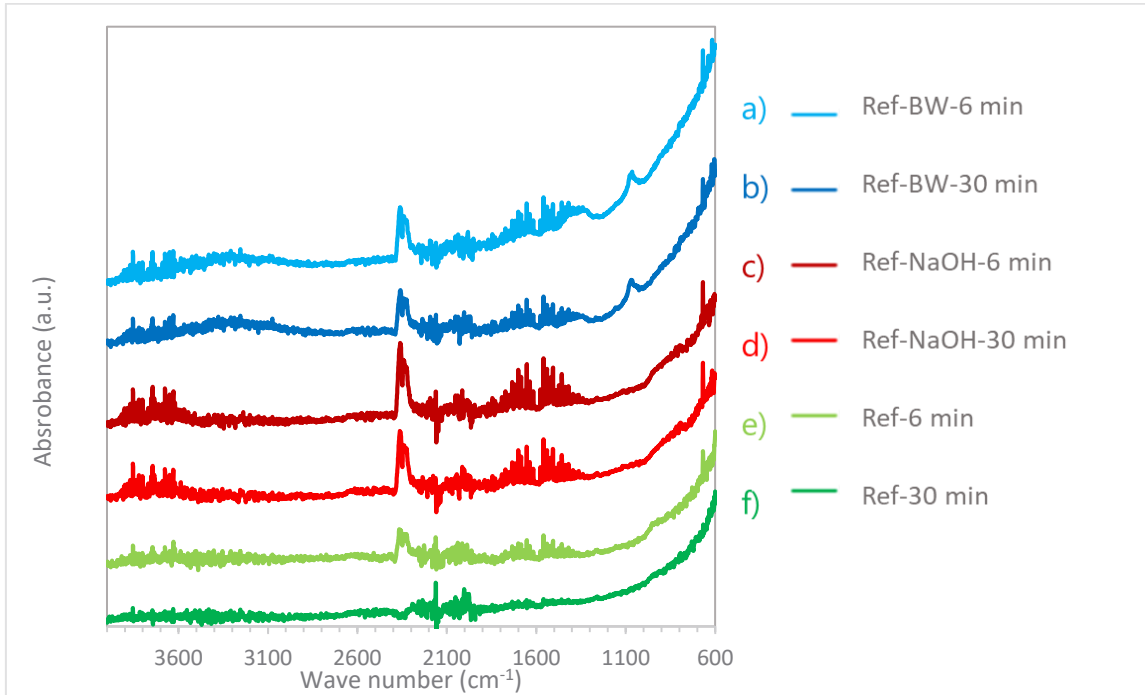


Figure 117: Impact of the cleaning duration

The figure shows the impact of the different cleaning durations on the cleaned and etched aluminum samples. The BW etched samples exhibit a peak around 1100 cm^{-1} , indicating the -OH bonds, and a broad band around $3600\text{-}3000\text{ cm}^{-1}$ suggesting water absorption on the surface. BW etching is identified as the most effective treatment.

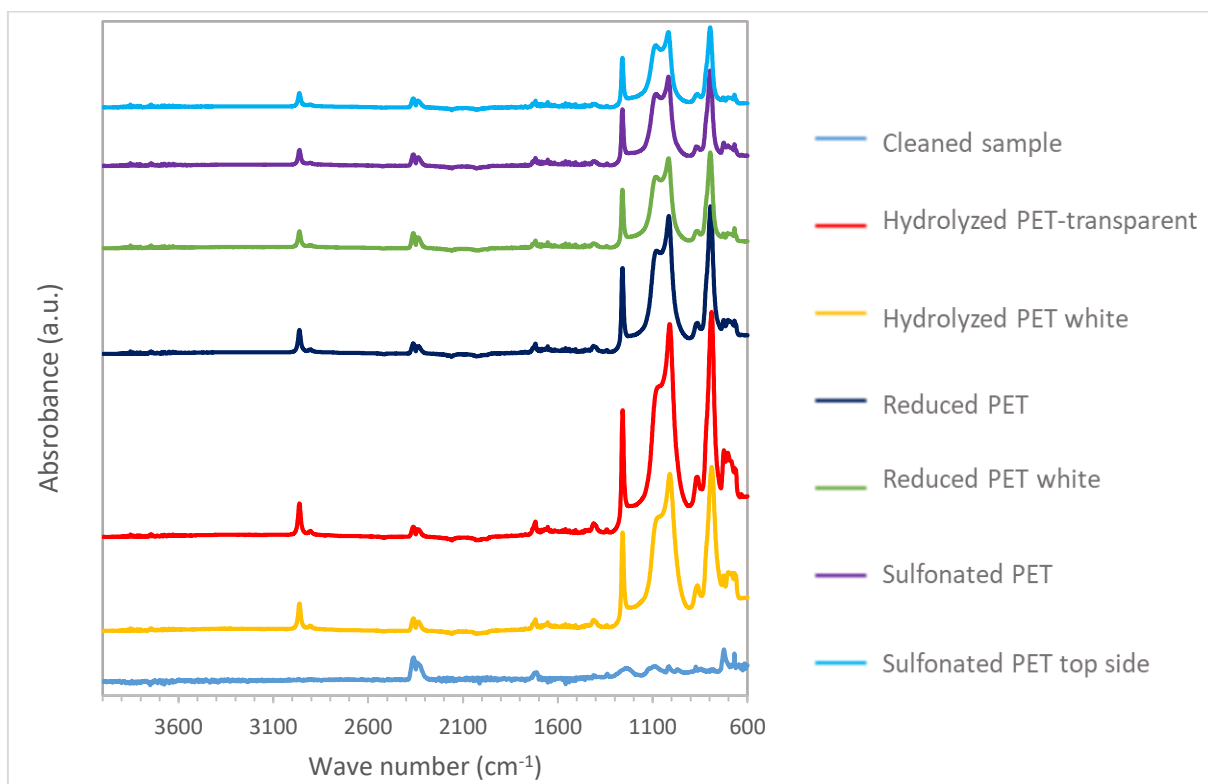


Figure 118: Whole spectra of the PET samples

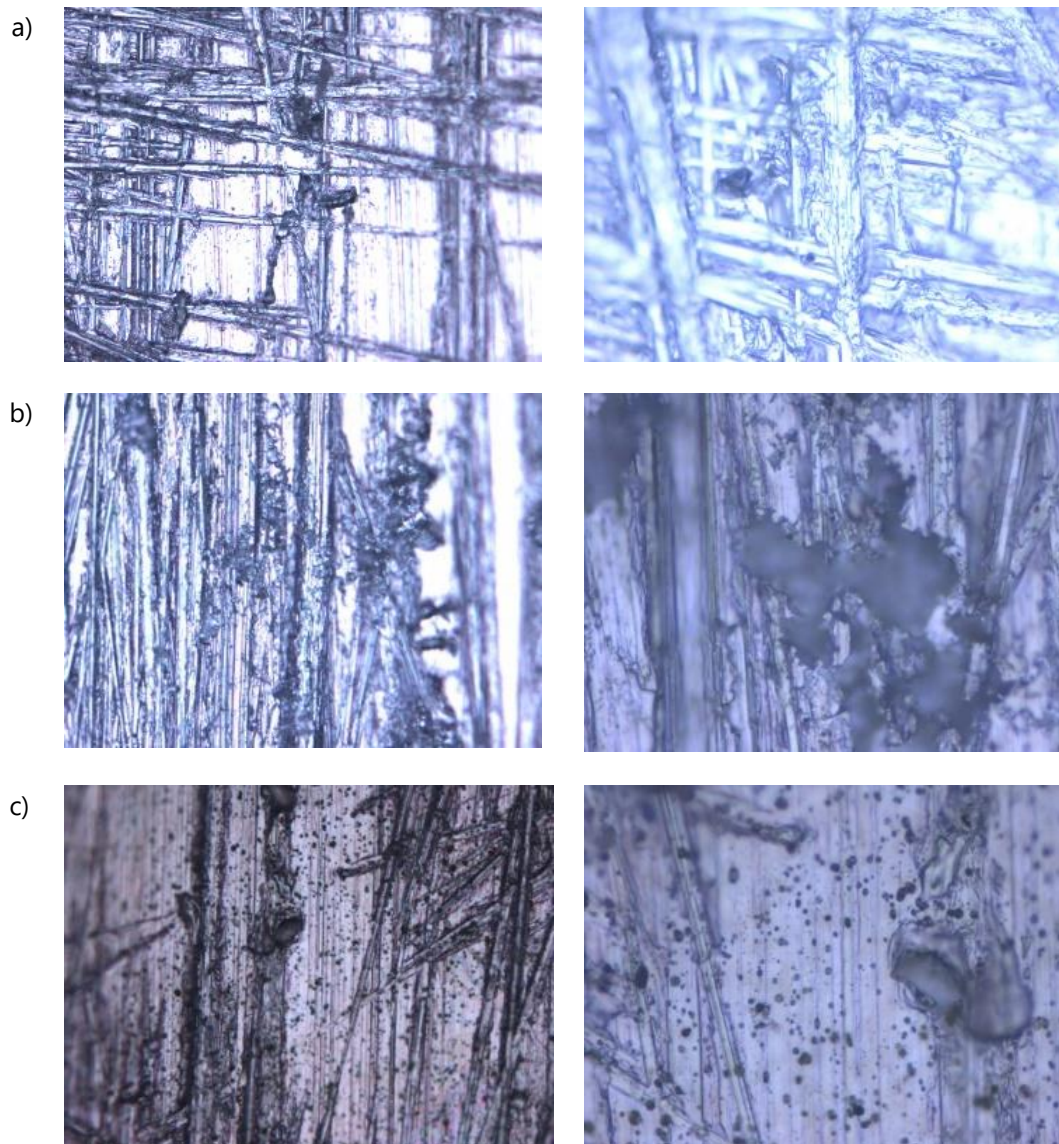


Figure 119: Optical microscopy images of shiny side of the polished samples etched with three etching methods a) Polished Shiny- NaOH-HNO_3 (magnified x20 and x50) b) Polished shiny- $\text{HCl-H}_2\text{O}_2$ (x20 and x50) c) Polished shiny -BW (x20 and x50)

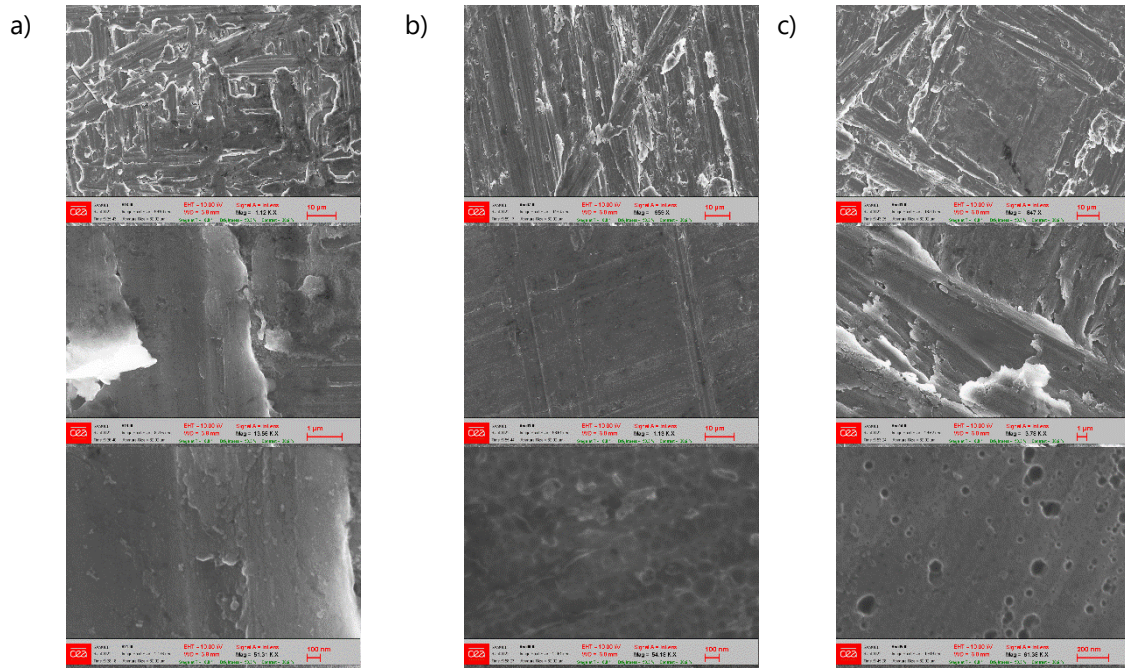
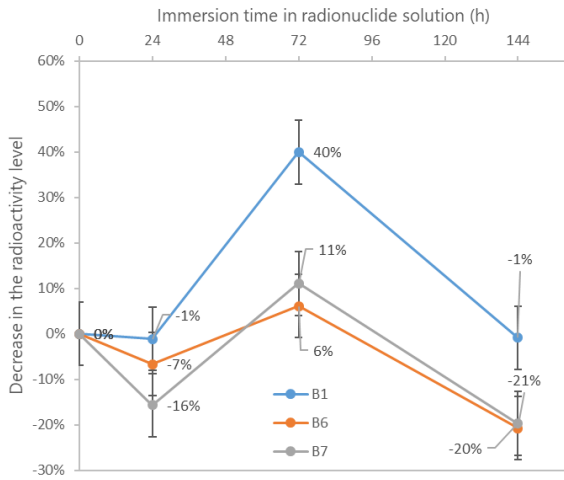
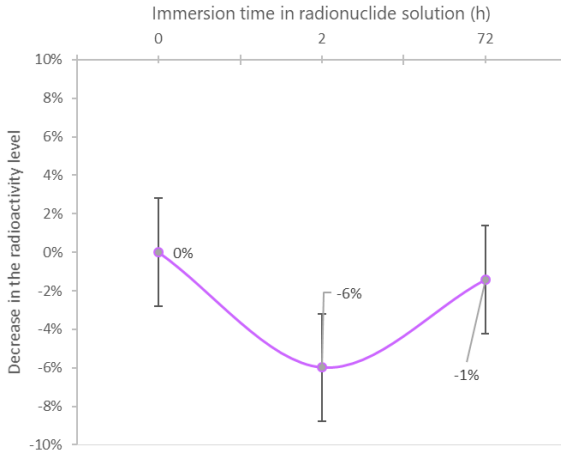


Figure 120: SEM images of the polished samples a) Polished matte side etched with NaOH-HNO₃ b) Polished matte side c) polished shiny side etched with NaOH-HNO₃

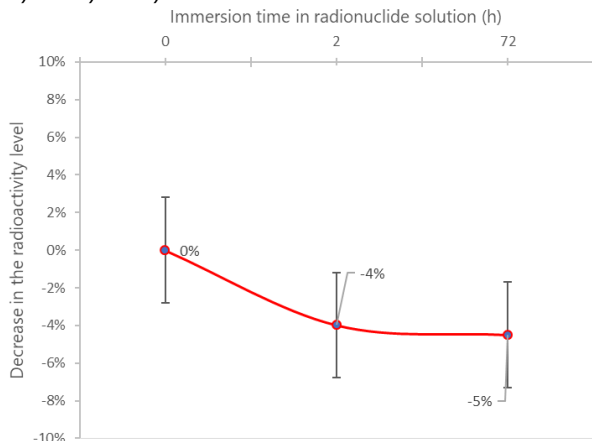
Appendices



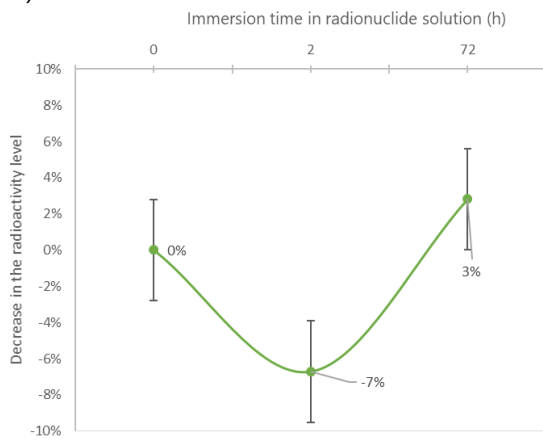
a) B1 b) B6 c) B7



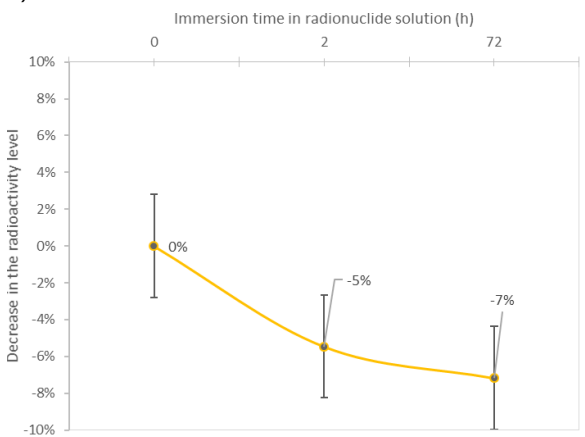
d) C6



e) C8



f) C9



g) D10

Figure 121: Kinetic behaviors of ^{152}Eu onto the grafted samples with a thickness of 0.03 mm a) $\text{Si-PO}_3\text{-2.5h}$ b) Si-N-2.5h , c) $\text{PO}_3\text{-PO}_3\text{-Na}_2\text{SO}_4\text{-pH8-10h}$, d) $\text{PO}_3\text{-PO}_3\text{-Na}_2\text{SO}_4\text{-10h}$, e) $\text{Si-SO}_3\text{-20h}$

Table 43: Impact of the different grid sizes on the uniformity values of the produced sources

Sample name	2x2	3x3
E4 (Raw PET) ¹⁵² Eu	(100 ± 10)%	(95 ± 10)%
E7 (Sulfonated PET) ¹⁵² Eu	(42 ± 10)%	(47 ± 10)%
E2 (~0.30- 30 min-80°C) ¹⁵² Eu	(90 ± 10)%	(60 ± 10)%
F2 (~0.30-60 min-80°C) ¹⁵² Eu	(82 ± 10)%	(75 ± 10)%
G2 (~0.30-60 min-80°C) ¹⁵² Eu	(86 ± 10)%	(70 ± 10)%
E3 (ACN-16 h-70°C) ¹⁵² Eu	(45 ± 10)%	(47 ± 10)%
F3 (ACN-3h@70°C+16h@22°C) ¹⁵² Eu	(80 ± 10)%	(46 ± 10)%
G3 (ACN-3h@70°C+16h (@22°C)) ¹⁵² Eu	(80 ± 10)%	(70 ± 10)%
K1 (Oxidized) ²⁴¹ Am	(75 ± 10)%	(70 ± 10)%
K2 (Oxidized) ²⁴¹ Am	(90 ± 10)%	(85 ± 10)%
K3 (Oxidized) ²⁴¹ Am	(90 ± 10)%	(83 ± 10)%
L1 (Sulfonated) ²⁴¹ Am	(75 ± 10)%	(46 ± 10)%
L2 (Sulfonated) ²⁴¹ Am	(85 ± 10)%	(77 ± 10)%
L3 (Sulfonated) ²⁴¹ Am	(60 ± 10)%	(49 ± 10)%
D10 (Si-SO ₃ -20h), ¹⁵² Eu	(70 ± 10)%	(66 ± 10)%
J3 (0.27M-15min-50°C), ²⁴¹ Am	(93 ± 10)%	(92 ± 10)%

Drawing of the chemicals in this manuscript were generated using the online platform C6H6.org (Patiny et al., 2018).

LISTS OF FIGURES AND TABLES

Figure 1: Principles of radioactive waste classification in the French legislation (ASN, 2016).....	14
Figure 2: Curved surfaces encountered on nuclear sites: a) ceiling that was checked by hand (blue areas); b) a pipe.....	15
Figure 3: Approach of characterization of the contaminated surfaces (NEA, 2017).....	16
Figure 4: Radiation detection instruments.....	20
Figure 5: Porous anodic aluminum oxide surface (Lee and Park, 2014).....	26
Figure 6: Drop deposition of radioactive solution on a filter paper (Monsanglant-Louvet et al., 2015).....	27
Figure 7: Illustration of the electrodeposition method (Becerril et al., 1993).....	29
Figure 8: Glass framework for soaking large ion-exchange membrane (Yoshida and Martin, 1990).....	30
Figure 9: The structure of Nafion HP membrane (Chen et al., 2018).....	31
Figure 10: Diagram of the schematic device to prepare the source 1: RN solution, 2: quartz glass tank, 3: aluminum backing material, 4: PDMS, 5: ion exchange membrane (Chen et al., 2018).....	31
Figure 11: Illustration of the cell for electrochemical polymerization (Tsoumpko-Sitnikov et al., 2002).....	32
Figure 12: Immersion of the MnO ₂ coated thin film in RN solution (Surbeck, 2000).....	33
Figure 13: Scheme of the low efficiency alpha emitting resin sources (Chambon et al., 2022).....	35
Figure 14: Commercial surface sources produced on a 150 cm ² sized aluminum plaque a) alpha-beta hand source, Eckert & Ziegler b) © LEA - Cyril Crespeau, Orano.....	38
Figure 15: The comparison of the production methods of commercial surface sources (a) and approach (b).....	39
Figure 16: Surface sources produced with approach of the study a) aluminum foil, b) epoxy resin, c) PET.....	40
Figure 17: E-pH diagram of americium in 10 ⁻¹⁰ M solutions (Lehto and Hou, 2011).....	43
Figure 18: Relative species distribution (%) diagrams for a) Eu(III) (Plancque et al., 2003) and b) Am(III) as a function of pH in aqueous solution containing carbonates under ambient conditions (Ioannidis et al., 2023).....	43
Figure 19: Possible approaches to modify the surface of a substrate a) one step, b) two steps...	44
Figure 20: Principle of Ion exchange resins a) anion exchange resin, b) cation exchange resin	45
Figure 21: Functional groups found on some typical ion exchangers	46
Figure 22: Operating pH range of functional groups in cationic and anionic resins (Silva et al., 2018).....	47
Figure 23: Chemical structure of the epoxy resin a) Part A: Epoxy polymer, b) Part B: Amine oligomer.....	51
Figure 24: Epoxy/amine reaction scheme (Gonzalez et al., 2012).....	52
Figure 25: The pathway of the hydrolysis and reduction reactions	53
Figure 26: Oxidation of functional groups in the polymer chain (Siau et al., 2004a).....	54
Figure 27: The order of the polymer chain breakdown (Siau et al., 2004a)	55
Figure 28: Williamson ether synthesis (S _N 2 mechanism) with 1,4 butane sultone a) alcohol chain ends, b) deprotonation of alcohol and formation of alkoxide anion, c) substitution and elimination reaction.....	56

Figure 29: One step method to produce sulfonic acid group grafted on polybutylene terephthalate a) Butane diol (BD), b) Dimethyl terephthalate, c) 1, 4-butane sultone, d) Sodium carbonate	57
Figure 30: Hydrolysis (a) and condensation (b) reaction of aluminum surface (adapted from (Abel et al., 2006))	60
Figure 31: Schematic illustration of the influence of water content on the surface modification (Hubert Mutin et al., 2005)	60
Figure 32: The modification of the end functions on the hydrolysed aluminum surface	62
Figure 33: Possible binding modes of phosphonate ligand on the aluminum surface (Neouze and Schubert, 2008)	63
Figure 34: Schematic illustration of MnO ₆	65
Figure 35: Correlation between the surface density of MnO ₂ coating on polyamide discs as a function of the coating treatment duration (Eikenberg et al., 2001).....	66
Figure 36: E-pH diagram for aqueous manganese compounds in the solution containing 5 mmol/L KMnO ₄ (Kharitonov et al., 2020)	67
Figure 37: Examples of epoxy resin surface sources, mimicking a) a curved surface, b) a cement-like surface, c) a rough surface created with a rough mold	72
Figure 38: The molds used in the casting of epoxy resin samples a) Rigid white PTFE mold (5x5 cm ²), b) Flexible yellow mold (5x5 cm ²), and c) Blue metal mold (11x16 cm ²)	73
Figure 39: The methods for the PET modification.....	74
Figure 40: The functionalization method planned for epoxy resin	76
Figure 41: a) Experimental set up for the oxidation of epoxy samples, b) an oxidized sample before washing for 1 h, c) an oxidized sample after washing with acetic acid and DI water.....	78
Figure 42: Experimental set up of the sulfonation treatment a) dissolution of NaH (presented in a grey stone like substance) in solvent, b) mixing of 1,4-butane sultone with solvent, c) immersion of the pre-treated epoxy surface	79
Figure 43: Experimental setup of the RN binding experiment.....	82
Figure 44: Illustration of the autoradiography: a) exposure of a source (grey) on the imaging plate (white) b) autoradiography imaging system c) reading step in the scanner, d) signal of the source	83
Figure 45: a) Chemical structure of PET, schematic view of: b) raw PET, c) hydrolyzed PET, d) reduced PET, e) sulfonated PET, f) KMnO ₄ treated PET.....	84
Figure 46: Ester cleavage reaction of PET	85
Figure 47: ATR-FTIR spectrum of the PET samples a) raw PET, b) white part of hydrolyzed PET, c) transparent part of hydrolyzed PET, d) transparent part of reduced PET, e) white part of reduced PET, f) sulfonated PET, g) close up version of the raw PET spectrum	86
Figure 48: Chemical structure of epoxy resin a) component A, b) component B, c) a possible modification mechanism of epoxy resin	88
Figure 49: A possible mechanism on the hydroxyl end of the oxidized epoxy resin samples	89
Figure 50: The ATR-FTIR Spectrum of the epoxy sample from 4000 to 600 cm ⁻¹ a) raw cleaned epoxy resin, b) oxidized epoxy resin, c) sulfonated epoxy resin.....	89
Figure 51: Fingerprint region of the epoxy resin a) raw epoxy, b) oxidized epoxy resin, c) sulfonated epoxy resin.....	91
Figure 52: The attachment of ¹⁵² Eu on the PET samples a) E4 (raw PET), b) E5 (hydrolyzed PET), c) E6 (reduced PET), d) E7 (sulfonated PET), e) H5 (KMnO ₄ treated PET).....	94
Figure 53: Kinetic behavior of the fixation of ¹⁵² Eu onto epoxy samples a) raw epoxy (E1), b) oxidized epoxy (E2), c) sulfonated epoxy (E3).....	96

Figure 54: Kinetic behavior of the fixation of ^{152}Eu onto oxidized epoxy samples, a) E2, b) F2 and c) G2 samples.....	98
Figure 55: Pictures of the oxidized samples treated with ^{152}Eu a) E2, b) F2, and c) G2	99
Figure 56: Kinetic behavior of the fixation of ^{152}Eu onto sulfonated epoxy samples a) E3 (ACN-16h-70°C), b) H6 (DMSO-3h@70°C+16 h@22°C), c) G3 (ACN-3h@70°C+16h@22°C), d) F3 (ACN-3h@70°C+16h@22°C).....	100
Figure 57: Appearance of the sulfonated sample using DMSO solvent (H6).....	101
Figure 58: The kinetic behavior of ^{241}Am onto the oxidized epoxy resin samples a) J1, b) K1, c) K2 and d) K3.....	103
Figure 59: The kinetic behavior of the sulfonated samples immersed in ^{241}Am solution	104
Figure 60: Appearances of samples of the L series after the sulfonation treatment.....	105
Figure 61: Pictures of samples, phosphor imaging autoradiography images, uniformity and radioactivity levels of PET samples treated with ^{152}Eu a) E4, b) E7, c) H5	110
Figure 62: Pictures of samples, phosphor imaging autoradiography images, uniformity and radioactivity levels of the oxidized samples treated with ^{152}Eu a) E2, b) F2 and c) G2	112
Figure 63: Pictures, phosphor imaging autoradiography images, uniformity and activity of sulfonated epoxy samples treated with ^{152}Eu , a) E3, b) F3 and c) G3	113
Figure 64: Pictures, phosphor imaging autoradiography images, uniformity, and activity of ^{241}Am epoxy surface sources a) K1 (Oxidized), b) K2 (Oxidized), c) K3 (Oxidized), d) L1 (Sulfonated), e) L2 (Sulfonated), f) L3 (Sulfonated)	115
Figure 65: Experimental set up for the exposure with two screens.....	116
Figure 66: Phosphor imaging autoradiography images, and uniformity values of the K series (^{241}Am) with and without the alpha emissions from the smooth side of the sources, using 2 x 2 grids .	116
Figure 67: Phosphor imaging autoradiography images, and uniformity values of the L series (^{241}Am) with and without the alpha emissions from the smooth side of the sources, using 2 x 2 grids .	117
Figure 68: Autoradiography images of the samples after the non-contamination tests	119
Figure 69: Aluminum modification approaches (grafting and coating)	124
Figure 70: The chemical structure of the chemicals used in the grafting methods.....	125
Figure 71: Illustration of the etching methods a) NaOH-HNO ₃ b) HCl-H ₂ O ₂ c) Boiling water (BW) d) CuCl ₂ e) H ₂ O ₂ treatment	127
Figure 72: Experimental setup of the RN binding experiments.....	133
Figure 73: Images of the cleaned aluminum foil a) optical microscope image of cleaned Al foil shiny side (x50 magnification) b) optical microscope image of cleaned Al foil matte side (x50 magnification) c) top view SEM image of the cleaned Al foil matte side	135
Figure 74: ATR-FTIR spectra of Al samples a) clean matte side b) clean shiny side	135
Figure 75: Optical microscopy images of matte side of the polished samples before etching and after an etching step a) Polished without etching (magnified x50), b) Polished-NaOH-HNO ₃ (x50), c) Polished-HCl-H ₂ O ₂ (x50), d) Polished-BW (x50)	137
Figure 76: Appearance of the polished matte side of the regular aluminum foil (0.03 mm).....	137
Figure 77: Impacts of the different etching methods a) cleaned sample without etching, b) sample treated with NaOH-HNO ₃ , c) sample treated with boiling water	138
Figure 78: Top view SEM images of a) Cleaned sample b) Cleaned, etched with NaOH-HNO ₃ , c) Cleaned, and etched with boiling water sample (BW).....	139
Figure 79: Top view SEM images of the Si-N grafted samples a) Si-N-dipped, b) Si-N-dipped-BW, c) Si-N-dipped-NaOH-HNO ₃	140
Figure 80: Top view SEM images of boiling water treated and grafted samples a) PO ₃ -PO ₃ -BW b)	

Si-PO ₃ -BW	141
Figure 81 : Top view SEM images of the Si-PO ₃ grafted samples a) Si-PO ₃ -2.5h, b) Si-PO ₃ -12h, c) BW	141
Figure 82: Top view SEM images of a) BW treated sample, b) E8 sample (Si-SO ₃ -3 h)	142
Figure 83: ATR-FTIR of Al samples: a) Cleaned, b) BW, c) Si-N-dipped, d) Si-N-dipped-BW, e) Si-N-dipped-NaOH-HNO ₃ , f) Si-PO ₃ -dipped-BW, g) PO ₃ -PO ₃ -BW	143
Figure 84: Si-N chemical attaches onto the aluminum surface	144
Figure 85: ATR-FTIR spectra of aluminum surface after grafting with MPTMS (Si-SH) and subsequent sulfonation, to yield Si-SO ₃ groups a) Cleaned sample, b) BW treated sample, c) E8 (Si-SO ₃ -3h)	146
Figure 86: Possible binding modes of the Si-SO ₃ chemical onto aluminum surface	147
Figure 87: Top view SEM images of the Si-N grafted samples a) Si-N-1h, b) Si-N-2.5h, c) Si-N-6h, d) Si-N-12h, e) BW treated sample	148
Figure 88: Si-N (DMOAC) samples grafted for different durations a) Cleaned, b) Cleaned-BW, c) Si-N-1h, d) Si-N-2.5h, e) Si-N-6h, f) Si-N-12h	149
Figure 89: ATR-FTIR spectra of the Si-PO ₃ grafted samples a) Cleaned, b) Cleaned-BW, c) Si-PO ₃ -2.5h, d) Si-PO ₃ -12h	151
Figure 90: Possible binding modes of the Si-PO ₃ chemical a) binding from silanol group, b) binding from phosphonic acid group	151
Figure 91: Top view SEM images of the PO ₃ -PO ₃ grafted samples a) PO ₃ -PO ₃ -Na ₂ SO ₄ -1h-22°C,	152
Figure 92: ATR-FTIR spectra of the PO ₃ -PO ₃ grafted samples a) Cleaned, b) Cleaned-BW, c) PO ₃ -PO ₃ -Na ₂ SO ₄ -1h-22 °C, d) PO ₃ -PO ₃ -Na ₂ SO ₄ -2.5h, e) PO ₃ -PO ₃ -Na ₂ SO ₄ -10h, f) PO ₃ -PO ₃ -pH8-2.5h g) PO ₃ -PO ₃ -pH8-6h	153
Figure 93: Possible binding mode of PO ₃ -PO ₃ chemical on aluminum surface	154
Figure 94 : Top view SEM images of a) Cleaned sample, b) H3 sample treated with KMnO ₄ (0.3M-60 min-50°C) c) zoomed area of H3 sample treated with KMnO ₄	155
Figure 95: ATR-FTIR spectra of a KMnO ₄ treated sample and references a) Cleaned sample, b) H3 sample (0.30M-60min-50°C)	156
Figure 96: Top-view SEM images of the I2 sample treated with K ₂ Cr ₂ O ₇ (0.50M-H ₂ SO ₄ -60min-50°C) a) Cleaned sample, b) K ₂ Cr ₂ O ₇ (0.50M-H ₂ SO ₄ -60min-50°C)	157
Figure 97: ATR-FTIR spectra of the CrOx coated sample I2 and references a) Cleaned sample, b) I2 sample (0.50M-H ₂ SO ₄ -60min-50°C)	158
Figure 98: Kinetic behavior of the uptake of ¹⁵² Eu on sulfonated samples immersed in a ¹⁵² Eu solution (Al thickness of 0.03 mm) a) Si-SO ₃ -3 h b) Si-SO ₃ -20 h	161
Figure 99: Kinetic behavior of ²⁴¹ Am attachment onto sulfonated aluminum samples Si-SO ₃ -20 h with a thickness of 0.3 mm a) P3, b) P4, c) P1	162
Figure 100: Kinetic behavior of ¹⁵² Eu attachment onto the samples treated with K ₂ Cr ₂ O ₇ a) I2 (CrOx-10 min- 50 °C), b) I3 (CrOx-60min-50 °C)	165
Figure 101: Kinetic behavior of ²⁴¹ Am onto the J2 sample treated with K ₂ Cr ₂ O ₇ (CrOx-pH1-60 min-50°C)	166
Figure 102: Kinetic behavior of ¹⁵² Eu attachment onto KMnO ₄ treated samples produced in acidic conditions a) I4 (0.005 M-pH3-24h-22°C), b) I1 (0.27M-pH1-60min-50°C), and c) I5 (0.02 M-pH7-24h-22°C)	167
Figure 103: Kinetic behavior of ¹⁵² Eu onto the basic KMnO ₄ treated samples a) H2 (0.1M-Dipped-22°C), b) H4 (0.3M-Dipped-50°C), c) H1 (0.1 M-pH9-60min-22°C), d) H3 (0.3M-60min-50°C) ...	169

Figure 104: Appearance of the H3 sample a) before immersion in the RN solution b) after immersion in the RN solution 171

Figure 105: Kinetic behavior of ^{241}Am attachment onto KMnO_4 treated samples a) Y2 (0.28M-15 min -50°C), b) T1 (0.28M-15min-80°C), c) Y1 (0.28M-15min-50°C), d) Y3 (0.28M-15 min-50°C), e) J3* (0.27M-15min-50°C), f) R2 (0.28M-40min-80°C). Among these samples, J3 has a thickness of 0.03 mm, unlike the other samples. 172

Figure 106: The appearance of the KMnO_4 treated samples a) T series samples (0.30M-15min-80°C) series, b) R series samples (0.30M-40min-80°C)..... 174

Figure 107: Picture and autoradiography image of the sulfonated (Si-SO_3 -20h) D10 sample immersed in ^{152}Eu solution 176

Figure 108: Pictures, autoradiography images, uniformity and activity of the sulfonated (Si-SO_3) samples immersed in ^{241}Am a) P1, b) P3, c) P4, d) Other side of P1 e) Other side of P3 f) Other side of P4. DLU*: Total digital light unit for the sample 177

Figure 109: Pictures, autoradiography image, uniformity and activity of the KMnO_4 treated J3 sample immersed in ^{241}Am solution a) appearance of the sample after immersion in the RN solution from two sides, b) autoradiography..... 179

Figure 110: Pictures and, two sided autoradiography images, uniformity and activity of the MnOx coated samples from Y series (0.28M-15min-50°C) with ^{241}Am a) Y1, b) Y2, c) Y3, d) Other side of Y1 e) Other side of Y2 f) Other side of Y3. DLU*: Total digital light unit for the sample 180

Figure 111: Pictures, two sided autoradiography images, uniformity and activity of the MnOx coated samples treated with ^{241}Am a) Y3 (0.28M-15 min-50°C), b) T1 (0.28M-15min-80°C), c) R2 (0.28M-40min-80°C), d) other side of Y3, f) other side of T1, e) other side of R2..... 182

Figure 112: The fundamental vibrational regions with some characteristic group frequencies.. 190

Figure 113: The oscillating electric field of the photon generates oscillating, oppositely directed forces on the positive and negative charges of the molecular dipole..... 191

Figure 114: The diagram of a single reflection ATR crystal depicting the basic principles of the technique..... 191

Figure 115: Electromagnetic spectrum showing the size of the wavelength used in the light, scanning electron microscope (SEM) and transmission electron microscope (TEM)(UI-Hamid, 2018) 192

Figure 116: Placing of an autoradiography plate in the device 198

Figure 117: Impact of the cleaning duration 201

Figure 118: Whole spectra of the PET samples 202

Figure 119: Optical microscopy images of shiny side of the polished samples etched with three etching methods a) Polished Shiny-NaOH-HNO₃ (magnified x20 and x50) b) Polished shiny-HCl-H₂O₂ (x20 and x50) c) Polished shiny -BW (x20 and x50) 203

Figure 120: SEM images of the polished samples a) Polished matte side etched with NaOH-HNO₃ b) Polished matte side c) polished shiny side etched with NaOH-HNO₃ 204

Figure 121: Kinetic behaviors of ^{152}Eu onto the grafted samples with a thickness of 0.03 mm a) Si-PO₃-2.5h b) Si-N-2.5h, c) PO₃-PO₃-Na₂SO₄-pH8-10h, d) PO₃-PO₃- Na₂SO₄- 10h, 205

Table 1: Types of measurement methods (Amgarou and Herranz, 2021)	19
Table 2: Radionuclides for alpha-emitting standard sources (ISO 8769, 2020)	23
Table 3: Radionuclides for beta emitting standard sources (ISO 8769, 2020)	23
Table 4: Production methods for LARS	36
Table 5: Examples of resin types	49
Table 6: Silanol grafting chemicals and their experimental parameters	61
Table 7: Phosphonic acid grafting with some experimental parameters	63
Table 8: Chosen chemicals for the experimental procedures	71
Table 9: The experimental conditions for the PET functionalization methods	76
Table 10: Experimental conditions of the oxidation of epoxy resin	77
Table 11: Experimental conditions for sulfonation of epoxy resin	79
Table 12: Parameters of the RN binding experiments for polymeric surface sources	81
Table 13: Vibrational bands of raw PET samples (Pereira et al., 2017; Torres-Huerta et al., 2016)	87
Table 14: The vibrational frequencies of the raw epoxy resin (Çalı, 2019; Gao et al., 2017; Gonzalez et al., 2012; Han et al., 2011; Kallingal et al., 2023; Ouadah et al., 2018)	92
Table 15: The vibrational frequencies indicating oxidation and sulfonation (Çalı, 2019; Gao et al., 2017; Gonzalez et al., 2012; Han et al., 2011; Ouadah et al., 2018; Zhou et al., 2019)	93
Table 16: Maximum activity of the PET surface sources immersed in a ¹⁵² Eu solution	95
Table 17: Maximum radioactivity levels of the oxidized epoxy samples immersed in a ¹⁵² Eu solution	99
Table 18: Maximum radioactivity levels of sulfonated epoxy samples immersed in a ¹⁵² Eu solution	101
Table 19: Maximum activities of the oxidized epoxy sources immersed in a ²⁴¹ Am solution	103
Table 20: Maximum activities of the sulfonated epoxy sources immersed in ²⁴¹ Am	104
Table 21: Maximum fixation yields of the best samples that oxidized and sulfonated in ²⁴¹ Am	106
Table 22: Maximum fixation yields and activities of ¹⁵² Eu and ²⁴¹ Am onto KMnO ₄ treated epoxy samples	106
Table 23: Maximum fixation yields and activities of ¹⁵² Eu and ²⁴¹ Am onto sulfonated epoxy samples	107
Table 24: Comparison of PET and epoxy resin substrates with the best oxidized and sulfonated samples that were immersed in a ¹⁵² Eu solution	107
Table 25: Results of the dry and wet non-contamination tests on epoxy resin K1 and L1 samples spiked with ²⁴¹ Am	118
Table 26 : Chemicals used in the grafting methods and their parameters	129
Table 27: Parameters of manganese oxide coating methodologies (MnOx) and aluminum foils finish and thickness	131
Table 28: Parameters of the K ₂ Cr ₂ O ₇ treatment	131
Table 29: Parameters of the RN binding experiments for aluminum surface sources	132
Table 30: Peaks of the Si-N grafted samples and their attributions	144
Table 31: Attributions of the peaks from PO ₃ -PO ₃ grafted samples (Lushtinetz et al., 2007)	154
Table 32: Maximum radioactivity levels of some of the best aluminum foil grafted samples, tested with ¹⁵² Eu	159
Table 33: Maximum radioactivity levels on the sulfonated aluminum foils immersed in a ¹⁵² Eu solution	161
Table 34: Maximum radioactivity levels of the sulfonated aluminum foil immersed in a ²⁴¹ Am solution	163

Table 35: Comparison of the maximum fixation of ^{152}Eu and ^{241}Am onto Si-SO_3 treated samples	164
Table 36: Maximum radioactivity levels of the $\text{K}_2\text{Cr}_2\text{O}_7$ treated aluminum foils immersed in a ^{152}Eu solution.....	166
Table 37: Maximum radioactivity levels of the aluminum foils coated with MnOx produced in acidic or neutral conditions, immersed in a ^{152}Eu solution.....	168
Table 38: Maximum radioactivity levels of the aluminum foil samples coated with MnOx under basic conditions, immersed in a ^{152}Eu solution	170
Table 39: Maximum radioactivity levels of the aluminum foil samples coated with MnOx under basic conditions, immersed in a ^{241}Am solution	173
Table 40: Kinetic behavior of ^{152}Eu and ^{241}Am onto KMnO_4 treated samples produced in basic conditions.....	175
Table 41: Standard uncertainty budget for LSC measurements.....	197
Table 42: Effect of the grid size on the uniformity values.....	200
Table 43: Impact of the different grid sizes on the uniformity values of the produced sources.	206

REFERENCES

- Abel, M.-L., Allington, R.D., Digby, R.P., Porritt, N., Shaw, S.J., Watts, J.F., 2006. Understanding the relationship between silane application conditions, bond durability and locus of failure. *International Journal of Adhesion and Adhesives, Silane Coupling Agents* 26, 2–15. <https://doi.org/10.1016/j.jjadhadh.2005.03.009>
- Aggarwal, S.K., 2016. Alpha-particle spectrometry for the determination of alpha emitting isotopes in nuclear, environmental and biological samples: past, present and future. *Anal. Methods* 8, 5353–5371. <https://doi.org/10.1039/C6AY00920D>
- Alexandratos, S.D., 2009. Ion-Exchange Resins: A Retrospective from Industrial and Engineering Chemistry Research. *Ind. Eng. Chem. Res.* 48, 388–398. <https://doi.org/10.1021/ie801242v>
- Alexandratos, S.D., Quillen, D.R., 1990. Mechanism of polymer-based separations: II. Targeted metal ion complexation by reactive polymers. *Reactive Polymers, Ion Exchange Fundamentals and Applications* 13, 255–265. [https://doi.org/10.1016/0923-1137\(90\)90095-L](https://doi.org/10.1016/0923-1137(90)90095-L)
- Alexandratos, S.D., Shelley, C.A., Philip Horwitz, E., Chiarizia, R., 1998. A Mechanism for Enhancing Ionic Accessibility into Selective Ion Exchange Resins. *Solvent Extraction and Ion Exchange* 16, 951–966. <https://doi.org/10.1080/07366299808934562>
- Amersham™ Typhoon™ Catalogs, 2018.
- Amgarou, K., Herranz, M., 2021. State-of-the-art and challenges of non-destructive techniques for in-situ radiological characterization of nuclear facilities to be dismantled. *Nuclear Engineering and Technology* 53, 3491–3504. <https://doi.org/10.1016/j.net.2021.05.031>
- ASN, 2016. French National Plan for the Management of Radioactive Materials and Waste for 2016-2018. Autorité de sûreté nucléaire. <https://www.french-nuclear-safety.fr/asn-informs/publications/other-asn-reports/french-national-plan-for-the-management-of-radioactive-materials-and-waste-for-2016-2018>
- Balasubramanian, P.S., 1997. Anodically oxidised aluminium layer as a useful substrate for the fabrication of ¹⁴⁷Pm sources for beta-ray thickness gauges. *J Radioanal Nucl Chem* 223, 79–81. <https://doi.org/10.1007/BF02223367>
- Ballard, P.J., 1981. The calibration of health physics contamination instruments and the use of thin ion exchange resin membranes to produce large area radioactive sources. *J. Soc. Radiol. Prot.* 1, 27. <https://doi.org/10.1088/0260-2814/1/3/002>
- Bartoś, B., Bilewicz, A., Delmas, R., Loos-Neskovic, C., 1997. Synthesis and Ion Exchange Properties of Various Forms of Manganese Dioxide for Cations of the I and II Groups. *Solvent Extraction and Ion Exchange* 15, 533–546. <https://doi.org/10.1080/07366299708934492>
- Baudat, E., Gautier, C., Fichet, P., Destrel, E., Colin, C., Giuliani, M., Lambrot, G., 2021. Optimization of Sr-90 precipitation in nitric acid using design of experiments for radioactive waste characterization method. *J. Radioanal. Nucl. Chem.* 328, 637–650. <https://doi.org/10.1007/s10967-021-07680-5>
- Becerril, V.A., Meas, V.Y., Tejera, R.A., Ozil, P., 1993. An improved rotating disc cathode cell for electrodeposition of actinides. The case of plutonium. *Nuclear Instruments and Methods in Physics Research Section A: Accelerators, Spectrometers, Detectors and Associated Equipment* 328, 512–516. [https://doi.org/10.1016/0168-9002\(93\)90668-8](https://doi.org/10.1016/0168-9002(93)90668-8)
- Berti, C., Celli, A., Marianucci, E., Vannini, M., 2008. Modification of poly(butylene terephthalate)

References

- by reaction with 1,4-butane sultone; synthesis and thermal characterization of new telechelic PBT ionomers. *e-Polymers* 8. <https://doi.org/10.1515/epoly.2008.8.1.865>
- Bourrel, F., Courrière, P., 2003. Radionucléides - Application: biologie moléculaire. *Techniques d'analyse*. <https://doi.org/10.51257/a-v1-p3362>
- Boxus, T., Deldime-Rubbens, M., Mougenot, P., Schneider, Y.-J., Marchand-Brynaert, J., 1996. Chemical assays of end-groups displayed on the surface of poly(ethylene terephthalate) (PET) films and membranes by radiolabeling. *Polymers for Advanced Technologies* 7, 589–598. [https://doi.org/10.1002/\(SICI\)1099-1581\(199607\)7:7<589::AID-PAT551>3.0.CO;2-B](https://doi.org/10.1002/(SICI)1099-1581(199607)7:7<589::AID-PAT551>3.0.CO;2-B)
- Burgess, P.H., Iles, W.J., 1983. The Suitability of Different Sources for the Calibration of Beta Surface Contamination Monitors. *Radiation Protection Dosimetry* 5, 125–130. <https://doi.org/10.1093/oxfordjournals.rpd.a082682>
- Çalı, A., 2019. SYNTHESIS, CHARACTERIZATION OF SEPIOLITE AND KAOLINITE ADDED, THERMALLY CROSSLINKED SULFONATED POLY (ETHER ETHER KETONE) INORGANIC-ORGANIC COMPOSITE MEMBRANES FOR PROTON EXCHANGE MEMBRANE FUEL CELL APPLICATIONS.
- Chambon, L., Tüzün, D., Bobin, C., Corbel, M., Lourenço, V., 2022. Development of alpha-emitting large area radioactive surface sources tailored for decommissioning. *Nuclear Instruments and Methods in Physics Research Section A: Accelerators, Spectrometers, Detectors and Associated Equipment* 1033, 166732. <https://doi.org/10.1016/j.nima.2022.166732>
- Chen, Y., Zhao, C., He, L., Tang, F., 2018. Preparation of reference sources for calibration of surface contamination monitors using Nafion ion exchange membrane. *J Radioanal Nucl Chem* 318, 2307–2311. <https://doi.org/10.1007/s10967-018-6259-5>
- Chen, Y.-F., Hu, Y.-H., Chou, Y.-I., Lai, S.-M., Wang, C.-C., 2010. Surface modification of nano-porous anodic alumina membranes and its use in electroosmotic flow. *Sensors and Actuators B: Chemical* 145, 575–582. <https://doi.org/10.1016/j.snb.2009.12.061>
- Cherian, E., Rajan, A., Gurunathan, Dr.B., 2016. Synthesis of manganese dioxide nanoparticles using co-precipitation method and its antimicrobial activity 01, 17–22.
- Crawford, C.B., Quinn, B., 2017. 4 - Physiochemical properties and degradation, in: Crawford, C.B., Quinn, B. (Eds.), *Microplastic Pollutants*. Elsevier, pp. 57–100. <https://doi.org/10.1016/B978-0-12-809406-8.00004-9>
- Cyclone Plus Storage Phosphor System, 2011.
- Danilidis, I., Hunter, J., Scamans, G.M., Sykes, J.M., 2007. Effects of inorganic additions on the performance of manganese-based conversion treatments. *Corrosion Science* 49, 1559–1569. <https://doi.org/10.1016/j.corsci.2006.08.007>
- Das, G., Kalita, R.D., Deka, H., Buragohain, A.K., Karak, N., 2013. Biodegradation, cytocompatibility and performance studies of vegetable oil based hyperbranched polyurethane modified biocompatible sulfonated epoxy resin/clay nanocomposites. *Progress in Organic Coatings* 76, 1103–1111. <https://doi.org/10.1016/j.porgcoat.2013.03.007>
- Dean, J., Adsley, I., Burgess, P., 2007. Traceability for measurements of radioactivity in waste materials arising from nuclear site decommissioning. *Metrologia* 44, S140. <https://doi.org/10.1088/0026-1394/44/4/S18>
- del Olmo, R., Mohedano, M., Matykina, E., Arrabal, R., 2022. Permanganate loaded Ca-Al-LDH coating for active corrosion protection of 2024-T3 alloy. *Corrosion Science* 198, 110144. <https://doi.org/10.1016/j.corsci.2022.110144>
- Durmus, Z., Kavas, H., Baykal, A., Toprak, M.S., 2009. A green chemical route for the synthesis of Mn₃O₄ nanoparticles. *cent.eur.j.chem.* 7, 555–559. <https://doi.org/10.2478/s11532-009->

References

- 0049-4
- Eikenberg, J., Tricca, A., Vezzu, G., Bajo, S., Ruethi, M., Surbeck, H., 2001. Determination of ²²⁸Ra, ²²⁶Ra and ²²⁴Ra in natural water via adsorption on MnO₂-coated discs. *Journal of Environmental Radioactivity, Natural Radioactivity: Technological Enhancement, Detection and Migration* 54, 109–131. [https://doi.org/10.1016/S0265-931X\(00\)00170-3](https://doi.org/10.1016/S0265-931X(00)00170-3)
- Eisazadeh, A., Kassim, K., Nur, H., 2010. Physicochemical characteristics of phosphoric acid stabilized bentonite. *Electronic Journal of Geotechnical Engineering* 15D, 1–10.
- El Ouardi, Y., Virolainen, S., Massima Mouele, E.S., Laatikainen, M., Repo, E., Laatikainen, K., 2023. The recent progress of ion exchange for the separation of rare earths from secondary resources – A review. *Hydrometallurgy* 218, 106047. <https://doi.org/10.1016/j.hydromet.2023.106047>
- EZAG, 2022. Wide area sources. Eckert & Ziegler Strahlen- und Medizintechnik AG.
- Feng, L., Che, Y., Liu, Y., Qiang, X., Wang, Y., 2013. Fabrication of superhydrophobic aluminium alloy surface with excellent corrosion resistance by a facile and environment-friendly method. *Applied Surface Science* 283, 367–374. <https://doi.org/10.1016/j.apsusc.2013.06.117>
- Fichet, P., Bresson, F., Leskinen, A., Goutelard, F., Ikonen, J., Siitari-Kauppi, M., 2012. Tritium analysis in building dismantling process using digital autoradiography. *J Radioanal Nucl Chem* 291, 869–875. <https://doi.org/10.1007/s10967-011-1423-1>
- Fryxell, G.E., Wu, H., Lin, Y., Shaw, W.J., Birnbaum, J.C., Linehan, J.C., Nie, Z., Kemner, K., Kelly, S., 2004. Lanthanide selective sorbents: self-assembled monolayers on mesoporous supports (SAMMS). *J. Mater. Chem.* 14, 3356–3363. <https://doi.org/10.1039/B408181A>
- Gao, S., Xu, H., Luo, T., Guo, Y., Li, Z., Ouadah, A., Zhang, Y., Zhang, Z., Zhu, C., 2017. Novel proton conducting membranes based on cross-linked sulfonated polyphosphazenes and poly(ether ether ketone). *Journal of Membrane Science* 536, 1–10. <https://doi.org/10.1016/j.memsci.2017.04.065>
- Gautier, C., Laporte, E., Lambrot, G., Giuliani, M., Colin, C., Bubendorff, J., Crozet, M., Mougel, C., 2020. Accurate measurement of ⁵⁵Fe in radioactive waste. *J. Radioanal. Nucl. Chem.* 326, 591–601. <https://doi.org/10.1007/s10967-020-07332-0>
- GE Health Care, 2018. Storage Phosphor Screen BAS-IP.
- Gong, S., Niu, L., Kemp, L.K., Yiu, C.K.Y., Ryou, H., Qi, Y., Blizzard, J.D., Nikonov, S., Brackett, M.G., Messer, R.L.W., Wu, C.D., Mao, J., Bryan Brister, L., Rueggeberg, F.A., Arola, D.D., Pashley, D.H., Tay, F.R., 2012. Quaternary ammonium silane-functionalized, methacrylate resin composition with antimicrobial activities and self-repair potential. *Acta Biomaterialia* 8, 3270–3282. <https://doi.org/10.1016/j.actbio.2012.05.031>
- Gonzalez, M., Cabanelas, J., Baselga, J., 2012. Applications of FTIR on Epoxy Resins - Identification, Monitoring the Curing Process, Phase Separation and Water Uptake. <https://doi.org/10.5772/36323>
- Gray, J.E., Luan, B., 2002. Protective coatings on magnesium and its alloys — a critical review. *Journal of Alloys and Compounds* 336, 88–113. [https://doi.org/10.1016/S0925-8388\(01\)01899-0](https://doi.org/10.1016/S0925-8388(01)01899-0)
- Han, M., Zhang, G., Li, M., Wang, S., Liu, Z., Li, H., Zhang, Y., Xu, D., Wang, J., Ni, J., Na, H., 2011. Sulfonated poly(ether ether ketone)/polybenzimidazole oligomer/epoxy resin composite membranes in situ polymerization for direct methanol fuel cell usages. *Journal of Power Sources* 196, 9916–9923. <https://doi.org/10.1016/j.jpowsour.2011.08.049>
- Haudebourg, R., Fichet, P., 2016. A non-destructive and on-site digital autoradiography-based

References

- tool to identify contaminating radionuclide in nuclear wastes and facilities to be dismantled. *J Radioanal Nucl Chem* 309, 551–561. <https://doi.org/10.1007/s10967-015-4610-7>
- Hermassi, M., Granados, M., Valderrama, C., Skoglund, N., Ayora, C., Cortina, J.L., 2022. Impact of functional group types in ion exchange resins on rare earth element recovery from treated acid mine waters. *Journal of Cleaner Production* 379, 134742. <https://doi.org/10.1016/j.jclepro.2022.134742>
- Hesek, D., Lee, M., Noll, B.C., Fisher, J.F., Mobashery, S., 2009. Complications from Dual Roles of Sodium Hydride as a Base and as a Reducing Agent. *J Org Chem* 74, 2567–2570. <https://doi.org/10.1021/jo802706d>
- Horwitz, E., McAlister, D., Bond, A., Jr, R., 2005. Novel Extraction of Chromatographic Resins Based on Tetraalkyldiglycolamides: Characterization and Potential Applications. *Solvent Extraction and Ion Exchange - SOLVENT EXTR ION EXCH* 23, 319–344. <https://doi.org/10.1081/SEI-200049898>
- Horwitz, E.P., Chiarizia, R., Dietz, M.L., 1997. DIPEX: A new extraction chromatographic material for the separation and preconcentration of actinides from aqueous solution. *Reactive and Functional Polymers* 33, 25–36. [https://doi.org/10.1016/S1381-5148\(97\)00013-8](https://doi.org/10.1016/S1381-5148(97)00013-8)
- Horwitz, E.P., Dietz, M.L., Chiarizia, R., Diamond, H., Maxwell, S.L., Nelson, M.R., 1995. Separation and preconcentration of actinides by extraction chromatography using a supported liquid anion exchanger: application to the characterization of high-level nuclear waste solutions. *Analytica Chimica Acta* 310, 63–78. [https://doi.org/10.1016/0003-2670\(95\)00144-O](https://doi.org/10.1016/0003-2670(95)00144-O)
- Hubert Mutin, P., Guerrero, G., Vioux, A., 2005. Hybrid materials from organophosphorus coupling molecules. *Journal of Materials Chemistry* 15, 3761–3768. <https://doi.org/10.1039/B505422B>
- International Atomic Energy Agency, 2007. Strategy and Methodology for Radioactive Waste Characterization, Strategy and Methodology for Radioactive Waste Characterization. International Atomic Energy Agency.
- Ioannidis, I., Pashalidis, I., Raptopoulos, G., Paraskevopoulou, P., 2023. Radioactivity/Radionuclide (U-232 and Am-241) Removal from Waters by Polyurea-Crosslinked Alginate Aerogels in the Sub-Picomolar Concentration Range. *Gels* 9, 211. <https://doi.org/10.3390/gels9030211>
- Ion Chromatography*, 1990. . Elsevier.
- ISO 5725-1, 2023. Accuracy (trueness and precision) of measurement methods and results Part 1: General principles and definitions. ISO.
- ISO 7503-1, 2016. Measurement and evaluation of surface contamination Part 1: General principles. ISO.
- ISO 7503-2, 2016. ISO 7503-2. ISO.
- ISO 8769, 2020. Measurement of radioactivity - Alpha-, beta- and photon emitting radionuclides - Reference measurement standard specifications for the calibration of surface contamination monitors. Afnor EDITIONS.
- ISO 9978, 2020. ISO 9978:2020. ISO.
- ISO/IEC Guide 98-1, 2024. ISO/IEC Guide 98-1:2024. ISO.
- Isotrak Calibration Sources, E., 2022. Isotrak Calibration Sources. Eckert & Ziegler Strahlen- und Medizintechnik AG.
- Janssen, H., Klein, R., 1994. Characterization of large-area reference sources for the calibration of alpha-contamination monitors. *Nuclear Instruments and Methods in Physics Research*

References

- Section A: Accelerators, Spectrometers, Detectors and Associated Equipment 339, 318–321. [https://doi.org/10.1016/0168-9002\(94\)91824-4](https://doi.org/10.1016/0168-9002(94)91824-4)
- Janßen, H., Thieme, K., 2000. On the determination of activity profiles in wide-area reference sources. *Applied Radiation and Isotopes* 52, 533–537. [https://doi.org/10.1016/S0969-8043\(99\)00206-7](https://doi.org/10.1016/S0969-8043(99)00206-7)
- Kallingal, N., Sobolčiak, P., Akbar, H., Krupa, I., Novak, I., Popelka, A., 2023. An Enhancement of Compositional Stability of Phase Change Materials by Lamination with Aluminum Sheet. *Coatings* 13, 444. <https://doi.org/10.3390/coatings13020444>
- Kanekal, S., Sahai, A., Jones, R.E., Brown, D., 1995. Storage-phosphor autoradiography: A rapid and highly sensitive method for spatial imaging and quantitation of radioisotopes. *Journal of Pharmacological and Toxicological Methods* 33, 171–178. [https://doi.org/10.1016/1056-8719\(94\)00089-M](https://doi.org/10.1016/1056-8719(94)00089-M)
- Kang, J.-K., Kim, S.-B., 2020. Synthesis of quaternized mesoporous silica SBA-15 with different alkyl chain lengths for selective nitrate removal from aqueous solutions. *Microporous and Mesoporous Materials* 295, 109967. <https://doi.org/10.1016/j.micromeso.2019.109967>
- Kang, L., Zhang, M., Liu, Z.-H., Ooi, K., 2007. IR spectra of manganese oxides with either layered or tunnel structures. *Spectrochimica Acta Part A: Molecular and Biomolecular Spectroscopy* 67, 864–869. <https://doi.org/10.1016/j.saa.2006.09.001>
- Kharitonov, D.S., Makarova, I.V., Osipenko, M.A., Yanushevskii, V.I., Wrzesińska, A., Bobowska, I., Kurilo, I.I., 2020. The Deposition Mechanism and Protective Properties of Manganese-Based Conversion Coatings on the Surface of AD31 Aluminum Alloy. *Prot Met Phys Chem Surf* 56, 113–124. <https://doi.org/10.1134/S2070205120010128>
- Khaskhoussi, A., Calabrese, L., Proverbio, E., 2020. Superhydrophobic Self-Assembled Silane Monolayers on Hierarchical 6082 Aluminum Alloy for Anti-Corrosion Applications. *Applied Sciences* 10, 2656. <https://doi.org/10.3390/app10082656>
- Khodaei, M., Shadmani, S., 2019. Superhydrophobicity on aluminum through reactive-etching and TEOS/GPTMS/nano-Al₂O₃ silane-based nanocomposite coating. *Surface and Coatings Technology* 374, 1078–1090. <https://doi.org/10.1016/j.surfcoat.2019.06.074>
- Kim, G., Burnett, W.C., Horwitz, E.P., 2000. Efficient preconcentration and separation of actinide elements from large soil and sediment samples. *Anal Chem* 72, 4882–4887. <https://doi.org/10.1021/ac000417n>
- Knoll, G.F., 2010. *Radiation Detection and Measurement*. John Wiley & Sons.
- Kokatev, A.N., Lukiyanchuk, I.V., Yakovleva, N.M., Rudnev, V.S., Chupakhina, E.A., Yakovlev, A.N., Stepanova, K.V., 2016. Catalytically active composite materials with porous aluminum oxide matrix modified by γ -MnO₂ nanoparticles. *Prot Met Phys Chem Surf* 52, 832–838. <https://doi.org/10.1134/S2070205116050130>
- Krmpotić, M., Rožmarić, M., Benedik, L., 2018. Investigation of key factors in preparation of alpha sources by electrodeposition. *Applied Radiation and Isotopes* 136, 37–44. <https://doi.org/10.1016/j.apradiso.2018.02.011>
- Kulinich, S.A., Akhtar, A.S., 2012. On conversion coating treatments to replace chromating for Al alloys: Recent developments and possible future directions. *Russ. J. Non-ferrous Metals* 53, 176–203. <https://doi.org/10.3103/S1067821212020071>
- Kyriakou, N., Pizzoccaro-Zilamy, M.-A., Nijmeijer, A., Luiten-Olieman, M., Winnubst, L., 2020. Hydrolytic stability of PEG-grafted γ -alumina membranes: Alkoxysilane vs phosphonic acid linking groups. *Microporous and Mesoporous Materials* 307, 110516. <https://doi.org/10.1016/j.micromeso.2020.110516>

References

- Lafferty, B.J., Ginder-Vogel, M., Zhu, M., Livi, K.J.T., Sparks, D.L., 2010. Arsenite Oxidation by a Poorly-Crystalline Manganese Oxide 2. Results from X-ray Absorption Spectroscopy and X-ray Diffraction. *Environ Sci Technol* 44, 8467–8472. <https://doi.org/10.1021/es102016c>
- Larkin, P.J., 2018a. Chapter 6 - IR and Raman Spectra–Structure Correlations: Characteristic Group Frequencies, in: Larkin, P.J. (Ed.), *Infrared and Raman Spectroscopy (Second Edition)*. Elsevier, pp. 85–134. <https://doi.org/10.1016/B978-0-12-804162-8.00006-9>
- Larkin, P.J., 2018b. Chapter 2 - Basic Principles, in: Larkin, P.J. (Ed.), *Infrared and Raman Spectroscopy (Second Edition)*. Elsevier, pp. 7–28. <https://doi.org/10.1016/B978-0-12-804162-8.00002-1>
- Leblond, S., Fichet, P., Laumonier, R., Billon, S., Sardini, P., Colas, K., 2022. Development of a compact alpha and beta camera for dismantlement applications. *J Radioanal Nucl Chem* 331, 1075–1089. <https://doi.org/10.1007/s10967-021-08172-2>
- Lee, W., Park, S.-J., 2014. Porous Anodic Aluminum Oxide: Anodization and Templated Synthesis of Functional Nanostructures. *Chem. Rev.* 114, 7487–7556. <https://doi.org/10.1021/cr500002z>
- Lehto, J., Hou, X., 2011. *Chemistry and analysis of radionuclides: laboratory techniques and methodology*. Wiley-VCH-Verl, Weinheim.
- Leskinen, A., Fichet, P., Siitari-Kauppi, M., Goutelard, F., 2013. Digital autoradiography (DA) in quantification of trace level beta emitters on concrete. *J Radioanal Nucl Chem* 298, 153–161. <https://doi.org/10.1007/s10967-013-2535-6>
- Li, F., Yin, H., Zhu, T., Zhuang, W., 2024. Understanding the role of manganese oxides in retaining harmful metals: Insights into oxidation and adsorption mechanisms at microstructure level. *Eco-Environment & Health* 3, 89–106. <https://doi.org/10.1016/j.eehl.2024.01.002>
- Li, H., Belkind, A., Jansen, F., Orban, Z., 1997. An in situ XPS study of oxygen plasma cleaning of aluminum surfaces. *Surface and Coatings Technology* 92, 171–177. [https://doi.org/10.1016/S0257-8972\(97\)00079-0](https://doi.org/10.1016/S0257-8972(97)00079-0)
- Lourenço, V., Bobin, C., 2015. Weighing uncertainties in quantitative source preparation for radionuclide metrology. *Metrologia* 52, S18. <https://doi.org/10.1088/0026-1394/52/3/S18>
- Lubelli, B., Hees, R.P.J., 2007. Effectiveness of crystallization inhibitors in preventing salt damage in building materials. *Journal of Cultural Heritage - J CULT HERIT* 8, 223–234. <https://doi.org/10.1016/j.culher.2007.06.001>
- Luschtinetz, R., Seifert, G., Jaehne, E., Adler, H.-J.P., 2007. Infrared Spectra of Alkylphosphonic Acid Bound to Aluminium Surfaces. *Macromolecular Symposia* 254, 248–253. <https://doi.org/10.1002/masy.200750837>
- Ma, D.-Y., Zhang, Y.-M., Xu, J.-N., 2016. The synthesis and process optimization of sulfobutyl ether β -cyclodextrin derivatives. *Tetrahedron* 72, 3105–3112. <https://doi.org/10.1016/j.tet.2016.04.039>
- Madden, S.B., Scully, J.R., 2014. Inhibition of AA2024-T351 Corrosion Using Permanganate. *J. Electrochem. Soc.* 161, C162. <https://doi.org/10.1149/2.075403jes>
- Marinov, G.M., Marinova, A.P., Medvedev, D.V., Dadakhanov, J.A., Milanova, M.M., Happel, S., Radchenko, V.I., Filosofov, D.V., 2016. Determination of distribution coefficients (Kd) of various radionuclides on UTEVA resin. *Radiochimica Acta* 104, 735–742. <https://doi.org/10.1515/ract-2016-2582>
- Martin, D.F., Martin, B.B., Martin, D.F., Martin, B.B., 2013. *Column Chromatography*. <https://doi.org/10.5772/47823>

References

- Monsanglant-Louvet, C., Osmond, M., Ferreux, L., Liatimi, N., Maulard, A., Picolo, J.L., Marcillaud, B., Gensdarmes, F., 2015. Production of reference sources of radioactive aerosols in filters for proficiency testing. *Applied Radiation and Isotopes* 95, 13–22. <https://doi.org/10.1016/j.apradiso.2014.09.014>
- Mougenot, P., Koch, M., Dupont, I., Schneider, Y.-J., Marchand-Brynaert, J., 1996. Surface Functionalization of Polyethylene Terephthalate Film and Membranes by Controlled Wet Chemistry: II. Reactivity Assays of Hydroxyl Chain Ends. *Journal of Colloid and Interface Science* 177, 162–170. <https://doi.org/10.1006/jcis.1996.0017>
- Mui, T.S.M., Mota, R.P., Quade, A., Hein, L.R. de O., Kostov, K.G., 2018. Uniform surface modification of polyethylene terephthalate (PET) by atmospheric pressure plasma jet with a horn-like nozzle. *Surface and Coatings Technology* 352, 338–347. <https://doi.org/10.1016/j.surfcoat.2018.08.014>
- Muñoz, L., Tamayo, L., Gulppi, M., Rabagliati, F., Flores, M., Urzúa, M., Azócar, M., Zagal, J.H., Encinas, M.V., Zhou, X., Thompson, G., Páez, M., 2018. Surface Functionalization of an Aluminum Alloy to Generate an Antibiofilm Coating Based on Poly(Methyl Methacrylate) and Silver Nanoparticles. *Molecules* 23. <https://doi.org/10.3390/molecules23112747>
- Nähle, O., Kossert, K., 2012. Characterization of photon-emitting wide area reference sources. *Applied Radiation and Isotopes, Proceedings of the 18th International Conference on Radionuclide Metrology and its Applications* 70, 2018–2024. <https://doi.org/10.1016/j.apradiso.2012.02.076>
- Nayak, N., Huertas, R., Crespo, J.G., Portugal, C.A.M., 2019. Surface modification of alumina monolithic columns with 3-aminopropyltetraethoxysilane (APTES) for protein attachment. *Separation and Purification Technology* 229, 115674. <https://doi.org/10.1016/j.seppur.2019.115674>
- N. Bùì, L., Thompson, M., B. McKeown, N., D. Romaschin, A., G. Kalman, P., 1993. Surface modification of the biomedical polymer poly(ethylene terephthalate). *Analyst* 118, 463–474. <https://doi.org/10.1039/AN9931800463>
- NEA, 2017. Radiological Characterisation from a Waste and Materials End-State Perspective: Practices and Experience | en | OECD.
- Neouze, M.-A., Schubert, U., 2008. Surface Modification and Functionalization of Metal and Metal Oxide Nanoparticles by Organic Ligands. *Monatshefte für Chemie - Chemical Monthly* 139, 183–195. <https://doi.org/10.1007/s00706-007-0775-2>
- Nuc Film Discs, 2015. NucFilm Discs [WWW Document]. TrisKem International - Reagents for environmental monitoring, bioassay, geochemistry, radiopharmacy and decommissioning. URL <https://www.triskem-international.com/nucfilm-discs.php> (accessed 3.2.23).
- OECD/NEA, 2003. The Decommissioning and Dismantling of Nuclear Facilities: Status, Approaches, Challenges, Radioactive Waste Management. OECD. <https://doi.org/10.1787/9789264184886-en>
- Ohshiro, M., Shiina, T., Yamada, T., 2016. Uniformity measurement of wide area reference sources for beta emitters. *Applied Radiation and Isotopes* 109, 397–401. <https://doi.org/10.1016/j.apradiso.2015.12.015>
- Orano, 2023. Wide area α and β sources - Rectangular and Square. LEA.
- Ouadah, A., Luo, T., Gao, S., Zhu, C., 2018. Controlling the degree of sulfonation and its impact on hybrid cross-linked network based polyphosphazene grafted butylphenoxy as proton exchange membrane. *International Journal of Hydrogen Energy* 43, 15466–15480. <https://doi.org/10.1016/j.ijhydene.2018.06.105>

References

- Özkanat, Ö., Salgin, B., Rohwerder, M., Mol, J.M.C., de Wit, J.H.W., Terryn, H., 2012. Scanning Kelvin Probe Study of (Oxyhydr)oxide Surface of Aluminum Alloy. *J. Phys. Chem. C* 116, 1805–1811. <https://doi.org/10.1021/jp205585u>
- Patiny, L., Zasso, M., Kostro, D., Bernal, A., Castillo, A.M., Bolaños, A., Asencio, M.A., Pellet, N., Todd, M., Schloerer, N., Kuhn, S., Holmes, E., Javor, S., Wist, J., 2018. The C₆H₆ NMR repository: An integral solution to control the flow of your data from the magnet to the public. *Magn Reson Chem* 56, 520–528. <https://doi.org/10.1002/mrc.4669>
- Peng, H., Luo, Z., Li, L., Xia, Z., Du, J., Zheng, B., 2019. Facile fabrication of superhydrophobic aluminum surfaces by chemical etching and its anti-icing/self-cleaning performances. *Mater. Res. Express* 6, 096586. <https://doi.org/10.1088/2053-1591/ab3173>
- Pereira, A.P., Silva, M., Jr, É., Paula, A., Tommasini, F., 2017. Processing and Characterization of PET Composites Reinforced With Geopolymer Concrete Waste. *Materials Research* 20. <https://doi.org/10.1590/1980-5373-mr-2017-0734>
- Pérot, B., Jallu, F., Passard, C., Gueton, O., Allinei, P.-G., Loubet, L., Estre, N., Simon, E., Carasco, C., Roure, C., Boucher, L., Lamotte, H., Comte, J., Bertaux, M., Lyoussi, A., Fichet, P., Carrel, F., 2018. The characterization of radioactive waste: a critical review of techniques implemented or under development at CEA, France. *EPJ Nuclear Sci. Technol.* 4, 3. <https://doi.org/10.1051/epjn/2017033>
- Petrovic, J., Thomas, G., 2008. Reaction of Aluminum with Water to Produce Hydrogen.
- Plancque, G., Moulin, V., Toulhoat, P., Moulin, C., 2003. Europium speciation by time-resolved laser-induced fluorescence. *Analytica Chimica Acta* 478, 11–22. [https://doi.org/10.1016/S0003-2670\(02\)01486-1](https://doi.org/10.1016/S0003-2670(02)01486-1)
- Plueddemann, E.P., 1991. Nature of Adhesion Through Silane Coupling Agents, in: Plueddemann, E.P. (Ed.), *Silane Coupling Agents*. Springer US, Boston, MA, pp. 115–152. https://doi.org/10.1007/978-1-4899-2070-6_5
- Rahimi, M., Fojan, P., Gurevich, L., Afshari, A., 2014. Effects of aluminium surface morphology and chemical modification on wettability. *Applied Surface Science* 296, 124–132. <https://doi.org/10.1016/j.apsusc.2014.01.059>
- Ren, Y., Bao, H., Wu, Q., Wang, H., Gai, T., Shao, L., Wang, S., Tang, H., Li, Y., Wang, X., 2020. The physical chemistry of uranium (VI) immobilization on manganese oxides. *Journal of Hazardous Materials* 391, 122207. <https://doi.org/10.1016/j.jhazmat.2020.122207>
- Riaz, S., Ashraf, M., Hussain, T., Hussain, M.T., 2019. Modification of silica nanoparticles to develop highly durable superhydrophobic and antibacterial cotton fabrics. *Cellulose* 26, 5159–5175. <https://doi.org/10.1007/s10570-019-02440-x>
- Rodič, P., Milošev, I., 2019. One-step ultrasound fabrication of corrosion resistant, self-cleaning and anti-icing coatings on aluminium. *Surface and Coatings Technology* 369, 175–185. <https://doi.org/10.1016/j.surfcoat.2019.03.082>
- Sardini, P., Caner, L., Mossler, P., Mazurier, A., Hellmuth, K.-H., Graham, R., Rossi, A., Siitari-Kauppi, M., 2015. Calibration of digital autoradiograph technique for quantifying rock porosity using ¹⁴C-PMMA method. *Journal of Radioanalytical and Nuclear Chemistry* 303. <https://doi.org/10.1007/s10967-014-3617-9>
- Sato, Y., Hino, Y., Yamada, T., Matsumoto, M., 2004. The new fabrication method of standard surface sources. *Applied Radiation and Isotopes, Proceedings of the 14th International Conference on Radionuclide Metrology and its Applications, ICRM 2003* 60, 543–546. <https://doi.org/10.1016/j.apradiso.2003.11.074>
- Siau, S., Vervaet, A., Schacht, E., Calster, A.V., 2004a. Influence of Chemical Pretreatment of Epoxy

References

- Polymers on the Adhesion Strength of Electrochemically Deposited Cu for Use in Electronic Interconnections. *J. Electrochem. Soc.* 151, C133. <https://doi.org/10.1149/1.1639159>
- Siau, S., Vervaet, A., Schacht, E., Degrande, S., Callewaert, K., Van Calster, A., 2005. Chemical Modification of Buildup Epoxy Surfaces for Altering the Adhesion of Electrochemically Deposited Copper. *Journal of The Electrochemical Society* 152, 136. <https://doi.org/10.1149/1.1952727>
- Siau, S., Vervaet, A., Van Calster, A., Swennen, I., Schacht, E., 2004b. Epoxy Polymer Surface Roughness Modeling Based on Kinetic Studies of Wet Chemical Treatments. *Journal of The Electrochemical Society* 151, 54. <https://doi.org/10.1149/1.1766314>
- Silva, I.A., Siqueira, P. de T.D., Nascimento, E. do, Yoriyaz, H., Sordi, G.-M.A.A., Vivolo, V., Potiens, M. da P.A., 2020. Correction factors for non-uniform large-area reference sources. *Applied Radiation and Isotopes* 160, 109082. <https://doi.org/10.1016/j.apradiso.2020.109082>
- Silva, R.A., Hawboldt, K., Zhang, Y., 2018. Application of resins with functional groups in the separation of metal ions/species – a review. *Mineral Processing and Extractive Metallurgy Review* 39, 395–413. <https://doi.org/10.1080/08827508.2018.1459619>
- Song, M.-S., Deng, Q.-S., Toh, R.J., Cole, I., Chen, X., 2022. Permanganate, Molybdate and Vanadate Conversion Coatings Vanadate conversion coatings, in: Saji, V.S., Sankara Narayanan, T.S.N., Chen, X. (Eds.), *Conversion Coatings for Magnesium and Its Alloys*. Springer International Publishing, Cham, pp. 113–131. https://doi.org/10.1007/978-3-030-89976-9_5
- Stéphan, O., Carrier, M., 1997. Preparation of Thin α -Particle Sources Using Polypyrrole Films Functionalized by Alkylammonium Groups. *Radiochimica Acta* 76, 29–36. <https://doi.org/10.1524/ract.1997.76.12.29>
- Surbeck, H., 2000. Alpha spectrometry sample preparation using selectively adsorbing thin films. *Applied Radiation and Isotopes* 53, 97–100. [https://doi.org/10.1016/S0969-8043\(00\)00119-6](https://doi.org/10.1016/S0969-8043(00)00119-6)
- Švec, A., Janßen, H., Pernická, L., Klein, R., 2006. A modified method for the characterisation and activity determination of large area sources. *Applied Radiation and Isotopes, Proceedings of the 15th International Conference on Radionuclide Metrology and its Applications* 64, 1207–1210. <https://doi.org/10.1016/j.apradiso.2006.02.022>
- Szlamkiewicz, I., Stanberry, J., Lugo, K., Murphy, Z., Ruiz Garcia, M., Hunley, L., Qafoku, N.P., Anagnostopoulos, V., 2023. Role of Manganese Oxides in Controlling Subsurface Metals and Radionuclides Mobility: A Review. *ACS Earth Space Chem.* 7, 1–10. <https://doi.org/10.1021/acsearthspacechem.2c00113>
- Talvitie, N.A., 1972. Electrodeposition of actinides for .alpha. spectrometric determination. *Anal. Chem.* 44, 280–283. <https://doi.org/10.1021/ac60310a013>
- Torres-Huerta, A., Del Angel, D., Domínguez-Crespo, M.A., Palma Ramírez, D., Perales-Castro, M., Flores-Vela, A., 2016. Morphological and Mechanical Properties Dependence of PLA Amount in PET Matrix Processed by Single-Screw Extrusion. *Polymer-Plastics Technology and Engineering* 55. <https://doi.org/10.1080/03602559.2015.1132433>
- Tsoumpko-Sitnikov, V., Picolo, J.L., Carrier, M., Peulon, S., Moutard, G., 2002. A novel method for large-area sources preparation for the calibration of β - and α -contamination monitors. *Applied Radiation and Isotopes, Proceedings of the Conference on Radionuclide Metrology and its Applications, ICRM'01* 56, 21–29. [https://doi.org/10.1016/S0969-8043\(01\)00161-0](https://doi.org/10.1016/S0969-8043(01)00161-0)

References

- Tüzün, D., Chambon, L., Kergadallan, Y., Lourenço, V., 2023. Novel production method for traceable surface sources by aluminium functionalisation. *Applied Radiation and Isotopes* 202, 111045. <https://doi.org/10.1016/j.apradiso.2023.111045>
- Ul-Hamid, A., 2018. *A Beginners' Guide to Scanning Electron Microscopy*. Springer International Publishing, Cham. <https://doi.org/10.1007/978-3-319-98482-7>
- Umehara, H., Takaya, M., Terauchi, S., 2003. Chrome-free surface treatments for magnesium alloy. *Surface and Coatings Technology, Proceedings of Frontiers of Surface Engineering* 169–170, 666–669. [https://doi.org/10.1016/S0257-8972\(03\)00052-5](https://doi.org/10.1016/S0257-8972(03)00052-5)
- Uyama, Y., Kato, K., Ikada, Y., 1998. Surface Modification of Polymers by Grafting, in: Galina, H., Ikada, Y., Kato, K., Kitamaru, R., Lechowicz, J., Uyama, Y., Wu, C. (Eds.), *Grafting/Characterization Techniques/Kinetic Modeling, Advances in Polymer Science*. Springer, Berlin, Heidelberg, pp. 1–39. https://doi.org/10.1007/3-540-69685-7_1
- Vuurman, M.A., Wachs, I.E., Stufkens, D.J., Oskam, A., 1993. Characterization of chromium oxide supported on Al₂O₃, ZrO₂, TiO₂, and SiO₂ under dehydrated conditions. *Journal of Molecular Catalysis* 80, 209–227. [https://doi.org/10.1016/0304-5102\(93\)85079-9](https://doi.org/10.1016/0304-5102(93)85079-9)
- Wang, Z., Giammar, D.E., 2015. Metal Contaminant Oxidation Mediated by Manganese Redox Cycling in Subsurface Environment, in: *Advances in the Environmental Biogeochemistry of Manganese Oxides, ACS Symposium Series*. American Chemical Society, pp. 29–50. <https://doi.org/10.1021/bk-2015-1197.ch002>
- Xia, L., McCreery, R.L., 1998. Chemistry of a Chromate Conversion Coating on Aluminum Alloy AA2024-T3 Probed by Vibrational Spectroscopy. *J. Electrochem. Soc.* 145, 3083. <https://doi.org/10.1149/1.1838768>
- Xu, F., Zhang, G., Zhang, F., Zhang, Y., 2015. Facile preparation of super-hydrophilic poly(ethylene terephthalate) fabric using dilute sulfuric acid under microwave irradiation. *Applied Surface Science* 349, 437–444. <https://doi.org/10.1016/j.apsusc.2015.05.018>
- Yamada, T., Matsumoto, M., Yamamoto, S., Sato, Y., Yunoki, A., Hino, Y., 2012. Performance test and quality control of large area reference sources fabricated by the ink-jet printing technique. *Applied Radiation and Isotopes, Proceedings of the 18th International Conference on Radionuclide Metrology and its Applications* 70, 1964–1968. <https://doi.org/10.1016/j.apradiso.2012.02.024>
- Yin, L., Wang, Y., Ding, J., Wang, Q., Chen, Q., 2012. Water condensation on superhydrophobic aluminum surfaces with different low-surface-energy coatings. *Applied Surface Science* 258, 4063–4068. <https://doi.org/10.1016/j.apsusc.2011.12.100>
- Yoshida, M., Martin, R.H., 1990. Preparation of extended sources with homogeneous polyethylene ion-exchange membranes. *International Journal of Radiation Applications and Instrumentation. Part A. Applied Radiation and Isotopes* 41, 387–394. [https://doi.org/10.1016/0883-2889\(90\)90148-A](https://doi.org/10.1016/0883-2889(90)90148-A)
- Zheng, M., Zhang, H., Gong, X., Xu, R., Xiao, Y., Dong, H., Liu, X., Liu, Y., 2013. A simple additive-free approach for the synthesis of uniform manganese monoxide nanorods with large specific surface area. *Nanoscale research letters* 8, 166. <https://doi.org/10.1186/1556-276X-8-166>
- Zhou, S., Liu, X., Lai, J., Zheng, M., Liu, W., Xu, Q., Yin, D., 2019. Covalently linked organo-sulfonic acid modified titanate nanotube hybrid nanostructures for the catalytic esterification of levulinic acid with n-butyl alcohol. *Chemical Engineering Journal* 361, 571–577. <https://doi.org/10.1016/j.cej.2018.12.111>